



Norwegian University of
Science and Technology

Rational Upscaling and Modelling of a Semi-Submersible Floating Offshore Wind Turbine

Mareike Leimeister

Wind Energy

Submission date: May 2016

Supervisor: Erin Bachynski, IMT


Co-supervisor: Michael Muskulus, BAT
Andrei Metrikine, TU Delft
Philipp Thomas, Fraunhofer IWES

Norwegian University of Science and Technology
Department of Marine Technology

Rational Upscaling and Modelling of a Semi-Submersible Floating Offshore Wind Turbine

Mareike Leimeister

1st June, 2016

 European Wind Energy Master
Erasmus Mundus MSc program
Offshore Engineering track



Rational Upscaling and Modelling of a Semi-Submersible Floating Offshore Wind Turbine

MASTER OF SCIENCE THESIS

For obtaining the degree of Master of Science in “Technology-Wind Energy” at Norwegian University of Science and Technology, and in “Offshore Engineering and Dredging” at Delft University of Technology.

Mareike Leimeister

NTNU: 763391
TU Delft: 143525

1st June, 2016

European Wind Energy Master - EWEM

Delft University of Technology
Faculty of Mechanical, Maritime and Materials Engineering
Department of Maritime and Transport Technology
Section of Offshore and Dredging Engineering

Norwegian University of Science and Technology
Faculty of Engineering Science and Technology
Department of Marine Technology



Copyright © Mareike Leimeister
All rights reserved.

Cover photo - Fukushima floating offshore wind project, courtesy of Bloomberg [58]

Statement in Lieu of an Oath

I hereby make an affirmation in lieu of an oath that I have written this master's thesis report on my own without any help from anyone else and that I have used no source material or aids other than those indicated.

Trondheim, Norway

Place

1st June, 2016

Date

Marika Leimisto

Signature

MSC THESIS IN MARINE TECHNOLOGY

SPRING 2016

FOR

Mareike Leimeister

Rational upscaling and modelling of a semi-submersible floating offshore wind turbine

Rasjonell oppskalering og modellering av en halvt nedsenkbar flytende offshore vindturbin
Rationeel opschalen en modelleren van een half-afzinkbare zwevende offshore windturbin

Background:

The recent trend in the offshore wind industry is going to larger wind turbines and deeper water, implicating the necessity to concentrate on the development of floating structures. Those will be more challenging than bottom-fixed offshore wind turbines because of more complex conditions. The large displacements and rotations of floating structures are coupled to the rotor-nacelle motions. Low frequency modes can influence the aerodynamic damping, which could have an effect on the stability of the entire system. The mooring also adds an extra system. Furthermore, the non-slender and non-cylindrical shape of the floating platform will cause radiation and diffraction effects. [60]

Those additional aspects, that have to be considered in the aero-hydro-servo-elastic analysis, also involve unique challenges in upscaling of floating offshore wind turbines. The scaling of a whole wind turbine, based on the turbine rating, is a well-known procedure. But there are no scaling laws that consider the different behavior of the offshore and onshore wind turbine control systems. Furthermore, for floating structures the accurate representations of frequencies and internal modes are more important than just following the geometrically scaling. Also the mooring system has to be treated separately, focusing on the needed stiffness in the full size.

The complexity of floating structures regarding the dynamic behavior is one of the aspects considered in the Offshore Code Comparison Collaboration Continuation (OC4) project. The 5MW DeepCwind semi-submersible floating offshore wind turbine has already been studied numerically within the OC4-project, and tested at 1:50 scale in the ocean basin at MARIN.

For further research, reference turbines reproducing realistic data are needed. Due to the fact that limited information about modern wind turbines is provided by the manufacturers, and that the mainly used reference turbines are no longer representing the state of the art, Fraunhofer IWES has designed a new reference wind turbine within the joint "Smart Blades" project. This is designed for onshore purposes and optimized regarding the tower structure and rotor blades. An offshore equivalent of the IWT-7.5-164 turbine has also been recently designed, including monopile and transition piece.

In the project work, an initial upscaling of the DeepCwind semi-submersible platform is carried out, so that a floating platform, including station-keeping system, for the onshore IWT-7.5 MW turbine is designed. A simple analysis process is developed, and the natural periods, stability, and hydrodynamic characteristics of the upscaled platform are estimated. Potential problems with the upscaling are identified and suggestions for modification are made.

In the thesis work, the initial upscaling procedure, performed in the project work, should be adapted to the offshore IWT wind turbine design. The simple analysis process should be extended to a more detailed upscaling analysis of the DeepCwind semi-submersible wind turbine. The preliminary design should be implemented in Modelica as a rigid body with stiff braces, based on existing models in the OneWind Modelica Library. Based on the results of the preliminary design, unexpected effects in the dynamic behavior, modes, motion interactions and stability that result from the initial upscaling have to be identified. The upscaling should then be adapted in such a way, that undesired and unforeseen side effects are avoided. Based on the load cases of OC4 Phase II, simulations should be run in Dymola/Modelica, in order to prove reasonable behavior of the upscaled floating wind turbine system. Furthermore, the results obtained by hand calculations and both computer based simulations (HydroD and Modelica) should be compared.

The final goal of the master's thesis is to optimize the upscaling process of the DeepCwind floating turbine in order to find a reasonable design for a semi-submersible platform, which would fit the offshore IWT-7.5 MW wind turbine, is a producible structure and represents realistic dynamic behavior. An implementation of the upscaling would be desirable, so that it could be used for other scales, like the DTU 10 MW wind turbine, as well.

Assignment:

The following tasks should be addressed in the thesis work:

1. Literature study on additional aspects like control system for floating wind turbines, mooring dynamics, 2nd order wave loads and viscous effects.
2. Get familiar with Modelica. Work with the online book Modelica by Example and the tool Open Modelica. Familiarize with the existing models, especially for floating structures, available in the OneWind Modelica Library. Become acquainted with equation-based modelling.
3. Implement the preliminary design of the semi-submersible floating platform in Modelica and include also the wind turbine IWT-7.5-164 and mooring system. Analyze the system performance and compare with the results obtained by hand calculations and simulation with HydroD.
4. Optimize the original DeepCwind semi-submersible platform.
5. Adapt the upscaling procedure and design, based on the optimized DeepCwind floater, a reasonable semi-submersible platform for the offshore IWT-7.5-164 wind turbine. Implement the final design in Modelica and run simulations based on representative load cases. Analyze the system performance and compare with the results obtained by hand calculations and simulation with HydroD.
6. Report and conclude on the investigation. Summarize the upscaling criteria and optimization approaches. Give a kind of guideline for the upscaling procedure of a semi-submersible platform depending on the predefined parameters.
7. Write the master's thesis report.

Theories and conclusions should be based on mathematical derivations and/or logic reasoning, identifying the various steps in the deduction.

The candidate should utilize the existing possibilities for obtaining relevant literature.

The original contribution of the candidate and material taken from other sources shall be clearly defined. Work from other sources shall be properly referenced using an acknowledged referencing system.

The thesis report should be organized in a rational manner to give a clear exposition of results, assessments, and conclusions. The text should be brief and to the point, with a clear language. Telegraphic language should be avoided.

The thesis report shall contain the following elements: A text defining the scope, preface, list of contents, main body of the project report, conclusions with recommendations for further work, list of symbols and acronyms, reference and (optional) appendices. All figures, tables and equations shall be numerated.

Supervisors:

| | |
|------------------|--|
| NTNU: | Erin Bachynski Michael Muskulus Torgeir Moan |
| TU Delft: | Andrei Metrikine Eliz-Mari Lourens |
| Fraunhofer IWES: | Philipp Thomas |

Deadline: 01.06.2016

Summary

Floating offshore wind turbines are taking on more and more prominence, as the industry moves towards larger turbines, farther offshore, in deeper water. The increase in turbine size can reduce the costs of offshore wind energy, but requires larger support structures. Rather than redesigning the structure completely, a rational methodology for upscaling an existing floating substructure can improve the efficiency of the design process. This work presents a guideline for the optimization and upscaling of a semi-submersible floating platform, addressing also special challenges related to changes in turbine technology, as well as design criteria for floating platforms.

The OC4 semi-submersible platform is used as starting point of this study. Based on analysis results of an initial elementary upscaling procedure, the main criteria, when dealing with a semi-submersible floating platform, are specified. Optimization is then carried out, focusing on stability and eigenfrequencies. Reducing the upper column diameter and changing the ballast position within the columns, yields longer natural periods in heave and pitch, a lighter and cheaper platform, and a less over-conservative, but still stable and safe system.

Based on this optimized design, a guideline for an upscaling procedure for any other turbine is given. The main scaling factor is determined from the mass ratio of the top structures, rather than the turbine rating. The main column is scaled, so that it fits the new tower base diameter. The scaling factor for the upper columns is computed, based on the ratio of the overturning moments, and considers the contribution of the different columns to the stiffness component in pitch. The mooring line length is scaled, such that it can yield a predefined stiffness. Finally, the controller gains are recalculated, based on the expected natural frequency in pitch.

The optimization and upscaling process is carried out for Fraunhofer's offshore wind turbine IWT-7.5-164 and the DTU 10 *MW* reference wind turbine. The floating wind turbines are analyzed, modelled and simulated by means of simplified spreadsheet methods, linear frequency-domain calculations (in DNV's software HydroD), and detailed equation-based models (in Fraunhofer's software Modelica). The systems are evaluated regarding their eigenfrequencies, nominal pitch, stability and global performance in selected sea states, taking variable buoyancy and center of buoyancy into account, and adjusting the blade-pitch controller gains. The results, obtained from both computer programs and the initial hand calculations, are comparable and satisfying. The structural integrity is proved by a simplified approach, using tank pressure and sea pressure for computing the equivalent stress. More detailed strength checks for fatigue and ultimate limit states, as well as optimization of the mooring system, are left for future work.

Preface

This master's thesis is realized within the European Wind Energy Master (EWEM) program in the Offshore Engineering track. The thesis work is partly carried out at Fraunhofer Institute for Wind Energy and Energy System Technology (IWES) in Bremerhaven, Germany, and partly at the Department of Marine Technology of the Norwegian University of Science and Technology (NTNU) in Trondheim, Norway. Due to the double degree master program, also the Delft University of Technology (TU Delft), in the Netherlands, is involved in supervision.

Sending an unsolicited application to Fraunhofer, I got into contact with Mareike Strach-Sonsalla and Philipp Thomas in July 2015. Together, we worked out some ideas for a master's thesis and preceding research project, about upscaling and modelling of a semi-submersible floating wind turbine, including simulations for comparison with the OC4-project. Beginning of August, those ideas were revised and the scientific question of finding an optimized upscaling procedure was formulated. From September to December, I worked on this thesis topic within the framework of a preceding research project at NTNU. With the beginning of this year 2016, I continued with the final master's thesis work. In February, I moved to Bremerhaven, in order to perform the main part and simulations at Fraunhofer IWES. I finished the last simulations end of April and went back to Trondheim for finalizing the thesis work. In the last month, I wrote the thesis report, had my greenlight meeting, attended the poster presentation at NTNU, and, finally, had my thesis defense on 1st of June 2016.

At NTNU, I had weekly meetings with Erin Bachynski, and some also together with Michael Muskulus, in order to discuss the main steps, results and further procedure. During the time at IWES, the regular exchange was done via email or Skype. In the kick-off and progress meetings, also Andrei Metrikine, my supervisor at TU Delft, and Philipp Thomas, from Fraunhofer IWES, were involved.

I want to thank Erin Bachynski from NTNU for her supervision, constructive discussions and feedback. She was supporting me during the entire time of the preceding research project and master's thesis. Even from the distance, a regular contact and helpful supervision was possible. Besides the supervision, I also want to thank Michael Muskulus from NTNU for encouraging me to send an abstract, based on my project work, to DeepWind. This way, I had the opportunity to participate in the 13th Deep Sea Offshore Wind R&D Conference in January 2016, where I had a poster presentation, and also had the chance to have a paper accepted to be published in Energy Procedia, expected in August 2016, which can be found in Appendix A.8.

Thanks to Philipp Thomas from Fraunhofer IWES, who arranged that I could already work from Norway with Fraunhofer's simulation tools and libraries. He provided me all information about Fraunhofer's reference wind turbine, and introduced me to the modelling environment. I also want to thank all other employees at Fraunhofer IWES, for being open for questions to and discussions about existing models and designs. I am looking forward to continuing my work there as an assistant after my thesis defense.

Finally, I also want to thank Andrei Metrikine and Eliz-Mari Lourens from TU Delft, for being open to the topic and new ideas to include, as well as Zhen Gao from NTNU and Marysa Dunant from TU Delft, for helping with general questions regarding the organization of the master's thesis procedure. A special thank goes to Linda Gaffel, the main coordinator of the EWEM program, and to my fellow students - thanks for having such a great time together, during this unique master program.

Mareike Leimeister

Contents

| | |
|--|--------------|
| Thesis Work Description | iii |
| Summary | vii |
| Preface | ix |
| Contents | xi |
| List of Figures | xv |
| List of Tables | xvi |
| List of Source Codes | xvii |
| List of Symbols | xix |
| Abbreviations | xxiii |
| 1 Introduction | 1 |
| 1.1 Onshore Versus Offshore | 1 |
| 1.2 Floating Wind Turbines | 1 |
| 1.3 Upscaling | 2 |
| 1.4 Content | 3 |
| 2 Reference Structures | 5 |
| 2.1 DeepCwind Semi-Submersible | 5 |
| 2.2 IWES IWT-7.5-164 | 8 |
| 2.3 DTU 10 MW Reference Wind Turbine | 9 |
| 3 Theory | 11 |
| 3.1 Upscaling Procedure for Wind Turbines | 11 |
| 3.1.1 Theoretical Upscaling Based on Geometric Self-Similarity | 11 |
| 3.1.1.1 Assumptions and Basics | 11 |
| 3.1.1.2 Scaling Laws | 11 |
| 3.1.1.3 Limits of Standard Upscaling Procedure | 12 |
| 3.1.2 Real Upscaling Based on Existing Wind Turbines | 14 |
| 3.2 Stable Floating Systems | 16 |
| 3.2.1 The Principle of Floatation | 16 |
| 3.2.2 Stability | 16 |
| 3.2.2.1 General Definitions | 16 |
| 3.2.2.2 Simplified Hand Calculations | 17 |
| 3.2.2.3 Detailed Stability Calculations | 19 |
| 3.2.2.4 Intact Floating Stability | 19 |
| 3.3 Natural Frequencies of Floating Structures | 20 |
| 3.3.1 Motions of a Floating Structure | 20 |
| 3.3.2 Natural Frequency in Heave | 21 |
| 3.3.3 Natural Frequency in Pitch | 22 |
| 3.4 Viscous Forces and Damping | 24 |
| 3.4.1 Morison's Equation | 24 |
| 3.4.2 Drag Coefficient Determination | 24 |
| 3.5 Station-Keeping Systems for Floating Structures | 26 |
| 3.5.1 Overview of Existing Design Concepts | 26 |
| 3.5.2 Calculations of Elastic Catenaries | 26 |

| | | |
|----------|---|-----------|
| 3.5.3 | Mooring Stiffness | 28 |
| 3.6 | Control Systems for Floating Wind Turbines | 29 |
| 3.6.1 | Wind Turbine Control | 29 |
| 3.6.2 | Blade-Pitch Controller | 29 |
| 4 | Analyses of the Platform Designs and Floating Systems | 31 |
| 4.1 | Analysis Based on Hand Calculations | 31 |
| 4.2 | Analysis Based on GeniE and HydroD | 31 |
| 4.2.1 | Implementation in GeniE and HydroD | 31 |
| 4.2.2 | Results from HydroD and Wadam | 32 |
| 4.2.3 | Motion Response Analysis | 33 |
| 4.3 | Analysis Based on Modelica and Dymola | 34 |
| 4.3.1 | Implementation in Modelica | 35 |
| 4.3.1.1 | Top Structure | 35 |
| 4.3.1.2 | Support Structure | 35 |
| 4.3.1.3 | Station-Keeping System | 36 |
| 4.3.1.4 | Environment | 36 |
| 4.3.2 | Simulation and Results | 36 |
| 4.3.2.1 | Free Decay Tests | 37 |
| 4.3.2.2 | Full-System Analysis | 37 |
| 4.4 | Verification of the Analysis Methods and Implemented Models | 37 |
| 4.4.1 | Verification of the Determination of the Drag Coefficients | 38 |
| 4.4.2 | Verification of the Static Analysis Methods | 38 |
| 4.4.2.1 | System Matrices | 38 |
| 4.4.2.2 | Nominal Pitch | 40 |
| 4.4.2.3 | Stability | 40 |
| 4.4.2.4 | Natural Periods | 40 |
| 4.4.2.5 | Controller Gains | 41 |
| 5 | Initial Upscaling of the DeepCwind Semi-Submersible Platform | 43 |
| 5.1 | Initial Upscaling Procedure | 43 |
| 5.2 | Analysis of the Initially Upscaled Platform Designs | 45 |
| 5.2.1 | Static Analysis | 45 |
| 5.2.1.1 | System Matrices | 45 |
| 5.2.1.2 | Nominal Pitch | 47 |
| 5.2.1.3 | Stability | 47 |
| 5.2.1.4 | Natural Periods | 48 |
| 5.2.2 | Dynamic Analysis | 49 |
| 5.2.2.1 | Response Amplitude Operators | 49 |
| 5.2.2.2 | Response Spectra | 50 |
| 5.2.2.3 | Standard Deviations | 50 |
| 6 | Criteria for Optimization and Upscaling | 53 |
| 6.1 | Top Structure | 53 |
| 6.2 | Eigenfrequencies | 53 |
| 6.3 | Stability | 53 |
| 6.4 | Mooring System | 54 |
| 6.5 | Environment | 54 |
| 6.6 | Structural Strength | 54 |
| 6.7 | Producibility | 56 |
| 6.8 | Costs | 56 |

| | | |
|----------|--|-----------|
| 7 | Optimization of the DeepCwind Semi-Submersible Platform | 57 |
| 7.1 | Optimization Procedure | 57 |
| 7.2 | Optimized DeepCwind Semi-Submersible Platform Design | 59 |
| 7.2.1 | Static Analysis | 59 |
| 7.2.1.1 | System Matrices | 59 |
| 7.2.1.2 | Nominal Pitch | 59 |
| 7.2.1.3 | Stability | 60 |
| 7.2.1.4 | Natural Periods | 60 |
| 7.2.1.5 | Controller Gains | 61 |
| 7.2.2 | Dynamic Analysis | 61 |
| 7.2.3 | Structural Analysis | 64 |
| 8 | Upscaling of the Optimized DeepCwind Semi-Submersible Platform Design | 65 |
| 8.1 | Upscaling Process - A Guideline | 65 |
| 8.1.1 | Main Scaling Factor | 65 |
| 8.1.2 | Scaling Factor for the Main Column | 65 |
| 8.1.3 | Scaling Factor for the Upper Columns | 65 |
| 8.1.4 | Further Adjustments | 68 |
| 8.1.4.1 | Drag Coefficients | 68 |
| 8.1.4.2 | Mooring System | 68 |
| 8.1.4.3 | Ballast System | 68 |
| 8.1.4.4 | Controller Gains | 68 |
| 8.2 | Upscaled Semi-Submersible Platform Design for the IWT-7.5-164 | 69 |
| 8.2.1 | Static Analysis | 69 |
| 8.2.1.1 | System Matrices | 69 |
| 8.2.1.2 | Nominal Pitch | 69 |
| 8.2.1.3 | Stability | 71 |
| 8.2.1.4 | Natural Periods | 71 |
| 8.2.1.5 | Controller Gains | 73 |
| 8.2.2 | Dynamic Analysis | 74 |
| 8.2.3 | Structural Analysis | 76 |
| 8.3 | Upscaled Semi-Submersible Platform Designs for the DTU 10 MW | 77 |
| 8.3.1 | Static Analysis | 77 |
| 8.3.1.1 | System Matrices | 77 |
| 8.3.1.2 | Nominal Pitch | 79 |
| 8.3.1.3 | Stability | 79 |
| 8.3.1.4 | Natural Periods | 80 |
| 8.3.1.5 | Controller Gains | 81 |
| 8.3.2 | Dynamic Analysis | 81 |
| 8.3.3 | Structural Analysis | 82 |
| 9 | Conclusion and Recommendation | 83 |
| 9.1 | Conclusion | 83 |
| 9.2 | Recommendation | 84 |
| A | Appendix | 91 |
| A.1 | Detailed Stability Calculation | 91 |
| A.2 | Parameters for Controller Gain Calculation | 98 |
| A.3 | The OneWind [®] Modelica Library | 103 |
| A.4 | Initial Bottom Contact Lengths of the Mooring Lines | 105 |
| A.5 | Mooring Line Length for the Upscaled System | 108 |
| A.6 | Adjustment of the Ballast Position | 109 |
| A.7 | Summary of the Designed Semi-Submersible Floating Wind Turbine Systems | 111 |

A.8 Successfully Submitted Paper 113

List of Figures

| | | |
|-----|--|-----|
| 1.1 | The most common design concepts of floating platforms | 2 |
| 2.1 | Design of the DeepCwind floating wind turbine | 5 |
| 3.1 | Stability conditions of a floating structure | 17 |
| 3.2 | Critical positions where the submerged geometry could change first | 18 |
| 3.3 | Coordinates of the centers of gravity and buoyancy in tilted position | 18 |
| 3.4 | Righting moment and wind heeling moment curves | 19 |
| 3.5 | Coordinate system of a floating semi-submersible wind turbine | 20 |
| 3.6 | Drag coefficient depending on the Reynolds number | 24 |
| 3.7 | Geometry and parameters of the catenary mooring line | 27 |
| 4.1 | Implementation of the semi-submersible platform in GeniE and HydroD | 32 |
| 4.2 | Pierson-Moscowitz wave spectra for different environmental conditions | 34 |
| 4.3 | Floating wind turbine system in Dymola, based on Modelica | 36 |
| 4.4 | Frequency-dependent added mass terms of the original OC4 system | 39 |
| 4.5 | Frequency-dependent damping terms of the original OC4 system | 39 |
| 4.6 | Moment curves of the original OC4 system | 40 |
| 4.7 | Free decay time series of the original OC4 system | 40 |
| 4.8 | Best-fit line of pitch sensitivity above rated wind speed for the NREL 5 MW | 41 |
| 5.1 | Frequency-dependent system matrices of the initially upscaled platforms | 46 |
| 5.2 | Moment curves of the initially upscaled platforms | 47 |
| 5.3 | Response amplitude operators | 49 |
| 5.4 | Response spectra for condition number 15 | 50 |
| 5.5 | Dynamic response of one initially upscaled platform | 51 |
| 7.1 | Moment curves of the optimized DeepCwind platform design | 60 |
| 7.2 | Free decay time series of the optimized DeepCwind platform design | 61 |
| 7.3 | Dynamic response of the optimized DeepCwind platform design | 62 |
| 7.4 | Response of the optimized DeepCwind platform design at different wind speeds | 63 |
| 7.5 | Mean and dynamic response of the optimized DeepCwind platform design | 63 |
| 8.1 | Moment curves of the upscaled platform for the IWT-7.5-164 | 71 |
| 8.2 | Free decay time series of the upscaled platform for the IWT-7.5-164 | 72 |
| 8.3 | Best-fit line of pitch sensitivity above rated wind speed for the IWT-7.5-164 | 73 |
| 8.4 | Dynamic response of the upscaled platform for the IWT-7.5-164 | 74 |
| 8.5 | Mean and dynamic response of the upscaled platform for the IWT-7.5-164 | 75 |
| 8.6 | Response of the upscaled platform for the IWT-7.5-164 at different wind speeds | 76 |
| 8.7 | Moment curves of the upscaled platforms for the DTU 10 MW | 80 |
| 8.8 | Dynamic response of the IWT-based upscaled platform for the DTU 10 MW | 81 |
| A.1 | Parameters of cylindrical geometries | 93 |
| A.2 | Six cases of the column position with respect to the water line | 93 |
| A.3 | Geometrical arrangement for the roll motion of the fairlead at column 3 | 106 |

List of Tables

| | | |
|------|--|-----|
| 1.1 | Typical natural periods and frequencies of semi-submersible floating platforms . . . | 2 |
| 2.1 | Main dimensions of the DeepCwind semi-submersible platform | 6 |
| 2.2 | Main dimensions of the DeepCwind semi-submersible mooring system | 7 |
| 2.3 | Main dimensions of the tower of the DeepCwind system | 7 |
| 2.4 | Main characteristics of the turbine of the DeepCwind system | 7 |
| 2.5 | Main dimensions of Fraunhofer's wind turbine IWT-7.5-164 | 8 |
| 2.6 | Main dimensions of the tower of the IWT-7.5-164 offshore adaption | 9 |
| 2.7 | Main dimensions of the DTU 10 MW reference wind turbine | 9 |
| 2.8 | Main dimensions of the tower of the DTU 10 MW reference wind turbine | 9 |
| 3.1 | Physical equations and scaling proportionalities for wind turbine parameters . . . | 12 |
| 3.2 | Actual scaling proportionalities for wind turbine parameters | 15 |
| 3.3 | Technology dependent scaling proportionalities for wind turbine masses | 15 |
| 3.4 | Representative sea states of OC4 | 25 |
| 4.1 | Wave parameters of 15 representative environmental conditions | 34 |
| 4.2 | Comparison of the drag coefficients of the original OC4 floating system | 38 |
| 4.3 | Comparison of the system matrices of the original OC4 floating system | 38 |
| 4.4 | Comparison of the natural periods of the original OC4 floating system | 41 |
| 4.5 | Sensitivity of aerodynamic power to blade-pitch for the NREL 5 MW | 42 |
| 5.1 | Main dimensions of the initially upscaled semi-submersible platforms | 44 |
| 5.2 | Main dimensions of the two ballast systems | 45 |
| 5.3 | Comparison of the system matrices of the initially upscaled platforms | 46 |
| 5.4 | Nominal pitch of the initially upscaled platforms | 47 |
| 5.5 | Comparison of the natural periods of the initially upscaled platforms | 48 |
| 5.6 | Dynamic response of the initially upscaled platforms | 50 |
| 6.1 | Steel (S355) yield stress depending on the wall thickness | 56 |
| 7.1 | Modified dimensions of the optimized DeepCwind platform design | 59 |
| 7.2 | Comparison of the system matrices of the optimized DeepCwind platform design | 60 |
| 7.3 | Comparison of the natural periods of the optimized DeepCwind platform design | 61 |
| 7.4 | Dynamic response of the optimized DeepCwind platform design | 62 |
| 7.5 | Equivalent stress calculation for the optimized DeepCwind platform design . . . | 64 |
| 8.1 | Main dimensions of the upscaled platform for the IWT-7.5-164 | 70 |
| 8.2 | Comparison of the system matrices of the upscaled platform for the IWT-7.5-164 | 71 |
| 8.3 | Comparison of the natural periods of the upscaled platform for the IWT-7.5-164 | 72 |
| 8.4 | Sensitivity of aerodynamic power to blade-pitch for the IWT-7.5-164 | 73 |
| 8.5 | Blade-pitch angles at different wind speeds for the IWT-7.5-164 | 74 |
| 8.6 | Dynamic response of the upscaled platform for the IWT-7.5-164 | 74 |
| 8.7 | Equivalent stress calculation for the upscaled platform for the IWT-7.5-164 . . . | 76 |
| 8.8 | Scaling factors for the floating platforms for the DTU 10 MW | 77 |
| 8.9 | Main dimensions of the upscaled platforms for the DTU 10 MW | 78 |
| 8.10 | Comparison of the system matrices of the upscaled platforms for the DTU 10 MW | 79 |
| 8.11 | Comparison of the natural periods of the upscaled platforms for the DTU 10 MW | 80 |
| 8.12 | Dynamic response of the upscaled platforms for the DTU 10 MW | 82 |
| 8.13 | Equivalent stress calculation for the upscaled platforms for the DTU 10 MW . . | 82 |
| A.1 | Summary of the main dimensions of the semi-submersible floater designs | 111 |
| A.2 | Summary of the main performances of the semi-submersible floater designs . . . | 112 |

List of Source Codes

| | | |
|-----|---|-----|
| A.1 | Reading in of airfoil data | 98 |
| A.2 | Input parameters for the BEM calculation | 98 |
| A.3 | Determination of the blade-pitch angles at wind speeds above rated | 100 |
| A.4 | Linearization analysis of the power for slightly varied blade-pitch angles | 102 |
| A.5 | Input parameters for the initial bottom contact length calculation | 105 |
| A.6 | Determination of $l_{\text{tot,hor}}$ and h for each mooring line at initial displacement | 106 |
| A.7 | Iterative computation of l_{eff} and τ_{hor} | 107 |
| A.8 | Determination of l_{tot} of the upscaled system for constant stiffness in surge | 108 |

List of Symbols

Latin Symbols

| | | |
|-----------------|---------------------------------------|--|
| A | $[kg, kgm, kgm^2]$ | Added mass matrix (6x6) with elements A_{11} to A_{66} |
| A | $[m^2]$ | Area |
| AOA | $[rad]$ or $[^\circ]$ | Angle of attack |
| a | $[-]$ | Axial induction factor |
| a' | $[-]$ | Tangential induction factor |
| B | $[kgs^{-1}, kgms^{-1}, kgm^2s^{-1}]$ | Damping matrix (6x6) with elements B_{11} to B_{66} |
| B | $[-]$ | Number of blades |
| C | $[kgs^{-2}, kgms^{-2}, kgm^2s^{-2}]$ | Stiffness matrix (6x6) with elements C_{11} to C_{66} |
| C_* | $[-]$ | Dimensionless coefficient of parameter * |
| c | $[m]$ | Chord length |
| D | $[m]$ | Diameter |
| d | $[m]$ | Distance or thickness |
| E | $[Nm^{-2}]$ | Young's modulus |
| \underline{F} | $[N, Nm]$ | Excitation force vector (6x1) with elements F_1 to F_6 |
| F | $[N]$ | Force |
| f | $[Hz]$ | Frequency |
| GK | $[-]$ | Gain-correction factor |
| g | $[ms^{-2}]$ | Acceleration due to gravity |
| H | $[m]$ | Wave height |
| h | $[m]$ | Height |
| $I_{*/**}$ | $[m^4] / [kgm^2]$ | Area/mass moment of inertia (one/two subscripts) |
| K_D | $[s^2]$ | Derivative controller gain |
| K_I | $[-]$ | Integral controller gain |
| K_P | $[s]$ | Proportional controller gain |
| k | $[-]$ | Scaling factor |
| l | $[m]$ | Length |
| M | $[kg, kgm, kgm^2]$ | Mass matrix (6x6) with elements M_{11} to M_{66} |
| M | $[Nm]$ | Moment |
| m | $[kg]$ | Mass |
| N_{gear} | $[-]$ | Gearbox ratio |
| P | $[W]$ | Power |
| p | $[Pa]$ | Pressure |
| \underline{q} | $[m, rad]$ or $[m, ^\circ]$ | Vector of system DoFs (6x1) with elements q_1 to q_6 |
| R | $[m]$ | Radius |
| Re | $[-]$ | Reynolds number |
| r | $[m]$ | Local radial position |
| S | $[m^2Hz^{-1}]$ or $[^\circ^2Hz^{-1}]$ | Spectral density |
| s | $[-]$ | Coordinate and direction along the mooring line |
| T | $[s]$ | Period |
| t | $[s]$ | Time |
| V | $[m^3]$ | Volume |
| v | $[ms^{-1}]$ | Velocity |
| W | $[N]$ | Weight |
| x | $[-]$ | Coordinate and direction of surge |
| y | $[-]$ | Coordinate and direction of sway |
| z | $[-]$ | Coordinate and direction of heave |

Greek Symbols

| | | |
|------------|-----------------------|--|
| α | $[-]$ | Wind shear exponent |
| β | $[rad]$ or $[^\circ]$ | Angle between local and global reference axes |
| Γ | $[-]$ | Glauert correction factor |
| γ | $[-]$ | Load factor |
| ϵ | $[m]$ | Length value for avoiding division by zero in Modelica |
| ζ | $[-]$ | Damping factor |
| η | $[-]$ | Generator efficiency |
| θ | $[rad]$ or $[^\circ]$ | Pitch angle |
| κ | $[m^{-1}]$ | Wave number |
| Λ | $[-]$ | Eigenvalue |
| λ | $[-]$ | Tip speed ratio |
| μ | $[kgm^{-1}]$ | Mass per length |
| ν | $[m^2s^{-1}]$ | Kinematic viscosity |
| ξ | $[rad]$ or $[^\circ]$ | Blade twist angle |
| Π | $[-]$ | Prandtl's tip loss correction factor |
| ρ | $[kgm^{-3}]$ | Density |
| Σ | $[-]$ | Solidity |
| σ | $[m]$ or $[^\circ]$ | Standard deviation |
| σ | $[Nm^{-2}]$ | Stress |
| τ | $[N]$ | Tension |
| τ^* | $[m]$ | Normalized mooring line pretension |
| φ | $[rad]$ or $[^\circ]$ | Roll angle |
| χ | $[rad]$ or $[^\circ]$ | Flow angle |
| ψ | $[rad]$ or $[^\circ]$ | Angle between mooring line and x -axis |
| Ω | $[rad s^{-1}]$ | Angular velocity |
| ω | $[rad s^{-1}]$ | Angular frequency |

Subscripts

| | |
|------------|--|
| 0 | Undisturbed |
| 1 | First DoF (surge) |
| 2 | Second DoF (sway) |
| 3 | Third DoF (heave) |
| 4 | Fourth DoF (roll) |
| 5 | Fifth DoF (pitch) |
| 6 | Sixth DoF (yaw) |
| a | Added mass |
| aimed | Aimed value |
| air | Parameter of the air |
| ax | Axial component |
| B | Buoyant |
| b | Bottom end |
| ballast | Parameter of the ballast |
| C | Centrifugal |
| c | Parameter of the controller |
| char | Characteristic value |
| crit | Critical value |
| cylinder | Parameter of the circular cylinder |
| cyl. hoof | Parameter of the cylindrical hoof |
| D | Drag |
| d | Damped/Damping |
| draft | Parameter at the draft of the platform |
| drivetrain | Parameter of the drivetrain |
| E | Environmental load |
| eff | Effective value |
| equ | Equivalent parameter |
| G | Gravitational/permanent load |
| gen | Parameter of the wind turbine generator |
| HSS | High speed shaft |
| hor | Horizontal projection/component |
| hub | At the hub |
| i | Running index |
| initial | Parameter of the initial design |
| K | Value at doubled blade-pitch sensitivity |
| L | Lift |
| LSS | Low speed shaft |
| lp | Load point under consideration |
| M | Torque moment |
| mat | Parameter of the material |
| max | Maximum value |
| min | Minimum value |
| moor | Parameter of the mooring system |
| n | Normal component |
| nat | Natural |
| orig | Parameter of the original design |
| P | Power |
| PM | Pierson-Moscowitz |
| p | Peak value |
| Q | Variable load |

| | |
|----------|--|
| R | Reference value |
| r | Radial component |
| rated | Rated value |
| rest | Resting component |
| rotor | Parameter of the wind turbine rotor |
| s | Significant value |
| seabed | At the seabed |
| steel | Parameter of steel |
| system | Entire floating wind turbine system |
| T | Thrust |
| t | Tangential component |
| tank | Parameter of the tank/filled column |
| tip | Parameter at blade tip |
| tot | Total value |
| tower | Parameter of the tower |
| upscaled | Parameter of the upscaled design |
| vert | Vertical projection/component |
| WP | Waterplane |
| WT | Wind turbine |
| water | Parameter of/in the water |
| wind | Parameter of the wind |
| x | In x -direction/around the x -axis |
| y | In y -direction/around the y -axis |
| yield | Yield value |
| z | In z -direction/around the z -axis |

Abbreviations

| | |
|---------|---|
| B | Center of buoyancy |
| BC | Base column |
| BEM | Blade element momentum |
| CB | Cross brace |
| DL | Lower delta pontoon |
| DoF | Degree of freedom |
| DU | Upper delta pontoon |
| FEM | Finite element method |
| FFT | Fast Fourier transform |
| G | Center of gravity |
| GM | Metacentric height |
| GZ | Righting lever |
| JONSWAP | Joint North Sea Wave Project |
| M | Metacenter |
| MC | Main column |
| OC | Offset column |
| OC4 | Offshore Code Comparison Collaboration, Continuation |
| OC5 | Offshore Code Comparison Collaboration Continuation, with Correlation |
| O&M | Operations and maintenance |
| RAO | Response amplitude operator |
| RNA | Rotor nacelle assembly |
| SWL | Still water level |
| TLP | Tension leg platform |
| UC | Upper column |
| ULS | Ultimate Limit State |
| YL | Lower Y pontoon |
| YU | Upper Y pontoon |

1 Introduction

Wind energy is an important source of emission-free and self-sufficient energy production. With the free of cost energy source and the good complementarity with both solar energy for compensating the wind fluctuations, and hydro power for energy storage, wind energy is a competitive component on the energy market. [25]

1.1 Onshore Versus Offshore

Despite the positive aspects of renewable and emission-free power production, wind energy also has some disadvantages.

Onshore wind turbines are often subjectively perceived to be unsightly in the landscape. Navigation lights on wind turbines, or the so called “disco-effect” due to rotating blade shadows and reflections, strengthen the argument of visual pollution more objectively. Also noise during transport, erection and production affects neighboring areas. Furthermore, the maximum power production is limited onshore, as the available wind is slowed down due to the roughness of the territory, there is only a limited number of available sites where it is efficient and possible to place wind turbines, wind turbine sizes are restricted due to overland transportation constraints and local legislations, and maximum rotational speed and sometimes also the operational time are prescribed, based on noise limits and tolerated hours of shadow flickering [15].

The impacts and limitations, that come with onshore wind energy, make offshore wind more attractive. Still, the use of offshore wind power is sometimes economically controversial because of higher installation and O&M costs, limited time windows for installation and transport, more difficult accessibility, higher loads on the structure due to waves, current and increased wake effects, arising foundation issues like scour processes, and electrical energy transport to the shore. On the other hand, more potential areas are available offshore, turbines more than 10 *km* from the shore no longer cause any visual impact, transportation of large wind turbines is easier by sea, and many densely populated coastal regions have huge energy consumption but little opportunities for locating onshore wind turbines [25]. In addition, the power generation per wind turbine is higher offshore, as the small roughness length over open sea leads to higher wind speeds with less turbulence at already smaller heights, bigger wind turbines can be installed due to feasible transportation and absent size restrictions, and capacity factors of around 40 – 50% can be achieved [14] because of higher and more consistent wind resource potential, as well as less restricted operational time due to noise or visual impact limits.

1.2 Floating Wind Turbines

Many promising sites are at deeper water depths (> 50 *m*), where bottom-fixed foundations no longer could be used [43]. This brings floating structures more into the focus of interest. In addition to the advantages of reduced noise during erection, no required scour protection and cheap anchor installation for the mooring system, challenges like dynamic interaction between floating structure and wind turbine, or wave excitation frequencies have to be faced.

The most common types of floating platforms under study for offshore wind turbines are spars, tension leg platforms (TLP) and semi-submersibles, shown in Figure 1.1. Design concepts for multiple-units or innovative approaches, like for vertical axis wind turbines, also exist. [61]

Semi-submersibles, or also called column-stabilized platforms, consist mostly of three or four cylindrical columns, which are interconnected by pontoons and/or braces, and make up a floatable structure [35]. The big distance between the columns and the large waterplane area provide stability, as well as restoring forces and moments [2]. Heave plates, attached to the bottom of

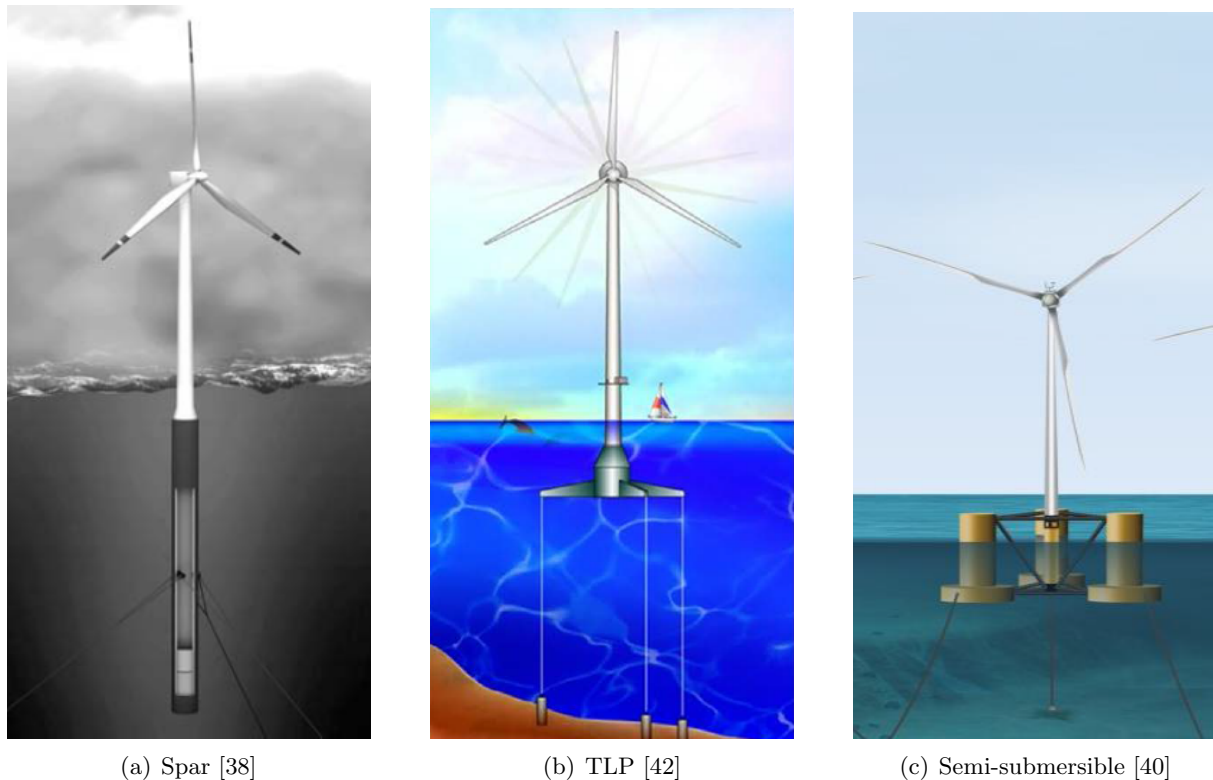


Figure 1.1: The most common design concepts of floating platforms

the columns, increase added mass, damping and drag [2]. This way, natural periods outside the range of wave excitation can be achieved, as given in Table 1.1, which leads to reduced platform motions and thus less downtime of the wind turbine [35].

Table 1.1: Typical natural periods and frequencies of semi-submersible floating platforms, based on [61]

| Translational motion | Unit | Surge | Sway | Heave |
|----------------------|------|------------|------------|-------------------|
| Natural period | s | > 40 | > 40 | $17 - 40$ |
| Natural frequency | Hz | < 0.0250 | < 0.0250 | $0.0250 - 0.0588$ |

| Rotational motion | Unit | Roll | Pitch | Yaw |
|-------------------|------|-------------------|-------------------|------------|
| Natural period | s | $25 - 50$ | $25 - 50$ | > 3 |
| Natural frequency | Hz | $0.0200 - 0.0400$ | $0.0200 - 0.0400$ | < 0.3333 |

The low draft of semi-submersible floaters gives the opportunity to assemble the platform onshore and then tow it as a complete structure to the location offshore. Thereby, the installation time and effort can be reduced, which is a very important advantage for offshore wind turbines. [35]

1.3 Upscaling

From an economical point of view, installation of bigger wind turbines is preferred, but only offshore more feasible. So, existing wind turbines are normally scaled up to larger sizes based on the power rating. Recent technology developments and new designs, however, make this simple upscaling insufficient. Furthermore, the support structure carrying the upscaled wind turbine

has to be adjusted, so that floatation and stability are maintained. But floating platforms come with coupled dynamic motions, wave interaction, low frequency response, and additional components like mooring system. Those are all further aspects why simple upscaling, based on the turbine rating, cannot be applied in the case of floating offshore wind turbine systems.

1.4 Content

This master's thesis examines the criteria that have to be fulfilled during upscaling of a semi-submersible platform carrying a predefined wind turbine, and gives a guideline for the optimization and upscaling procedure.

In Chapter 1, an introduction to wind energy, with the focus on offshore floating wind turbines, is given, and the problem of upscaling is presented, which is the motivation for this thesis work.

Chapter 2 introduces the reference structures used for this study. Those are the DeepCwind semi-submersible floating platform, which deals as basic floater design for the optimization and upscaling procedure, Fraunhofer's IWT-7.5-164 reference wind turbine, and the DTU 10 MW reference wind turbine, for which both a semi-submersible platform is to be designed.

Chapter 3 provides the theoretical background. This includes upscaling (Section 3.1), principles of floatation and stability (Section 3.2), determination of the natural frequencies of a floating structure (Section 3.3), viscous forces and damping (Section 3.4), station-keeping systems (Section 3.5), as well as control systems for floating wind turbines (Section 3.6).

In Chapter 4, the three different methods, based on which the designed floating systems will be analyzed, are presented and verified.

In Chapter 5, an initial semi-submersible platform design is obtained for the IWT-7.5-164, based on an elementary upscaling procedure, and analyzed with respect to its static and dynamic performance.¹

The main criteria for optimization and upscaling of a semi-submersible floating platform are defined, based on the results of this initial upscaling, and presented in Chapter 6.

Using those factors, the original DeepCwind semi-submersible platform is optimized and analyzed in Chapter 7.

This optimized floater design is used in Chapter 8 as basis for upscaling to larger wind turbines. In Section 8.1 a guideline for the upscaling procedure is presented. This is applied in Sections 8.2 and 8.3, and semi-submersible floating platforms for the IWT-7.5-164 and DTU 10 MW reference wind turbines are designed, analyzed and compared. For the DTU wind turbine two floaters are designed, one based on the optimized DeepCwind platform, and the other one using the floater for the IWT-7.5-164 as basis for the upscaling procedure.

Finally, Chapter 9 recapitulates the developed rational and optimized upscaling procedure, summarizes the obtained semi-submersible floating wind turbine systems, and gives recommendations for future work on upscaling of a semi-submersible floating platform.

¹This chapter mainly covers the work performed in the preceding research project, corresponding to the specialization project TMR4590 at NTNU, and thus does not count to the final master's thesis TMR 5950. At TU Delft, however, the preceding research project counts to the final thesis work.

2 Reference Structures

The upscaling procedure shall be carried out on the basis of the DeepCwind semi-submersible floater, which is originally designed for the NREL 5 MW wind turbine. The target scale, however, is Fraunhofer's 7.5 MW offshore wind turbine. The generality of the upscaling procedure is proved in a final step, by designing a semi-submersible platform for the DTU 10 MW.

In the following, all three reference structures are introduced.

2.1 DeepCwind Semi-Submersible

Within the framework of the OC4 (Offshore Code Comparison Collaboration, Continuation) project, hydrodynamic calculations and code-to-code comparisons were performed for the NREL 5 MW wind turbine on top of the DeepCwind semi-submersible platform [41]. Later on, in OC5 (Offshore Code Comparison Collaboration Continuation, with Correlation), the floating system was retested at MARIN at a 1:50 model scale [40].

The DeepCwind semi-submersible platform, designed for a water depth of 200 m, consists of three offset columns (OC) and one smaller central main column (MC). The latter one carries the NREL 5 MW wind turbine. The offset columns are each subdivided into an upper column (UC) and a base column (BC) of larger diameter, representing a heave plate and thus serving as motion suppression device. The offset columns are placed on the edges of an equilateral triangle

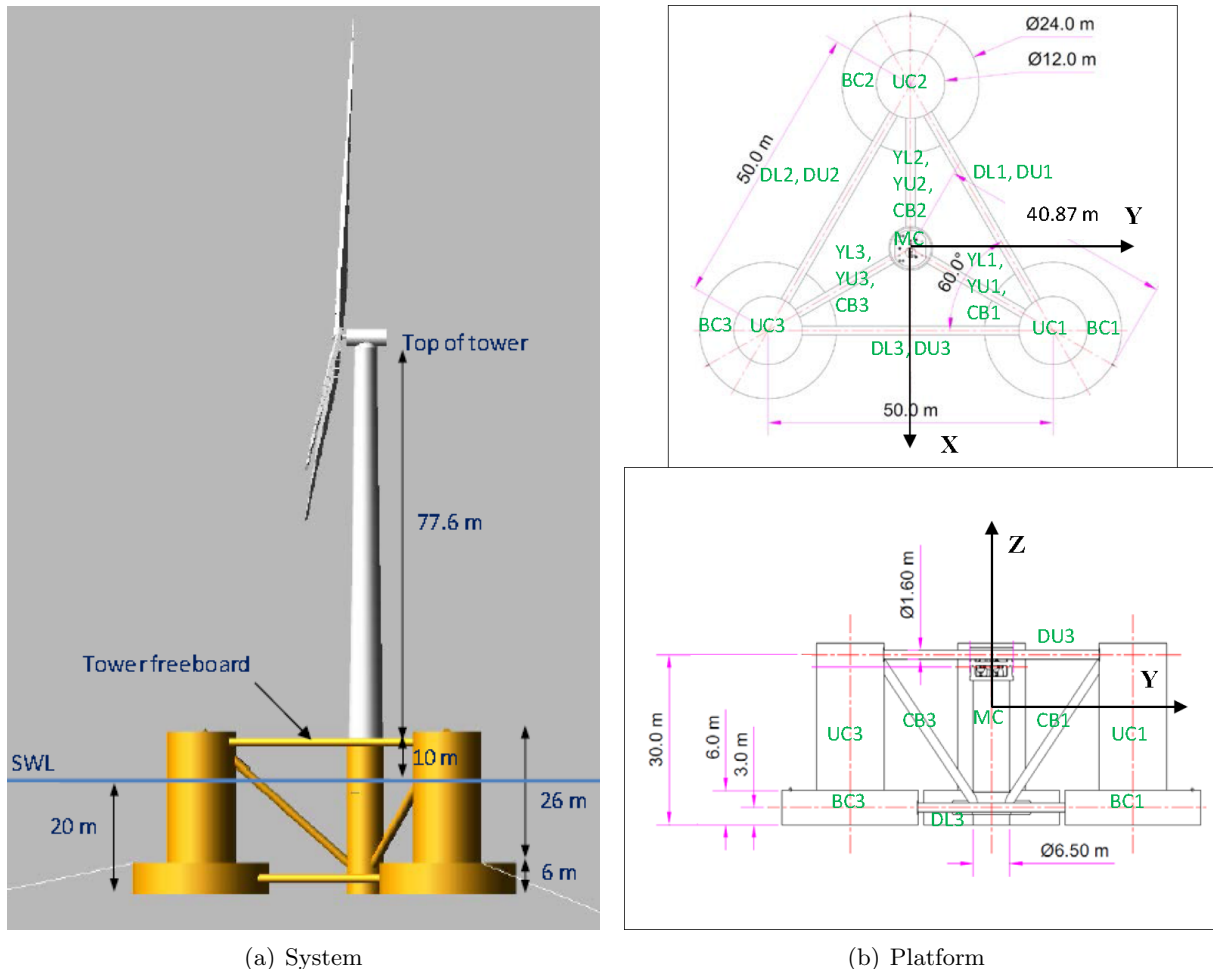


Figure 2.1: Design of the DeepCwind floating wind turbine [41]

of side length 50.0 *m*, having the main column at its centroid. Offset columns and main column are interconnected by twelve pontoons and three cross braces. The cross braces (CB) connect the bottom of the main column to the top of each upper column. The pontoons are subdivided into delta and Y pontoons. The upper (DU) and lower (DL) delta pontoons interconnect the offset columns at the top and bottom, respectively, in form of a triangle. The upper (YU) and lower (YL) Y pontoons, however, build up a Y-connection between the main column and the top, respectively bottom, of the offset columns. The design of the DeepCwind semi-submersible floating wind turbine and the arrangement of columns and braces are presented in Figure 2.1. The platform itself is made out of steel. In order to balance weight and buoyancy, the offset columns are ballasted with water. As a result, the natural frequencies of the floating system are below the wave frequency range. The final main dimensions are given in Table 2.1. [41]

Table 2.1: Main dimensions of the DeepCwind semi-submersible platform [41, 42]

| Element | Diameter [<i>m</i>] | Wall thickness [<i>m</i>] | Length [<i>m</i>] | Drag coefficient |
|---------|-----------------------|-----------------------------|---------------------|--------------------------|
| MC | 6.5 | 0.03 | 30 | 0.56 |
| UC | 12 | 0.06 | 26 | 0.61 |
| BC | 24 | 0.06 | 6 | 0.68 ($C_{D,z} = 4.8$) |
| DU | 1.6 | 0.0175 | 38 | 0.63 |
| DL | 1.6 | 0.0175 | 26 | 0.63 |
| YU | 1.6 | 0.0175 | 19.62 | 0.63 |
| YL | 1.6 | 0.0175 | 13.62 | 0.63 |
| CB | 1.6 | 0.0175 | 32.04 | 0.63 |

| | |
|--|-----------------|
| Elevation of OC above SWL | 12 <i>m</i> |
| Elevation of MC (tower base) above SWL | 10 <i>m</i> |
| Elevation of upper pontoons above SWL | 10 <i>m</i> |
| Elevation of upper end of CBs above SWL | 9.13 <i>m</i> |
| Spacing between OCs | 50 <i>m</i> |
| Depth to lower end of CBs below SWL | 16.2 <i>m</i> |
| Depth to lower pontoons below SWL | 17 <i>m</i> |
| Depth of platform base below SWL (total draft) | 20 <i>m</i> |
| Ballast height in UCs | 7.83 <i>m</i> |
| Ballast height in BCs | 5.0478 <i>m</i> |

| | |
|-----------------------------|---------------------|
| Density of metal (steel) | 7,850 kgm^{-3} |
| Total metal mass | 3.8522E+6 <i>kg</i> |
| Density of ballast (water) | 1,025 kgm^{-3} |
| Total ballast mass | 9.6208E+6 <i>kg</i> |
| Total platform mass | 1.3473E+7 <i>kg</i> |
| Center of gravity below SWL | 13.46 <i>m</i> |

The floating platform is moored with three catenary lines, which are at an angle of 120° to each other. The fairleads are at the top of each base column and the anchors are at the sea bottom 200 *m* below SWL. The station-keeping system properties are presented in Table 2.2. [41]

Table 2.2: Main dimensions of the DeepCwind semi-submersible mooring system [41]

| | |
|---|---|
| Depth to fairleads below SWL | 14 <i>m</i> |
| Depth to anchors below SWL | 200 <i>m</i> |
| Radius to fairleads from platform centerline | 40.868 <i>m</i> |
| Radius to anchors from platform centerline | 837.6 <i>m</i> |
| Unstretched mooring line length | 835.5 <i>m</i> |
| Mooring line diameter | 0.0766 <i>m</i> |
| Equivalent mooring line mass density, mass in water | 113.35 <i>kgm</i> ⁻¹ , 108.63 <i>kgm</i> ⁻¹ |
| Equivalent mooring line extensional stiffness | 7.536E+8 <i>N</i> |
| Gravity force in undisplaced position | -1.839E+6 <i>N</i> |

The wind turbine on top of the DeepCwind semi-submersible platform is mainly based on the NREL 5 *MW* [31]. Only the tower dimensions are adjusted such that the hub height of 90 *m* remains the same. The main properties of tower and turbine are given in Tables 2.3 and 2.4.

Table 2.3: Main dimensions of the tower of the DeepCwind system [31,41]

| | |
|---|--------------------------------|
| Elevation of tower top above SWL | 87.6 <i>m</i> |
| Elevation of tower base above SWL | 10 <i>m</i> |
| Overall tower length | 77.6 <i>m</i> |
| Tower top diameter and thickness | 3.87 <i>m</i> , 0.019 <i>m</i> |
| Tower base diameter and thickness | 6.5 <i>m</i> , 0.027 <i>m</i> |
| Tower steel density | 8,500 <i>kgm</i> ⁻³ |
| Overall (integrated) tower mass | 249,718 <i>kg</i> |
| Center of gravity above SWL on tower centerline | 43.4 <i>m</i> |

Table 2.4: Main characteristics of the turbine of the DeepCwind system [31]

| | |
|--------------------------------------|---|
| Rated power | 5 <i>MW</i> |
| Cut-in, rated and cut-out wind speed | 3 <i>ms</i> ⁻¹ , 11.4 <i>ms</i> ⁻¹ , 25 <i>ms</i> ⁻¹ |
| Cut-in and rated rotor speed | 6.9 <i>rpm</i> , 12.1 <i>rpm</i> |
| Rated tip speed | 80 <i>ms</i> ⁻¹ |
| Overhang, shaft tilt and precone | 5 <i>m</i> , 5°, 2.5° |
| Hub height above SWL | 90 <i>m</i> |
| Hub diameter | 3 <i>m</i> |
| Rotor diameter | 126 <i>m</i> |
| Number of blades | 3 |
| Rotor mass | 1.100E+5 <i>kg</i> |
| Nacelle mass | 2.400E+5 <i>kg</i> |

The high-speed drive and multiple-stage gearbox are directly taken from the NREL 5 *MW* [31]. However, the variable-speed, blade-pitch-to-feather controller, originally for onshore purpose, has to be adjusted. In order to avoid negative damping, the pitch controller gains are reduced and the generator control system is modified from constant power to constant torque. [41]

The entire floating system - wind turbine, platform and lifted parts of the mooring lines together - weighs $1.426\text{E} + 7 \text{ kg}$. The natural frequencies are 0.009 Hz in surge, 0.058 Hz in heave and 0.037 Hz in pitch. [41,42]

2.2 IWES IWT-7.5-164

The 7.5 MW wind turbine was designed by Fraunhofer IWES within the “Smart Blades” project [59], for the purpose of having a state-of-the-art onshore reference turbine. This was then modified to an offshore-adapted wind turbine within the joint project “TANDEM” [8]. The concept is in general based on the IEC61400-1 standard and assumes worst case conditions by utilizing wind class IEC 1A. A direct drive mechanism, meaning a generator without gearbox, is used. The main technical properties of the IWT-7.5-164 wind turbine are given in Table 2.5. [46]

Table 2.5: Main dimensions of Fraunhofer’s wind turbine IWT-7.5-164 [46]

| | |
|--|---|
| Rated power | 7.5 MW |
| Cut-in, rated and cut-out wind speed | 3 ms^{-1} , $\approx 11 \text{ ms}^{-1}$, 25 ms^{-1} |
| Cut-in and rated rotor speed | 5 rpm, 10 rpm |
| Rated tip speed | 85.9 ms^{-1} |
| Design tip speed ratio | 8.4 |
| Overhang, shaft tilt and precone | 6.13 m, 5° , 2° |
| Hub height (without offshore-adaption) | 111.6 m (120 m) |
| Hub diameter | 4 m |
| Rotor diameter | 164 m |
| Number of blades | 3 |
| Rotor mass | 158,053 kg |
| Nacelle mass | 335,311 kg |

An optimized design of the rotor blades is the main focus of the “Smart Blades” project. Three Fraunhofer airfoils and four airfoils developed by TU Delft are used for the rotor blades. Between the different airfoils, blade parameters, like relative thickness, chord length and twist angle, are numerically interpolated. The blades are pre-bent in flapwise direction, in order to increase the tower clearance. The blade-pitch system allows individual pitching. Each pitch drive is equipped with a backup system and a passive break system. Furthermore, an individual pitch control aims the minimization of the loads on the blades. The turbine control itself is based on a combined torque pitch controller for variable speed wind turbines. An additional peak shaver, which activates the blade-pitch control already shortly before rated wind speed, ensures a smoother transition to rated power, and reduces high thrust and fatigue loads. [46]

Within the “TANDEM” project, the tower design was modified, and a monopile and transition piece were added as offshore support structure. With changing the original hybrid tower to a pure steel tower and shortening the overall tower length, the tower mass could be reduced by a factor of four and the hub height was decreased from 120 m (onshore) to 111.6 m (offshore). The basic parameters for the tower are presented in Table 2.6. For a water depth of 30 m, a monopile of 27.6 m length and 8 m diameter is designed. A 24 m long transition piece connects monopile and tower. The Young’s modulus of the support structure ($E = 1.92\text{E} + 11 \text{ Nm}^{-2}$) differs slightly from the material parameter of the tower ($E = 2.10\text{E} + 11 \text{ Nm}^{-2}$). This way, a system first mode frequency of 0.234 Hz , lying between 1P and 3P, is obtained. [7]

Table 2.6: Main dimensions of the tower of the IWT-7.5-164 offshore adaption [7]

| | |
|-----------------------------------|-----------------------------|
| Elevation of tower top above SWL | 107.6 <i>m</i> |
| Elevation of tower base above SWL | 21.6 <i>m</i> |
| Overall tower length | 86 <i>m</i> |
| Tower top diameter and thickness | 3 <i>m</i> , 0.025 <i>m</i> |
| Tower base diameter and thickness | 7 <i>m</i> , 0.035 <i>m</i> |
| Tower steel density | 7,850 kgm^{-3} |
| Overall (integrated) tower mass | 362,750 <i>kg</i> |

2.3 DTU 10 MW Reference Wind Turbine

The DTU 10 MW wind turbine was designed as reference wind turbine for the “Light Rotor” project and used in the “European InnWind” project [5]. The main properties of the DTU 10 MW wind turbine are given in Table 2.7.

Table 2.7: Main dimensions of the DTU 10 MW reference wind turbine [4]

| | |
|--------------------------------------|---|
| Rated power | 10 MW |
| Cut-in, rated and cut-out wind speed | 4 ms^{-1} , 11.4 ms^{-1} , 25 ms^{-1} |
| Cut-in and rated rotor speed | 6 rpm, 9.6 rpm |
| Rated tip speed | 90 ms^{-1} |
| Design tip speed ratio | 7.5 |
| Overhang, shaft tilt and precone | 7.07 <i>m</i> , 5°, 2.5° |
| Hub height | 119 <i>m</i> |
| Hub diameter | 5.6 <i>m</i> |
| Rotor diameter | 178.3 <i>m</i> |
| Number of blades | 3 |
| Rotor mass | 230,667 <i>kg</i> |
| Nacelle mass | 446,036 <i>kg</i> |

A detailed design of a light rotor with good aerodynamic behavior was the main objective. The final blades are 3 *m* pre-bent. The rotor control was adjusted, in order to account for instabilities due to coinciding frequencies. Furthermore, individual pitch is used for avoiding vibrations in stand still. The overall variable-speed, collective-pitch control system is based on the DTU wind energy controller [23]. A medium speed drivetrain with multiple stage gearbox is used. [5]

The tower is designed from scratch. An effective material density higher than steel accounts for secondary structures. The basic tower parameters are presented in Table 2.8. [4]

Table 2.8: Main dimensions of the tower of the DTU 10 MW reference wind turbine [4]

| | |
|-------------------------------------|-------------------------------|
| Elevation of tower top above ground | 118.38 <i>m</i> |
| Tower top diameter and thickness | 5.5 <i>m</i> , 0.020 <i>m</i> |
| Tower base diameter and thickness | 8.3 <i>m</i> , 0.038 <i>m</i> |
| Tower effective density | 8,500 kgm^{-3} |
| Overall (integrated) tower mass | 628,442 <i>kg</i> |

3 Theory

3.1 Upscaling Procedure for Wind Turbines

Wind energy would become more attractive, if the cost of electricity production from wind turbines is decreased. Bigger turbines can produce more power per plant, and thus fewer wind turbines are needed for generating the same amount of electricity. This leads to reduced maintenance effort and lower costs for installation and operation. [26]

In the following, the scaling laws for the upscaling procedure from existing smaller wind turbines to bigger ones are explained, first based on structural and physical relations, and then based on comparisons of existing wind turbines.

3.1.1 Theoretical Upscaling Based on Geometric Self-Similarity

3.1.1.1 Assumptions and Basics A bigger wind turbine with equal optimal performance is the main goal of upscaling. The dimensionless power, thrust and torque moment coefficients C_P , C_T and C_M , defining the wind turbine performance, thus have to follow the same curves for both initial and upscaled wind turbines [19]. This implies identical flow dynamics around the blade profiles, and similar aerodynamic behavior of the wind turbines. Neglecting Reynolds effects, this can be obtained by maintaining the tip speed ratio λ [13]. Based on this requirement, all dimensions of the wind turbine should then be scaled, so that also geometric self-similarity is fulfilled. Furthermore, the same wind turbine concept, with equal number of blades and similar blade profiles, should theoretically be used for the upscaled design. In order to obtain the same lift and drag coefficients C_L and C_D , the same materials should be used for the blades [19].

However, the coefficients also depend on the Reynolds number Re , which is not considered in the scaling laws based on geometric self-similarity. The results are still comparable, if the Reynolds number is not smaller than the critical value of $Re_{crit} = 200,000$ [19]. Further assumptions in the theoretical upscaling procedure are a linear behavior of the structure, only stationary loads being considered, and negligible second-order aerodynamic effects [47].

In the end of this section, in Paragraph 3.1.1.3, the limits of this upscaling procedure are described in more detail.

3.1.1.2 Scaling Laws The scaling factor k , used in the scaling laws, is normally determined by means of the power rating of new and initial wind turbine designs, as the power is usually the predefined value of the desired upscaled turbine. But for an easier handling, the power rating is expressed in terms of a ratio of lengths, so that the scaling factor follows Equation 1.

$$k = \frac{l_{\text{upscaled}}}{l_{\text{initial}}} \quad (1)$$

This way, the entire geometry is scaled by a factor of k . Other physical parameters, like forces, stresses, or frequencies, have to be written as a function of a length, mostly the rotor diameter D_{rotor} , so that the scaling proportionalities can be determined based on the physical equations.

The requirement of a constant tip speed ratio for aerodynamic similarity, and thus Equation 2, can be used to obtain the scaling proportionalities for frequency values.

$$\lambda = \frac{\Omega R_{\text{rotor}}}{v_0} \quad (2)$$

As presented later on in Table 3.1, it can be found that frequency ratios remain unchanged during upscaling, based on structural scaling laws. This means that a wind turbine, which was

designed to operate in a frequency range outside resonance, will still operate free of resonance when it is scaled up based on geometric and aerodynamic self-similarity [19].

The scaling proportionalities for several parameters, relevant for wind turbines, are presented in Table 3.1. For a better understanding of the derivation of the scaling proportionalities, the physical equations of the considered parameters are included.

Table 3.1: Physical equations and scaling proportionalities for several parameters relevant to wind turbines, based on [19]

| Parameter | Equation | Proportionality |
|------------------------------------|---|-----------------|
| Mass | $m = \rho_{\text{mat}}V$ with $V \sim k^3$ | k^3 |
| Weight | $W = mg$ | k^3 |
| Area moment of inertia | $I_y = \int_A x^2 dA$ | k^4 |
| Young's modulus | E constant for same material | k^0 |
| Bending stiffness | EI | k^4 |
| Rotational speed | $\Omega = \frac{2\lambda v_0}{D_{\text{rotor}}}$ | k^{-1} |
| Natural frequencies | $f_{\text{nat}} = \frac{4\Lambda^2}{D_{\text{rotor}}^2} \sqrt{\frac{EI}{\mu}}$ | k^{-1} |
| Frequency ratio | $\frac{\Omega}{f_{\text{nat}}}$ | k^0 |
| Power | $P = \frac{\rho_{\text{air}}}{2} C_P(\lambda) \frac{D_{\text{rotor}}^2}{4} \pi v^3$ | k^2 |
| Aerodynamic forces (e.g. thrust) | $F_T = \frac{\rho_{\text{air}}}{2} C_T(\lambda) \frac{D_{\text{rotor}}^2}{4} \pi v^2$ | k^2 |
| Aerodynamic moments (e.g. torque) | $M = \frac{\rho_{\text{air}}}{2} C_M(\lambda) \frac{D_{\text{rotor}}^3}{8} \pi v^2$ | k^3 |
| Stresses due to aerodynamic loads | $\sigma = \frac{Ml}{I}$ | k^0 |
| Centrifugal forces | $F_C = ml\Omega^2$ | k^2 |
| Stresses due to centrifugal forces | $\sigma_C = \frac{F_C}{A}$ with $A \sim k^2$ | k^0 |
| Bending moment due to self-weight | $M_G = Wl$ | k^4 |
| Stresses due to self-weight | $\sigma_G = \frac{M_G l}{I}$ | k |

From Table 3.1 it can be determined that the aeroelastic stability of the rotor is maintained during upscaling, as both centrifugal forces and aerodynamic loads scale with k^2 and the corresponding moments with k^3 , but angular displacements are scale invariant [29].

3.1.1.3 Limits of Standard Upscaling Procedure Increasing the power by a factor of the length scale squared yields a mass increase by a factor of the length scale cubed, as given in Table 3.1. This implies higher loads due to self-weight, brings structural disadvantages, and also sets a limit to the highest possible scaling value. Stresses due to self-weight scale linearly with the scaling factor, while stresses due to aerodynamic or centrifugal forces remain unchanged. But since all stresses contribute to the total stress, this linear dependency on the scaling factor

in the part due to self-weight could cause that the design stress limit is exceeded and buckling or failure could occur. [47]

This maximum possible scaling factor could be extended, if the bending yield strength is higher but the material density smaller. This can be obtained by using glass- or carbon-fiber reinforced plastics instead of aluminum, as they are stronger but at the same time lighter and scale just with a factor of approximately the scaling factor to the power of 2.2 instead of 3. Lighter but sufficiently strong designs for bigger wind turbines are feasible with lighter materials. [19]

However, also the effect of self-weight on the blade tip deflection has to be taken into account. Just considering scaling of turbine dimensions and bending moments due to aerodynamic loads, the tower clearance would be maintained. Including dynamic motions of the blades due to self-weight, bending moments could conflict with the desired tower clearance. [29]

The theoretical upscaling procedure does not account for Reynolds effects, as already mentioned in Paragraph 3.1.1.1. The Reynolds number Re gives the ratio of inertia forces to viscous forces, and depends linearly on a characteristic length value, as shown in Equation 3.

$$Re = \frac{v l_{\text{char}}}{\nu} \quad (3)$$

Good performing wind turbine blades are designed, so that they have a turbulent boundary layer on the blades during operation. A turbulent condition occurs for Reynolds numbers above the critical value of $Re_{\text{crit}} = 2 \cdot 10^5$. The Reynolds number would increase during upscaling, following Equation 3, and thus the lift and drag coefficients would remain the same. This means that Reynolds effects would only influence the flow condition, if the Reynolds number becomes smaller than the critical value. This will only be the case when downsizing, for example in order to make small wind turbine models for wind tunnel tests. [19]

Wind shear is also not included in the scaling laws. The wind velocity follows a logarithmic profile and increases with the altitude as $v \sim h^\alpha$, with the wind shear exponent α . The hub height scales linearly with the scaling factor k . With the power proportional to the wind speed cubed and the diameter squared, the power scales with $k^{2+3\alpha}$. The bending moment on the blades is proportional to the wind speed squared and the diameter cubed, and thus scales with $k^{3+2\alpha}$. This means that both power and blade bending moment scale more than k^2 and k^3 , respectively, when considering the wind shear effect. Thus, the risk of failure due to buckling, fracture or fatigue is increased, and the material strength has to be checked carefully. [47]

Besides wind shear also wind turbulence should be considered, as the resultant loads are mostly design driving. Having a bigger rotor diameter and thus a larger swept area, more different loading due to turbulence will act on the rotor blades. [29]

The scaling laws should be applied to the entire wind turbine system, but not all components can be scaled that directly. The drivetrain, with cubically varying torque and constant speed as determining parameters, is one example. Simplifications and further considerations lead to the approximation that the generator mass can be scaled by k^2 , and in case of direct drive by k^3 . [47]

In reality, also prevailing basic conditions have to be considered. The recommended ratio of hub height to rotor diameter, for example, depends on the location of the wind turbines. Big onshore turbines should have high towers, in order to avoid the impact of the bottom boundary layer. The hub height to rotor diameter ratio for onshore wind turbines should therefore be bigger than 1 or even 2 for small turbines. Offshore, however, the hub height to rotor diameter ratio could be smaller than 1, as water has a quite small roughness value. [19]

The control system is another parameter that has to be different for onshore, offshore fixed and offshore floating wind turbines, and that does not follow any geometric scaling law. The modification of the controller for floating systems is covered in detail in Section 3.6.

Besides the physical properties, also the cost parameter is an essential value for wind turbines. The square-cube law describes the scaling proportionality of power ($\sim k^2$) and costs (dependent on the amount of material and thus $\sim m \sim k^3$). From this, it can be found that the cost per unit capacity scales with k , if only the wind turbine system is considered. However, not only mass but also manufacturing, installation and infrastructure are driving parameters of wind turbine costs. Complex cost models are needed for describing the scaling behavior of the costs. [29]

To conclude, the scaling laws can be used for obtaining a roughly upscaled design. Caution should be exercised with resulting stresses, especially due to weight, and both yield strength and buckling limit have to be checked. Furthermore, the upscaled design has to be adjusted to local or case-specific predefined conditions and requirements. The costs of the upscaled system have to be estimated, based on detailed cost models.

3.1.2 Real Upscaling Based on Existing Wind Turbines

New technologies and design developments are not covered by theoretical physical laws. Based on existing wind turbines, trend lines in the scaling factors of relevant parameters can be determined. The results from such a comparative study [48] are presented in Table 3.2 and compared with the theoretical scaling proportionalities, following the previously introduced scaling laws and the results from Table 3.1. In the comparative study, a distinction is made between wind turbines with gearbox and direct drive wind turbines, as they sometimes scale with a slightly different factor. Table 3.2 is then supplemented by real scaling proportionalities for tower base and blade root bending moments, taken from [47].

Some remarks about the results of the comparative study, presented in Table 3.2, have to be made, based on [48]. It strikes that the tower height does not scale linearly with the rotor diameter. The hub height is in general increasing with the rotor diameter, but the real proportionality depends on the actual location of the wind turbine, as already discussed in Paragraph 3.1.1.3. The linearly scaling of lengths is also not valid for blade root and tip chord lengths. Both are increasing with increasing rotor diameter, as the blades have to bear higher loads. The trend, however, is slower than a linear increase for the blade root chord, and faster for the blade tip chord. Reasons may be new blade designs and light-weight materials, used for larger blades.

A direct drive has a bigger top mass than a geared wind turbine. The generator of an upscaled direct drive wind turbine has to be larger, includes more poles and should be quite stiff in order to deal with the high torque. This leads to a higher nacelle mass than generator and gearbox of a geared turbine have together. The blade mass of a direct drive wind turbine, however, is slightly smaller, as the mostly larger hub diameters lead to a smaller effective blade length. The total rotor mass of a direct drive wind turbine, however, is larger again, as the rotor mass also includes the hub itself. This is mostly bigger for a direct drive turbine, because it has to fit to the large sized nacelle. The total top mass of a direct drive wind turbine, thus, is bigger compared to the top mass of a geared wind turbine. But still, the mass scaling is rather quadratic than cubic.

The tip speed of existing wind turbines is not exactly kept constant. Noise limitations and environmental restrictions are the determining factors that influence the theoretical upscaling of the tip speed. Comparing the minimum possible rotor speed shows that direct drive turbines can already start energy generation at lower speed than geared wind turbines can do. The reason lies within the principle of direct drive generators, which have the opportunity to control the number of activated poles, so that the grid frequency can already be reached at lower rotor speed.

Table 3.2: Actual scaling proportionalities for several parameters relevant to wind turbines, based on [47, 48], given as exponent to the base k

| Parameter | Geared | Direct drive | Theoretical |
|---------------------------------|---------|--------------|-------------|
| Blade length | 1 | | 1 |
| Blade root chord length | 0.6988 | | 1 |
| Blade tip chord length | 1.4833 | | 1 |
| Tower height | 0.6958 | | 1 |
| Blade mass | 1.934 | 1.92 | 3 |
| Rotor mass | 1.748 | 2.31 | 3 |
| Nacelle mass | 1.45 | 1.859 | 3 |
| Top mass | 1.683 | 2.088 | 3 |
| Tip speed | 0.1999 | | 0 |
| Cut-in rotor speed | -1.256 | -0.821 | -1 |
| Rated rotor speed | -0.8814 | -0.8748 | -1 |
| Rated power | 1.92 | 1.896 | 2 |
| Nominal power | 1.71 | 1.496 | 2 |
| Tower base bending moment M_x | 3.2351 | | 3-4 |
| Tower base bending moment M_y | 2.3381 | | 3-4 |
| Tower base bending moment M_z | 4.0526 | | 3-4 |
| Blade root bending moment M_x | 3.2504 | | 3-4 |
| Blade root bending moment M_y | 2.8648 | | 3-4 |
| Blade root bending moment M_z | 2.7273 | | 3-4 |

The real scaling factor of the bending moments coincides well with the theoretical value, showing the influence of self-weight, as explained in Paragraph 3.1.1.2.

Besides different drivetrain types, considered in the comparative study [48], also design site and wind conditions, manufacturer's preferences, and especially the stage of technology influence the real scaling proportionalities. Considering this last issue of time history, it is found that new designs, which are still in technology development, follow more or less the theoretical scaling proportionalities regarding the masses, as presented in Table 3.3. However, advanced designs, with technology improvements and further developments for mass and cost reduction, appear to scale significantly less than theoretically. This shows the limited direct application of the theoretical scaling laws based on geometric self-similarity. [29]

Table 3.3: Technology dependent scaling proportionalities for wind turbine masses, based on [29], given as exponent to the base k

| Parameter | Undeveloped | Developed | Theoretical |
|--------------|-------------|-----------|-------------|
| Blade mass | ~ 3 | 2.1 | 3 |
| Nacelle mass | 3.0 | 1.8 | 3 |
| Top mass | 2.8 | 2.1 | 3 |

3.2 Stable Floating Systems

As floating offshore wind turbines are not rigidly fixed to the bottom, they need some special consideration of buoyancy and weight. Based on Archimedes' law, floatation and stability of a floating system are covered in this chapter.

3.2.1 The Principle of Floatation

A semi-submersible floating platform should be designed, such that it is floating with a certain draft in calm seas with no wind. In this neutral position, floatation is met when the weight W of the entire system equals the buoyancy force F_B , as shown in Equation 4.

$$W \stackrel{!}{=} F_B \quad (4)$$

All single components, like blades, hub, nacelle, tower, platform, and also the lifted parts of the mooring lines, count to the weight of the floating wind turbine system. The mass of the components itself is either directly given or can be calculated from volume V and material density ρ_{mat} . Equation 5 summarizes the computation of the weight of the floating system.

$$W = \sum_i W_i = g \sum_i m_i = g \sum_i V_i \rho_{\text{mat},i} \quad (5)$$

The buoyancy force corresponds to the weight of the displaced water volume. With the predefined draft, the displaced water volume can be determined from the submerged bodies, which are mostly a part of the floater and the lifted elements of the mooring lines. Multiplication with the water density and gravity yields the buoyancy force, as shown in Equation 6.

$$F_B = \rho_{\text{water}} g \sum_i V_i |_{z \leq 0} \quad (6)$$

If weight and buoyancy are initially not in equilibrium, the design has to be adjusted. The buoyancy force cannot be changed, as the draft of the floating system is predefined. However, the weight of the system can be changed by adding (or removing) ballast. The amount of ballast is directly given by the difference between buoyancy force and initial weight. The required ballast volume always has to be checked against the available interior volume of the structure. Considering different ballast types of various densities, provides many opportunities to adjust the weight of the entire system, in order to obtain a floatable structure with predefined draft.

3.2.2 Stability

Wind turbines, orientated with the rotor area perpendicular to the main wind direction and having the rotor at the hub far above SWL, must deal with high thrust forces in surge direction and resulting large moments around the y -axis. As existing floating structures, like oil and gas platforms, have a more compact and heavy structure on top, but quite a large footprint, the stability criterion, especially in pitch, is an emerging relevant issue for floating offshore wind turbines. The concrete definitions of the turbine motions and coordinate system are introduced in Subsection 3.3.1. For simplification reasons, only static stability is considered in the following.

3.2.2.1 General Definitions In a stable position, the system's centers of gravity and buoyancy, denoted as G and B , are lying on one vertical axis, as it can be seen in Figure 3.1(a). This is no longer the case, if the system tilts out. The intersection point, between the initial vertical axis through the center of buoyancy in neutral position and the actual vertical axis through the new center of buoyancy, is defined as metacenter M . Depending on the relative location of G and M , the gravity force and righting lever GZ lead to a stabilizing or destabilizing moment. If the metacentric height GM is positive for a positive tilt angle, meaning the center of gravity lies

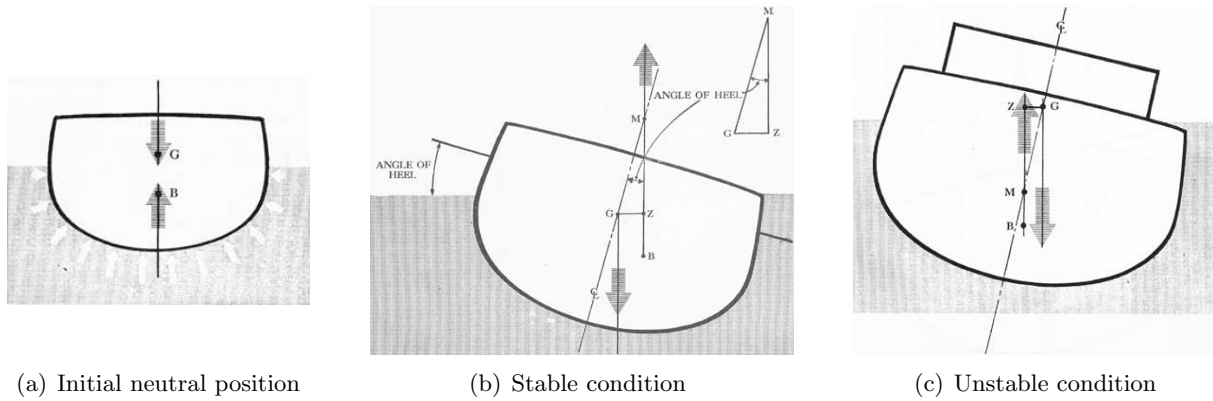


Figure 3.1: Stability conditions of a floating structure [11]

below the metacenter as shown in Figure 3.1(b), the system rotates back into its initial stable position. But if $GM < 0$ for a positive tilt, the center of gravity is above the metacenter like in Figure 3.1(c), and the system will capsize. The same applies analogously to negative tilt angles.

A stability analysis can be carried out by plotting the metacentric height or the righting lever with respect to the tilt angle. The stability limit is directly at the first zero crossing point of the GM- or GZ-curve, which comes after the zero crossing point at the initial neutral position.

Determining the metacentric height or righting lever for different pitch angles by means of this method is generally valid, but quite complex. Only for small tilt angles, the metacenter can be assumed to be fixed. If the system contains movable components, like liquid ballast, the center of gravity will change during pitching. Another consequence of large tilt angles is that the displaced water volume would vary, when just rotating around the y -axis. For a system without any openings, the entire weight is not changing, and the buoyancy force has to remain constant to maintain floatation. This means that after tilting, the vertical position of the structure has to be adjusted. Only then, the correct location of the center of buoyancy corresponding to the actual pitch angle can be determined and the metacenter found. Those steps include some iterations and should therefore be carried out with the help of a computer program.

3.2.2.2 Simplified Hand Calculations Estimating the stability limit already by means of hand calculations, requires some simplifications. All system components, even the ballast, are assumed to be fixed. Furthermore, the center of buoyancy is only calculated based on the rotatory pitch motion, neglecting the vertical translation, required for meeting the force equilibrium for floatation. Those simplified hand calculations do not allow to determine the exact stability limit. It should rather be checked if the system remains stable during operation. The maximum allowable operational pitch angle is assumed to be 10° , based on conventional values [27,32].

The simplified calculation procedure is explained based on a semi-submersible platform, like the DeepCwind floater introduced in Section 2.1. As the center of buoyancy depends on the pitch angle, first the smallest angle, up to which no additional element is submerged or emerged, has to be identified. This simplifies the calculation because the geometries for the volume calculation remain similar in this pitch range and can be expressed in terms of the angle. For example, the base columns are initially totally submerged, and thus full cylinders in the displaced water volume calculation. If the base column starts emerging, the cylindrical geometry would have to be adjusted for the emerged cylindrical hoof. Figure 3.2 shows the six critical locations where the initial submerged geometries could change first, θ_I to θ_{III} (in green) for positive pitch and θ_{IV} to θ_{VI} (in orange) for negative pitch. Those are the outer top edge of the base columns (θ_I and θ_{IV}), the outer top edge of the upper columns (θ_{II} and θ_V), and the bottom edge of the upper brace

contact points to the offset columns (θ_{III} and θ_{VI}). If the smallest of those angles, according to amount, is already distinctly bigger than the assumed maximum allowable operational pitch angle of 10° , the calculations only have to be carried out for this initial submerged geometry.

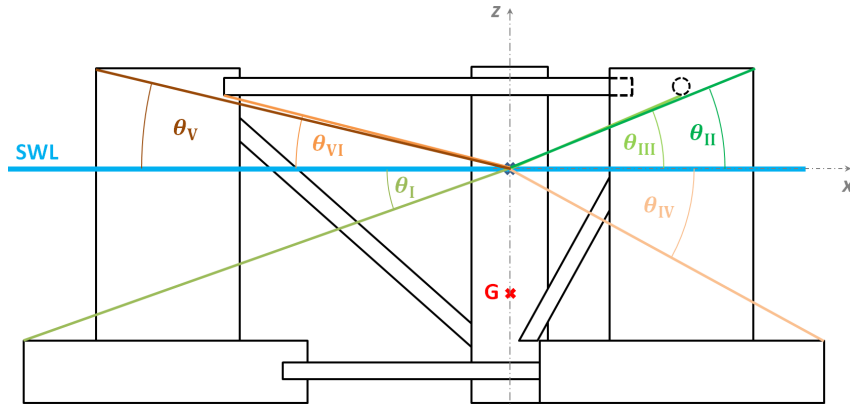


Figure 3.2: Critical positions where the submerged geometry could change first

The submerged volume of the first calculation range can be split up into nine cylinders (three for the base columns, six for the lower horizontal braces), and seven one-sided truncated cylinders (three for the upper columns, one for the main column, three for the diagonal cross braces). The dimensions of the truncated cylinders are expressed in terms of the pitch angle θ . For each geometry, the location of its center of buoyancy is determined and transferred to the global body-fixed coordinate system of the structure (denoted with $\tilde{\sim}$), leading to the coordinates \tilde{x}_{B_i} and \tilde{z}_{B_i} , as visualized in Figure 3.3.

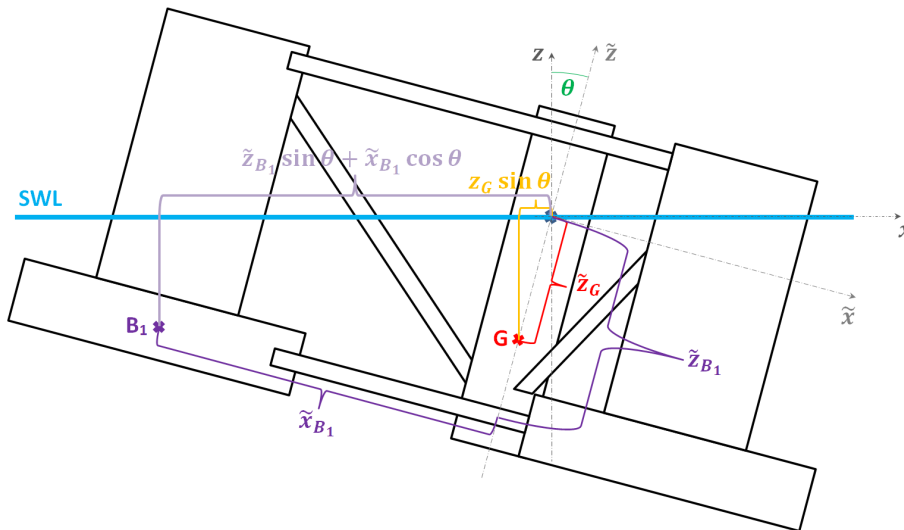


Figure 3.3: Coordinates of the centers of gravity and buoyancy in tilted position

The x -coordinate of each single element's center of buoyancy can be computed by means of Equation 7, and for the entire system's center of buoyancy by means of Equation 8, written as function of the pitch angle.

$$x_{B_i}(\theta) = \tilde{z}_{B_i} \sin \theta + \tilde{x}_{B_i} \cos \theta \quad (7)$$

$$x_B(\theta) = \frac{\sum_i x_{B_i}(\theta) V_i(\theta)}{\sum_i V_i(\theta)} \quad (8)$$

For the stability analysis also the x -coordinate of the center of gravity has to be computed depending on the pitch angle, as given in Equation 9.

$$x_G(\theta) = \tilde{z}_G \sin \theta \quad (9)$$

This way, the x -coordinates of the centers of gravity and buoyancy, as well as their difference, corresponding to the righting lever GZ , can be determined and plotted with respect to the pitch angle. From the graphs, it can be seen whether the system is stable within the considered range of pitch, following the description given in Paragraph 3.2.2.1. However, this is still an estimation, even if the calculations yield a stable system up to pitch angles distinctly above 10° .

3.2.2.3 Detailed Stability Calculations For a detailed stability calculation, program-based analyses of the floating wind turbines are performed in HydroD and Modelica, as introduced later on in Sections 4.2 and 4.3. HydroD already has a stability analysis tool included. In the equation-based simulation program Modelica, however, the stability calculation has to be implemented manually. The detailed computation can be found in Appendix A.1.

3.2.2.4 Intact Floating Stability According to Offshore Standard DNV-OS-J103 [53], stability of the floating system has to be ensured during operation at highest rotor thrust. This occurs at rated wind speed or in a fault situation. For a column-stabilized structure, the requirements for intact stability are a positive righting moment from upright position to the second intercept of righting and wind heeling moment curves, and that “the area under the righting moment curve to the angle of downflooding shall be equal to or greater than 130% of the area under the wind heeling moment curve to the same limiting angle.” [53, p.81] A schematic representation of the moment curves and angles is given in Figure 3.4.

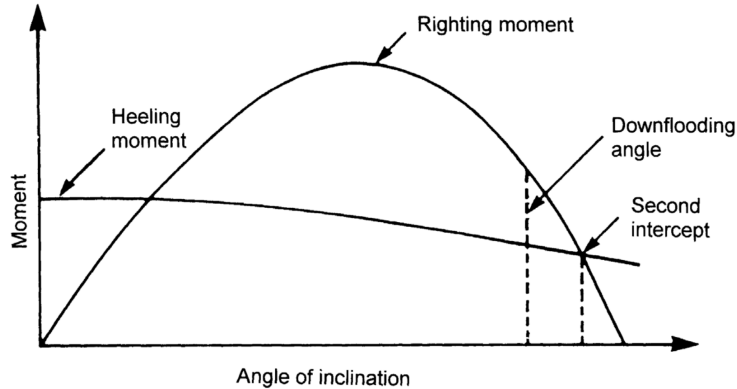


Figure 3.4: Righting moment and wind heeling moment curves [53]

In order to check this criterion, the angle at the second intercept of righting and wind heeling moment curves is taken as downflooding angle, as the semi-submersible platform has no openings [57]. The wind heeling moment is determined for the maximum thrust force, obtained at rated wind speed, and expressed in Equation 10 as function of the pitch angle θ .

$$\begin{aligned} M_{\text{wind}} &= F_{T,\text{rated}} l \cos^2 \theta \\ &= \frac{1}{2} \rho_{\text{air}} \frac{D_{\text{rotor}}^2}{4} \pi C_T v_{\text{rated}}^2 l \cos^2 \theta \end{aligned} \quad (10)$$

The lever arm l is the distance between the force application point, taken at the hub, and the point of rotation. The latter one is variable for a moving half-submerged floating system. As the point of rotation of a body is normally at the center of gravity, however for a fully submerged body at its center of buoyancy [37], a conservative approach is to set the lever arm equal to the distance from hub to center of buoyancy of the floating system.

3.3 Natural Frequencies of Floating Structures

The natural frequencies of floating structures should be outside the range of wave excitation, in order to avoid large motions and resonance. For a semi-submersible floating wind turbine, the main focus lies on heave and pitch motion. Therefore, the determination of the natural frequencies in those two degrees of freedom (DoFs) are covered in Subsections 3.3.2 and 3.3.3, after a general introduction to the coordinate system, terminology, and equations of motion for a floating wind turbine in the following Subsection 3.3.1.

3.3.1 Motions of a Floating Structure

The coordinate system of a floating wind turbine is defined with its origin at still water level (SWL), the x -axis pointing in the main wind direction, perpendicular to the untilted rotor plane, the z -axis coinciding with the centerline of the tower and pointing upwards, and the y -axis perpendicular to both x - and z -axis, so that x , y and z make up a right-handed coordinate system. The rotations around the coordinate axes are defined positive, following the right-hand rule. The orientation and position of the coordinate system are presented in Figures 3.5(a) and 3.5(b). The floating system has six DoFs, which are combined in the vector q . The first three DoFs q_1 to q_3 are the translational motions surge, sway and heave, while the remaining DoFs q_4 to q_6 are the rotations roll, pitch and yaw. The terminology is presented in Figure 3.5(c).

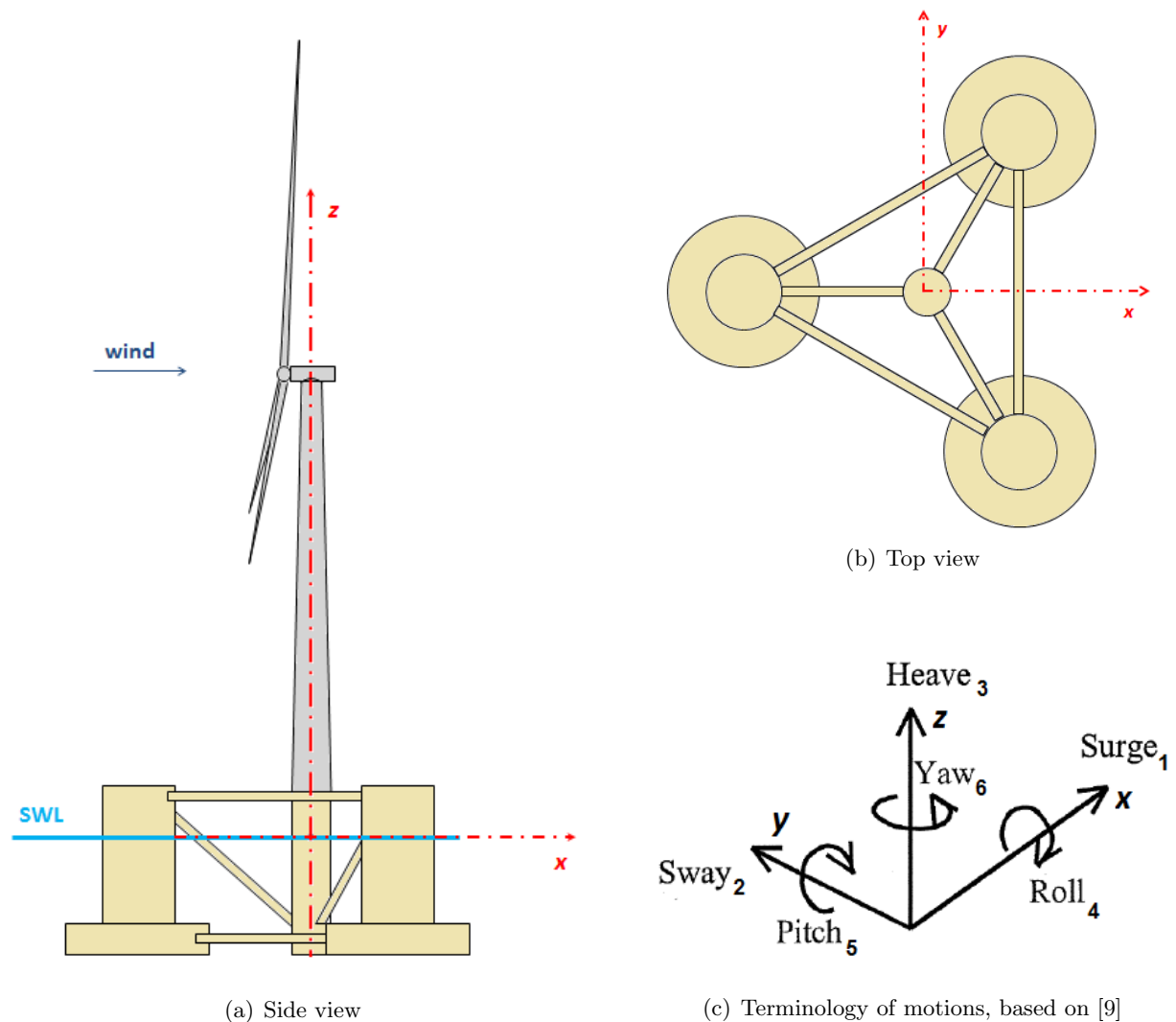


Figure 3.5: Coordinate system of a floating semi-submersible wind turbine

The governing equation of motion for a floating structure is given by Equation 11, with the parameters in time domain indicated by $\hat{\cdot}$. Transformation into frequency domain, by expressing the system motion as harmonic with complex number notation, yields Equation 12.

$$\left[\hat{\mathbf{M}} + \hat{\mathbf{A}} \right] \ddot{\underline{\hat{q}}}(t) + \hat{\mathbf{B}} \dot{\underline{\hat{q}}}(t) + \hat{\mathbf{C}} \underline{\hat{q}}(t) = \underline{\hat{F}}(t) \quad (11)$$

$$\left[-\omega^2 (\mathbf{M} + \mathbf{A}(\omega)) + i\omega \mathbf{B}(\omega) + \mathbf{C} \right] \underline{q}(\omega) = \underline{F}(\omega) \quad (12)$$

The mass and stiffness matrices \mathbf{M} and \mathbf{C} , as well as the frequency-dependent added mass and damping matrices \mathbf{A} and \mathbf{B} , are all of size 6x6. The cross-diagonal terms include the coupling between different DoFs. The frequency-dependent excitation forces and moments \underline{F} , and the system DoFs \underline{q} are vectors of size 6x1, with an element for each DoF.

The undamped natural frequencies of the system can be determined by equating both damping and excitation in Equation 12 to zero. Solving for the angular frequency ω , by setting successively all but one element of the system DoFs \underline{q} equal to zero, and then dividing by a factor of 2π , yields the undamped natural frequency in each DoF. In the simplified hand calculations, however, the coupling terms are neglected, and the undamped natural frequencies $f_{\text{nat},i}$ are just determined based on the diagonal matrix elements, as presented in Equation 13.

$$f_{\text{nat},i} = \frac{1}{2\pi} \omega_{\text{nat},i} = \frac{1}{2\pi} \sqrt{\frac{C_{ii}}{M_{ii} + A_{ii}(\omega_{\text{nat},i})}} \quad (13)$$

Including the damping term, the damped natural angular frequency $\omega_{d,i}$ can be expressed as function of the undamped parameter. The damped natural frequency $f_{d,i}$ is then again obtained by division by 2π , following Equation 14, with the damping factor ζ , defined by Equation 15. [12]

$$f_{d,i} = \frac{1}{2\pi} \omega_{d,i} = \frac{1}{2\pi} \omega_{\text{nat},i} \sqrt{1 - \zeta_i^2} = f_{\text{nat},i} \sqrt{1 - \zeta_i^2} \quad (14)$$

$$\zeta_i = \frac{B_{ii}}{(M_{ii} + A_{ii}(\omega_{\text{nat},i})) 2\omega_{\text{nat},i}} \quad (15)$$

Added mass and damping are in general frequency-dependent parameters. However, this is not considered in the hand calculations. As also the coupling terms of the matrices are neglected, only explicit expressions for the components C_{33} , C_{55} , M_{33} , M_{55} , A_{33} and A_{55} are needed, in order to estimate the natural frequencies in heave and pitch. The derivation is done in the following Subsections 3.3.2 and 3.3.3, based on the assumption of small displacements.

3.3.2 Natural Frequency in Heave

The stiffness component in heave C_{33} follows Equation 16. [16]

$$C_{33} = \rho_{\text{water}} g A_{\text{WP}} \quad (16)$$

The waterplane area A_{WP} of the semi-submersible platform in its initial position, shown in Figure 3.5(a), consists of four cylindrical intersections (three from the upper columns, one from the main column) and three elliptical intersections from the cross braces. The stiffness component in heave can be expressed in terms of column and cross brace diameters, cross brace length and its vertical projection Δz_{CB} . The final formula, given by Equation 17, is based on the wall-sided assumption and can be used as a good approximation for small displacements and motions [6].

$$C_{33} = \rho_{\text{water}} g \frac{\pi}{4} \left[3 \left(D_{\text{UC}}^2 + D_{\text{CB}}^2 \frac{l_{\text{CB}}}{\Delta z_{\text{CB}}} \right) + D_{\text{MC}}^2 \right] \quad (17)$$

The mass component in heave M_{33} is equal to the total system mass, following Equation 18. [9]

$$M_{33} = \sum_i m_i = \sum_i V_i \rho_{\text{mat},i} \quad (18)$$

A good approximation for the low-frequency limit of the added mass component in heave A_{33} is obtained by Equation 19, based on [21, 52], considering upper, base and main columns, but neglecting the pontoons and cross braces.

$$A_{33} = \frac{\rho_{\text{water}}}{6} D_{\text{MC}}^3 + 3 \left\{ \frac{\rho_{\text{water}}}{3} D_{\text{BC}}^3 - \left[\frac{\pi \rho_{\text{water}}}{8} D_{\text{UC}}^2 \left(D_{\text{BC}} - \sqrt{D_{\text{BC}}^2 - D_{\text{UC}}^2} \right) + \frac{\pi \rho_{\text{water}}}{24} \left(D_{\text{BC}} - \sqrt{D_{\text{BC}}^2 - D_{\text{UC}}^2} \right)^2 \left(2D_{\text{BC}} + \sqrt{D_{\text{BC}}^2 - D_{\text{UC}}^2} \right) \right] \right\} \quad (19)$$

Substituting C_{33} , M_{33} and A_{33} in Equation 13 yields finally the natural frequency in heave.

Regarding the upscaling of wind turbine parameters, the stiffness component in heave is expected to scale with k^2 , as it is proportional to an area, and thus a length squared. The mass and added mass components, however, are volumetric dimensions, and therefore expected to scale with k^3 . Based on this calculation, the natural frequency in heave is rather expected to scale with $k^{-0.5}$, than with k^{-1} following the structural scaling laws, given in Table 3.1 in Subsection 3.1.1.

3.3.3 Natural Frequency in Pitch

The stiffness component in pitch C_{55} is given by Equation 20. [9]

$$\begin{aligned} C_{55} &= W(z_{\text{B}} - z_{\text{G}}) + \rho_{\text{water}} g I_y \\ &= W(z_{\text{B}} - z_{\text{G}}) + \rho_{\text{water}} g \int_{A_{\text{WP}}} x^2 dA \end{aligned} \quad (20)$$

W is the total weight of the system, as defined in Equation 5, and z_{B} and z_{G} the vertical coordinates of the center of buoyancy and gravity, respectively. Those can be obtained for composite bodies based on Equation 8, by replacing x by z and setting θ equal to zero for considering the undisplaced position. I_y is the second-order moment of waterplane area about the y -axis.

The local second-order moment of area for the circular intersections of upper and main columns $\bar{I}_{y,\text{UC/MC}}$ can be calculated by means of Equation 21. [56]

$$\bar{I}_{y,\text{UC/MC}} = \frac{\pi}{64} D_{\text{UC/MC}}^4 \quad (21)$$

The local second-order moment of area for the elliptical intersections of the cross braces $\bar{I}_{y,\text{CB}}$ follows Equation 22. β represents the angle between the major symmetry axis of the elliptical intersection and the global y -axis, and amounts 30° for cross braces 1 and 3, and 90° for cross brace 2, with the numbering following Figure 2.1(b).

$$\bar{I}_{y,\text{CB}} = \frac{\pi}{64} D_{\text{CB}}^4 \frac{l_{\text{CB}}}{\Delta z_{\text{CB}}} \left[\left(\frac{l_{\text{CB}}}{\Delta z_{\text{CB}}} \right)^2 \sin^2(\beta) + \cos^2(\beta) \right] \quad (22)$$

For each intersection, the local second-order moment of area about the axis through its centroid has to be transferred to the global y -axis, by adding the product of intersection area and distance to the parallel axis squared, which is known as the parallel axis theorem [56]. Summing up the second-order moments of area about the global y -axis of all seven intersections, yields the total second-order moment of waterplane area, needed in Equation 20 for calculating the stiffness component in pitch.

The mass component in pitch M_{55} is equal to the mass moment of inertia about the y -axis over the entire body, as written in Equation 23. [9]

$$M_{55} = I_{yy} = \int_{\text{system}} x^2 + z^2 dV \quad (23)$$

The mass moments of inertia have to be calculated for each component of the floating wind turbine structure, transferred to the global coordinate system, and finally added up.

For calculating the added mass component in pitch A_{55} , strip theory is used. By assuming 2D potential flow theory, leading to an added mass coefficient of 1 for a circular cylinder in surge motion [9], and neglecting pontoons and braces, a good approximation for the low-frequency limit of the added mass component in pitch can be obtained by Equation 24, based on [21].

$$A_{55} = 3\rho_{\text{water}} \frac{\pi}{4} D_{\text{BC}}^2 \left(\frac{|z_{\text{b,BC}}|^3}{3} + (z_{\text{G,BC}} - z_{\text{b,BC}})^2 |z_{\text{b,BC}}| + (z_{\text{G,BC}} - z_{\text{b,BC}}) |z_{\text{b,BC}}|^2 \right) \\ + \rho_{\text{water}} \frac{\pi}{4} D_{\text{MC}}^2 \left(\frac{|z_{\text{b,MC}}|^3}{3} + (z_{\text{G,MC}} - z_{\text{b,MC}})^2 |z_{\text{b,MC}}| + (z_{\text{G,MC}} - z_{\text{b,MC}}) |z_{\text{b,MC}}|^2 \right) \quad (24)$$

Substituting C_{55} , M_{55} and A_{55} in Equation 13 results in the natural frequency in pitch.

The stiffness component in pitch, given in Equation 20, has the dimension of an area moment of inertia, corresponding to a weight times a length. Thus, it is expected that the stiffness component in pitch scales with k^4 during the upscaling procedure. The mass component in pitch is expressed by mass moments of inertia, and the added mass component in pitch is proportional to a length to the power of five. Therefore, it is expected that both mass and added mass components in pitch scale with k^5 . Based on this calculation, the natural frequency in pitch is, as in heave, rather expected to scale with $k^{-0.5}$, than with k^{-1} following the structural scaling laws, given in Table 3.1 in Subsection 3.1.1.

3.4 Viscous Forces and Damping

Severe sea states with long waves and high wave heights, viscous forces, and flow separation have to be considered in hydrodynamic analyses of cylindrical structures with small diameters. [22]

3.4.1 Morison's Equation

A typical approach for hydrodynamic load calculations, including viscous forces, is Morison's equation, given in Equation 25. This can be applied in case of flow separation, if diffraction effects are simplified using the long wave approximation, and radiation damping is neglected. [41]

$$\begin{aligned} \partial F = & \frac{1}{2} \rho_{\text{water}} C_D D (v_{\text{water}} - \dot{q}) |v_{\text{water}} - \dot{q}| \partial z \\ & + \rho_{\text{water}} (1 + C_a) \frac{\pi D^2}{4} \dot{v}_{\text{water}} \partial z \\ & - \rho_{\text{water}} C_a \frac{\pi D^2}{4} \ddot{q} \partial z \end{aligned} \quad (25)$$

Equation 25 is split up into three terms, considering quadratic drag, inertia and added mass. The force on one cylinder element ∂z of diameter D is thus not only dependent on the fluid and cylinder velocities v_{water} and \dot{q} , respectively, but also on the drag and added mass coefficients C_D and C_a .

In the following work, an added mass coefficient of $C_a = 0.63$ is used for the analysis in HydroD, based on the selection in the original OC4 semi-submersible design [41]. From this analysis, the low-frequency added mass limit in surge is obtained, with which the added mass coefficient is adjusted for the further analysis in Modelica, as explained in Paragraph 4.3.1.2.

The drag coefficients of all platform members, however, are already calculated ahead of any computer-based analysis. The determination method is presented in the following Subsection 3.4.2, based on [41].

3.4.2 Drag Coefficient Determination

The drag coefficient depends on the Reynolds number Re , as shown in Figure 3.6 [10].

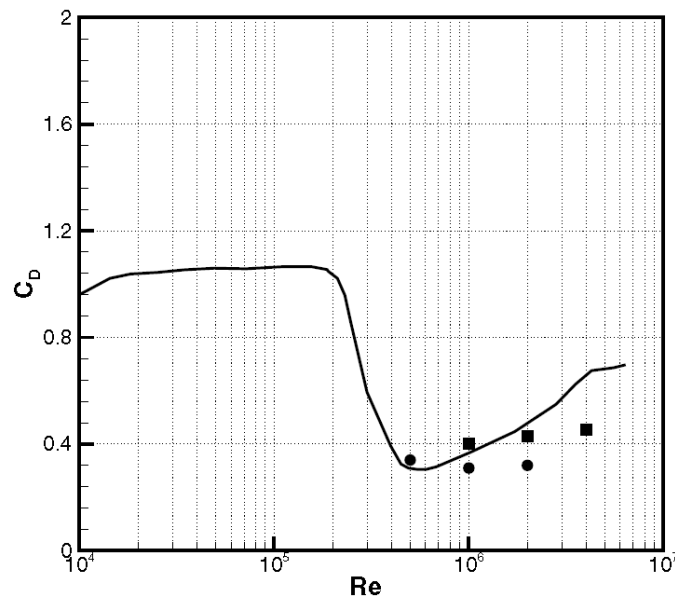


Figure 3.6: Drag coefficient depending on the Reynolds number [10]

The Reynolds number is already introduced in Paragraph 3.1.1.3 by Equation 3. For the considered cylinder in transverse and steady flow, the characteristic length scale is given by the cylinder diameter. The velocity equals the amplitude of the water velocity acting perpendicular on the cylinder, given by Equation 26. The water velocity itself depends on the sea state, defined by wave height H and wave period T , water depth $|z_{\text{seabed}}|$, wave number κ , defined by the dispersion relation given in Equation 27, and the vertical position z . [41]

$$v_{\text{water}} = \frac{\pi H}{T} \frac{\cosh[\kappa(z + |z_{\text{seabed}}|)]}{\sinh(\kappa|z_{\text{seabed}}|)} \quad (26)$$

$$\kappa \tanh(\kappa|z_{\text{seabed}}|) = \frac{4\pi^2}{gT^2} \quad (27)$$

This means that the drag coefficient not only depends on the diameter of the column, but also varies along the column in vertical direction, and changes with the sea conditions. For a detailed hydrodynamic analysis, all those factors should be included, as the drag coefficient could vary quite a lot from around 0.3 to 1.06, as it can be seen in Figure 3.6. However, for the analyses performed in this work, an estimate of the drag coefficient for each column is used. The approximate determination of the drag coefficients follows the method applied in [41] for the original OC4 semi-submersible platform.

Table 3.4: Representative sea states of OC4 [41]

| Sea state | 1 | 2 | 3 | 4 | 5 | 6 | 7 | 8 |
|-----------|------|------|------|------|------|------|------|-------|
| T [s] | 2.0 | 4.8 | 6.5 | 8.1 | 9.7 | 11.3 | 13.6 | 17.0 |
| H [m] | 0.09 | 0.67 | 1.40 | 2.44 | 3.66 | 5.49 | 9.14 | 15.24 |

Thus, for each of the eight representative sea states, given in Table 3.4, a mean water velocity is computed, based on Equation 28, as average from SWL to the platform's draft [41]. The wave number κ is determined for each sea state, by iteratively solving of Equation 27.

$$\bar{v}_{\text{water}} = \frac{\pi H}{-z_{\text{draft}} T \kappa} \left[1 - \frac{\sinh(\kappa z_{\text{draft}} + \kappa |z_{\text{seabed}}|)}{\sinh(\kappa |z_{\text{seabed}}|)} \right] \quad (28)$$

For each average velocity, the Reynolds number is computed for the considered column, by means of Equation 3, and using a kinematic viscosity of water of $1.004\text{E-}6 \text{ m}^2\text{s}^{-1}$. The corresponding drag coefficients are read from the graph in Figure 3.6. This way, eight values are found for each column. The final estimated drag coefficient is taken as their average.

3.5 Station-Keeping Systems for Floating Structures

Floating offshore wind turbines require a station-keeping system, that keeps the displacements within the allowable range. This is, for example, dictated by the load-bearing capacity of the entire system, including mooring line strength and load capacity of the anchors, geometric constraints, like wind farm layout and clearance requirements, or equipment limitations. Furthermore, station-keeping systems may allow controlling the orientation of the wind turbine, and help limiting the tower top acceleration and tilt. [61]

3.5.1 Overview of Existing Design Concepts

Two main concepts of station-keeping systems exist: active systems, like dynamic positioning or thruster-assisted mooring, in which the mooring line tension can be changed or the system is steered by thrusters, and passive station-keeping systems, like spread mooring systems, tendons or single point mooring systems. Active station-keeping systems, as well as single point mooring systems, with an integrated turret that enables weathervaning, are more common for ships and often needed in offshore oil and gas operations, where the big floating structures are sensitive to the directionality of the environmental conditions. The less sensitive floating platforms for wind turbines, however, usually have tendons or spread mooring systems. The only disadvantage of the latter one is the large spread of the mooring lines, which could complicate the layout of an offshore wind farm. [61]

Depending on the floating platform type, different passive station-keeping systems are used. Tension leg platforms are moored with vertical tendons, whereas spars and semi-submersible floaters are supported by a spread mooring system with catenaries, semi-taut or taut lines. The mooring lines are made out of chains, wires, ropes, fibers or some combination, and can also include buoys or clump weights. On the seabed, the mooring lines are fixed by anchors, anchor piles or suction piles. The entire station-keeping system is thus defined by the type of the mooring system, the layout, number and material of the lines, and the anchor type and properties. Beyond those components, pretension, elasticity, total line length, and submerged weight of the suspended lines are very important parameters for a catenary mooring system. [61]

3.5.2 Calculations of Elastic Catenaries

Catenary mooring lines provide the needed restoring force due to the gravity of the lifted part of the chain. In case of elastic catenary mooring lines, which are used for the DeepCwind semi-submersible platform, also the axial/extensional stiffness EA has to be considered.

For accurate ballasting of the floating system, the lifted parts of the mooring lines have to be included in the weight calculation. The geometry of the catenary mooring line, including the definitions of the total length l_{tot} , the length of the lifted part l_{eff} , their horizontal projections $l_{\text{tot,hor}}$ and $l_{\text{eff,hor}}$, the length of the catenary part lying on the seabed l_{rest} , the height of the fairleads above the seabed h , and the local coordinate systems, is presented in Figure 3.7. The mathematical relation between those parameters is given in Equation 29, based on [1].

$$l_{\text{rest}} = l_{\text{tot}} - l_{\text{eff}} = l_{\text{tot,hor}} - l_{\text{eff,hor}} \quad (29)$$

Both effective length and its horizontal projection are unknown. The other two lengths are predetermined by the geometry of the floating system. Using Equation 30 for the normalized mooring line pretension τ^* , with the horizontal tension τ_{hor} at the touch down point and the equivalent mooring line mass in water $\mu_{\text{moor,water}}$, the horizontal projection of the effective length can be expressed by Equation 31 [36] and substituted into Equation 29, yielding Equation 32.

$$\tau^* = \frac{\tau_{\text{hor}}}{\mu_{\text{moor,water}} g} \quad (30)$$

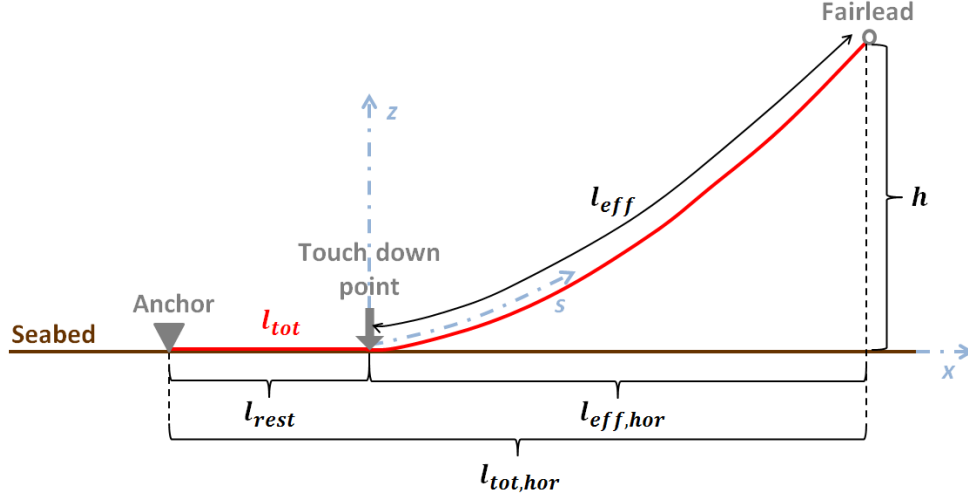


Figure 3.7: Geometry and parameters of the catenary mooring line

$$l_{\text{eff,hor}} = \tau^* \sinh^{-1} \left(\frac{l_{\text{eff}}}{\tau^*} \right) + \frac{\tau_{\text{hor}} l_{\text{eff}}}{EA} \quad (31)$$

$$l_{\text{tot}} - l_{\text{eff}} = l_{\text{tot,hor}} - \tau^* \sinh^{-1} \left(\frac{l_{\text{eff}}}{\tau^*} \right) - \frac{\tau_{\text{hor}} l_{\text{eff}}}{EA} \quad (32)$$

As Equation 32 has still two unknowns, l_{eff} and τ_{hor} , another equation is needed for determining the effective length. The z -coordinate of the lifted part of the mooring line, as function of s in line direction, is introduced by Equation 33, based on [36]. Evaluation at $s = l_{\text{eff}}$, with the corresponding local z -value of $z_{\text{moor}} = h$, results in Equation 34.

$$z_{\text{moor}}(s) = \frac{\mu_{\text{moor,water}} g s^2}{2EA} + \tau^* \left(\sqrt{1 + \left(\frac{s}{\tau^*} \right)^2} - 1 \right) \quad (33)$$

$$h = \frac{\mu_{\text{moor,water}} g l_{\text{eff}}^2}{2EA} + \tau^* \left(\sqrt{1 + \left(\frac{l_{\text{eff}}}{\tau^*} \right)^2} - 1 \right) \quad (34)$$

Equations 32 and 34 are solved for the two unknowns l_{eff} and τ_{hor} , with the help of MATLAB.

The mass contribution of the mooring lines m_{moor} to the total system mass is obtained by multiplying the effective length with the equivalent mooring line mass in water and the number of mooring lines, resulting in Equation 35.

$$W_{\text{moor}} = g m_{\text{moor}} = 3g \mu_{\text{moor,water}} l_{\text{eff}} \quad (35)$$

The mooring line's center of gravity is calculated based on Equation 36, representing the general equation for the centroid of a line, transferred to the global coordinate system of the floating structure. Substituting Equation 33 into Equation 36 and solving the integral expression yields Equation 37 for the center of gravity of the lifted mooring line.

$$z_{\text{G,moor}} = z_{\text{seabed}} + \frac{1}{l_{\text{eff}}} \int_0^{l_{\text{eff}}} z_{\text{moor}}(s) ds \quad (36)$$

$$z_{G,moor} = z_{seabed} + \frac{\mu_{moor,water} g l_{eff}^2}{6EA} + \frac{1}{2} \sqrt{(\tau^*)^2 + l_{eff}^2} - \tau^* + \frac{1}{2l_{eff}} (\tau^*)^2 \ln \left(\frac{l_{eff}}{\tau^*} + \sqrt{1 + \left(\frac{l_{eff}}{\tau^*} \right)^2} \right) \quad (37)$$

3.5.3 Mooring Stiffness

The additional stiffness of the mooring system restrains the system motions. The effect is the most in surge and yaw direction. As the determination of the mooring stiffness components is quite extensive, only the stiffness component in surge is covered in the hand calculations. For one line, the mooring stiffness in surge follows Equation 38 [16].

$$C_{11,moor} = \mu_{moor,water} g \left[\frac{-2}{\sqrt{1 + 2\frac{\tau^*}{h}}} + \cosh^{-1} \left(1 + \frac{h}{\tau^*} \right) \right]^{-1} \quad (38)$$

The total stiffness in surge of all three mooring lines is defined by Equation 39 [16].

$$C_{11,moor,tot} = \sum_{i=1}^3 C_{11,moor,i} \cos^2 \psi_i \quad (39)$$

With the angles $\psi_1 = 60^\circ$, $\psi_2 = 180^\circ$ and $\psi_3 = -60^\circ$ between the three mooring lines and the x -axis, the total stiffness component in surge is finally given in Equation 40.

$$C_{11,moor,tot} = \frac{3}{2} C_{11,moor} = \frac{3}{2} \mu_{moor,water} g \left[\frac{-2}{\sqrt{1 + 2\frac{\tau_{hor}}{\mu_{moor,water} gh}}} + \cosh^{-1} \left(1 + \frac{\mu_{moor,water} gh}{\tau_{hor}} \right) \right]^{-1} \quad (40)$$

3.6 Control Systems for Floating Wind Turbines

3.6.1 Wind Turbine Control

The control systems of onshore, offshore fixed and offshore floating wind turbines differ from each other, as already mentioned in Paragraph 3.1.1.3.

Conventional onshore wind turbines have a blade-pitch-to-feather control system and are regulated to constant generator power (or torque). At wind speeds below rated and at rotor speeds below the maximum value, the blades are not pitched and the wind turbine operates with optimum power coefficient at optimum tip speed ratio. In the transition range to rated power, mainly the rotor speed has to be kept at the maximum allowable value due to noise restrictions. Above rated wind speed the wind turbine starts pitching the blades, in order to maintain constant power output (or generator torque). With pitching the blades, the thrust force is decreased, leading to reduced loads on the wind turbine.

Using such a controller for a floating offshore wind turbine, could cause negative damping and large impermissible motions. Floating wind turbine systems, except wind turbines on TLPs, have very low natural frequencies. An onshore blade-pitch controller is too fast compared to the system motions, meaning that it would measure the decrease in relative wind speed and rotor thrust if the platform moves backwards due to hydrodynamic loads, and react by pitching the blades back in order to avoid a power drop. This, however, would lead to an increased thrust, which sustains the backward motion and could lead to an unstable system. Similar behavior is obtained when the floating wind turbine is moving forward due to hydrodynamic loads. [3]

Negative damping can be avoided by setting the blade-pitch controller frequency smaller than the smallest natural frequency of the floating system, and thus reducing the gains in the blade-pitch-to-feather control system [34]. Other options are active damping control strategies, in which a pitch controller, regulated on basis of the tower velocity, is added to the control system, or a notch filter is incorporated, which diminishes the pitch natural frequency and the corresponding resonant motions [38]. A variable power pitch control, which allows higher energy extraction in forward motions, leading to thrust increase and countering of the tower motion, and less energy extraction in backward motions, inducing thrust reduction and again counteracting the tower motion, is as well a possible concept [33].

3.6.2 Blade-Pitch Controller

The blade-pitch controller is adjusted for a floating wind turbine by reducing the controller gains. The proportional and integral controller gains K_P and K_I can be determined by Equations 41 and 42, respectively. The derivative gain K_D is neglected and set equal to $0s^2$. [23]

$$K_P = \frac{2I_{\text{drivetrain,LSS}} \Omega_{\text{rated,LSS}} \zeta_c \omega_{c,\text{nat}}}{N_{\text{gear}} \left(-\frac{\partial P}{\partial \theta}\right)} \quad (41)$$

$$K_I = \frac{I_{\text{drivetrain,LSS}} \Omega_{\text{rated,LSS}} \omega_{c,\text{nat}}^2}{N_{\text{gear}} \left(-\frac{\partial P}{\partial \theta}\right)} \quad (42)$$

The drivetrain inertia with respect to the low speed shaft $I_{\text{drivetrain,LSS}}$ can be computed from the high speed shaft value $I_{\text{drivetrain,HSS}}$ by multiplication with the gearbox ratio N_{gear} squared. The rated low speed shaft rotational speed $\Omega_{\text{rated,LSS}}$ is given as a property of the wind turbine. The damping ratio ζ_c and natural frequency $\omega_{c,\text{nat}}$ of the response, associated with the equation of motion for the rotor-speed error, are recommended to be chosen as $\zeta_c \cong 0.6 - 0.7$ and $\omega_{c,\text{nat}} \cong 0.6 \text{ rad s}^{-1}$ [23]. However, as the negative damping, introduced by the generator torque

control, is neglected in the determination of the proportional gain, the upper limit of 0.7 should be taken for the damping, in order to compensate for this. The sensitivity of the aerodynamic power to the rotor-collective blade-pitch angle $\frac{\partial P}{\partial \theta}$ depends on the pitch angle and can be linearly approximated by means of Equation 43, which can be transformed into Equation 44. [31]

$$\frac{\partial P}{\partial \theta} = \frac{\frac{\partial P}{\partial \theta} \Big|_{\theta_{\text{rated}}}}{\theta_{\text{K}}} \theta + \frac{\partial P}{\partial \theta} \Big|_{\theta_{\text{rated}}} \quad (43)$$

$$\frac{1}{\frac{\partial P}{\partial \theta}} = \frac{1}{\frac{\partial P}{\partial \theta} \Big|_{\theta_{\text{rated}}} \left(1 + \frac{\theta}{\theta_{\text{K}}}\right)} \quad (44)$$

θ_{K} is the rotor-collective blade-pitch angle, at which the pitch sensitivity has doubled from its rated value. By making use of Equation 44 and defining the gain-correction factor GK , as given in Equation 45, Equations 41 and 42 can be rewritten into Equations 46 and 47, respectively. [31]

$$GK(\theta) = \frac{1}{1 + \frac{\theta}{\theta_{\text{K}}}} \quad (45)$$

$$K_{\text{P}} = \frac{2I_{\text{drivetrain,LSS}} \Omega_{\text{rated,LSS}} \zeta_{\text{c}} \omega_{\text{c,nat}}}{N_{\text{gear}} \left(-\frac{\partial P}{\partial \theta} \Big|_{\theta_{\text{rated}}} \right)} GK(\theta) \quad (46)$$

$$K_{\text{I}} = \frac{I_{\text{drivetrain,LSS}} \Omega_{\text{rated,LSS}} \omega_{\text{c,nat}}^2}{N_{\text{gear}} \left(-\frac{\partial P}{\partial \theta} \Big|_{\theta_{\text{rated}}} \right)} GK(\theta) \quad (47)$$

Based on BEM theory, a MATLAB code is written for determining the blade-pitch sensitivity at rated and θ_{K} , depending on the wind turbine and blade properties. The derivations and the code can be found in Appendix A.2.

The proportional and integral gains for a floating wind turbine system are then determined, based on Equations 45 to 47, by choosing the natural frequency $\omega_{\text{c,nat}}$ smaller than the system's natural angular frequency in pitch. From the comparison of the adjusted gains for the OC4 floater and the original gains of the NREL 5 MW, it is found that the natural frequency $\omega_{\text{c,nat}}$ for the controller gain calculation is approximately the pitch natural angular frequency divided by a factor of around 1.3. Thus, it is decided to use Equation 48 as a conservative approach for choosing the controller natural frequency depending on the system's pitch natural frequency.

$$\omega_{\text{c,nat}} \approx \frac{\omega_{\text{nat},5}}{1.3} \quad (48)$$

4 Analyses of the Platform Designs and Floating Systems

Three different methods are used for analyzing the designed floating systems. Those are presented in Sections 4.1 to 4.3, and finally verified in Section 4.4.

4.1 Analysis Based on Hand Calculations

The hand calculations only allow a simplified stability check, as introduced in Paragraph 3.2.2.2.

The stiffness, mass and added mass components, as well as the natural frequencies in heave and pitch are computed based on Equations 13 and 17 to 24, given in Section 3.3. As the calculation of the added mass components is just an approximation, additionally also the original added mass values of the basic floating platform design is scaled up with the main scaling factor k to the power of three for the heave DoF, and to the power of five for pitch, neglecting the different scaling of other components, like main column or upper columns. Similarly, the original stiffness matrix of the basic floater design is also scaled up (DoF 3 with k^2 , DoF 5 with k^4) for comparison, even though the equation-based stiffness calculation is expected to be quite accurate.

The maximum pitch during operation of the wind turbine is, besides stability and natural frequencies, also of major interest. The common maximum allowable operational pitch angle is 10° [27, 32], which should not be exceeded. For determining the pitch displacement, a static analysis is sufficient. The general equation of motion, given by Equation 12 in Subsection 3.3.1, can thus be reduced to Equation 49.

$$\mathbf{C}q = \underline{F} \quad (49)$$

Neglecting coupling terms, when solving Equation 49 for the system DoF in pitch, results in Equation 50.

$$q_5 = \frac{F_{55}}{C_{55}} \quad (50)$$

The maximum pitch is obtained at maximum thrust. Not considering any fault situation, the thrust force is the highest at rated wind speed, as the blades start pitching at higher wind speeds, which decreases the area facing the wind, and thus also thrust force and pitch displacement. The overturning moment $F_{55, rated}$ resulting from the maximum thrust force can be computed based on Equation 10, with neglecting the inclination, meaning $\cos \theta \approx 1$. The lever arm l should be taken as the distance from hub to center of buoyancy, as already discussed in Paragraph 3.2.2.4. This might be inconsistent with the determination of the stiffness with respect to the origin of the coordinate system of the floating wind turbine, but makes up a conservative approach.

4.2 Analysis Based on GeniE and HydroD

More detailed and also frequency-dependent analysis results are obtained by means of DNV's SESAM software. GeniE, an extensive design analysis tool, contains, inter alia, finite element analyses, load calculations, as well as hydrodynamic and structural analyses, including nonlinearities, combined structures, and interactions [54]. Hydrostatic and stability analyses, as well as motion response, hydrodynamic parameter, and load calculations can be carried out in HydroD [55]. The wave load calculation is executed in this work by Wadam, which is based on Morison's equation and potential flow theory.

4.2.1 Implementation in GeniE and HydroD

The platform design is first implemented in DNV's software GeniE. Input parameters are total draft, heights, diameter and spacing of the columns, as well as diameter, thickness and elevation

of pontoons and cross braces. Using GeniE's finite element mesh generation tool, a panel model for the columns and a Morison model for the pontoons and cross braces are created. The final implemented model, including the wetted surface marked in orange, is presented in Figure 4.1(a).

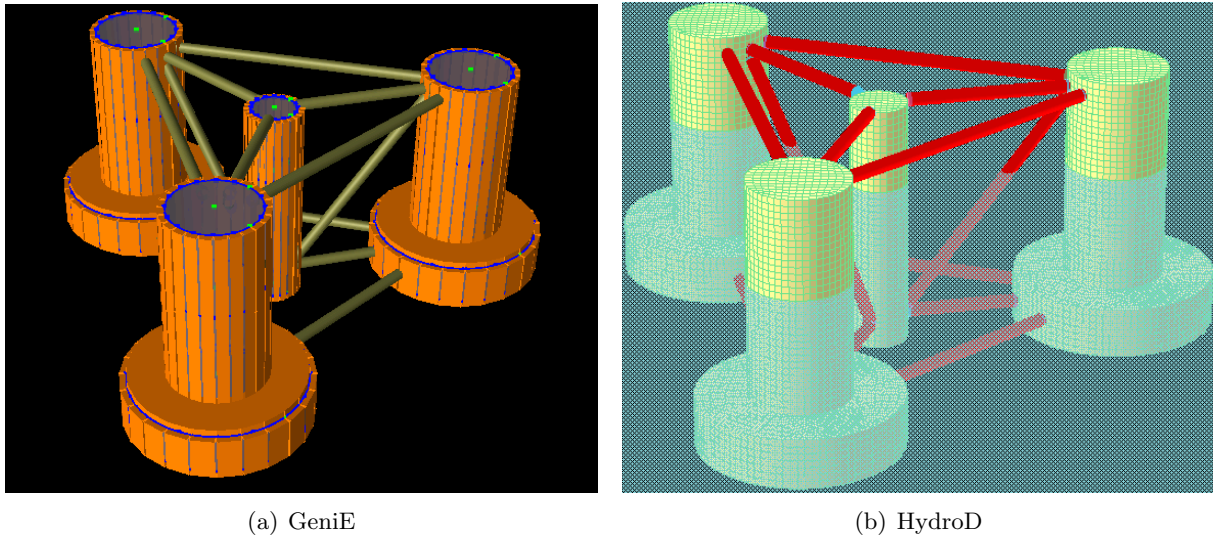


Figure 4.1: Implementation of the semi-submersible platform in GeniE and HydroD

Panel and Morison model are read into HydroD. The environment is defined by the location, water depth, water and air properties, a set of 26 wave angular frequencies from 0.13 rad s^{-1} to 6.28 rad s^{-1} , and the wave direction of 0° , meaning waves propagating in positive x -direction. A mass model is defined, based on the computed mass components M_{ij} , the corresponding radii of gyration, center of gravity of the entire system, and the level of still water. For the linearized viscous drag calculation, Morison 3D sections are specified for the columns by their drag and added mass coefficients, determined based on the procedure described in Subsection 3.4.2. Pressure area elements are generated for all pontoons and braces. The resulting model in HydroD, including SWL (blue), mesh of the columns (green) and Morison elements (red), is shown in Figure 4.1(b). Based on the implemented model, a stability analysis in pitch and a Wadam run for the global response are carried out.

4.2.2 Results from HydroD and Wadam

The stability analysis by HydroD considers the variation of buoyancy and its center, when the platform is pitched. Thus, the stability limits, obtained from the GZ- and restoring moment curves, are assumed to be accurate. A wind heeling moment curve, based on the calculation in Paragraph 3.2.2.4, can be added to the stability analysis. The areas below restoring and wind heeling moment curves to the intersection of both curves can directly be computed by HydroD. This way, also the intact floating stability criteria can be checked.

The Wadam output file, including mass, total restoring, added mass, and damping matrices, exciting forces and moments, motion response, and eigensolutions to the rigid body motion, is read into MATLAB for further post-processing. As the area for the computation of the stiffness matrix components is discretized by a finite element mesh in HydroD, it is expected that the Wadam results are more accurate than the hand calculated ones. The total added mass matrix considers both the panel and the Morison model, meaning all columns, pontoons and cross braces. The total damping matrix includes potential damping and damping due to viscous drag, following Morison's theory. Both matrices are computed by Wadam for each of the predefined 26 wave frequencies, allowing a visualization of the frequency dependence of added mass and damping, by plotting the matrix components with respect to the wave frequency.

Further calculations, based on the system matrices, are performed in MATLAB. The natural frequencies in heave and pitch are determined by means of Equation 13, given in Subsection 3.3.1. With the frequency-dependent added mass components, different results are obtained for the 26 wave frequencies. The real natural frequency is determined as the intersection point between the interpolated calculated results plotted against the wave frequency, and the angle bisector, representing the wave frequencies plotted against the wave frequencies itself. Those natural frequencies can be compared with the eigensolutions from Wadam, as well as with the results from the hand calculations.

The nominal pitch is computed based on Equation 50, given in Section 4.1, with the stiffness component in pitch obtained from the Wadam output.

4.2.3 Motion Response Analysis

The analysis of the motion response is, besides the previously determined parameters, also based on the excitation \underline{F} . The main excitation is in surge, heave and pitch, due to the loading direction at zero heading. The exciting forces and moments are complex values.

The response amplitude operator (RAO) for each single DoF can be computed by means of Equation 51, based on the equation of motion for floating structures, given in Equation 12 in Subsection 3.3.1.

$$\left| \text{RAO}_{\underline{q}}(\omega) \right| = \left| [\mathbf{C} + i\omega\mathbf{B}(\omega) - \omega^2(\mathbf{M} + \mathbf{A}(\omega))]^{-1} \underline{F}(\omega) \right| \quad (51)$$

In Equation 51, matrix left division is executed, written in terms of pre-multiplication with the inverse of the matrix in the square brackets. The RAO is, as presented in Equation 51, the absolute value of the complex calculation. The peak of the RAO is expected to occur at the natural frequency of the considered DoF.

The standard deviation of the motion response $\sigma_{\underline{q}}$ is a good measure of the dynamic response. The standard deviation can be obtained from the response spectrum $S_{\underline{q}}(\omega)$, which in turn depends on the wave spectrum. 15 wave spectra for different representative environmental conditions [3], given in Table 4.1, are generated by means of Pierson-Moscowitz's wave spectrum definition, given in Equation 52 [44]. The environmental conditions are defined by the significant wave height H_s and peak wave period T_p , from which the peak wave frequency f_p directly follows as its inverse. The resulting wave spectra are shown exemplarily for five condition numbers in Figure 4.2.

$$S_{\text{PM}}(f) = 0.3125 H_s^2 f_p^4 f^{-5} \exp \left[-1.25 \left(\frac{f_p}{f} \right)^4 \right] \quad (52)$$

Based on the wave spectra and the previous derived RAOs, the response spectra can be computed by means of Equation 53 [28]. The wave spectrum as function of the angular frequency is obtained by substituting the frequency f in Equation 52 by $\omega(2\pi)^{-1}$.

$$S_{\underline{q}}(\omega) = S_{\text{PM}}(\omega) \left| \text{RAO}_{\underline{q}}(\omega) \right|^2 \quad (53)$$

The standard deviations of the motions are finally obtained based on the generated response spectra, as given in Equation 54 [28].

$$\sigma_{\underline{q}} = \sqrt{\int_0^{\infty} S_{\underline{q}}(\omega) d\omega} \quad (54)$$

Table 4.1: Wave parameters of 15 representative environmental conditions [3]

| Condition number | Significant wave height H_s [m] | Peak wave period T_p [s] | Peak wave frequency f_p [Hz] |
|------------------|--------------------------------------|-------------------------------|-----------------------------------|
| 1 | 1.25 | 4 | 0.250 |
| 2 | 1.25 | 6 | 0.167 |
| 3 | 1.25 | 8 | 0.125 |
| 4 | 2.75 | 6 | 0.167 |
| 5 | 2.75 | 8 | 0.125 |
| 6 | 2.75 | 10 | 0.100 |
| 7 | 2.75 | 12 | 0.083 |
| 8 | 3.75 | 6 | 0.167 |
| 9 | 3.75 | 8 | 0.125 |
| 10 | 3.75 | 10 | 0.100 |
| 11 | 3.75 | 12 | 0.083 |
| 12 | 5.25 | 8 | 0.125 |
| 13 | 5.25 | 10 | 0.100 |
| 14 | 5.25 | 12 | 0.083 |
| 15 | 6.75 | 12 | 0.083 |

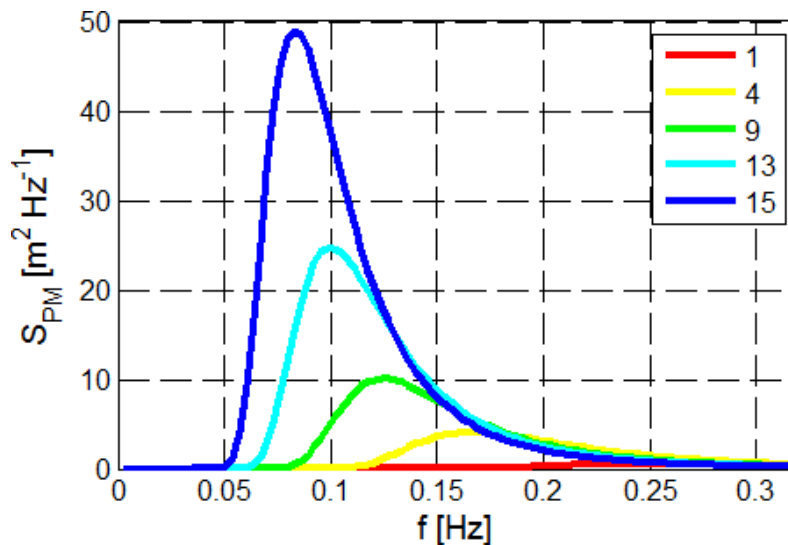


Figure 4.2: Pierson-Moscowitz wave spectra for different environmental conditions

4.3 Analysis Based on Modelica and Dymola

For simulation of the entire floating wind turbine system, Modelica and Dymola are used. The modelling language Modelica is perfectly suited for describing complex physical systems, as it supports several domains, like electrical, mechanical, hydraulic, and control objects. Programming in Modelica is equation-based and object-oriented. With single models being interconnected, complex dynamic systems can be simulated. Dymola, originally standing for Dynamic Modelling Language, but then developed into Dynamic Modelling Laboratory, is used as simulation environment for Modelica. Besides a Modelica compiler, it also includes a graphic user interface and text editor, so that Modelica models can directly be edited within Dymola. [18]

4.3.1 Implementation in Modelica

The floating wind turbine system is implemented in Modelica by means of several single models, using the OneWind[®] Modelica Library (see Appendix A.3 for further information). Each component has frames, which could be connected with each other, and at which forces, moments, displacements, and rotations are transferred. The model world is used as reference, with the coordinate system fixed to the SWL, and the earth acceleration acting in negative z -direction.

4.3.1.1 Top Structure The top structure is divided into rotor, nacelle, operating control, and tower. The rotor model consists of the hub and one blade model, extended to a three-bladed rotor. The blades are implemented as flexible bodies, based on a FEM model. The aerodynamic parameters, needed for the BEM calculation, are also defined in the model of the rotor.

The model of the nacelle includes drivetrain, generator, and yaw controller. A separate model contains all input parameters, like nacelle mass, dimensions and inertias, drivetrain properties, and generator type.

The operating control covers pitch and generator torque control, bus system between operating control, nacelle and rotor, as well as different operating phases, like idling or shutdown. A separate model, again, defines all input parameters for the control units. There, the blade-pitch controller gains and the value of the pitch angle at doubled blade-pitch sensitivity have to be changed according to the designed floating system.

The tower is modelled either as rigid or flexible body. The original wind turbines (NREL 5 MW, IWT 7.5 MW and DTU 10 MW) are designed with a tower reaching to ground or SWL level. For the floating system designs, the tower model is adjusted by removing all tower elements below the top level of the main column, and shortening the now remaining lowest element, so that it starts directly on top of the main column. For the rigid tower model, the procedure is implemented by means of functions, and directly executed when running the simulation. However, for the flexible tower model, the FEM model has to be created, based on the new tower dimensions, prior to the simulation.

4.3.1.2 Support Structure The semi-submersible platform is implemented by interconnecting cylindrically shaped structure elements for the columns, pontoons and cross braces, as well as for the ballast in the columns. By specifying material density and cylinder dimensions, weight and center of gravity of the platform are directly included.

The hydrostatic forces on the floating platform, however, have to be added manually. Buoyancy force and center of buoyancy are calculated for each column at each time step, depending on the actual local heave and pitch, following the detailed stability calculation in Appendix A.1. By setting the buoyancy force application point at the center of buoyancy, the resulting waterplane restoring moment does not have to be defined separately.

The hydrodynamic forces are computed based on Morison's equation, given in Equation 25 in Subsection 3.4.1. Only upper, base and main columns are considered, Morison loads on cross braces and pontoons are neglected. The columns are divided into several elements, shorter at the upper parts close to SWL, in order to improve the accuracy of the Morison load calculation. Due to the large column diameters, MacCamy-Fuchs approximation has to be used for the determination of the added mass coefficient. For the added mass of the heave plates in vertical direction, a reference volume V_R is defined, replacing the term $\frac{1}{4}D^2\pi \partial z$ in the added mass part of Morison's equation (Equation 25). This reference volume is computed based on Equation 55, using the low-frequency limit of the added mass in heave, obtained by the Wadam calculation in HydroD, and setting the added mass coefficient in z -direction equal to $C_{a,z} = 1$. [62]

$$V_R = \frac{\frac{1}{3} A_{33}|_{\omega \rightarrow 0}}{\rho_{\text{water}} C_{a,z}} \quad (55)$$

The factor of $\frac{1}{3}$ in Equation 55 is based on the assumption that the added mass in heave mainly comes from the three base columns, and the contribution of the main column can be neglected.

The platform parameters are defined in a separate model. The main data, like cylinder diameters, wall thicknesses, heights, drag and added mass coefficients, pontoon elevations, initial draft, steel and ballast densities, column distances, and ballast heights, have to be given as input. All other parameters, like pontoon lengths and position of the columns with respect to the world coordinate system, as well as the variable buoyancy force, are defined based on those values.

4.3.1.3 Station-Keeping System The mooring system was implemented within the bachelor's thesis [17]. The mooring lines are divided into several elements, each modelled as mass-spring-damping system. Velocity dependent damping (Morison damping), as well as inner damping are considered. Weight and buoyancy due to the lifted parts of the mooring lines are computed. Furthermore, bottom contact reaction forces are taken into account. The shape of the mooring lines and the effective lengths are internally determined at each time step, based on catenary equation, mooring line parameters, and actual fairlead positions. For the first time step, however, an initial value for the bottom contact length has to be provided as input. This can be computed according to Appendix A.4.

4.3.1.4 Environment The environmental conditions are given by wind and waves, not considering any currents. In the wind model, the wind type can be chosen, for example steady, ramped or turbulent wind, but also up- or downwind turbines can be modelled, and the wake can be additionally calculated. The general parameters, like hub wind speed, density and dynamic viscosity of air, wind direction, and flow inclination, have to be specified in the input data model. Furthermore, tower shadow and gust can be taken into account, as well as wind shear, based on the specified guideline and wind turbine class.

Two wave models exist, either for regular or irregular waves. Water depth and density, significant wave height, peak period, and phase angle, as well as the stretching method (Wheeler, linear extrapolation or none) have to be defined for both models. In addition, wave spectrum model (Pierson Moskowitz or JONSWAP), as well as number of frequencies and number of seeds, for generating the different waves with random phase angles, have to be specified for the irregular wave model.

4.3.2 Simulation and Results

Figure 4.3 shows the implemented floating wind turbine system, simulated in Dymola.

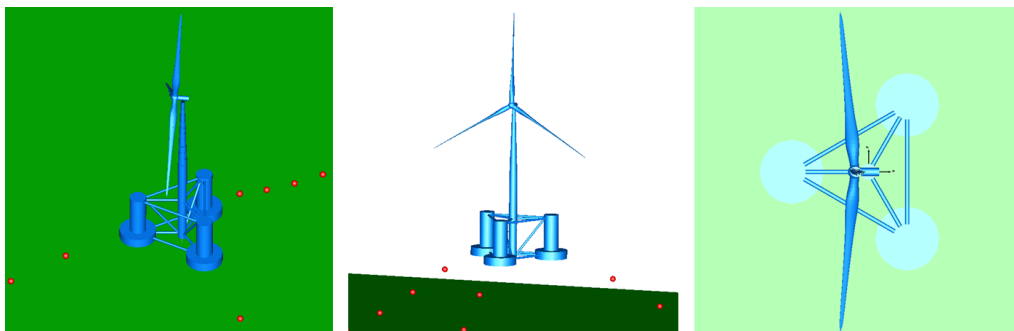


Figure 4.3: Floating wind turbine system in Dymola, based on Modelica

For the analysis of the floating wind turbine systems, different simulations are run in Dymola.

4.3.2.1 Free Decay Tests At first, free decay tests in surge, heave, pitch and yaw are performed with no waves, no air, the generator locked, the controllers turned off, and the blades in idling position, with one blade pointing straight upwards. The initial displacements and the simulation lengths are directly taken from the load case description for OC4 [42]. The initial bottom contact length of each mooring line is re-calculated, based on the initial displacements, the geometrical arrangement, and Source Codes A.5 to A.7 in Appendix A.4.

From the resulting time series, the natural frequencies can either be determined by counting the number of oscillations and dividing by the time, or by performing a FFT calculation in Dymola. The accuracy of the latter method, however, depends on the chosen output interval length for the simulation. A smaller interval length would improve the FFT results, but at the same time increase the simulation effort. As time and capacities are limited, it is rather recommended to obtain the natural frequencies from the counting method.

4.3.2.2 Full-System Analysis Based on the results from the free decay test in pitch, the integral and proportional controller gains, as well as the value for the blade-pitch angle at doubled blade-pitch sensitivity are re-calculated, following the method explained in Subsection 3.6.2, and modified in the Modelica models.

Those floating-adapted wind turbine systems are simulated at different wind speeds without waves. A ramped wind model is defined, starting at a wind speed at hub height of 1 ms^{-1} and going in 13 steps of each 2 ms^{-1} up to 27 ms^{-1} , covering the entire operational range of the wind turbine. Each wind speed is run for 1000 s. The duration of the linear rise at the ramps is set to 10 s. From those time series, the platform performance depending on the wind speed can be analyzed, and also the controller settings checked.

A separate simulation is performed at rated or in the range of rated wind speed, in order to obtain the nominal pitch at maximum thrust, directly before the blades start pitching.

The dynamic performance of the floating wind turbine system is analyzed by simulating at the same wind speeds as before, but now with irregular waves. Due to limited time, only one sea state is considered. Eight different periodic sea states were defined in the OC4-project [41], as given in Table 3.4 in Subsection 3.4.2. The second most severe sea state number seven is chosen, as its significant wave height $H_s = 9.14 \text{ m}$ corresponds approximately to the average of the significant wave heights with a return period of one year at the different offshore regions, presented in the Offshore Standard DNV-OS-J103 [53]. The corresponding peak period is $T_p = 13.6 \text{ s}$ [41]. Ten frequencies are used for the irregular wave. The JONSWAP wave spectrum is selected, although a two-peaked spectrum model would represent the environment more accurate [53].

Based on the simulations in Dymola without and with irregular waves at different wind speeds, the mean values and standard deviations for the main platform motions (surge, heave, pitch) and the blade-pitch angle are computed with the help of MATLAB. Excluding the transient response at the beginning of each wind speed, only the second 500 s are used for the analysis.

4.4 Verification of the Analysis Methods and Implemented Models

In order to examine the accuracy of the analysis methods and verify the correctness of the implemented models in HydroD and Modelica, the system performance of the original OC4 semi-submersible floater, carrying the adjusted NREL 5 MW wind turbine, is analyzed by means of the three methods, presented in Sections 4.1 to 4.3. The results are compared with each other, as well as with the data from the OC4 definition [41] and the code-to-code comparisons [42].

4.4.1 Verification of the Determination of the Drag Coefficients

First of all, the approximate determination of the drag coefficients for the columns, described in Subsection 3.4.2, is verified. The manually determined values are presented in Table 4.2, together with the specified values [41].

Table 4.2: Comparison of the drag coefficients of the original OC4 floating system

| | CB ($D = 1.6 \text{ m}$) | MC ($D = 6.5 \text{ m}$) | UC ($D = 12 \text{ m}$) | BC ($D = 24 \text{ m}$) |
|---------------|----------------------------|----------------------------|---------------------------|---------------------------|
| Manually | 0.54 | 0.62 | 0.67 | 0.70 |
| Original [41] | 0.63 | 0.56 | 0.61 | 0.68 |

It can be seen that there is a difference between the manually determined drag coefficients and those, defined for the original OC4 semi-submersible floater. This is on the one hand due to inaccuracies in reading out the correct values from a printed graph. The main reason for this discrepancy, however, may be due to differences in the plots, as [41] also refers to [10], but the printed graph deviates from Figure 3.6 by [10], presented in Subsection 3.4.2. Since the latter one is the initial source, Figure 3.6 is, despite those discrepancies, still used for the determination of the drag coefficients in the further work.

4.4.2 Verification of the Static Analysis Methods

4.4.2.1 System Matrices For the comparison and verification of the analysis methods, the obtained mass, added mass and stiffness matrices in heave and pitch are presented in Table 4.3, together with the data of the original DeepCwind semi-submersible floater [41]. Figures 4.4 and 4.5 show, additionally, the frequency dependence of added mass and damping, comparing the results obtained by the Wadam run in HydroD with the original data from [41].

Table 4.3: Comparison of the system matrices of the original OC4 floating system

| Parameter | Unit | Calculated | HydroD | Modelica | Original [41] | |
|-----------|----------------|------------------------------|----------|----------|---------------|----------|
| M_{33} | kg | 14.26E+6 | 14.26E+6 | 14.26E+6 | 14.26E+6 | |
| M_{55} | kgm^2 | 1.71E+10 | 1.71E+10 | — | — | |
| A_{33} | kg | $ \omega \rightarrow 0$ | 13.37E+6 | 15.26E+6 | — | |
| | | $ \omega \rightarrow \infty$ | — | 14.53E+6 | — | 14.70E+6 |
| A_{55} | kgm^2 | $ \omega \rightarrow 0$ | 6.08E+9 | 7.66E+9 | — | — |
| | | $ \omega \rightarrow \infty$ | — | 7.24E+9 | — | 7.21E+9 |
| C_{33} | $kg s^{-2}$ | 3.822E+6 | 3.819E+6 | — | 3.836E+6 | |
| C_{55} | $kgm^2 s^{-2}$ | 1.241E+9 | 1.325E+9 | — | 1.235E+9 | |

From Table 4.3 it can be observed that the system matrices, obtained by the Wadam run in HydroD, correlate very well with the original values. The low-frequency limits for the added mass components, as well as concrete values for the damping, are not explicitly given for the original floater. But from the comparison with the available plots in Figures 4.4(b) and 4.5(b), the conclusion could be drawn that the chosen discretization of the finite element mesh in GeniE and the implemented model in HydroD are very accurate. Only small variations in the frequency-dependent curves could not be covered by HydroD, as a limited number of frequencies is selected for the analysis. If more frequencies and finer intervals were chosen, it is expected to obtain more detailed frequency-dependent curves, even more similar to the original plots.

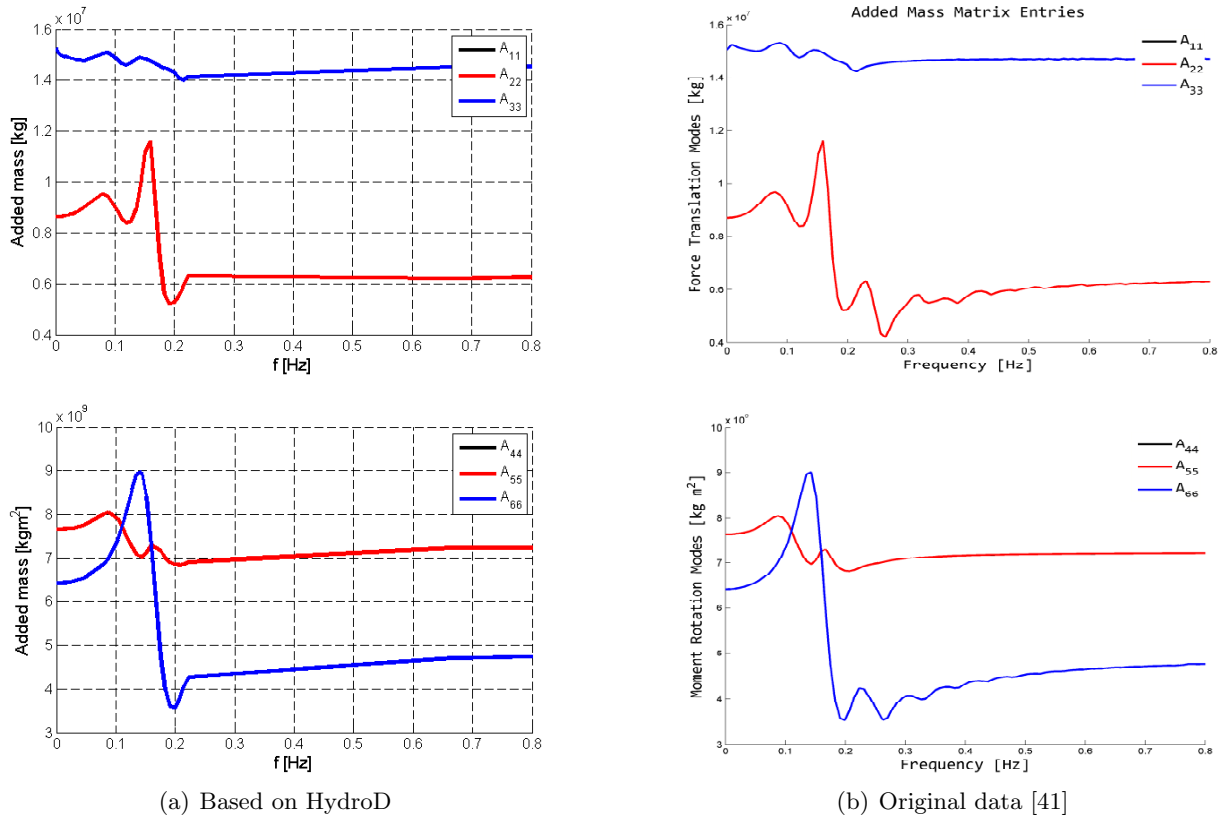


Figure 4.4: Diagonal terms of the frequency-dependent added mass matrix of the original OC4 system

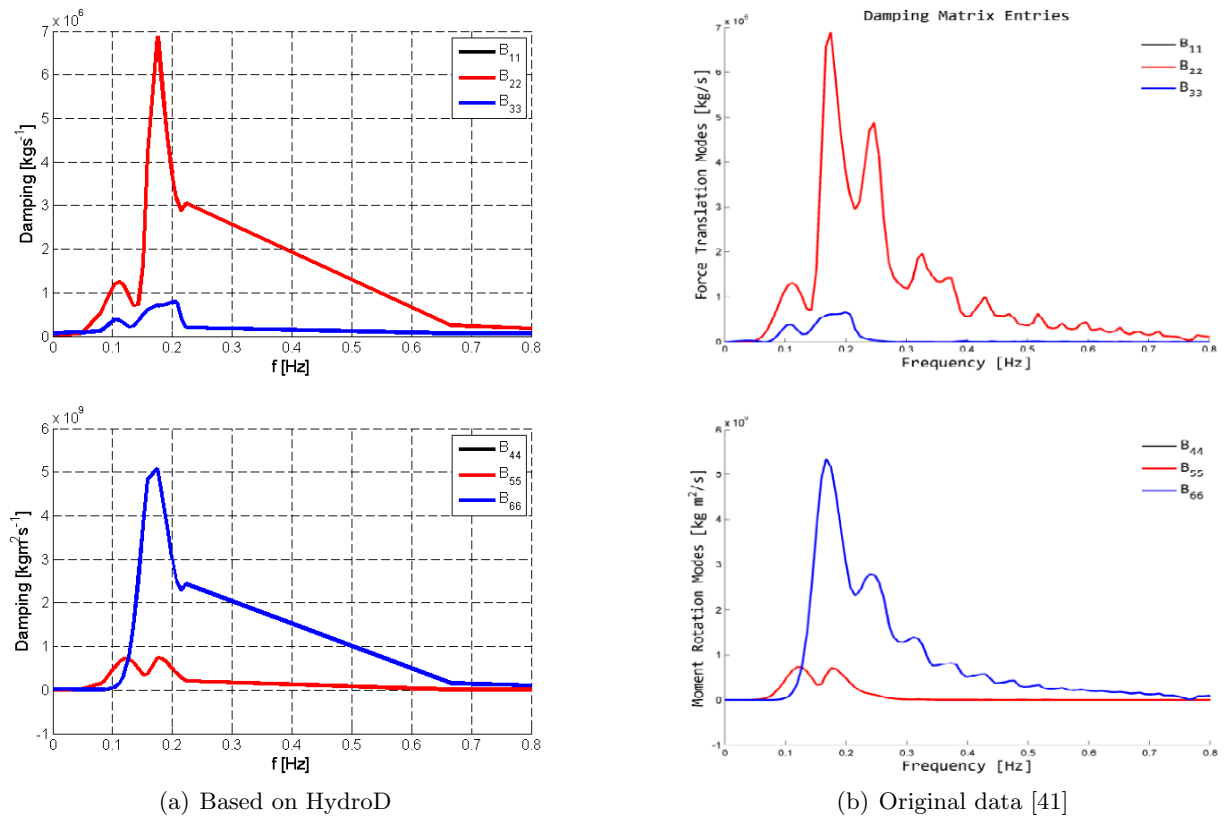


Figure 4.5: Diagonal terms of the frequency-dependent damping matrix of the original OC4 system

The equation-based determination of the stiffness components is quite accurate. Comparison of the calculated low-frequency added mass limits with the HydroD results, shows that the hand computations underestimate the added mass by up to 20%. This leads to the conclusion that Equations 19 and 24, presented in Section 3.3, are only rough estimates for the added mass.

From the analysis based on Modelica, no further system matrices besides the mass can be obtained, as those parameters are not explicitly defined as output.

4.4.2.2 Nominal Pitch As the stiffness matrix components are comparable for all analysis methods, also the nominal pitch is similar and amounts 3.0° , when considering the lever from hub to center of buoyancy (-13.17 m), as explained in Paragraph 3.2.2.4 and Section 4.1, and using a rated thrust force of $6.774\text{E} + 5\text{ N}$, based on calculations in [3]. The simulation in Dymola yields a slightly larger nominal pitch of around 3.16° . The difference may result from the mooring line model in Modelica, as well as the fact that the real point of rotation differs from the center of buoyancy. The latter one, however, would rather result in a smaller nominal pitch, leaving the mooring system as the main reason for the increased nominal pitch.

4.4.2.3 Stability The hand calculations yield that the system should be stable within the range of $[-19.0^\circ, 18.9^\circ]$. From the detailed stability analysis in HydroD the moment curve, shown in Figure 4.6, is obtained. This analysis results in a stability range of $[-103.6^\circ, 97.9^\circ]$.

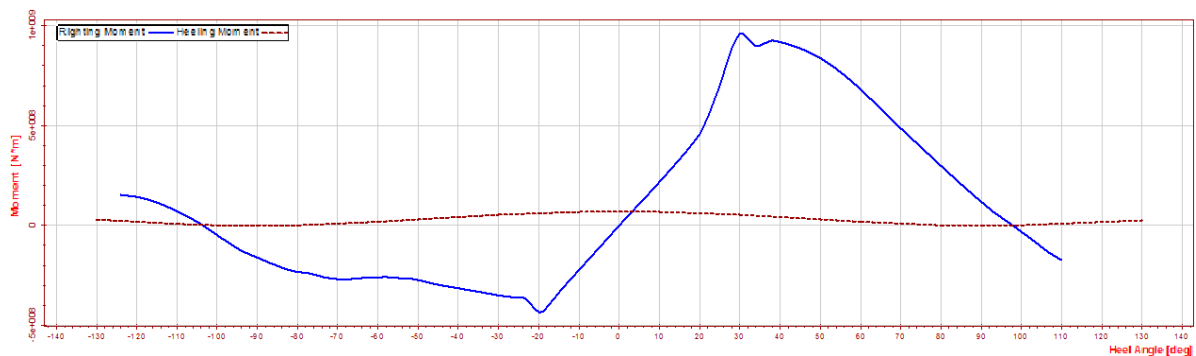


Figure 4.6: Moment curves of the original OC4 system

The area under the righting moment curve to the second intercept with the wind heeling moment curve is by a factor of 16 larger than the area under the wind heeling moment curve to the same limiting angle. In this entire range, the righting moment is positive. Thus, the intact floating stability criteria, specified in Paragraph 3.2.2.4, are fulfilled.

4.4.2.4 Natural Periods Figure 4.7 shows a comparative plot of the free decay time series. However, no numerical data for the time series in pitch of the original OC4 floater is available [42].

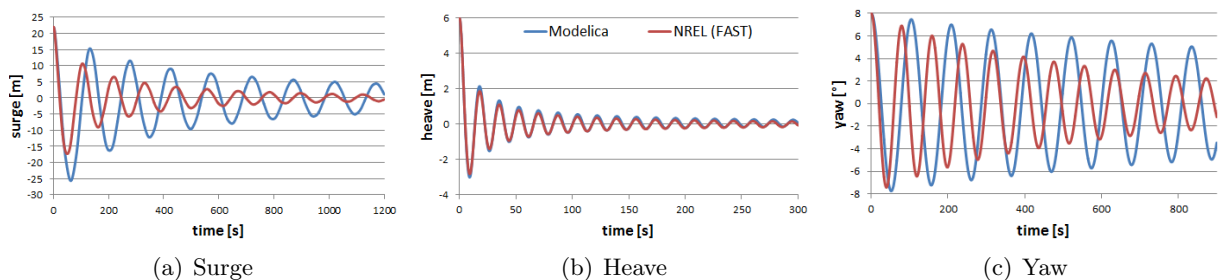


Figure 4.7: Free decay time series of the original OC4 system, Modelica and FAST-calculation by NREL [42] in comparison

Table 4.4: Comparison of the natural periods of the original OC4 floating system

| Parameter | Unit | Calculated | HydroD | | Modelica | | Original [41] |
|--------------------|------|------------|----------|---------------|----------|-------|------------------|
| | | | Computed | Eigensolution | Counted | FFT | |
| $T_{\text{nat},1}$ | s | — | 113.0 | — | 146.4 | 150.0 | 112.2 |
| $T_{\text{nat},3}$ | s | 16.7 | 17.4 | 17.4 | 17.4 | 17.6 | 17.4 |
| $T_{\text{nat},5}$ | s | 26.3 | 27.2 | 26.2 | 25.7 | 25.0 | 27.0 |
| $T_{\text{nat},6}$ | s | — | 79.4 | — | 104.3 | 100.0 | 79.3 |

The obtained natural periods are compared in Table 4.4. The hand calculated values are slightly smaller than the original ones, because the equation-based added mass components are underestimated, as already discussed. The results for the natural periods, obtained by computations based on the Wadam output, are more accurate. Wadam’s eigenanalysis, however, is incomplete and less accurate, as it yields no results for the natural periods in surge and yaw, and underestimates the pitch natural period. Thus, the eigensolutions are not used in the further analyses of the designed floating platforms. From the simulation in Modelica two values for each natural period can be obtained, as described in Paragraph 4.3.2.1. As already indicated there, the FFT calculation is not as accurate as the counting method. The heave natural period is comparable with the original value. The natural period in pitch is slightly underestimated. The natural periods in surge and yaw, however, are significantly higher than the original values. This is mainly due to the implemented mooring system, which is also one of the reasons for the differences in the code-to-code comparison in the OC4-project [42].

4.4.2.5 Controller Gains Finally, also the method for the determination of the blade-pitch sensitivity at rated and the rotor-collective blade-pitch angle at doubled pitch sensitivity, covered in Appendix A.2, has to be proved. The computed values are presented in Figure 4.8(a) and compared with the original data used for the OC4 semi-submersible [31], shown in Figure 4.8(b).

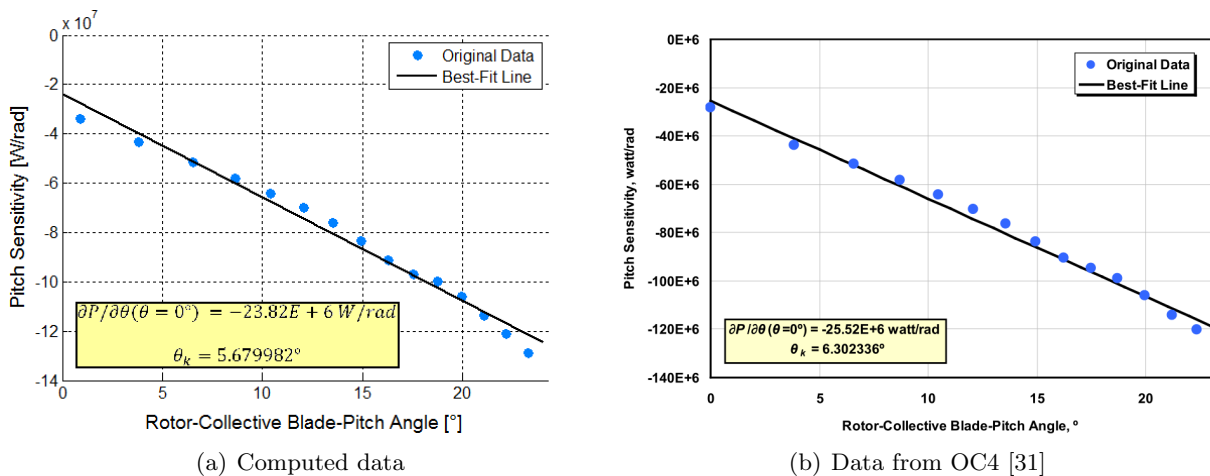


Figure 4.8: Best-fit line of pitch sensitivity above rated wind speed for the NREL 5 MW

The calculated and original values seem to correlate quite well, except for the first point. This one is computed directly at rated wind speed of 11.4 ms^{-1} . The concrete numbers for the pitch angles and blade-pitch sensitivities at discrete wind speeds are presented in Table 4.5, for a more detailed comparison. It can be seen that the values are not exactly the same, however, the differences are, for both pitch angles and pitch sensitivities at wind speeds above rated, maximum 2%, and mostly even less than 1%. Directly at rated wind speed, a pitch angle of

Table 4.5: Sensitivity of aerodynamic power to blade-pitch for the NREL 5 MW

| Wind speed [$m s^{-1}$] | Rotor speed [rpm] | Calculated values | | Original values [31] | |
|------------------------------|--------------------------|-------------------------------|---|-------------------------------|---|
| | | Pitch angle [$^{\circ}$] | $\partial P/\partial\theta$ [$W rad^{-1}$] | Pitch angle [$^{\circ}$] | $\partial P/\partial\theta$ [$W rad^{-1}$] |
| 11.4 - rated | 12.1 | 0.90 | -33.61E+6 | 0.00 | -28.24E+6 |
| 12.0 | 12.1 | 3.78 | -43.34E+6 | 3.83 | -43.73E+6 |
| 13.0 | 12.1 | 6.51 | -51.38E+6 | 6.60 | -51.66E+6 |
| 14.0 | 12.1 | 8.60 | -57.88E+6 | 8.70 | -58.44E+6 |
| 15.0 | 12.1 | 10.39 | -64.10E+6 | 10.45 | -64.44E+6 |
| 16.0 | 12.1 | 12.02 | -69.78E+6 | 12.06 | -70.46E+6 |
| 17.0 | 12.1 | 13.52 | -76.03E+6 | 13.54 | -76.53E+6 |
| 18.0 | 12.1 | 14.92 | -83.32E+6 | 14.92 | -83.94E+6 |
| 19.0 | 12.1 | 16.25 | -91.12E+6 | 16.23 | -90.67E+6 |
| 20.0 | 12.1 | 17.51 | -96.74E+6 | 17.47 | -94.71E+6 |
| 21.0 | 12.1 | 18.74 | -99.52E+6 | 18.70 | -99.04E+6 |
| 22.0 | 12.1 | 19.93 | -105.95E+6 | 19.94 | -105.90E+6 |
| 23.0 | 12.1 | 21.07 | -113.79E+6 | 21.18 | -114.30E+6 |
| 24.0 | 12.1 | 22.17 | -121.07E+6 | 22.35 | -120.20E+6 |
| 25.0 | 12.1 | 23.24 | -128.56E+6 | 23.47 | -125.30E+6 |

0.90° is computed instead of the original value of 0.00° . The discrepancy in the corresponding blade-pitch sensitivity amounts around 19%.

As the trend line through all those single points is used for the further controller gain calculation, a closer look is taken at the blade-pitch sensitivity at rated $\left.\frac{\partial P}{\partial\theta}\right|_{\theta_{\text{rated}}}$ and the rotor-collective blade-pitch angle θ_K , at which the pitch sensitivity has doubled from its rated value. Those parameters are already presented in Figures 4.8(a) and 4.8(b) for the manually determination method and the original OC4 floating wind turbine system, respectively. Taking the pitch sensitivity at the computed rated pitch angle would slightly overestimate the parameters in amount, while taking the value at zero pitch slightly underestimates the parameters in amount. The latter method is minimal more accurate.

For the final controller gain values, this means a discrepancy of around 7% between the computed values and the original data. This, however, is taken as insignificantly small. Thus, the method for determining $\left.\frac{\partial P}{\partial\theta}\right|_{\theta_{\text{rated}}}$ and θ_K , presented in Appendix A.2, is assumed to be accurate enough.

5 Initial Upscaling of the DeepCwind Semi-Submersible Platform

In order to obtain an initial floating platform design for the IWT-7.5-164 wind turbine, an elementary upscaling procedure is performed, based on the original DeepCwind semi-submersible platform. By means of hand calculations and computations in HydroD, the system's performance is analyzed, and potential problems with the upscaling are identified. This chapter mainly covers the work done in the preceding research project.

5.1 Initial Upscaling Procedure

The initial upscaling of the semi-submersible floater mainly follows the theoretical scaling laws, introduced in Subsection 3.1.1. The scaling factor is thus determined in Equation 56 from the power rating of the two wind turbines IWT-7.5-164 and NREL 5 *MW* to be $k = 1.225$.

$$k = \sqrt{\frac{7.5}{5}} \approx 1.225 \quad (56)$$

Because of geometrical boundary conditions, this scaling factor cannot be applied to the entire floating platform, as the main column would then have a diameter of 7.96 *m*, and thus be larger than the given tower base diameter (7.0 *m*) of Fraunhofer's wind turbine. The diameter of the main column, therefore, has to be scaled with a smaller scaling factor of $k_{MC} \approx 1.077$, so that it matches the tower base dimension. To maintain the proportions, the wall thickness of the main column is also scaled with this smaller scaling factor. Draft and vertical positions of brace and pontoon connections are, however, scaled with the initial factor based on the power rating. The lengths of braces and pontoons can be determined from the geometrical arrangement. The fixed hub height at 111.6 *m* above SWL makes up another boundary condition. As the wind turbine is placed on top of the main column, which scales with k_{MC} , the bottom part of the tower has to be cut at the top level of the upscaled main column, meaning at 12.25 *m*.

For the mooring system design, it is assumed that the upscaled floater is located at the same water depth (200 *m*), and anchor positions, as well as mooring line dimensions and physical parameters remain unchanged. Effective length, weight and center of gravity of the lifted mooring line parts are computed based on Equations 32, 34, 35 and 37, derived in Subsection 3.5.2.

The final dimensions are given in Table 5.1, including the data of the original DeepCwind floater and the applied scaling factors. The reference values for the drag coefficients are based on the procedure described in Subsection 3.4.2, the original values from [41] are added in brackets. The center of buoyancy of the initially upscaled design is located 16.18 *m* below SWL.

The total weight of the upscaled system, including wind turbine, mooring system and platform, but excluding any ballast in the offset columns, is computed to be $W = 7.954E + 7$ *N*, based on Equation 5 in Subsection 3.2.1. The buoyancy force amounts $F_B = 25.441E + 7$ *N*, following Equation 6 in Subsection 3.2.1. At this stage, the offshore wind turbine system is not yet a floating structure. In order to fulfill Equation 4, while maintaining the upscaled draft of the platform, 1.783E+7 *kg* ballast are to be added. Focusing on stability, a deep as possible system's center of gravity is aimed, and achieved by ballasting first the base columns, and only if needed then also filling the upper columns. The required ballast volume depends on the density of the chosen ballast. Two different designs are considered, one with water, as it is used in the original DeepCwind floater, and the other one with concrete with a specific weight of 2.50E+4 *Nm*⁻³, corresponding to a density of 2,548.42 *kgm*⁻³. Concrete is chosen, because of its higher density. Thus, a deeper center of gravity can be obtained as less volume is needed. The final dimensions of the two ballast systems, with which equilibrium is achieved, are presented in Table 5.2.

Table 5.1: Main dimensions of the initially upscaled semi-submersible platforms, including the original DeepCwind platform dimensions and applied scaling factors

| Element | Parameter | Unit | k | Initially upscaled | Original OC4 [41] |
|----------------|---------------------------------|------|----------|--------------------|-------------------|
| MC | Diameter | m | k_{MC} | 7.00 | 6.50 |
| | Wall thickness | m | k_{MC} | 0.032 | 0.030 |
| | Elevation above SWL | m | k | 12.25 | 10.00 |
| | Depth of base below SWL | m | k | 24.49 | 20.00 |
| | Drag coefficient | — | — | 0.62 | 0.62 (0.56) |
| OC | Wall thickness | m | k | 0.073 | 0.060 |
| | Elevation above SWL | m | k | 14.70 | 12.00 |
| | Spacing between OCs | m | k | 61.24 | 50.00 |
| | Depth of base below SWL | m | k | 24.49 | 20.00 |
| UC | Diameter | m | k | 14.70 | 12.00 |
| | Length | m | k | 31.84 | 26.00 |
| | Drag coefficient | — | — | 0.67 | 0.67 (0.61) |
| BC | Diameter | m | k | 29.39 | 24.00 |
| | Length | m | k | 7.35 | 6.00 |
| | Drag coefficient | — | — | 0.70 | 0.70 (0.68) |
| Pontoons, CBs | Diameter | m | k | 1.96 | 1.60 |
| | Wall thickness | m | k | 0.0214 | 0.0175 |
| | Drag coefficient | — | — | 0.55 | 0.54 (0.63) |
| Upper pontoons | Length DU | m | k | 46.54 | 38.00 |
| | Length YU | m | — | 24.51 | 19.62 |
| | Elevation above SWL | m | k | 12.25 | 10.00 |
| Lower pontoons | Length DL | m | k | 31.84 | 26.00 |
| | Length YL | m | — | 17.16 | 13.62 |
| | Depth below SWL | m | k | 20.82 | 17.00 |
| CB | Length | m | — | 39.53 | 32.04 |
| | Elevation above SWL | m | k | 11.18 | 9.13 |
| | Depth below SWL | m | k | 19.84 | 16.20 |
| Mooring system | Depth to fairleads below SWL | m | k | 17.15 | 14.00 |
| | Depth to anchors below SWL | m | 1 | 200 | 200 |
| | Radius to fairleads | m | k | 47.91 | 40.87 |
| | Radius to anchors | m | 1 | 837.6 | 837.6 |
| | Unstretched mooring line length | m | 1 | 835.5 | 835.5 |
| | Effective mooring line length | m | — | 475.2 | 594.4 |
| Masses | RNA | kg | — | 4.934E+5 | 3.500E+5 |
| | Tower | kg | — | 443,434 | 249,718 |
| | Platform steel | kg | — | 7.016E+6 | 3.852E+6 |

Table 5.2: Main dimensions of the two ballast systems

| Ballast | | Water | Concrete |
|--|------------|----------|----------|
| Density | kgm^{-3} | 1,025 | 2,548.42 |
| Total volume | m^3 | 17,390.6 | 6,994.7 |
| Height in UC | m | 5.7665 | 0 |
| Height in BC | m | 7.2015 | 3.4705 |
| Center of gravity of ballast below SWL | m | 16.25 | 22.65 |
| Center of gravity of system below SWL | m | 14.29 | 16.31 |

In the water ballasted system, the base columns are completely filled and the upper columns partly, whereas in the concrete ballasted system only the base columns are partly filled. For both designs, it is assumed that there are no internal structures in the columns, so that the entire inner volume can be used for ballasting. Table 5.2 shows that a deeper center of gravity, of both ballast and the entire system, is obtained for the concrete ballasted design.

5.2 Analysis of the Initially Upscaled Platform Designs

The analysis of the two initially upscaled semi-submersible floater designs for the IWT-7.5-164 covers static and dynamic performance, and is carried out based on hand calculations and simulations with HydroD, as introduced in Sections 4.1 and 4.2.

5.2.1 Static Analysis of the Initially Upscaled Platform Designs

5.2.1.1 System Matrices The system matrices for both initially upscaled floaters, with the two different ballast systems, are presented in Table 5.3, together with the values of the original DeepCwind semi-submersible platform for comparison.

The total system mass scales less than with the main scaling factor of 1.225 to the power of three, as the ratio of the top structure masses would yield a much smaller factor of just 1.160. This shows that technical development is not included in the theoretical upscaling. Comparing the two ballast systems, it can be seen from Table 5.3 that the mass components in the rotational DoFs are different, larger for the concrete ballasted design, due to the deeper center of gravity.

Added mass and damping are the same for both designs, as those values just depend on the geometry and not on the center of gravity. Figure 5.1 presents the frequency-dependencies of added mass and damping, which have similar trends compared to the original DeepCwind floater, shown in Figures 4.4 and 4.5 in Section 4.4. Due to symmetry, surge and sway, as well as roll and pitch components are the same. The added mass in heave is much larger than in surge and sway, which is caused by the bigger base columns, acting as heave plates. The added mass values in brackets, in Table 5.3, reflect that the approximate computation (upscaling of the given DeepCwind added mass parameters) is much more accurate than the hand calculated equation-based values. The added mass in heave is then just by 3.5% underestimated, and in pitch by 5.4%. The contribution of the main column to the added mass is hence almost negligible. Thus, the added mass components should rather be determined by upscaling of the original values with the main scaling factor, than computed based on the approximation Equations 19 and 24, given in Section 3.3. This recommendation, however, will only be a good advice, if the main relevant geometrical parts are scaled with the same scaling factor.

The hand calculation of the stiffness components, based on Equations 17 and 20 in Section 3.3, is very accurate and yields just by maximum 0.4% higher values than obtained in HydroD.

Table 5.3: Comparison of the system matrices of the initially upscaled platforms, added mass in brackets based on upscaling, values in brackets for the original OC4 floater from HydroD

| Parameter | Unit | Ballast | Calculated | HydroD | Original [41] | |
|-----------|---------------------------------|----------|------------|------------------------|---------------|------------|
| M_{33} | kg | water | 25.93E+6 | 25.93E+6 | 14.26E+6 | |
| | | concrete | 25.93E+6 | 25.93E+6 | | |
| M_{55} | kgm^2 | water | 3.84E+10 | 3.84E+10 | (1.71E+10) | |
| | | concrete | 4.25E+10 | 4.25E+10 | | |
| A_{33} | $ _{\omega \rightarrow 0}$ | kg | water | 24.54E+6 (27.01E+6) | 27.98E+6 | (15.26E+6) |
| | | | concrete | 24.54E+6 (27.01E+6) | 27.98E+6 | |
| | $ _{\omega \rightarrow \infty}$ | water | — | 26.54E+6 | 14.70E+6 | |
| | | concrete | — | 26.54E+6 | | |
| A_{55} | $ _{\omega \rightarrow 0}$ | kgm^2 | water | 16.47E+9 (19.87E+9) | 21.00E+9 | (7.66E+9) |
| | | | concrete | 16.47E+9 (19.87E+9) | 21.00E+9 | |
| | $ _{\omega \rightarrow \infty}$ | water | — | 19.87E+9 | 7.21E+9 | |
| | | concrete | — | 19.87E+9 | | |
| C_{33} | $kg s^{-2}$ | water | 5.620E+6 | 5.598E+6 | 3.836E+6 | |
| | | concrete | 5.620E+6 | 5.598E+6 | | |
| C_{55} | $kgm^2 s^{-2}$ | water | 2.810E+9 | 2.806E+9 | 1.235E+9 | |
| | | concrete | 3.324E+9 | 3.320E+9 | | |

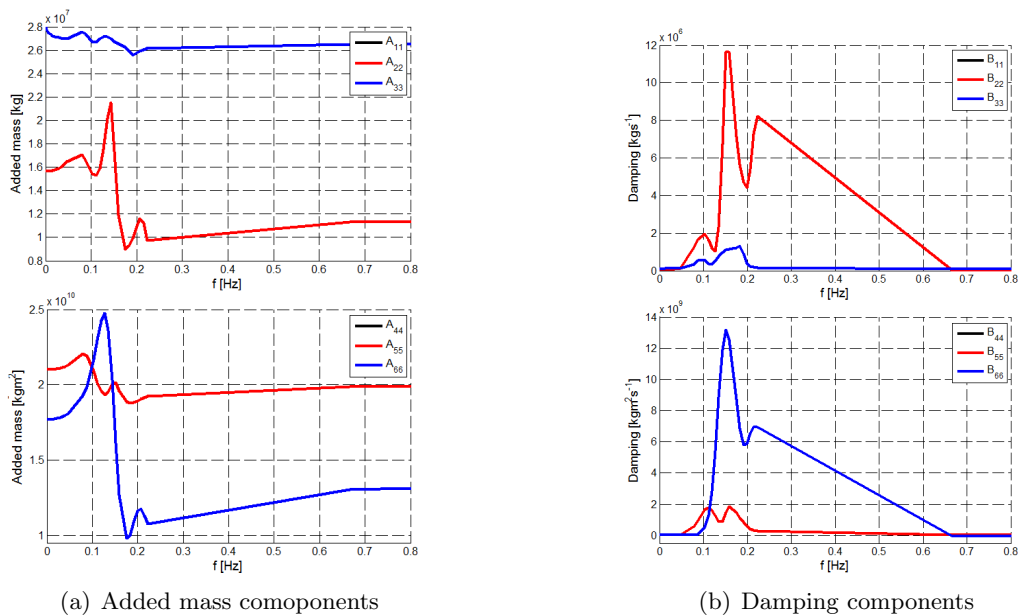


Figure 5.1: Diagonal terms of the frequency-dependent added mass and damping matrices of the initially upscaled platforms

Comparison with the original DeepCwind floater shows, that the stiffness in heave scales less than theoretically the scaling factor squared, which is mainly the effect of the smaller scaling of the main column. The stiffness component in pitch, however, is larger than the theoretically upscaled original value from the OC4 floater, as the ballast system is changed. Due to the deeper center of gravity in the concrete ballasted design, the corresponding stiffness component in pitch is larger than in the water ballasted system. As consequence, it is expected that the concrete ballasted floater design is more stable, but has a smaller natural period in pitch.

5.2.1.2 Nominal Pitch Including the mooring stiffness, the nominal pitch is computed for both designs, using the rated thrust force of the IWT-7.5-164 of about $F_{T,\text{rated}} = 1.155\text{E} + 6 \text{ N}$. The results are presented in Table 5.4. Due to the similar stiffness values based on the hand calculations and computations in HydroD, the same nominal pitch angles are obtained by both analysis methods. However, as the water ballasted system has a smaller stiffness in pitch than the concrete ballasted one, the first one experiences a by 0.44° higher nominal pitch.

Table 5.4: Nominal pitch of the initially upscaled platforms

| Ballast | Water | Concrete |
|-------------------|-------|----------|
| Nominal pitch [°] | 2.92 | 2.48 |

The nominal pitch is reduced from the original value of 3.0° for the OC4 floating system. According to the theoretical scaling laws, a decrease by a factor of k^{-1} is expected. This, however, is only in the concrete ballasted design almost obtained. The nominal pitch angle of the water ballasted design remains nearly unchanged. One reason for this different behavior is the increased stiffness in pitch due to the different ballasting method. The other reason is that thrust force and hub height scale higher than based on the main scaling factor. Thus, for the water ballasted design, the higher scaling of thrust force and hub height prevail, and counteract the theoretical scaling of the nominal pitch. For the concrete ballasted design, however, the larger scaling of the stiffness in pitch prevails and nearly compensates the higher scaling of thrust force and hub height, so that a decrease in the nominal pitch angle is obtained, which is coincidentally similar to the expected change following the theoretical scaling laws.

5.2.1.3 Stability Following the steps of the simplified stability analysis, explained in Paragraph 3.2.2.2, the outer top edge of the left upper column and the outer top edge of the left base column are determined as the first locations, at which the initial submerged geometry would change. The corresponding angles are $\theta_V = -16.7^\circ$ and $\theta_I = 18.9^\circ$. In this range, the initially upscaled floating systems are proved to be stable, based on the simplified check.

The more detailed stability analysis in HydroD yields a stability range of $[-104.2^\circ, 98.4^\circ]$ for the water ballasted design, and more than $[-124.0^\circ, 110.0^\circ]$ for the concrete ballasted design. The moment curves are plotted in Figure 5.2 (blue water, brown concrete ballasted floater).

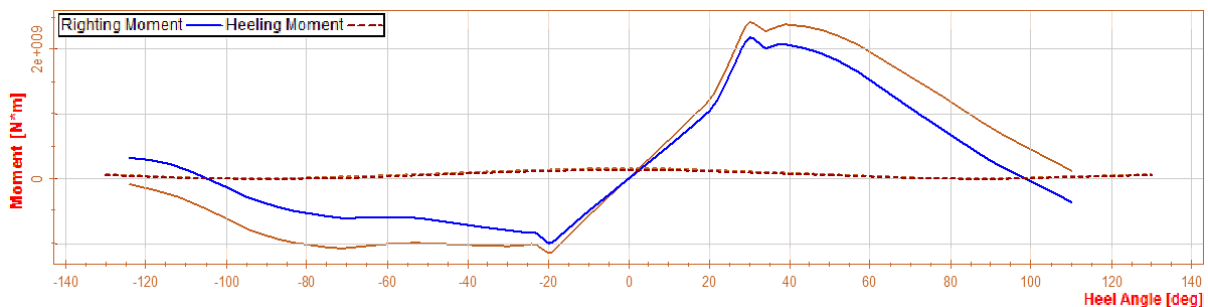


Figure 5.2: Moment curves of the initially upscaled platforms, blue line for water ballasted design, brown line for concrete ballasted design

The area under the righting moment curve to the second intercept with the wind heeling moment curve is by a factor of 16.7 for the water ballasted design, and even by a factor of at least 21.9 for the concrete ballasted design, larger than the area under the wind heeling moment curve to the same limiting angle. The intact floating stability requirements are more than fulfilled. The initially upscaled platforms rather turn out to be over-conservatively designed with respect to stability. Thus, some ballast could be moved into the upper columns without losing relevant stability, and a change in the ballast type, for obtaining higher stability, is not needed.

5.2.1.4 Natural Periods The natural periods of the initially upscaled designs for the IWT-7.5-164 are presented in Table 5.5, together with the values of the DeepCwind floater for the NREL 5 MW. The values in brackets are based on the added mass components determined by upscaling, as this turned out to be a more appropriate method than the equation-based one.

Table 5.5: Comparison of the natural periods of the initially upscaled platforms, added mass in brackets based on upscaling

| Parameter | Unit | Ballast | Calculated | HydroD | Original [41] |
|--------------------|------|----------|----------------|--------|---------------|
| $T_{\text{nat},1}$ | s | water | – | 152.1 | 112.2 |
| | | concrete | – | 152.1 | |
| $T_{\text{nat},3}$ | s | water | 18.8 (19.3) | 19.3 | 17.4 |
| | | concrete | 18.8 (19.3) | 19.3 | |
| $T_{\text{nat},5}$ | s | water | 27.3 (28.2) | 28.5 | 27.0 |
| | | concrete | 26.1 (26.9) | 27.2 | |
| $T_{\text{nat},6}$ | s | water | – | 132.3 | 79.3 |
| | | concrete | – | 132.6 | |

According to the theoretical scaling laws, it is expected that the natural periods scale with \sqrt{k} , and thus increase, which is a positive side effect of upscaling. The natural period in heave follows almost this theoretical scaling, as the different scaling of the main column has a minor effect. The natural period in pitch, however, scales with less than \sqrt{k} , because of the adjusted ballast system and the resulting deeper center of gravity. This effect is intensified in the concrete ballasted design, which has a by 1.3 s even more reduced natural period compared to the water ballasted one, and thus remains almost the same as for the original OC4 floater. This is another aspect, next to the over-conservatively dimensioned stability, why a change of the ballast type is not recommended, but rather the center of gravity should be lifted again, to obtain a higher natural period in pitch. Even if the natural period in heave is already increased due to upscaling, it is still on the lower bound of the typical range for semi-submersible floating platforms, close to the wave excitation period (see Table 1.1 in Section 1.2). A higher natural period in heave can be obtained by either decreasing the stiffness in heave and/or increasing the mass and/or added mass in heave. Choosing a smaller diameter for the upper columns and a larger diameter for the base columns, would decrease the waterplane area and thus the stiffness in heave, but increase the added mass. The change of the geometry would probably also influence the amount of displaced water volume, meaning that also an adjustment of the ballast and a change in the resulting total system mass have to be considered in the calculations for the optimization procedure.

The natural periods in surge and yaw are more increased than by a factor of \sqrt{k} , as the same mooring system parameters are used as in the OC4 design. Due to the unscaled radius of the anchor positions and the unchanged mooring line length, the mooring stiffness is significantly reduced. This leads to an increase in the natural periods, especially in surge and yaw, which are mainly influenced by the mooring system. It is thus recommended, also to adjust the mooring system parameters of the upscaled platform design, so that more reasonable values for the natural periods in surge and yaw are obtained.

5.2.2 Dynamic Analysis of the Initially Upscaled Platform Designs

5.2.2.1 Response Amplitude Operators Based on the hydrodynamic analysis in HydroD, the RAOs are determined, according to Equation 51 in Subsection 4.2.3. The RAOs for the translational motions are identical, due to the same stiffness and mass matrix components, and thus only once plotted in Figure 5.3(a). The RAOs for the rotational motions, however, differ for the two ballast systems, and are shown in Figures 5.3(b) and 5.3(c).

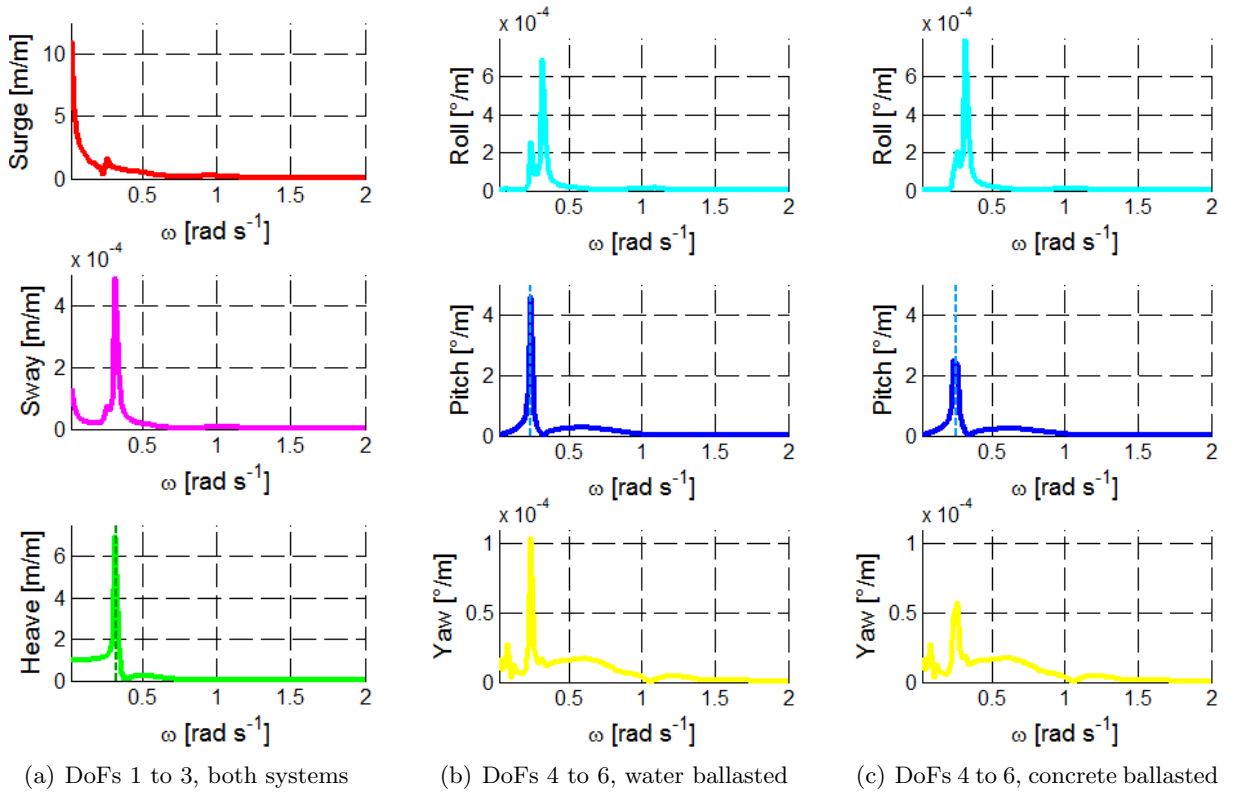


Figure 5.3: Response amplitude operators

The highest response is in general in surge, heave and pitch, due to the wave directionality. The responses in sway, roll and yaw, obtained by HydroD, are marginal and assumed to be purely numerical.

The heave RAO has a damping-dependent peak at its natural angular frequency of 0.325 rad s^{-1} , as presented in Figure 5.3(a). At lower frequencies the RAO is stiffness dominated and approaches the static value of 1 for infinitely small frequency. Above the natural frequency, the RAO is inertia dominated and tends to approach zero with infinitely high frequency.

The RAOs in the rotational DoFs, shown in Figures 5.3(b) and 5.3(c), slightly differ for the two initially upscaled designs, due to the differences in the stiffness and mass matrix components. The peaks occur at different frequencies, corresponding to the system's natural frequencies, but

are expected to be of equal height for both designs, as this only depends on the damping, which is equal for both floaters. This may also be the case, but as the natural frequencies of the two systems are slightly different, and only some discrete frequencies are used for the computations in HydroD, not exactly the highest value for the RAO is obtained. If the chosen frequency set is refined around the rotational natural frequencies, or directly includes them, it is expected that the RAOs in the rotational DoFs have same high peaks for both designs.

5.2.2.2 Response Spectra The further dynamic analysis, based on the representative environmental conditions given in Table 4.1 in Subsection 4.2.3, yields 15 response spectra for the initially upscaled systems, shown in Figure 5.4 exemplarily for the most severe sea state.

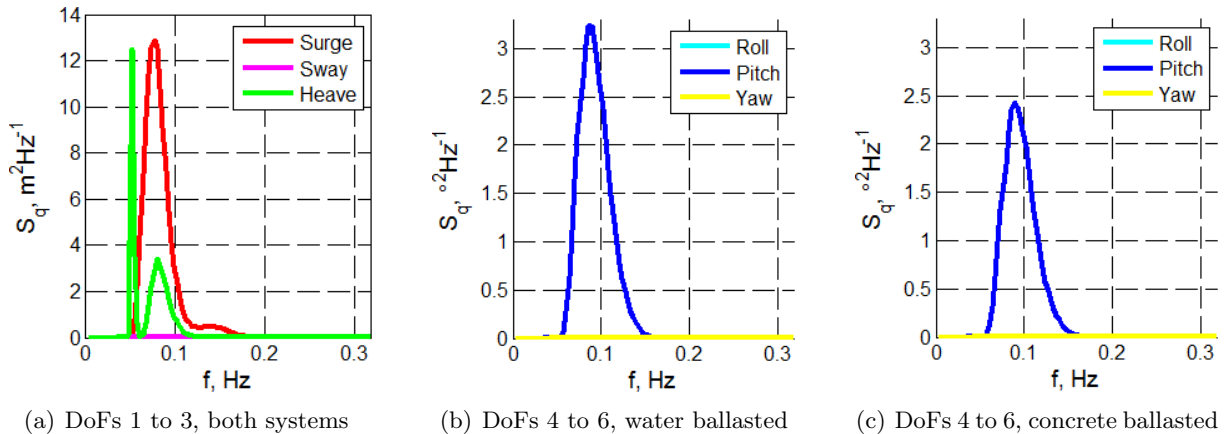


Figure 5.4: Response spectra for condition number 15

The response spectra in the translational DoFs are identical for both designs, as the RAOs are equal. The different RAOs in the rotational DoFs, lead to the assumption that the response spectra also differ. This discrepancy, however, is small, because the wave frequencies are above the system's natural frequencies, where the response is inertia dominated. As the mass matrix components in the rotational DoFs differ by around 10% for the two designs, the corresponding response spectra can only be distinguished one from the other by the height of the peak.

The peak of the spectra occurs at the peak wave frequency. Only the response spectrum in heave shows a second peak at the system's natural frequency in heave, as this is the closest to the wave excitation frequency. This again gives reason to further improve the upscaling procedure by applying different scaling factors, especially for the upper columns, so that a higher natural period in heave could be obtained.

5.2.2.3 Standard Deviations Figure 5.5 presents the standard deviations for the water ballasted design. The dynamic motion in the translational DoFs is the same for the concrete ballasted floater, but the standard deviations in the rotational DoFs are slightly smaller in amount, however, show a similar increasing trend as shown in Figure 5.5(b). For comparison of the maximum dynamic motions of both platform designs at the most severe sea state, the standard deviations in surge, heave and pitch are presented in Table 5.6.

Table 5.6: Dynamic response of the initially upscaled platforms, based on HydroD

| Parameter | Unit | Water ballasted | Concrete ballasted | Original OC4 floater |
|-------------------|----------|-----------------|--------------------|----------------------|
| $\sigma_{q1,max}$ | m | 0.64 | 0.64 | 0.78 |
| $\sigma_{q3,max}$ | m | 0.36 | 0.36 | 2.11 |
| $\sigma_{q5,max}$ | $^\circ$ | 0.37 | 0.32 | 0.36 |

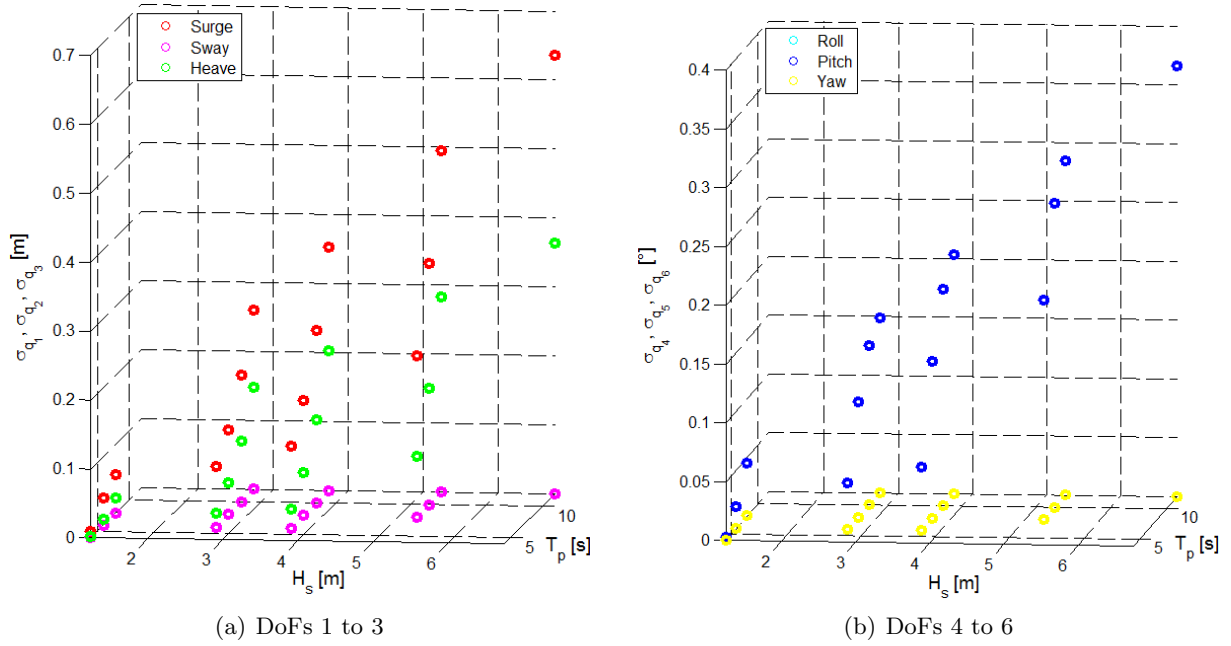


Figure 5.5: Dynamic response of one initially upscaled platform, water ballasted design

The dynamic motion in the translational DoFs is reduced, compared to the original DeepCwind semi-submersible platform. A significant reduction can be obtained in the maximum standard deviation in heave, which is mainly due to the natural period in heave, shifted more outside the range of wave excitation. This, however, cannot directly be considered positive, as the relative heave motion is the more important parameter, but not covered in this analysis. The dynamic motion in pitch is slightly increased for the water ballasted design, but decreased for the concrete ballasted floater, as there a higher stability and stiffer system is obtained by the deeper center of gravity. Roll and yaw show, as well as sway, almost no dynamic response, as those DoFs are not directly influenced by the incoming waves.

Comparing those standard deviations with the maximum mean displacement, represented by the nominal pitch at rated wind speed and obtained in Subsection 5.2.1, yields that the maximum dynamic pitch motion, occurring at the most severe environmental condition, is for both systems around 13% of the mean pitch displacement.

6 Criteria for Optimization and Upscaling

Based on the results of the initial upscaling and the recommendations given in Chapter 5, the main issues for optimization, upscaling, and design of semi-submersible platforms are defined.

6.1 Top Structure

The predefined wind turbine for the upscaled floater prescribes parameters like top structure mass (RNA and tower) and center of gravity, tower base diameter, hub height, rotational frequency range, rated rotor thrust, and rated power. The only adjustment regarding the dimensions, that is to be done, is that the tower bottom part is cut at the top level of the main column, so that the hub height of the floating system remains the same as before. This, however, would affect the tower eigenfrequencies, and should be analyzed in future work. Furthermore, it has to be checked that the nacelle accelerations do not exceed the limit of $0.2g$ [51].

The blade-pitch control has to be changed as well, when putting an onshore or bottom fixed wind turbine on top of a floating platform. The adjustment of the controller gains, based on the system's natural frequency in pitch, is explained in Subsection 3.6.2.

6.2 Eigenfrequencies

The system's frequencies should neither be coupled to 1P or 3P, nor lie in the range of wave excitation. Regarding 1P and 3P, the minimum rotational frequency is the most relevant. As this is for existing turbines around 5 or 6 *rpm*, which corresponds to a period of 10 to 12 *s*, it is disregarded as being not critical for the rigid body frequencies of the entire system. More crucial is the wave excitation, as wave peak periods could range from 5 to 25 *s* [57]. Semi-submersibles are designed to have their natural frequencies below the wave excitation frequency, as mentioned in Section 1.2. Based on the typical eigenfrequencies of semi-submersible platforms, following natural periods are aimed: $\gtrsim 20$ *s* in heave, $\gtrsim 30$ *s* in roll and pitch, and ≈ 100 *s* in surge, sway and yaw, whereas the latter value rather depends on the mooring system.

Those aims could be achieved by changing the upper column diameter, as this contributes mainly to the waterplane area, and thus also to the stiffness of the system. Also the ballast system could be adjusted, as it influences the total center of gravity, which has an effect on the stiffness and mass in the pitch DoF. And, as already mentioned above, the mooring system could be modified, such that the natural periods in surge, sway and yaw are optimized. Based on the final system's eigenfrequency in pitch, the blade-pitch controller gains have to be re-calculated.

6.3 Stability

For the floatability of the system, top structure mass, platform, and buoyancy play a role. When changing the platform dimensions, the displaced water volume would vary more than the volume of the material, as hollow structure elements are used. Buoyancy and weight can be balanced by adjusting the amount of ballast. The available inner volume of the columns has to be proved to be sufficient for the needed ballast volume. The cheapest ballast, water, is preferred. However, if less inner space is available than needed, other ballast types, like concrete, are to be considered.

Stability in pitch includes nominal pitch and intact floating stability. The latter one is checked by means of HydroD, according to Paragraph 3.2.2.4, taking the variable center of buoyancy and buoyancy volume into account. A nominal pitch of maximum 5° is aimed. This leaves a safety factor of two for higher loads in fault situations, without exceeding the typical maximum allowable pitch during operation of 10° [27, 32]. In fact, the safety factor is even higher, considering that the real point of rotation lies above the center of buoyancy. The nominal pitch value could be influenced by adjusting the location of the ballast within the columns.

6.4 Mooring System

The mooring system is mainly relevant for the surge, sway, and yaw natural frequencies, as well as for keeping the system's offsets within the allowable limits. The final design of the station-keeping system is, however, not covered in this work, as mooring lines make up a separate, very complex system. Still including the mooring system in a first approach, the mooring line length is computed by means of Source Code A.8 in Appendix A.5, such that the original mooring stiffness in surge is maintained.

The detailed mooring system design is left for future work. Within this, it has to be checked that no vertical force is acting on the anchors, and the maximum tension in the mooring lines versus the breaking strength has to be elaborated. The mooring line design could be adjusted in line diameter, material, and extensional stiffness, or by adding buoys or clump weights.

6.5 Environment

The environment is predefined by water depth, sea states, currents, and wind velocities at the location of interest for the floating wind turbine. The turbine is designed for optimum power performance at that site. Wind loads affect system pitch and aerodynamic damping. Waves and currents have an influence on dynamic motions, viscous forces and damping, mooring system, as well as pressure on the columns. The latter one is related to the structural design of the platform and covered a little bit more in detail in Section 6.6. Finally, the sea states also define the range of wave excitation frequencies, which is relevant for the design with respect to the system's eigenfrequencies.

6.6 Structural Strength

The structural integrity is of high relevance for the floating platform design, especially if the up-scaling procedure, covered in Section 8.1, does not follow structural scaling laws. However, only a simplified strength check is performed in this work, based on recommendations given in the Offshore Standard DNV-OS-J103 [53], as a detailed structural analysis would be too extensive.

The simplified strength check concentrates on the upper columns, as they are assumed to be one of the most critical components, because of their large height to diameter ratio and the strong impact of wave loads. The Offshore Standard [53] provides Equation 57 for the design tank pressure p_{tank} acting on the inner wall of the filled column, and Equation 58 for the design sea pressure p_{water} acting on the outer wall of the column.

$$p_{\text{tank}} = \rho_{\text{ballast}} g(z_{\text{ballast}} - z_{\text{lp}}) (\gamma_{\text{G,Q}} + 0.25\gamma_{\text{E}}) \quad (57)$$

$$p_{\text{water}} = \rho_{\text{water}} g \left[-z_{\text{lp}} \gamma_{\text{G,Q}} + \left(\frac{1}{2} H_{\text{max}} - z_{\text{lp}} \right) \gamma_{\text{E}} \right] \quad (58)$$

z_{ballast} is the z -coordinate of the ballast level in the column, and z_{lp} the z -coordinate of the considered load point on the column, both with respect to SWL. $\gamma_{\text{G,Q}}$ and γ_{E} are load factors for permanent and variable loads, and environmental loads, respectively. For the ULS calculation, they are to be taken as $\gamma_{\text{G,Q}} = 1.25$ and $\gamma_{\text{E}} = 0.7$ [53]. The elevation of the wave crest above SWL is substituted in Equation 58 by one half of the maximum wave height H_{max} .

The strength check is performed for the combinations of maximum tank pressure and minimum sea pressure, as well as for minimum tank pressure and maximum sea pressure, based on recommendations in [53]. The load point under consideration is taken at the base of the upper column. For maximum and minimum tank pressure, the two borderline cases of a completely

filled, and an empty column are considered. This means that the term $(z_{\text{ballast}} - z_{\text{lp}})$ in both cases equals the height of the upper column. The only difference is, that for the minimum tank pressure air is used instead of the real ballast material, leading to Equations 59 and 60.

$$\begin{aligned} p_{\text{tank,max}} &= \rho_{\text{ballast}} g h_{\text{UC}} (\gamma_{\text{G,Q}} + 0.25\gamma_{\text{E}}) \\ &= 1.425 \rho_{\text{ballast}} 9.81 \frac{m}{s^2} h_{\text{UC}} \end{aligned} \quad (59)$$

$$\begin{aligned} p_{\text{tank,min}} &= \rho_{\text{air}} g h_{\text{UC}} (\gamma_{\text{G,Q}} + 0.25\gamma_{\text{E}}) \\ &= 1.425 \cdot 1.225 \frac{kg}{m^3} 9.81 \frac{m}{s^2} h_{\text{UC}} \end{aligned} \quad (60)$$

For the minimum sea pressure the wave height is taken to be zero, and set equal to $1.86H_s$ for the maximum sea pressure. A significant wave height for 50 year return period of $H_s = 12.85m$ is used in this approach, taken as average of the considered environments in the Offshore Standard [53]. This leads to Equations 61 and 62 for the maximum and minimum sea pressure, respectively.

$$\begin{aligned} p_{\text{water,max}} &= \rho_{\text{water}} g \left[-z_{\text{b,UC}} \gamma_{\text{G,Q}} + \left(\frac{1}{2} \cdot 1.86H_s - z_{\text{b,UC}} \right) \gamma_{\text{E}} \right] \\ &= 1025 \frac{kg}{m^3} 9.81 \frac{m}{s^2} (11.95 m \cdot 0.7 - 1.95z_{\text{b,UC}}) \end{aligned} \quad (61)$$

$$\begin{aligned} p_{\text{water,min}} &= \rho_{\text{water}} g [-z_{\text{b,UC}} \gamma_{\text{G,Q}} - z_{\text{b,UC}} \gamma_{\text{E}}] \\ &= -1025 \frac{kg}{m^3} 9.81 \frac{m}{s^2} \cdot 1.95z_{\text{b,UC}} \end{aligned} \quad (62)$$

Combining minimum and maximum inner tank and outer sea pressures in the way described above, the tangential, radial, and axial stresses σ_t , σ_r , and σ_{ax} can be computed based on Equations 63 to 65 [45], with the wall thickness of the upper column denoted as d_{UC} .

$$\begin{aligned} \sigma_t &= \frac{1}{R_{\text{UC}}^2 - (R_{\text{UC}} - d_{\text{UC}})^2} \left[p_{\text{water}} R_{\text{UC}}^2 \left(1 + \frac{(R_{\text{UC}} - d_{\text{UC}})^2}{(R_{\text{UC}} - \delta d_{\text{UC}})^2} \right) \right. \\ &\quad \left. - p_{\text{tank}} (R_{\text{UC}} - d_{\text{UC}})^2 \left(1 + \frac{R_{\text{UC}}^2}{(R_{\text{UC}} - \delta d_{\text{UC}})^2} \right) \right] \end{aligned} \quad (63)$$

$$\begin{aligned} \sigma_r &= \frac{1}{R_{\text{UC}}^2 - (R_{\text{UC}} - d_{\text{UC}})^2} \left[p_{\text{water}} R_{\text{UC}}^2 \left(1 - \frac{(R_{\text{UC}} - d_{\text{UC}})^2}{(R_{\text{UC}} - \delta d_{\text{UC}})^2} \right) \right. \\ &\quad \left. - p_{\text{tank}} (R_{\text{UC}} - d_{\text{UC}})^2 \left(1 - \frac{R_{\text{UC}}^2}{(R_{\text{UC}} - \delta d_{\text{UC}})^2} \right) \right] \end{aligned} \quad (64)$$

$$\sigma_{\text{ax}} = \frac{p_{\text{tank}} (R_{\text{UC}} - d_{\text{UC}})^2 - p_{\text{water}} R_{\text{UC}}^2}{R_{\text{UC}}^2 - (R_{\text{UC}} - d_{\text{UC}})^2} \quad (65)$$

Tangential and radial stresses depend on the radial position of the load point. This is expressed in terms of δ , ranging from 0 to 1. In the simplified strength check, three different radial positions are considered: on the outer wall ($\delta = 0$), in the wall center ($\delta = 0.5$), and on the inner wall ($\delta = 1$).

For each considered load point and pressure combination, an equivalent stress σ_{equ} can be computed based on the shape modification hypothesis, as given in Equation 66 [45].

$$\sigma_{\text{equ}} = \sqrt{\sigma_t^2 + \sigma_r^2 + \sigma_{\text{ax}}^2 - \sigma_t\sigma_r - \sigma_t\sigma_{\text{ax}} - \sigma_r\sigma_{\text{ax}}} \quad (66)$$

The equivalent stress has to be compared with the yield stress σ_{yield} . Yield stress values for steel S355 are presented in Table 6.1 for different wall thicknesses [50].

Table 6.1: Steel (S355) yield stress depending on the wall thickness [50]

| d [m] | $d \leq 0.016$ | $0.016 < d \leq 0.040$ | $0.040 < d \leq 0.063$ | $0.063 < d \leq 0.080$ |
|-------------------------------|----------------|------------------------|------------------------|------------------------|
| σ_{yield} [MPa] | 355 | 345 | 335 | 325 |

For structural integrity the equivalent stress should not exceed the yield stress limit. However, a too large safety factor would imply an over-conservative and too expensive design.

A detailed strength check should include buckling and structural fatigue checks for all platform elements and the joints. Based on this, the structural design could be further improved, either by adjusting the wall thicknesses or by adding inner struts in the columns for more stability.

6.7 Producibility

Infrastructure and production site are of relevance for the total costs of floating wind turbines. The location of European shipyards, in which floating platforms could be produced, is examined in [20]. If floating platforms are getting bigger with larger wind turbines, the number of suitable docks for production decreases enormously. In order to avoid long, expensive, and weather-dependent transportation, local shipyards, close to the final construction site of the floating wind turbine, are preferred to be used. This, however, means that the overall size of the platform should be kept within limits. Limitations in draft could be mitigated by ballasting later or adding floaters to the platform, leaving the width of the dock as main limiting dimension. [20]

However, limiting the overall size would lead to a reduced waterplane inertia and a more compact platform design with less spacing between the heave plates. [30] recommends a distance between the base columns of more than $1.5D_{\text{BC}}$. The heave added mass could be negatively influenced, if the spacing is less than $1.3D_{\text{BC}}$ [30]. Using the original DeepCwind semi-submersible platform, with already just a distance of $1.1D_{\text{BC}}$ between the heave plates, as design basis, it is not advised to limit the overall platform size during upscaling or even reduce the outer dimensions.

6.8 Costs

One main aim of moving towards larger wind turbines, is to reduce the overall costs. From the structural side, costs could be cut if the design is less over-conservative, meaning that less material can be used as smaller dimensions or thinner walls would still be sufficient. By using the cheapest ballast type, namely water, further costs can be saved. However, it has to be checked that the available space within the columns is enough for the required amount of ballast. If this is not the case, still cheap but denser ballast, like concrete, should be used.

Also manufacturing costs contribute a lot to the total costs of floating wind turbines. Those include working hours for construction, time for transportation, and installation. Thus, local docks are preferred, as well as the method of towing the floating wind turbine fully assembled to the offshore site, which is feasible with semi-submersible platforms due to their shallow draft.

7 Optimization of the DeepCwind Semi-Submersible Platform

The DeepCwind semi-submersible floating platform is used as starting point for this study. The main properties are introduced in Section 2.1, and the performance is presented in Section 4.4. The system's stability is far exceeding the minimum requirements given by [53], the nominal pitch is quite small, the platform is with $1.35\text{E} + 7 \text{ kg}$ very heavy, and the natural periods in heave and pitch lie with 17.4 s and 27.0 s within the typical range for semi-submersible floating platforms, but very close to the lower bound. Thus, the original semi-submersible design is assessed to be over-conservative. The DeepCwind semi-submersible platform is therefore, first optimized before it is used as basis for upscaling to larger wind turbine sizes.

In the following Sections 7.1 and 7.2, the optimization procedure for the OC4 floater, and the resulting optimized semi-submersible platform for the NREL 5 MW wind turbine are presented.

7.1 Optimization Procedure

The aims of the optimization procedure are higher eigenperiods of at least 20 s in heave and 30 s in pitch, a more critical but still reasonable nominal pitch of around 5° , and a lighter total system.

The natural frequency in heave can be decreased, and thus the natural period increased, by reducing the stiffness in heave, and/or increasing added mass and mass in heave, according to Equation 13 in Subsection 3.3.1. Following Equations 17 to 19 in Subsection 3.3.2, a smaller stiffness component in heave can be achieved by reducing the upper column diameter. The same, or also an increased base column diameter would lead to a larger added mass component in heave. An increased mass would come in general with bigger dimensions. However, as a lighter platform is aimed, and the spacing between the base columns is already quite marginal, it is decided to adjust the diameter of the upper columns.

Aiming for an eigenperiod of 20 s in heave, the natural frequency should scale with k_3^{-1} , with k_3 based on the ratio of the aimed period to the original value, as given by Equation 67.

$$k_3 = \frac{T_{\text{nat},3,\text{aimed}}}{T_{\text{nat},3,\text{orig}}} = \frac{20 \text{ s}}{17.4 \text{ s}} \quad (67)$$

If only the upper column diameter is to be adjusted, its contribution to the system parameters has to be further analyzed. A decreasing upper column diameter would lead to a decreased mass. However, the upper columns make up less than 10% of the total system mass. The added mass component in heave, on the other hand, would increase with decreasing upper column diameter. However, the diameter of the base column dominates in the computation of the added mass component in heave. As mass and added mass are summed up in the denominator for the computation of the natural frequency, it is approximated that the small and contrary trend of mass and added mass would have a cancelling effect. Thus, the denominator in the natural frequency computation would remain almost unchanged, when only adjusting the upper column diameter.

Still aiming for a natural heave frequency decreased by a factor of k_3^{-1} , the stiffness component in heave has to scale with k_3^{-2} . However, only the part in the stiffness component, that depends on the upper column diameter, would change. The required scaling factor of the upper columns $k_{3,\text{UC}}$ is determined based on Equation 68, including the contribution of the cross sectional area of all three upper columns to the total waterplane area.

$$\frac{1}{k_3^2} = \frac{\frac{3}{4}D_{\text{UC}}^2\pi}{A_{\text{WP}}}k_{3,\text{UC}}^2 + \left(1 - \frac{\frac{3}{4}D_{\text{UC}}^2\pi}{A_{\text{WP}}}\right) \quad (68)$$

Solving Equation 68 for the scaling factor of the upper columns $k_{3,UC}$, results in Equation 69.

$$k_{3,UC} = \sqrt{1 + \frac{4A_{WP}}{3D_{UC}^2\pi} (k_3^{-2} - 1)} \quad (69)$$

With the parameters of the original semi-submersible platform, a scaling factor of $k_{3,UC} = 0.853$ is computed. If the upper column diameter is scaled just with this factor, the nominal pitch of the system would be around 4.53° , according to hand calculations, which is still below the aimed more critical value of 5° . Thus, a second scaling factor k_5 , with which the nominal pitch should scale, is introduced in Equation 70, based on the aimed and current nominal pitch.

$$k_5 = \frac{q_{5,rated,aimed}}{q_{5,rated}} = \frac{5^\circ}{4.53^\circ} \quad (70)$$

The nominal pitch depends on the overturning moment at rated wind speed and the stiffness component in pitch, as defined by Equation 50 in Section 4.1. Changing the upper column diameter would influence the center of buoyancy, and thus also the overturning moment. This is, however, assumed to be negligible with respect to the entire lever up to the hub. Therefore, the nominator in the nominal pitch computation can be approximated to remain constant, when just the upper column diameter is changed. In order to obtain the aimed nominal pitch of 5° , the stiffness component in pitch then has to scale with k_5^{-1} . The contribution of the upper columns to the stiffness, and their different scaling is expressed in Equation 71, using $d_{UC,i}$ for the distance of the center of upper column i to the system's centerline (z -axis). The explicit calculation of the additional scaling factor $k_{5,UC}$ for the upper columns is given by Equation 72.

$$\frac{1}{k_5} = \frac{3\rho_{water} g \frac{\pi}{64} D_{UC}^4}{C_{55}} k_{5,UC}^4 + \frac{\rho_{water} g \frac{\pi}{4} D_{UC}^2 \sum_{i=1}^3 d_{UC,i}^2}{C_{55}} k_{5,UC}^2 + \left(1 - \frac{\rho_{water} g \frac{\pi}{4} D_{UC}^2 \left(\frac{3}{16} D_{UC}^2 + \sum_{i=1}^3 d_{UC,i}^2 \right)}{C_{55}} \right) \quad (71)$$

$$k_{5,UC} = \sqrt{\frac{-\sum_{i=1}^3 d_{UC,i}^2 + \sqrt{\left(\sum_{i=1}^3 d_{UC,i}^2 \right)^2 - \frac{3C_{55}}{\rho_{water} g \pi} (1 - k_5^{-1}) + \frac{3}{4} D_{UC}^2 \left(\frac{3}{16} D_{UC}^2 + \sum_{i=1}^3 d_{UC,i}^2 \right)}}{\frac{3}{8} D_{UC}^2}} \quad (72)$$

The additional scaling factor is computed to $k_{5,UC} = 0.960$, based on the already scaled upper columns ($k_{3,UC} = 0.853$).

The upper column diameter of the original DeepCwind semi-submersible is, hence, scaled with a total factor of $k_{UC} = k_{3,UC} k_{5,UC} = 0.853 \cdot 0.960 = 0.819$, from originally 12 m to 9.83 m . This value is finally rounded up to decimeter, leading to an upper column diameter of 9.9 m for the optimized design. Based on this, the drag coefficient for the upper columns is adjusted, according to the procedure explained in Subsection 3.4.2. This leads to a slightly reduced drag coefficient of $C_{d,UC} = 0.66$.

Platform weight and displaced water volume have changed with the scaling of the upper column. For balancing buoyancy and weight, the ballast has to be adjusted. A total ballast mass of

$8.35E + 6$ kg is needed. This is initially filled into the columns, starting from the bottom up, thus that the base columns are completely filled with water and the ballast height in the upper columns is about 1.11 m. Adjusting the ballast position within base and upper columns, in order to obtain a nominal pitch of 5° , according to Appendix A.6, leads to the final ballast heights of 5.625 m in the base columns, and 2.630 m in the upper columns.

7.2 Optimized DeepCwind Semi-Submersible Platform Design

The final parameters of the optimized DeepCwind semi-submersible platform are summarized in Table 7.1 and compared with the original values from [41].

Table 7.1: Modified dimensions of the optimized DeepCwind platform design

| Parameter | Unit | Optimized floater | Original floater [41] |
|------------------|------|-------------------|-----------------------|
| D_{UC} | m | 9.90 | 12.00 |
| $h_{ballast,UC}$ | m | 2.63 | 7.83 |
| $h_{ballast,BC}$ | m | 5.6250 | 5.0478 |
| z_G | m | -12.43 | -11.59 |
| z_B | m | -13.93 | -13.17 |
| m_{steel} | kg | 3.5671E+6 | 3.8522E+6 |
| $m_{ballast}$ | kg | 8.3544E+6 | 9.6208E+6 |
| m_{tot} | kg | 1.1921E+7 | 1.3473E+7 |

Both center of gravity and center of buoyancy are deeper in the optimized design, compared to the original semi-submersible platform. This is due to the smaller upper columns, and thus less corresponding displaced water volume, as well as the changed ballast position. Furthermore, it can be seen from Table 7.1 that the steel mass is reduced by 7.4% and the ballast mass by 13.2%, leading to a by 11.5% lighter platform and a by 10.8% lighter total floating wind turbine system.

The drag coefficient of the upper columns is with 0.66 slightly smaller compared to the original OC4 floater (0.67). The drag coefficients for the main column (0.62), base column (0.70), cross braces and pontoons (0.54), however remain unchanged, as only the upper column diameter is adjusted in the optimized design.

7.2.1 Static Analysis of the Optimized DeepCwind Platform Design

The performance of the optimized DeepCwind semi-submersible platform design is analyzed based on the three different methods, introduced in Sections 4.1 to 4.3.

7.2.1.1 System Matrices The results for the system matrices are presented in Table 7.2, optimized and original design in comparison. It can be observed that the mass components have slightly decreased, while the added mass components have slightly increased. This is reasonable, as the upper column diameter was downsized. The reduction in the stiffness components is more significant, which was essentially aimed within the optimization process.

7.2.1.2 Nominal Pitch The nominal pitch could be increased from 3.0° to 4.5° . The aimed value of 5° is not achieved, as the computation in the optimization procedure is carried out with the system stiffness excluding the mooring lines. For the final nominal pitch performance, however, the mooring line stiffness is included, which leads to the smaller value. Simulation in Dymola, however, yield a higher nominal pitch (5.5°). This may result from the mooring system model implemented in Modelica, as already addressed in Section 4.4.

Table 7.2: Comparison of the system matrices of the optimized DeepCwind platform design, values in brackets for the original design from HydroD

| Parameter | Unit | Calculated | HydroD | Modelica | Original [41] | |
|-----------|----------------|------------------------------|----------|----------|---------------|------------|
| M_{33} | kg | 12.71E+6 | 12.71E+6 | 12.71E+6 | 14.26E+6 | |
| M_{55} | kgm^2 | 1.65E+10 | 1.65E+10 | — | (1.71E+10) | |
| A_{33} | kg | $ \omega \rightarrow 0$ | 13.84E+6 | 16.11E+6 | — | (15.26E+6) |
| | | $ \omega \rightarrow \infty$ | — | 15.42E+6 | — | 14.70E+6 |
| A_{55} | kgm^2 | $ \omega \rightarrow 0$ | 6.08E+9 | 8.00E+9 | — | (7.66E+9) |
| | | $ \omega \rightarrow \infty$ | — | 7.51E+9 | — | 7.21E+9 |
| C_{33} | $kg s^{-2}$ | 2.734E+6 | 2.712E+6 | — | 3.836E+6 | |
| C_{55} | $kgm^2 s^{-2}$ | 0.807E+9 | 0.804E+9 | — | 1.235E+9 | |

7.2.1.3 Stability Due to the geometrical changes, the stability range, based on the hand calculations, increased from $[-19.0^\circ, 18.9^\circ]$ to $[-19.5^\circ, 18.9^\circ]$. However, the real stability range, obtained by HydroD, could be slightly reduced from $[-103.6^\circ, 97.9^\circ]$ to $[-102.3^\circ, 97.9^\circ]$. The righting and wind heeling moment curves, presented in Figure 7.1, are still similar in shape compared to the original OC4 floater, shown as black line.

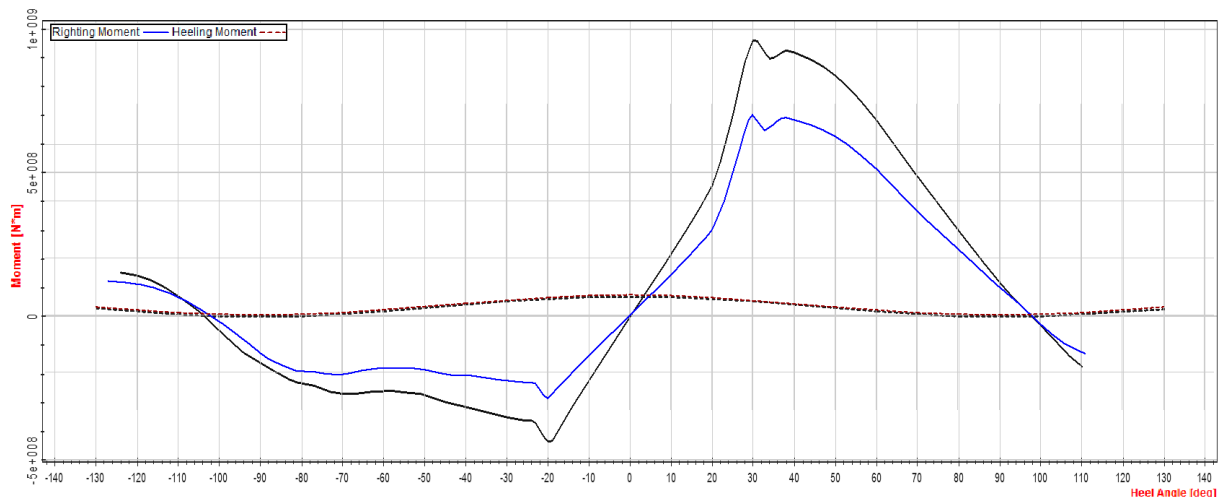


Figure 7.1: Moment curves of the optimized DeepCwind platform design, original OC4 platform in black

The area under the righting moment curve is no longer 16 times, but now only 11.4 times larger than the area under the wind heeling moment curve to the second intercept with the righting moment curve. This is, however, still much larger than the required factor of 1.3.

7.2.1.4 Natural Periods The natural periods of the optimized DeepCwind floating platform design are presented in Table 7.3, together with the values of the original OC4 design. A similar discrepancy between the different analysis methods can be seen, as already noted in Section 4.4. By means of the optimization procedure, the natural period in heave could be increased by 3 s to 20.4 s, and the natural period in pitch by more than 7 s to 34.7 s, based on the results obtained by HydroD. The natural periods in surge and yaw, however, are slightly decreased to 104.9 s and 73.7 s, respectively. The change in the natural periods could also be clearly seen in Figure 7.2, showing the time series from the free decay tests in Dymola, based on Modelica.

Table 7.3: Comparison of the natural periods of the optimized DeepCwind platform design

| Parameter | Unit | Calculated | HydroD | Modelica | | Original [41] |
|--------------------|------|------------|--------|----------|-------|---------------|
| | | | | Counted | FFT | |
| $T_{\text{nat},1}$ | s | — | 104.9 | 138.1 | 133.3 | 112.2 |
| $T_{\text{nat},3}$ | s | 19.3 | 20.4 | 20.4 | 20.0 | 17.4 |
| $T_{\text{nat},5}$ | s | 31.6 | 34.7 | 32.8 | 33.3 | 27.0 |
| $T_{\text{nat},6}$ | s | — | 73.7 | 97.7 | 100.0 | 79.3 |

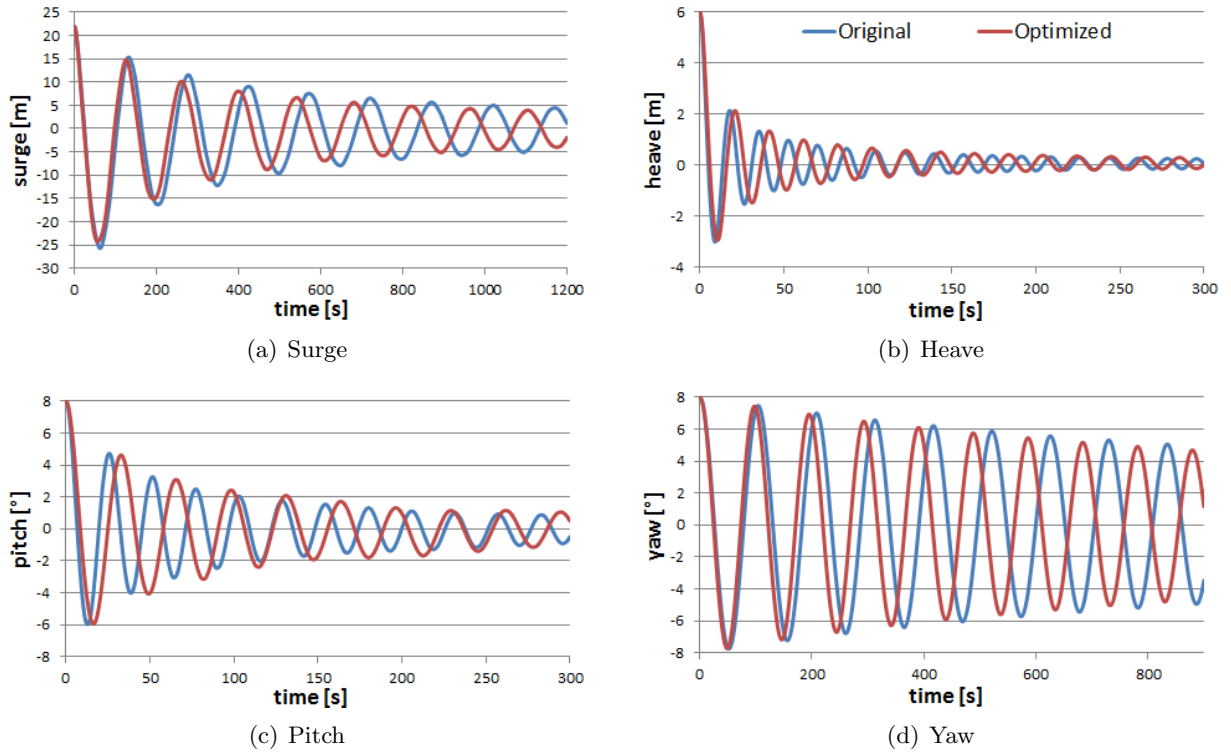


Figure 7.2: Free decay time series of the optimized OC4 system, in comparison with the original results, based on Modelica

7.2.1.5 Controller Gains Based on the results for the natural frequencies, the blade-pitch controller gains are re-calculated, by means of Equations 45 to 47 in Subsection 3.6.2, and with the parameters for the NREL 5 MW wind turbine of $\Omega_{\text{rated,LSS}} = 12.1 \text{ rpm}$, $N_{\text{gear}} = 97$, $I_{\text{drivetrain,HSS}} = 534.116 \text{ kgm}^2$, $\frac{\partial P}{\partial \theta} \Big|_{\theta_{\text{rated}}} = -25.52\text{E} + 6 \text{ W rad}^{-1}$ and $\theta_K = 6.302336^\circ$ [31]. Following the recommendations given in Subsection 3.6.2, $\omega_{\text{c,nat}} \approx \omega_{\text{nat},5}/1.3 \approx 0.14 \text{ rad s}^{-1}$ and $\zeta_c = 0.7$ are set. This way, the adjusted controller gains are determined to $K_P = 0.00481469 \text{ s}$ and $K_I = 0.000481469$ (at rated), and thus reduced, compared to the original values of 0.006275604 s and 0.0008965149 [41], respectively.

7.2.2 Dynamic Analysis of the Optimized DeepCwind Platform Design

The dynamic analysis in HydroD is performed for different sea states, as defined in Subsection 4.2.3. The dynamic motions, depending on significant wave height and peak period, are presented in Figure 7.3. It can be observed that the standard deviations are increasing with increasing wave height and period. Due to the directionality of the waves, the dynamic response is mainly

in surge, heave, and pitch. For the most severe sea state ($H_s = 6.75\text{ m}$, $T_p = 12\text{ s}$), considered in this analysis, the maximum dynamic motions are presented in Table 7.4.

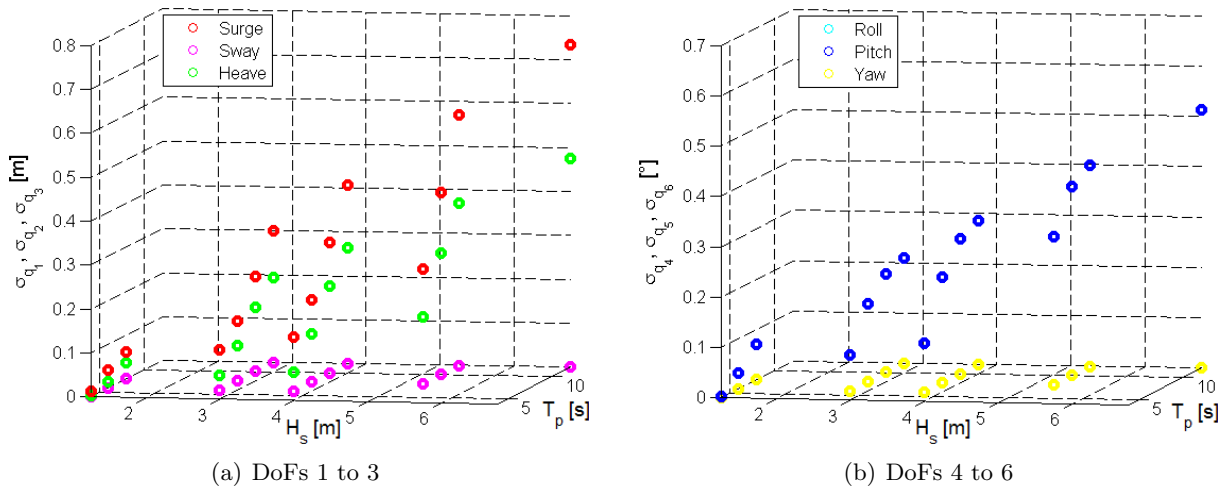


Figure 7.3: Dynamic response of the optimized DeepCwind platform design, based on HydroD

Table 7.4: Dynamic response of the optimized DeepCwind platform design, based on HydroD

| Parameter | Unit | Optimized floater | Original floater |
|--------------------|----------|-------------------|------------------|
| $\sigma_{q1,\max}$ | m | 0.73 | 0.78 |
| $\sigma_{q3,\max}$ | m | 0.48 | 2.11 |
| $\sigma_{q5,\max}$ | $^\circ$ | 0.51 | 0.36 |

Comparison with the original DeepCwind semi-submersible platform shows that the dynamic motion in surge is slightly decreased. The motion in heave is significantly reduced by more than 75%, which is expected to result from the increased added mass due to the smaller upper column diameter, and the considerably higher heave eigenperiod. What effects this will have on the more crucial relative heave motion, has to be analyzed in future work. The dynamic motion in pitch is enlarged by a factor of around 1.4. This is obvious, as the optimized platform is designed less over-conservative, and a more critical nominal pitch value was aimed.

The simulation in Dymola with ramped wind and without waves yields the time series, shown in Figure 7.4. It can be seen that the adjusted controller gains yield a stable floating wind turbine system. Above rated wind speed, the blade-pitch controller starts pitching the blades. The variation in platform pitch motion and blade-pitch angle is decreasing with the time at one considered wind speed, and also decreasing at higher wind speeds.

The mean and dynamic responses of the optimized semi-submersible floater are computed with the help of MATLAB and plotted with respect to the wind speed in Figure 7.5, together with the responses of the original OC4 floater design in dashed lines. Optimized and original design differ mainly in the mean pitch motion, as it can be seen in Figures 5(a) and 5(c). This is due to the aimed higher nominal pitch and less over-conservative design, obtained by the optimization procedure. The dynamic responses of optimized and original designs, presented in Figures 5(b) and 5(d), are quite comparable, except for the standard deviation in surge in the wind-only simulation, which is at rated wind speed by a factor of approximately two higher for the optimized floater.

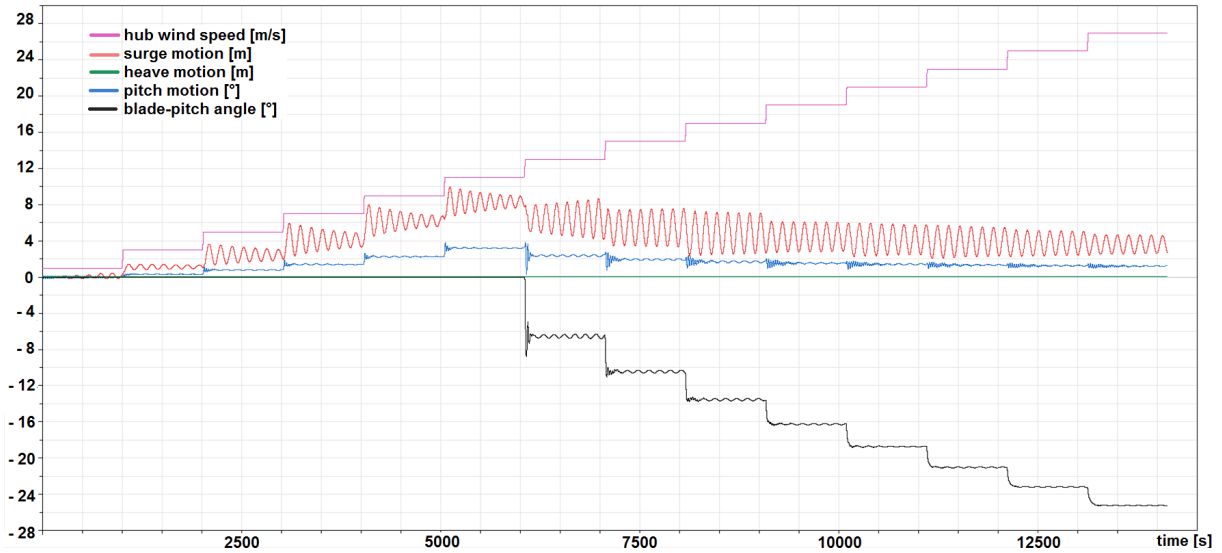


Figure 7.4: Response of the optimized DeepCwind platform design at different wind speeds

The mean displacements, as well as the dynamic variations in the platform motion response and the blade-pitch angle, are for both simulations, with or without waves, maximum at rated wind speed, but then decreasing again at higher wind speeds. This is caused by the similar behavior of the thrust force, which is correlated to the surge and pitch motion of the platform. However, the motion response in heave, mean and standard values, is not affected by the thrust force and thus remains nearly constant for different wind speeds.

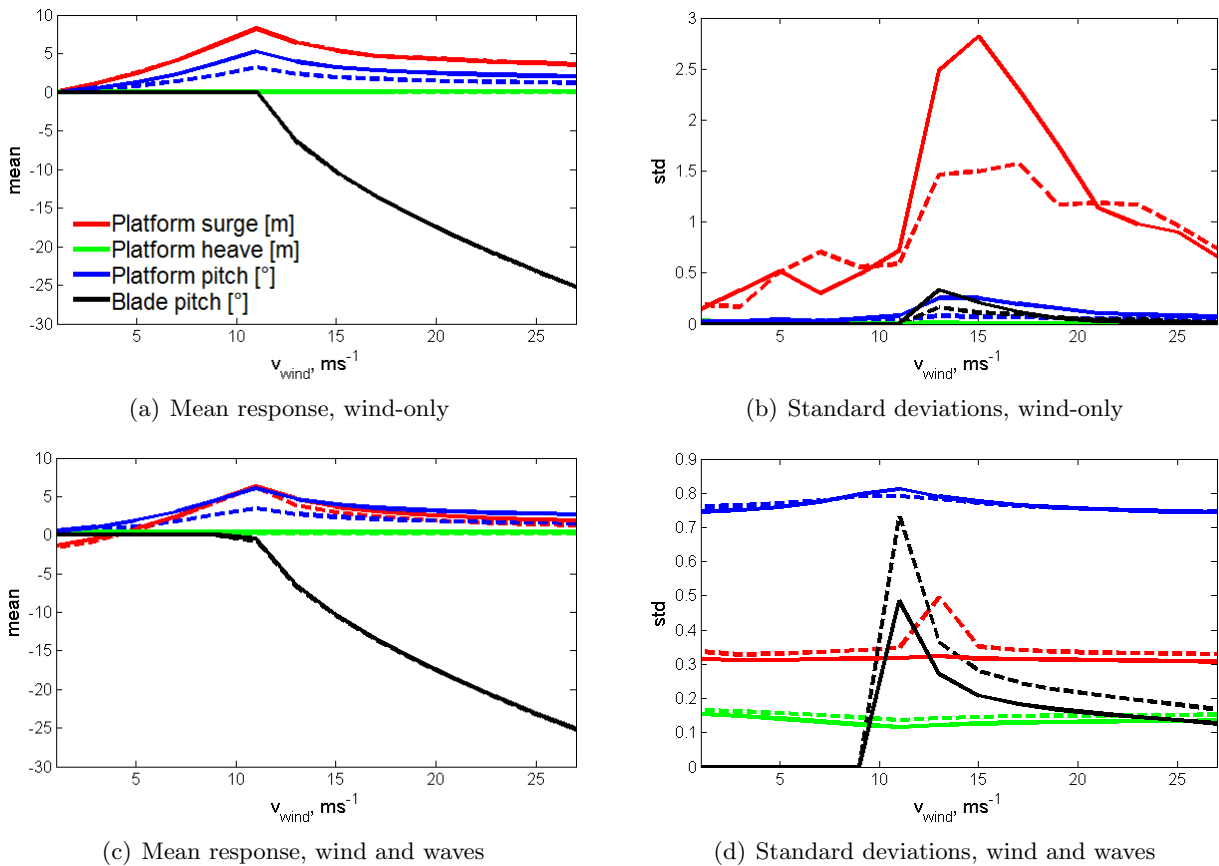


Figure 7.5: Mean and dynamic response of the optimized DeepCwind platform design, original OC4 platform responses in dashed lines

Comparing the wind-only and wind-and-wave simulations yields that, in the presence of waves, especially the platform motion in surge is significantly reduced, around 20% in the mean and even around 80% in the dynamic displacement. This shows the positive effect of coupled aero- and hydrodynamic motion and damping on the platform displacements. The results, obtained from the simulation with waves, are comparable to the dynamic response based on HydroD, presented in Figure 7.3 and Table 7.4. The values are not exactly the same, as different sea states are considered and HydroD does not include any wind, but they are in the same order of magnitude.

7.2.3 Structural Analysis of the Optimized DeepCwind Platform Design

Performing the structural strength check, as described in Section 6.6, leads to following equivalent stresses at the bottom of the upper column, presented in Table 7.5.

Table 7.5: Equivalent stress calculation for the optimized DeepCwind platform design, values given in MPa

| Pressure combination | Load point position | | |
|---|-----------------------------|--------------------------------|-----------------------------|
| | Outer wall ($\delta = 0$) | Wall center ($\delta = 0.5$) | Inner wall ($\delta = 1$) |
| $p_{\text{tank,min}}, p_{\text{water,max}}$ | 38.9 | 39.1 | 39.3 |
| $p_{\text{tank,max}}, p_{\text{water,min}}$ | 10.1 | 10.2 | 10.2 |

The yield stress for steel S355 for the unchanged wall thickness of the upper columns of 0.06 m amounts 335 MPa , based on Table 6.1 in Section 6.6. Comparing the equivalent stresses, given in Table 7.5, with the yield stress, results in a structural safety factor of 8.5 to 33.2. The more critical pressure combination is at minimum inner pressure, thus without any ballast in the upper columns, and maximum sea pressure. Furthermore, the stress is increasing from the outer wall through the column thickness to the inner side of the column wall. But still, the safety factor for the most critical condition and at the weakest point, is with 8.5, based on this simplified stress check, more than sufficient.

8 Upscaling of the Optimized DeepCwind Semi-Submersible Platform Design

The optimized semi-submersible floating platform, obtained and analyzed in Chapter 7, is used as basis for upscaling. In the following Section 8.1, the upscaling procedure is introduced, and applied as guideline for Fraunhofer's IWT-7.5-164 and the DTU 10 MW reference wind turbines in Sections 8.2 and 8.3, respectively.

8.1 Upscaling Process - A Guideline

Three different scaling factors are considered in the upscaling procedure: the main scaling factor k for most of the components of the platform, the scaling factor k_{MC} for the main column, based on geometrical constraints, and the scaling factor k_{UC} for the diameter of the upper columns, for an optimized upscaling procedure.

8.1.1 Main Scaling Factor

The main scaling factor k follows the theoretical upscaling based on geometric self-similarity, presented in Subsection 3.1.1. According to the theoretical scaling laws, the same scaling factor should be obtained by taking the square root of the power ratings, and by taking the third root of the ratio of the total masses. However, due to technological developments, the wind turbine designs are improved with respect to their weight. In order to take this technological progress into account, the main scaling factor is not determined based on the power rating, but rather based on the ratio of masses, following Equation 73.

$$k = \sqrt[3]{\frac{m_{WT,upscaled}}{m_{WT,initial}}} \quad (73)$$

The mass of the wind turbine, used for Equation 73, includes rotor (blades and hub), nacelle, and tower, taking the entire length to zero level into account. The shortened tower, which is finally used on top of the upscaled floating platform, is not considered in the computation of the main scaling factor, as the cut length depends itself on the scaling of the main column.

With this main scaling factor k , the entire platform is scaled, except main column diameter and wall thickness, as well as upper column diameter. Also pontoons and cross braces are only scaled in diameter, wall thickness, and elevation of the attachment points. Their final lengths result from the geometrical assembly.

8.1.2 Scaling Factor for the Main Column

As the tower base diameter is a predefined parameter of the upscaled system, a different scaling factor for the main column is needed. This can be computed by means of Equation 74, following just a length ratio.

$$k_{MC} = \frac{D_{b,tower,upscaled}}{D_{MC,initial}} \quad (74)$$

This scaling factor k_{MC} is applied to the diameter and wall thickness of the main column. The length, meaning draft and elevation, however, are scaled with the main scaling factor k , so that a consistent platform design is obtained.

8.1.3 Scaling Factor for the Upper Columns

The third scaling factor k_{UC} , used for upscaling of the upper column diameter, is determined based on the aim to maintain the nominal pitch of the initial design, which is assumed to be

critical optimized. This criterion is chosen, as the loads on the wind turbine occur in practice to depend more on the single turbine design, rather than follow the theoretical scaling laws.

The nominal pitch is given in Equation 50 in Section 4.1. Thus, the condition, for determining the scaling factor for the upper column diameter, is expressed in Equation 75.

$$q_{5,\text{rated}} = \frac{F_{55,\text{rated,initial}}}{C_{55,\text{initial}}} \stackrel{!}{=} \frac{F_{55,\text{rated,upscaled}}}{C_{55,\text{upscaled}}} \quad (75)$$

Thrust force at rated wind speed, hub height, as well as center of buoyancy, contribute to the overturning moment in the nominator. The first two parameters are given for the larger wind turbine. The position of the center of buoyancy, however, depends on the final platform design and is therefore influenced by the different scaling of main column, upper columns, and the remaining platform dimensions. The variation, however, is small compared to the entire lever arm starting at hub height. The z -coordinate of the center of buoyancy of the upscaled design is hence scaled with the main scaling factor, leading to Equation 76 for the overturning moment of the upscaled floater.

$$F_{55,\text{rated,upscaled}} = F_{T,\text{rated,upscaled}} (z_{\text{hub,upscaled}} - z_{B,\text{initial}}k) \quad (76)$$

The stiffness component in pitch follows Equation 20 in Subsection 3.3.3, and can be determined for the upscaled design, based on the initial platform, considering the different scaling of each component. The following distinctions have to be made:

- The local second-order moment of area of the upper columns $\bar{I}_{y,\text{UC}}$ is a function of the upper column diameter to the power of four, and thus should be scaled with k_{UC}^4 .
- The additional part in the global second-order moment of area of the upper columns, due to the parallel axis theorem, is proportional to the upper column diameter squared times the distance to the global y -axis squared. This part has to scale with $k_{\text{UC}}^2 k^2$.
- The main column is already centered at the global y -axis. Thus, only the basic equation for the second-order moment of area has to be considered, which again depends on the column diameter to the power of four, leading to a scaling of k_{MC}^4 for this part.
- The remaining second-order moments of area of the cross braces, as well as the term $W(z_B - z_G)$ in the stiffness component computation, are scaled with k^4 .

However, the weight of the platform is actually not following the k^3 -scaling, as the final weight has to be adjusted by ballasting to fit the buoyancy. The change of the latter one is considerably influenced by the different scaling of the upper columns. The different scaling of the main column, due to the geometrical constraints, would also influence the displaced water volume, but only with such a small contribution that this could be neglected. The difference in the buoyancy, and thus also in the weight, when scaling the upper columns with k_{UC} instead of k , could be computed by means of Equation 77.

$$\Delta W = \rho_{\text{water}} g \frac{3}{4} \pi D_{\text{UC,initial}}^2 (k_{\text{UC}}^2 - k^2) (-z_{b,\text{UC,initial}}) k \quad (77)$$

This way, the stiffness component in pitch of the upscaled design can be written as given in Equation 78, based on parameters of the initial design.

$$\begin{aligned}
 C_{55,\text{upscaled}} = & \rho_{\text{water}} g \left[\frac{3\pi}{64} D_{\text{UC,initial}}^4 k_{\text{UC}}^4 + \frac{\pi}{4} D_{\text{UC,initial}}^2 k_{\text{UC}}^2 \sum_{i=1}^3 d_{\text{UC,initial},i}^2 k^2 + \frac{\pi}{64} D_{\text{MC,initial}}^4 k_{\text{MC}}^4 \right. \\
 & + \left. \left(\frac{C_{55,\text{initial}}}{\rho_{\text{water}} g} - \frac{3\pi}{64} D_{\text{UC,initial}}^4 - \frac{\pi}{4} D_{\text{UC,initial}}^2 \sum_{i=1}^3 d_{\text{UC,initial},i}^2 - \frac{\pi}{64} D_{\text{MC,initial}}^4 \right) k^4 \right] \\
 & + \Delta W (z_{\text{B,initial}} - z_{\text{G,initial}}) k
 \end{aligned} \tag{78}$$

Substituting Equation 77 in Equation 78 and grouping the terms with the same scaling factors, yields Equation 79.

$$\begin{aligned}
 C_{55,\text{upscaled}} = & \rho_{\text{water}} g \frac{3\pi}{64} D_{\text{UC,initial}}^4 k_{\text{UC}}^4 \\
 & + \rho_{\text{water}} g \frac{\pi}{4} D_{\text{UC,initial}}^2 k^2 \left[\sum_{i=1}^3 d_{\text{UC,initial},i}^2 - 3z_{\text{b,UC,initial}} (z_{\text{B,initial}} - z_{\text{G,initial}}) \right] k_{\text{UC}}^2 \\
 & + \rho_{\text{water}} g \left[\frac{\pi}{64} D_{\text{MC,initial}}^4 k_{\text{MC}}^4 + \left(\frac{3}{4} \pi D_{\text{UC,initial}}^2 z_{\text{b,UC,initial}} (z_{\text{B,initial}} - z_{\text{G,initial}}) \right. \right. \\
 & + \left. \left. \frac{C_{55,\text{initial}}}{\rho_{\text{water}} g} - \frac{3\pi}{64} D_{\text{UC,initial}}^4 - \frac{\pi}{4} D_{\text{UC,initial}}^2 \sum_{i=1}^3 d_{\text{UC,initial},i}^2 - \frac{\pi}{64} D_{\text{MC,initial}}^4 \right) k^4 \right]
 \end{aligned} \tag{79}$$

The scaling factor for the upper column diameter can be computed based on Equations 76 and 79, and the conditional Equation 75. The final Equation 80 for k_{UC} only depends on parameters of the initial platform design, known values of the larger wind turbine, as well as on the two previously determined scaling factors k and k_{MC} .

$$k_{\text{UC}} = \sqrt{\frac{-Y + \sqrt{Y^2 - 4XZ}}{2X}} \tag{80}$$

Equation 80 is written in terms of the free variable parameters X , Y and Z , given in Equations 81 to 83.

$$X = \rho_{\text{water}} g \frac{3\pi}{64} D_{\text{UC,initial}}^4 \tag{81}$$

$$Y = \rho_{\text{water}} g \frac{\pi}{4} D_{\text{UC,initial}}^2 k^2 \left[\sum_{i=1}^3 d_{\text{UC,initial},i}^2 - 3z_{\text{b,UC,initial}} (z_{\text{B,initial}} - z_{\text{G,initial}}) \right] \tag{82}$$

$$\begin{aligned}
 Z = & \rho_{\text{water}} g \left[\frac{\pi}{64} D_{\text{MC,initial}}^4 k_{\text{MC}}^4 + \left(\frac{3}{4} \pi D_{\text{UC,initial}}^2 z_{\text{b,UC,initial}} (z_{\text{B,initial}} - z_{\text{G,initial}}) \right. \right. \\
 & + \left. \left. \frac{C_{55,\text{initial}}}{\rho_{\text{water}} g} - \frac{3\pi}{64} D_{\text{UC,initial}}^4 - \frac{\pi}{4} D_{\text{UC,initial}}^2 \sum_{i=1}^3 d_{\text{UC,initial},i}^2 - \frac{\pi}{64} D_{\text{MC,initial}}^4 \right) k^4 \right] \\
 & - \frac{F_{\text{T,rated,upscaled}} (z_{\text{hub,upscaled}} - z_{\text{B,initial}} k)}{F_{\text{T,rated,initial}} (z_{\text{hub,initial}} - z_{\text{B,initial}})} C_{55,\text{initial}}
 \end{aligned} \tag{83}$$

8.1.4 Further Adjustments

8.1.4.1 Drag Coefficients The new drag coefficients for the upscaled column, pontoon and cross brace diameters, have to be computed, following the procedure in Subsection 3.4.2.

8.1.4.2 Mooring System After scaling the semi-submersible floater with the above introduced scaling factors, the mooring line parameters have to be determined. As already addressed in Section 6.4, the mooring system is just included based on a rough estimate. For this first approach, line diameter, density, extensional stiffness, damping and added mass coefficients, as well as structural damping are taken over from the original OC4 floating wind turbine system design [41]. The mooring line length, however, is to be adjusted such that the same mooring stiffness in surge is obtained.

The new fairlead positions are defined by the upscaled platform. The radius from the platform centerline to the anchor positions is also scaled with the main scaling factor k . This way, both horizontal projection of the total mooring line length $l_{\text{tot,hor}}$ and height of the fairleads above the seabed h , can be determined. With the predefined mooring stiffness in surge and the unchanged line density, the horizontal tension at the touch down point τ_{hor} can be computed for the upscaled floating system, based on Equation 40 in Subsection 3.5.3. The effective line length and finally the total mooring line length can be computed by means of Equations 32 and 34, given in Subsection 3.5.2. This calculation is implemented in MATLAB in Source Code A.8 in Appendix A.5. Starting values for the effective and total line length have to be provided, for solving Equations 32 and 34. Those are taken as the parameters of the original OC4 floating system, scaled up with the main scaling factor k .

8.1.4.3 Ballast System The platform's structural mass, the mass of the lifted mooring line parts, as well as the rotor and nacelle masses of the predefined larger scale wind turbine, can directly be counted to the total system mass. The tower of the wind turbine, however, has to be cut at the elevation of the main column. Thus, only the tower mass without the bottom part, which is to be removed, contribute to the total system mass. This system weight has to be complemented by ballast in the columns, such that the total weight equals the buoyancy due to the displaced water volume of the upscaled platform. Knowing the needed amount of ballast, it has to be checked whether the available inner volume of the columns is enough, when water is used as ballast. If this is not the case, other ballast, like concrete, should be used, so that the inner space is sufficient.

The total ballast could first be distributed anyhow between upper and base column, but with the same levels for each column set. The final position of the ballast within the columns, is then determined based on the computation method given in Appendix A.6, with an aimed nominal pitch of 5° .

8.1.4.4 Controller Gains This final upscaled platform design could then be analyzed with respect to its structural strength, stability and eigenfrequencies. Before the system's dynamic performance is evaluated, the blade-pitch controller gains have to be adjusted, based on the eigenfrequency in pitch and following Subsection 3.6.2.

8.2 Upscaled Semi-Submersible Platform Design for the IWT-7.5-164

The guideline for upscaling of a semi-submersible platform, presented in Section 8.1, is applied to the optimized DeepCwind floater, derived in Section 7.2, and the aimed offshore wind turbine IWT-7.5-164 by Fraunhofer [7, 46], assuming the same water depth of 200 *m*.

The scaling factors for the main components, main column, and upper columns are determined, based on Equations 73, 74, and 80 to 83, to be $k = 1.172$, $k_{MC} = 1.077$, and $k_{UC} = 1.282$. This yields the final parameters of the upscaled semi-submersible platform for the IWT-7.5-164, summarized in Table 8.1 and compared with the values of the optimized DeepCwind floater.

The center of gravity of the upscaled system is located at -13.30 *m* and the center of buoyancy at -15.97 *m*. Compared to the optimized semi-submersible floater design, it can be observed that those positions scale with less than the main scaling factor, which is due to the considerably larger scaling factor for the upper columns.

From Table 8.1 it can be seen that the platform steel mass scales, with a factor of 1.184 to the power of three, slightly higher, compared to the main scaling factor. This is because of the larger scaling factor for the upper columns. The amount of ballast scales even higher, with a factor of 1.197 to the power of three, as it has to be accounted for the larger buoyancy volume due to the increased upper column diameter. The mass of the total floating wind turbine system, however, scales with a factor of 1.189 to the power of three, and is hence just by 1.5% higher than the main scaling factor based on the top structure mass ratio.

The re-calculation of the drag coefficients of the platform members yields unchanged coefficients for the main and base columns ($C_{D,MC} = 0.62$, $C_{D,BC} = 0.70$), and slightly increased coefficients of $C_{D,UC} = 0.67$ and $C_{D,CB} = 0.55$ for the upper columns, as well as cross braces and pontoons, compared to 0.66 and 0.54, respectively, for the optimized DeepCwind floater.

8.2.1 Static Analysis of the Upscaled Platform Design for the IWT-7.5-164

The performance of the upscaled semi-submersible platform design for the IWT-7.5-164 is analyzed based on the three different methods, introduced in Sections 4.1 to 4.3.

8.2.1.1 System Matrices The system matrices, upscaled and optimized DeepCwind design in comparison, are presented in Table 8.2. The values for the optimized OC4 floater are based on the results obtained by HydroD, given in Table 7.2 in Subsection 7.2.1.

The equation-based added mass calculation, introduced in Section 3.3, is not that accurate and underestimates the added mass components by 13% to 23%. More comparable results are obtained by upscaling the added mass values of the optimized DeepCwind floater. Those values, presented in brackets in Table 8.2, are, however, slightly higher than the low-frequency added mass limits obtained by HydroD, as the reducing effect of the larger scaling factor for the upper columns is not considered in this approximation based on the main scaling factor.

The equation-based stiffness calculation yields similar values as obtained by HydroD. However, scaling the stiffness parameters of the optimized DeepCwind platform based on the main scaling factor, would significantly underestimate the stiffness, as especially the stiffness component in heave, but also the component in pitch, are mainly influenced by the upper column diameter.

8.2.1.2 Nominal Pitch Even if the optimization procedure is performed without inclusion of the mooring stiffness, a nominal pitch of 4.8° is obtained, which is close to the aimed value of 5° . Simulation in Dymola, based on Modelica, yields with 4.6° a comparable result.

Table 8.1: Main dimensions of the upscaled platform for the IWT-7.5-164

| Element | Parameter | Unit | k | IWT floater | Optimized OC4 floater |
|----------------|---------------------------------|------|----------|-------------|-----------------------|
| MC | Diameter | m | k_{MC} | 7.00 | 6.50 |
| | Wall thickness | m | k_{MC} | 0.032 | 0.030 |
| | Elevation above SWL | m | k | 11.72 | 10.00 |
| | Depth of base below SWL | m | k | 23.45 | 20.00 |
| OC | Wall thickness | m | k | 0.070 | 0.060 |
| | Elevation above SWL | m | k | 14.07 | 12.00 |
| | Spacing between OCs | m | k | 58.62 | 50.00 |
| | Depth of base below SWL | m | k | 23.45 | 20.00 |
| UC | Diameter | m | k_{UC} | 12.70 | 9.90 |
| | Length | m | k | 30.48 | 26.00 |
| | Height of ballast (water) | m | — | 6.726 | 2.630 |
| BC | Diameter | m | k | 28.14 | 24.00 |
| | Length | m | k | 7.03 | 6.00 |
| | Height of ballast (water) | m | — | 6.215 | 5.625 |
| Pontoons, CBs | Diameter | m | k | 1.88 | 1.60 |
| | Wall thickness | m | k | 0.0205 | 0.0175 |
| Upper pontoons | Length DU | m | — | 45.92 | 40.10 |
| | Length YU | m | — | 24.00 | 20.67 |
| | Elevation above SWL | m | k | 11.72 | 10.00 |
| Lower pontoons | Length DL | m | k | 30.48 | 26.00 |
| | Length YL | m | — | 16.28 | 13.62 |
| | Depth below SWL | m | k | 19.93 | 17.00 |
| CB | Length | m | — | 38.18 | 32.69 |
| | Elevation above SWL | m | k | 10.70 | 9.13 |
| | Depth below SWL | m | k | 18.99 | 16.20 |
| Mooring system | Depth to fairleads below SWL | m | k | 16.41 | 14.00 |
| | Depth to anchors below SWL | m | 1 | 200 | 200 |
| | Radius to fairleads | m | k | 47.91 | 40.87 |
| | Radius to anchors | m | k | 982.0 | 837.6 |
| | Unstretched mooring line length | m | — | 972.4 | 835.5 |
| | Effective mooring line length | m | — | 586.7 | 594.4 |
| Masses | RNA | kg | — | 4.934E+5 | 3.500E+5 |
| | Tower | kg | — | 447,916 | 249,718 |
| | Platform steel | kg | — | 5.914E+6 | 3.567E+6 |
| | Ballast | kg | — | 1.433E+7 | 0.835E+7 |
| | Platform total | kg | — | 2.024E+7 | 1.192E+7 |
| | Total system | kg | — | 2.138E+7 | 1.271E+7 |

Table 8.2: Comparison of the system matrices of the upscaled platform for the IWT-7.5-164, added mass in brackets based on upscaling

| Parameter | Unit | Calculated | HydroD | Modelica | Optimized OC4 | |
|-----------|----------------|------------------------------|------------------------|----------|---------------|----------|
| M_{33} | kg | 21.38E+6 | 21.38E+6 | 21.38E+6 | 12.71E+6 | |
| M_{55} | kgm^2 | 3.21E+10 | 3.21E+10 | — | 1.65E+10 | |
| A_{33} | kg | $ \omega \rightarrow 0$ | 22.00E+6 (25.96E+6) | 25.28E+6 | — | 16.11E+6 |
| | | $ \omega \rightarrow \infty$ | — | 24.13E+6 | — | 15.42E+6 |
| A_{55} | kgm^2 | $ \omega \rightarrow 0$ | 13.31E+9 (17.72E+9) | 17.33E+9 | — | 8.00E+9 |
| | | $ \omega \rightarrow \infty$ | — | 16.34E+9 | — | 7.51E+9 |
| C_{33} | $kg s^{-2}$ | 4.315E+6 | 4.292E+6 | — | 2.712E+6 | |
| C_{55} | $kgm^2 s^{-2}$ | 1.689E+9 | 1.685E+9 | — | 0.804E+9 | |

8.2.1.3 Stability Due to the geometrical changes, the hand calculated stability range is decreased from $[-19.5^\circ, 18.9^\circ]$ to $[-16.7^\circ, 18.9^\circ]$, compared to the optimized DeepCwind floater.

The exact stability range, obtained by HydroD, is again slightly reduced from $[-102.3^\circ, 97.9^\circ]$ to $[-94.8^\circ, 90.7^\circ]$. The righting moment curve, shown together with the wind heeling moment curve in Figure 8.1, is thus steeper than the curve of the optimized platform, plotted in black.

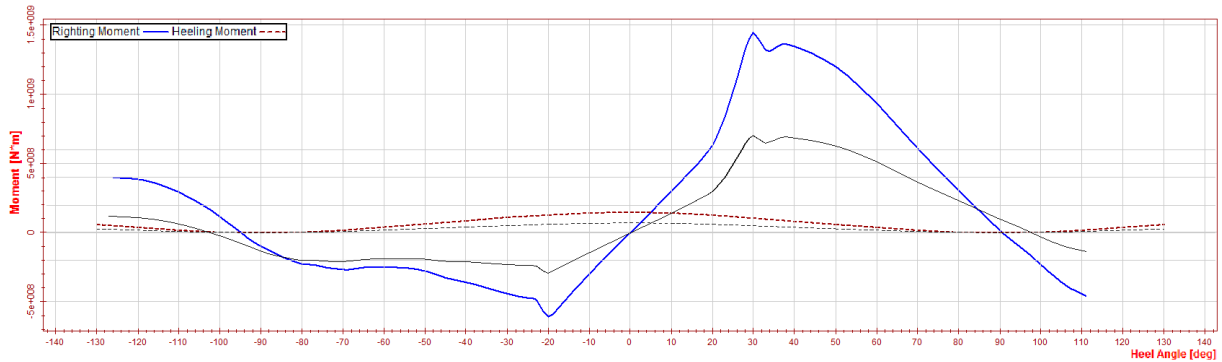


Figure 8.1: Moment curves of the upscaled platform for the IWT-7.5-164, optimized OC4 floater in black

The area under the righting moment curve is also further reduced from 11.4 to 10.2 times the area under the wind heeling moment curve to the second intercept with the righting moment curve. This factor is still considerably larger than the required value of 1.3, meaning that the intact floating stability criterion, given in Paragraph 3.2.2.4, is more than fulfilled.

8.2.1.4 Natural Periods The natural periods of the floating system for Fraunhofer's IWT-7.5-164 are presented in Table 8.3, together with the values of the optimized DeepCwind design. As two methods for determining the added mass components are applied in the hand calculations, the results based on the upscaled added mass values are added in brackets. Considering the hand calculations based on those upscaled added mass components, as well as the more accurate counting method in Dymola, it can be observed from Table 8.3 that the natural periods in heave and pitch are comparable for all methods. The natural periods in surge and yaw, obtained by HydroD and Dymola, however, again differ significantly, which is due to the implemented mooring system model in Modelica, as already noted in Section 4.4.

Table 8.3: Comparison of the natural periods of the upscaled platform for the IWT-7.5-164, added mass in brackets based on upscaling, values of the optimized OC4 floater design based on HydroD

| Parameter | Unit | Calculated | HydroD | Modelica | | Optimized OC4 |
|--------------------|------|----------------|--------|----------|-------|---------------|
| | | | | Counted | FFT | |
| $T_{\text{nat},1}$ | s | — | 136.9 | 181.3 | 171.4 | 104.9 |
| $T_{\text{nat},3}$ | s | 19.9 (20.8) | 20.6 | 20.7 | 20.0 | 20.4 |
| $T_{\text{nat},5}$ | s | 31.8 (33.3) | 33.2 | 33.1 | 33.3 | 34.7 |
| $T_{\text{nat},6}$ | s | — | 113.2 | 138.6 | 128.6 | 73.7 |

The upscaled floating system for the IWT-7.5-164 performs slightly better in heave than the optimized OC4 floater carrying the NREL 5 MW. The natural period in pitch, however, is around 1.5 s shorter, which is because of the larger scaling factor for the upper columns. But still, the pitch natural period (33.2 s) is above the aimed value of 30 s, defined in Section 6.2. The natural periods in surge and yaw are significantly larger compared to the optimized OC4 system. The reason for this is that the same mooring stiffness is assumed for the upscaled design, as initially used for the OC4 semi-submersible. An increased mooring stiffness would be more appropriate and then also reduce the natural periods in surge and yaw. However, the final design of the mooring system is left for future work, as indicated in Section 6.4. The change in the natural periods compared to the optimized DeepCwind floating system can also be seen in Figure 8.2, showing the time series from the free decay tests in Dymola. Slightly different results are obtained by the simulation in Dymola, as the pitch eigenperiod is increased by 0.3 s, when comparing the Modelica results.

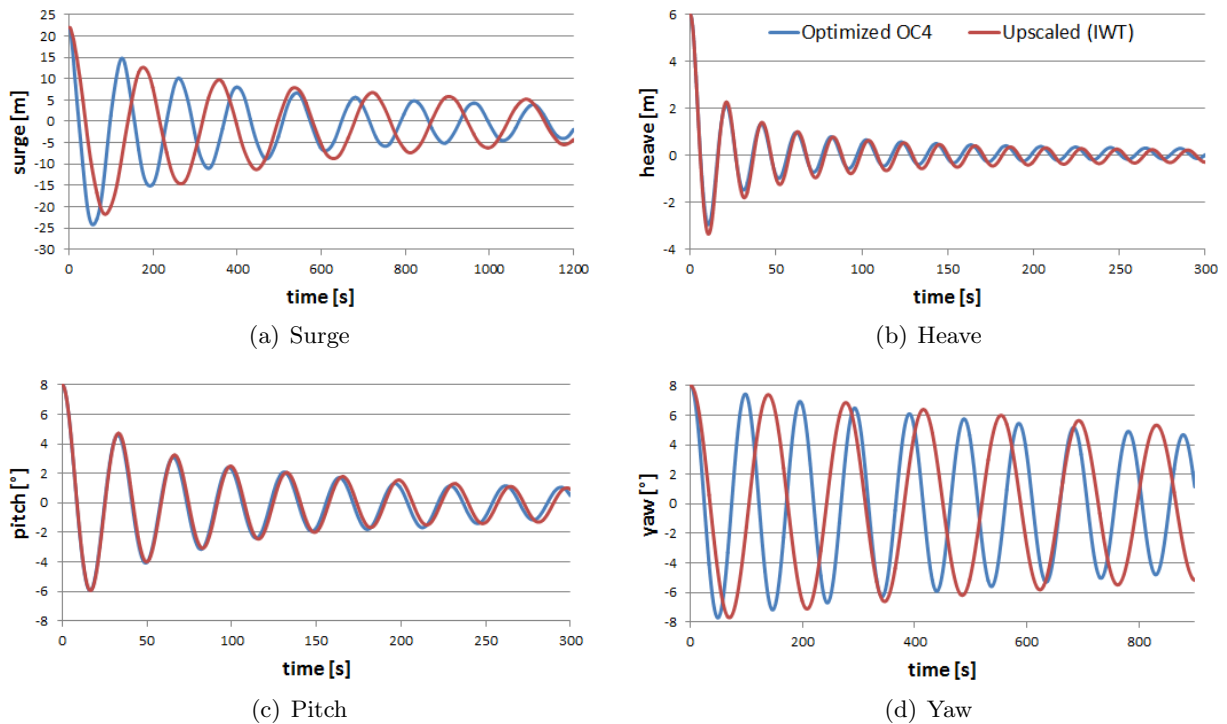


Figure 8.2: Free decay time series of the upscaled platform for the IWT-7.5-164, in comparison with the optimized OC4 floater, based on Modelica

8.2.1.5 Controller Gains Given parameters for the direct drive wind turbine IWT-7.5-164, needed in the controller gain calculation, are $\Omega_{\text{rated,LSS}} = 10.0 \text{ rpm}$ and $N_{\text{gear}} = 1$ [46]. As the available data sheet did not include the turbine inertias, all inertias, thus also the mass moment of inertia of the drivetrain, are estimated based on the given masses and dimensions of the components. With a generator rotor mass of $39,300 \text{ kg}$ and a generator inner diameter of 4.5 m , a mass moment of inertia of the drivetrain of $I_{\text{drivetrain,LSS}} = 99,478 \text{ kgm}^2$ is computed based on Equation 84. This is, due to the direct drive mechanism, independent of the shaft side.

$$I_{\text{drivetrain}} = \frac{1}{2} m_{\text{gen,rotor}} \frac{D_{\text{gen,rotor}}^2}{4} \quad (84)$$

The blade-pitch sensitivity at rated and the rotor-collective blade-pitch angle at doubled pitch sensitivity are determined for the IWT-7.5-164, based on the trend line shown in Figure 8.3 and the corresponding explicit values given in Table 8.4, obtained by the computations in MATLAB, presented in Appendix A.2. As, however, the wind turbine also uses a peak shaver, and thus the rated wind speed depends on the peak shaver, the blade-pitch sensitivity at rated is taken as the value at zero pitch. This way $\frac{\partial P}{\partial \theta} \Big|_{0^\circ} = -16.35E+6 \text{ W rad}^{-1}$ and $\theta_K = 2.679344^\circ$ are obtained. Using $\zeta_c = 0.7$ and $\omega_{c,\text{nat}} \approx 0.14 \text{ rad s}^{-1}$, based on the recommendations given in Subsection 3.6.2 and the determined system's pitch natural frequency, the adjusted blade-pitch controller gains are computed to be $K_P = 0.01196179 \text{ s}$ and $K_I = 0.001196179$.

Table 8.4: Sensitivity of aerodynamic power to blade-pitch for the IWT-7.5-164

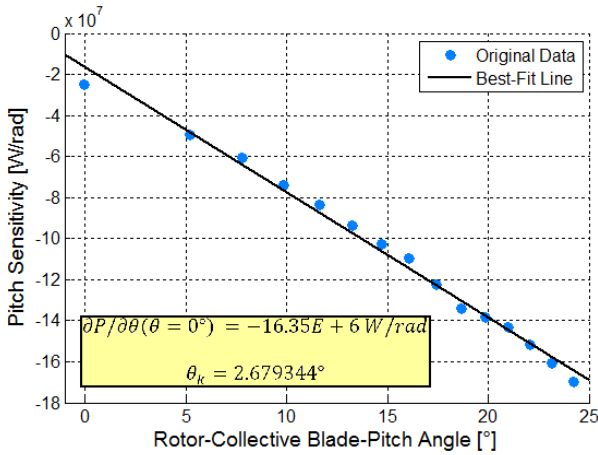


Figure 8.3: Best-fit line of pitch sensitivity above rated wind speed for the IWT-7.5-164

| Wind speed [ms^{-1}] | Pitch angle [$^\circ$] | $\partial P/\partial \theta$ [$W \text{ rad}^{-1}$] |
|-----------------------------|-----------------------------|--|
| 11.0 | -0.06 | -24.70E+6 |
| 12.0 | 5.18 | -49.16E+6 |
| 13.0 | 7.81 | -60.32E+6 |
| 14.0 | 9.86 | -73.86E+6 |
| 15.0 | 11.63 | -83.39E+6 |
| 16.0 | 13.23 | -93.36E+6 |
| 17.0 | 14.70 | -102.66E+6 |
| 18.0 | 16.07 | -109.50E+6 |
| 19.0 | 17.39 | -122.28E+6 |
| 20.0 | 18.64 | -133.93E+6 |
| 21.0 | 19.83 | -138.45E+6 |
| 22.0 | 20.97 | -143.19E+6 |
| 23.0 | 22.08 | -151.29E+6 |
| 24.0 | 23.15 | -160.41E+6 |
| 25.0 | 24.19 | -169.41E+6 |

In order to get an estimate of the accuracy of this calculation, the computed blade-pitch angles at discrete wind speeds are compared in Table 8.5 with the data for the IWT-7.5-164 [46]. Values for the blade-pitch sensitivity, however, were not available. The computed blade-pitch angles differ only by maximum 4% from the original values. However, close to rated wind speed, different pitch angles are specified in the original data [46], as this includes the peak shaver. Hence, the determination method is in general assumed to yield reliable results, but the blade-pitch sensitivity at rated is taken at zero pitch, as already indicated above.

Table 8.5: Blade-pitch angles at different wind speeds for the IWT-7.5-164

| Wind speed [ms^{-1}] | Pitch angle [$^{\circ}$] | | Wind speed [ms^{-1}] | Pitch angle [$^{\circ}$] | |
|-----------------------------|----------------------------|---------------|-----------------------------|----------------------------|---------------|
| | Computed | Original [46] | | Computed | Original [46] |
| 6.0 | – | 0.00 | 16.0 | 13.23 | 12.79 |
| 7.0 | – | 0.00 | 17.0 | 14.70 | 14.18 |
| 8.0 | – | 0.04 | 18.0 | 16.07 | 15.47 |
| 9.0 | – | 0.23 | 19.0 | 17.39 | 16.69 |
| 10.0 | – | 0.94 | 20.0 | 18.64 | 17.88 |
| 11.0 | -0.06 | 2.81 | 21.0 | 19.83 | 19.01 |
| 12.0 | 5.18 | 5.32 | 22.0 | 20.97 | 20.11 |
| 13.0 | 7.81 | 7.57 | 23.0 | 22.08 | 21.18 |
| 14.0 | 9.86 | 9.55 | 24.0 | 23.15 | 22.21 |
| 15.0 | 11.63 | 11.27 | 25.0 | 24.19 | 23.23 |

8.2.2 Dynamic Analysis of the Upscaled Platform Design for the IWT-7.5-164

The dynamic analysis in HydroD is performed for 15 sea states, as introduced in Subsection 4.2.3. The standard deviations of the motions, depending on significant wave height and peak period, are presented in Figure 8.4. This shows increasing dynamic response with increasing severity of the sea state. The maximum dynamic motions in the, by the wave directionality mainly affected, DoFs are presented in Table 8.6. Comparison with the optimized OC4 platform yields that the dynamic motions are reduced by 12% in surge, 23% in heave and 14% in pitch.

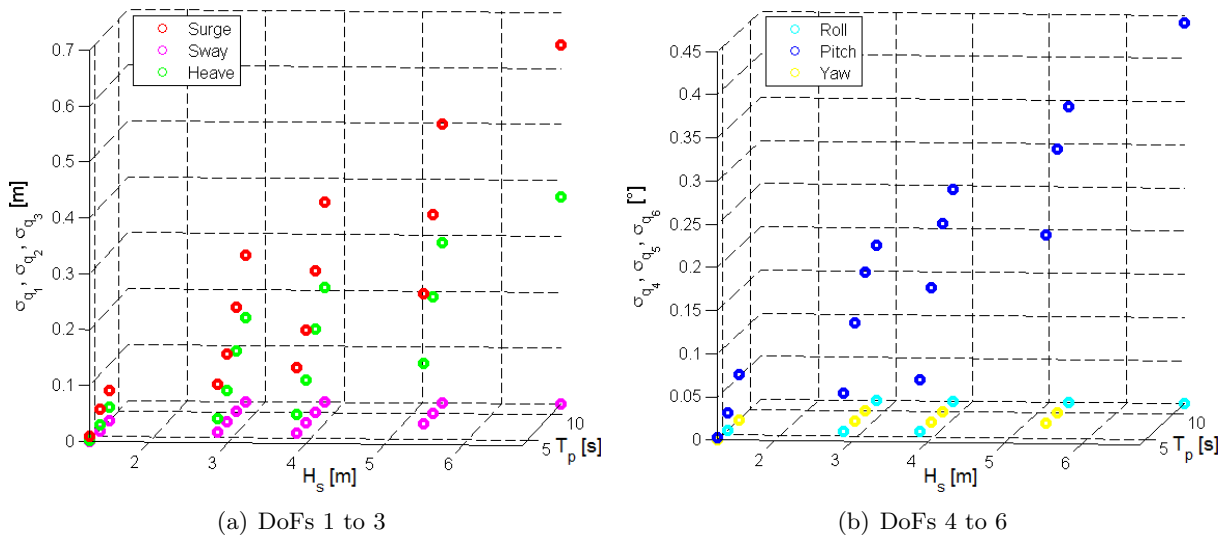


Figure 8.4: Dynamic response of the upscaled platform for the IWT-7.5-164, based on HydroD

Table 8.6: Dynamic response of the upscaled platform for the IWT-7.5-164, based on HydroD

| Parameter | Unit | IWT floater | Optimized OC4 floater |
|-------------------|------------|-------------|-----------------------|
| $\sigma_{q1,max}$ | m | 0.64 | 0.73 |
| $\sigma_{q3,max}$ | m | 0.37 | 0.48 |
| $\sigma_{q5,max}$ | $^{\circ}$ | 0.44 | 0.51 |

The dynamic analysis based on Modelica and Dymola, however, shows a slightly increased dynamic motion in surge in the wind and wave simulation, presented in Figure 8.5(d), while the standard deviation is decreased in the wind-only tests, shown in Figure 8.5(b), compared to the optimized OC4 floater plotted in dotted lines. But still, the dynamic motion in surge is much higher in the simulation without waves, compared to the coupled wind and wave simulation. This demonstrates that combined wind and waves could reduce the system's dynamic motion. The results from the simulation with waves are comparable in magnitude with the dynamic response data obtained by HydroD, presented in Figure 8.4 and Table 8.6. However, the decrease in the dynamic pitch motion is more significant in the results from Dymola.

The mean displacement in surge is increased, compared to the optimized platform design, and reaches around 12 m in the wind-only simulation and 10 m in the simulation with wind and irregular waves, shown in Figures 8.5(a) and 8.5(c), respectively. This higher motion is due to the mooring system, as already explained. The nominal platform pitch angle at rated wind speed of close to 5° is also visible in both simulations.

Overall, the platform's mean and dynamic displacements, as well as the blade-pitch angle, are increasing with increasing wind speed up to rated, and decreasing again at higher wind velocities. Hence, they show the same behavior as the optimized and original semi-submersible floaters, plotted in dotted and dashed lines, respectively, in Figure 8.5, influenced by the rotor thrust at different wind speeds.

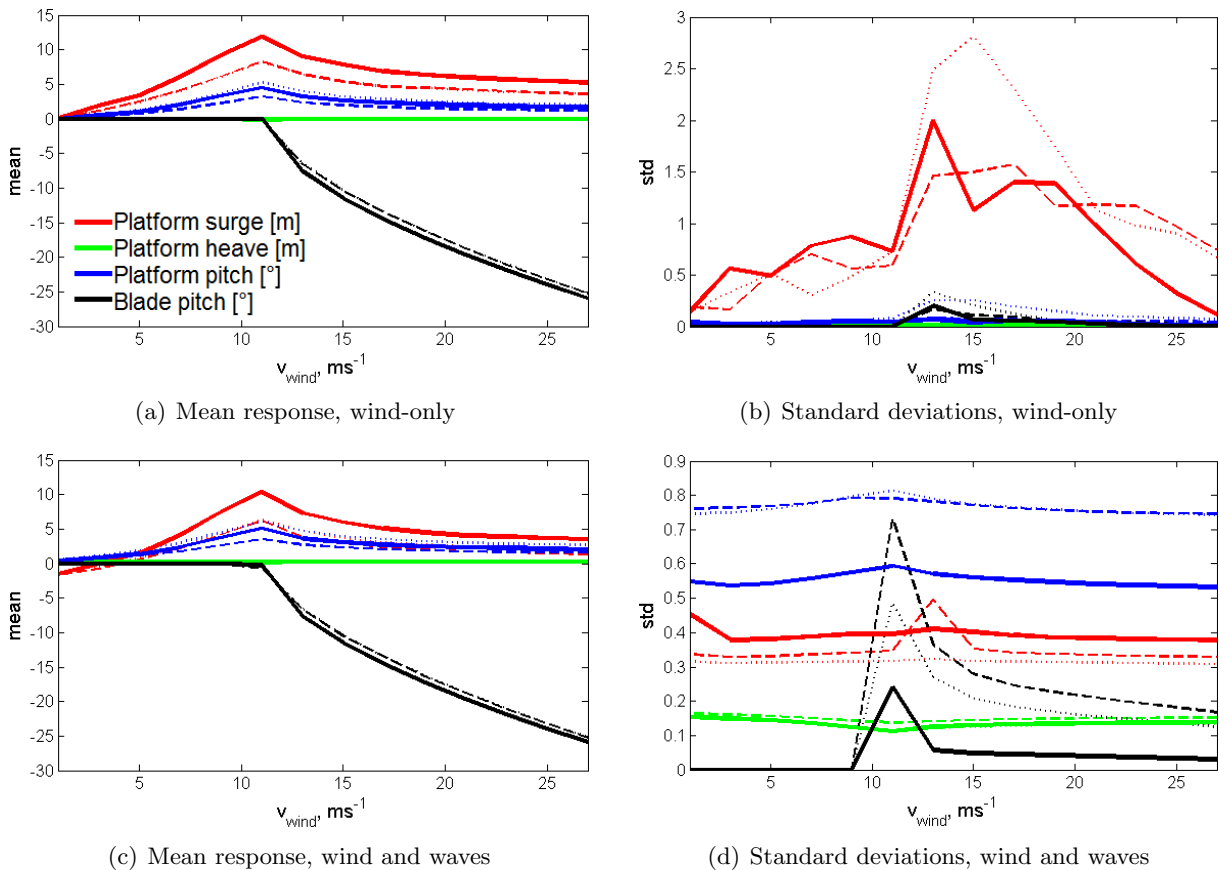


Figure 8.5: Mean and dynamic response of the upscaled platform for the IWT-7.5-164, in comparison with the optimized OC4 platform responses in dotted lines and the original OC4 platform responses in dashed lines

For the check of the adjusted blade-pitch controller gains, the time series of the simulation with ramped wind and without waves is presented in Figure 8.6. This demonstrates that the

computed controller gains yield a stable floating wind turbine system for the IWT-7.5-164. The dynamic motion response is the highest at rated wind speed when the blades just start pitching, which could be also obtained from Figure 8.5(b). However, for longer time duration and higher wind speeds, the variation in the pitch motion of the platform, as well as the oscillations in the blade-pitch angle are decreasing.

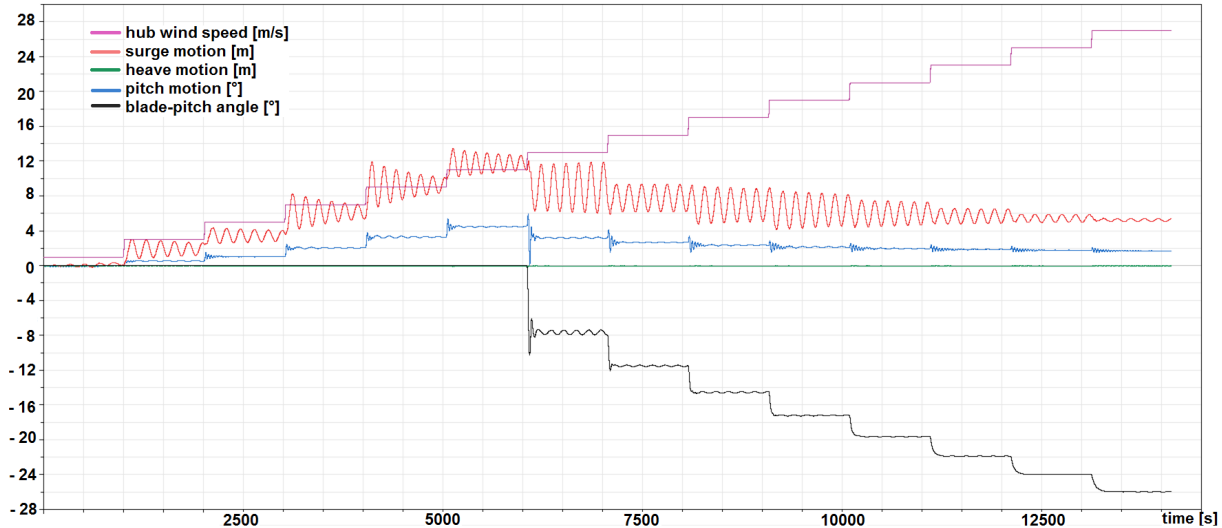


Figure 8.6: Response of the upscaled platform for the IWT-7.5-164 at different wind speeds

8.2.3 Structural Analysis of the Upscaled Platform Design for the IWT-7.5-164

Performing the structural strength check, as described in Section 6.6, leads to following equivalent stresses at the bottom of the upper column, presented in Table 8.7.

Table 8.7: Equivalent stress calculation for the upscaled platform for the IWT-7.5-164, values given in MPa

| Pressure combination | Load point position | | |
|---|-----------------------------|--------------------------------|-----------------------------|
| | Outer wall ($\delta = 0$) | Wall center ($\delta = 0.5$) | Inner wall ($\delta = 1$) |
| $p_{\text{tank,min}}, p_{\text{water,max}}$ | 48.2 | 48.5 | 48.7 |
| $p_{\text{tank,max}}, p_{\text{water,min}}$ | 13.0 | 13.1 | 13.2 |

The more critical pressure combination is at minimum inner pressure and maximum sea pressure, and the stress is increasing from the outer wall through the wall thickness to the inner side of the column wall, as it is the same trend for the optimized DeepCwind semi-submersible platform design.

The yield stress for steel S355, however, is due to the upscaled wall thickness of the upper columns (0.07 m) decreased to 325 MPa , based on Table 6.1 in Section 6.6. Comparing the equivalent stresses, given in Table 8.7, with the yield stress, results in a structural safety factor of 6.7 to 25.0. That is a reduction of around 21% for the minimum safety factor, compared to the optimized DeepCwind platform, but a safety factor of 6.7 is still conservative enough. However, a more detailed structural analysis is needed for ensuring structural integrity of the upscaled platform design, as mentioned in Section 6.6.

8.3 Upscaled Semi-Submersible Platform Designs for the DTU 10 MW

The upscaling guideline, given in Section 8.1, is also used for obtaining a floating platform for the DTU 10 MW reference wind turbine. This is done in two ways: one approach is based on the optimized OC4 semi-submersible, while the other one uses the upscaled floater for the IWT-7.5-164 as basis for applying the upscaling procedure. The scaling factors for both methods and the resulting platform parameters are presented in Tables 8.8 and 8.9, respectively.

Table 8.8: Scaling factors for the floating platforms for the DTU 10 MW

| Basic design | Optimized OC4 floater | IWT floater |
|--------------|-----------------------|-------------|
| k | 1.264 | 1.078 |
| k_{MC} | 1.277 | 1.186 |
| k_{UC} | 1.439 | 1.202 |

As it can be seen from Table 8.9, all dimensions, that are scaled with the main scaling factor or the scaling factor for the main column, are equal for both upscaled designs. This can be substantiated by comparing the scaling factors for the DTU floater based on the optimized OC4 floater ($k = 1.264$, $k_{MC} = 1.277$) with the product of the scaling factors for the IWT floater ($k = 1.172$, $k_{MC} = 1.077$) and the DTU floater based on the IWT floater ($k = 1.078$, $k_{MC} = 1.186$). As those scaling factors depend on predefined masses or dimensions, in total the same values are obtained, irrespectively of whether a direct or stepwise upscaling method is applied.

Comparison of the scaling factors for the upper columns, however, shows that, including $k_{UC} = 1.282$ for the IWT floater, a total scaling factor of 1.541 is obtained by means of the successive upscaling method. This is a by 7% higher factor than obtained by directly upscaling. The effects are seen in the different values for the upper column diameter, upper pontoon and cross brace lengths, ballast heights, as well as the centers of gravity and buoyancy. Those are $z_G = -14.04\text{ m}$ and $z_B = -16.96\text{ m}$ for the platform based on the optimized DeepCwind floater, and $z_G = -12.09\text{ m}$ and $z_B = -16.61\text{ m}$ for the IWT-based design. Thus, it is expected that the floating system, based on the iterative upscaling method, has a reduced stability range, compared to the system obtained by the direct upscaling approach. As successively upscaling yields a by 1 m larger upper column diameter, also the platform steel, ballast, and total system masses are increased. The corresponding semi-submersible platform is thus by 4.8% heavier than the floater obtained based on the optimized OC4 design.

Based on those outcomes, it is recommended to use directly the optimized platform design as basis for upscaling, rather than an already upscaled floater, as this is not that critically optimized.

Despite those divergences, the different upper column diameters do not affect the drag coefficient for the upper column. Thus, $C_{MC} = 0.57$, $C_{BC} = 0.70$, $C_{UC} = 0.67$, and $C_{CB} = 0.56$ are obtained for both upscaled designs, based on the method introduced in Subsection 3.4.2.

In the following Subsections 8.3.1 to 8.3.3, both obtained designs for the DTU 10 MW wind turbine are analyzed and compared, based on hand calculations and HydroD. A system analysis in Dymola, however, was, due to the time-consuming implementation and simulation based on Modelica, not feasible within the limited timeframe for this work.

8.3.1 Static Analysis of the Upscaled Platform Designs for the DTU 10 MW

8.3.1.1 System Matrices The results for the system matrices of both upscaled designs for the DTU 10 MW are presented, together with the HydroD results for the basic floater designs (optimized OC4 platform and IWT floater), in Table 8.10.

Table 8.9: Main dimensions of the upscaled platforms for the DTU 10 MW

| Element | Parameter | Unit | k | Basic floater design | |
|----------------|---------------------------------|------|----------|----------------------|----------|
| | | | | Opt. OC4 | IWT |
| MC | Diameter | m | k_{MC} | 8.30 | 8.30 |
| | Wall thickness | m | k_{MC} | 0.038 | 0.038 |
| | Elevation above SWL | m | k | 12.64 | 12.64 |
| | Depth of base below SWL | m | k | 25.28 | 25.28 |
| OC | Wall thickness | m | k | 0.076 | 0.076 |
| | Elevation above SWL | m | k | 15.17 | 15.17 |
| | Spacing between OCs | m | k | 63.21 | 63.21 |
| | Depth of base below SWL | m | k | 25.28 | 25.28 |
| UC | Diameter | m | k_{UC} | 14.30 | 15.30 |
| | Length | m | k | 32.87 | 32.87 |
| | Height of ballast (water) | m | — | 5.237 | 14.538 |
| BC | Diameter | m | k | 30.34 | 30.34 |
| | Length | m | k | 7.59 | 7.59 |
| | Height of ballast (water) | m | — | 7.376 | 5.340 |
| Pontoons, CBs | Diameter | m | k | 2.02 | 2.02 |
| | Wall thickness | m | k | 0.0221 | 0.0221 |
| Upper pontoons | Length DU | m | — | 48.91 | 47.91 |
| | Length YU | m | — | 25.19 | 24.69 |
| | Elevation above SWL | m | k | 12.64 | 12.64 |
| Lower pontoons | Length DL | m | k | 32.87 | 32.87 |
| | Length YL | m | — | 17.17 | 17.17 |
| | Depth below SWL | m | k | 21.49 | 21.49 |
| CB | Length | m | — | 40.75 | 40.44 |
| | Elevation above SWL | m | k | 11.54 | 11.54 |
| | Depth below SWL | m | k | 20.48 | 20.48 |
| Mooring system | Depth to fairleads below SWL | m | k | 17.70 | 17.70 |
| | Depth to anchors below SWL | m | 1 | 200 | 200 |
| | Radius to fairleads | m | k | 51.67 | 51.67 |
| | Radius to anchors | m | k | 1058.9 | 1058.9 |
| | Unstretched mooring line length | m | — | 1045.3 | 1045.3 |
| | Effective mooring line length | m | — | 582.6 | 582.6 |
| Masses | RNA | kg | — | 6.767E+5 | 6.767E+5 |
| | Tower | kg | — | 526,767 | 526,767 |
| | Platform steel | kg | — | 7.598E+6 | 7.822E+6 |
| | Ballast | kg | — | 1.877E+7 | 1.981E+7 |
| | Platform total | kg | — | 2.637E+7 | 2.763E+7 |
| | Total system | kg | — | 2.776E+7 | 2.902E+7 |

Table 8.10: Comparison of the system matrices of the upscaled platforms for the DTU 10 MW, added mass in brackets based on upscaling

| Parameter | Unit | Calculated | HydroD | Basic floater design | | |
|-----------|---------------------------------|------------|------------------------|----------------------|----------|----------|
| M_{33} | kg | 27.76E+6 | 27.76E+6 | 12.71E+6 | Opt. OC4 | |
| | | 29.02E+6 | 29.02E+6 | 21.38E+6 | IWT | |
| M_{55} | kgm^2 | 5.33E+10 | 5.33E+10 | 1.65E+10 | Opt. OC4 | |
| | | 5.12E+10 | 5.12E+10 | 3.21E+10 | IWT | |
| A_{33} | $ _{\omega \rightarrow 0}$ | kg | 27.39E+6 (32.55E+6) | 31.40E+6 | 16.11E+6 | Opt. OC4 |
| | | | 26.96E+6 (31.69E+6) | 30.83E+6 | 25.28E+6 | IWT |
| | $ _{\omega \rightarrow \infty}$ | — | 29.87E+6 | 15.42E+6 | Opt. OC4 | |
| | | — | 29.16E+6 | 24.13E+6 | IWT | |
| A_{55} | $ _{\omega \rightarrow 0}$ | kgm^2 | 19.65E+9 (25.84E+9) | 25.01E+9 | 8.00E+9 | Opt. OC4 |
| | | | 19.65E+9 (25.27E+9) | 24.56E+9 | 17.33E+9 | IWT |
| | $ _{\omega \rightarrow \infty}$ | — | 23.60E+9 | 7.51E+9 | Opt. OC4 | |
| | | — | 23.25E+9 | 16.34E+9 | IWT | |
| C_{33} | $kg s^{-2}$ | 5.512E+6 | 5.490E+6 | 2.712E+6 | Opt. OC4 | |
| | | 6.213E+6 | 6.189E+6 | 4.292E+6 | IWT | |
| C_{55} | $kgm^2 s^{-2}$ | 2.521E+9 | 2.515E+9 | 0.804E+9 | Opt. OC4 | |
| | | 2.514E+9 | 2.508E+9 | 1.685E+9 | IWT | |

As already found in the analysis of the IWT floater in Subsection 8.2.1, the added mass computation based on upscaling of the original values, using the main scaling factor, is despite the different scaling of upper and main columns, more accurate than the equation-based computation. Due to the higher scaling factor for the upper column diameter, the upscaled added mass values are slightly higher than those, obtained by HydroD at the low-frequency limit. Analogously to the findings in Subsection 8.2.1, the stiffness components would be significantly underestimated, if scaled up from the original values based on the main scaling factor, as the upper column diameter has a big influence. The stiffness values are only by less than 0.5% overestimated, following the equation-based calculation, which is thus a very accurate method.

Comparing the two platform designs for the DTU 10 MW, based on the values in Table 8.10, yields that the larger upper column diameter in the IWT-based design not only results into an enlarged system mass, but also in a reduced added mass, increased stiffness in heave, but decreased stiffness in pitch, which is all reasonable when looking at the dependencies of those parameters, defined in Subsections 3.3.2 and 3.3.3.

8.3.1.2 Nominal Pitch As the difference between the stiffness components in pitch of both upscaled designs is just less than 0.3%, both designs achieve a nominal pitch of 4.8°.

8.3.1.3 Stability Due to the different upper column diameters, the hand calculations yield a stability range of $[-19.2^\circ, 18.9^\circ]$ for the optimized OC4-based floater design, and a smaller range of $[-16.7^\circ, 18.9^\circ]$ for the IWT-based floater design.

The detailed stability analysis in HydroD also yields a reduced stability range for the successively upscaled floater, which is as expected, as already commented in the beginning of Section 8.3. The real stability ranges are thus $[-95.2^\circ, 90.6^\circ]$ and $[-72.5^\circ, 81.4^\circ]$ for the directly and iteratively upscaled platforms, respectively. This difference can clearly be seen in Figure 8.7, showing the righting and wind heeling moment curves, thin lines for the optimized OC4-based design, and thick lines for the IWT-based floater.

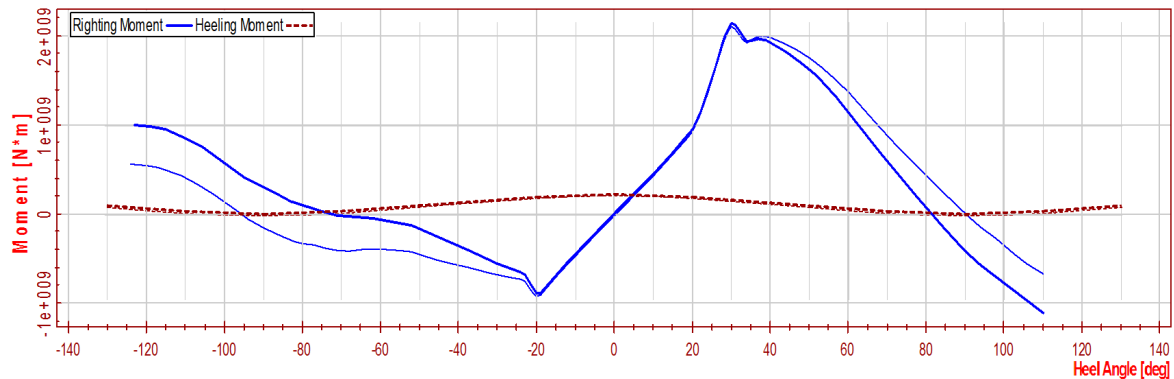


Figure 8.7: Moment curves of the upscaled platforms for the DTU 10 MW, thin line based on optimized OC4 floater, thick line based on IWT floater

As both floaters have quite similar centers of buoyancy, the wind heeling curves do not differ significantly. However, due to the different righting moment curves, the area under this curve to the second intercept with the wind heeling moment curve is for the optimized OC4-based floater by a factor of 10.0, and for the IWT-based design just by a factor of 9.0 larger than the area under the wind heeling moment curve to the same limiting angle. But still, the intact floating stability criteria, given in Paragraph 3.2.2.4, are for both designs more than fulfilled.

8.3.1.4 Natural Periods The natural periods of the two upscaled floater designs are presented in Table 8.11, together with the values of the basic floaters. The natural periods, based on the upscaled added mass components are added in brackets. This demonstrates again that the equation-based computation of the added mass is not that accurate, whereas the upscaling method yields comparable results for the natural periods in heave and pitch.

Table 8.11: Comparison of the natural periods of the upscaled platforms for the DTU 10 MW, added mass in brackets based on upscaling

| Parameter | Unit | Calculated | HydroD | Basic floater design | |
|--------------------|------|----------------|--------|----------------------|----------|
| $T_{\text{nat},1}$ | s | — | 156.7 | 104.9 | Opt. OC4 |
| | | — | 161.1 | 136.9 | IWT |
| $T_{\text{nat},3}$ | s | 19.7 (20.6) | 20.4 | 20.4 | Opt. OC4 |
| | | 18.8 (19.6) | 19.3 | 20.6 | IWT |
| $T_{\text{nat},5}$ | s | 33.2 (34.6) | 34.5 | 34.7 | Opt. OC4 |
| | | 32.8 (34.1) | 34.0 | 33.2 | IWT |
| $T_{\text{nat},6}$ | s | — | 139.6 | 73.7 | Opt. OC4 |
| | | — | 143.5 | 113.2 | IWT |

As the added mass values of the IWT-based floater are smaller than those of the optimized OC4-based design, and the stiffness component in heave is significantly larger, but in pitch just slightly smaller, the natural period in heave is by more than 5% and in pitch by around 1.5% smaller for the IWT-based platform. Thus, the heave natural period of the successively upscaled floater fell below the initially defined threshold of 20 s, while the natural period of 20.4 s could be maintained with the directly upscaled platform design. The heave frequency is not included in the calculation of the scaling factors. However, based on a rough approximation, using Equation 13 and the theoretical scaling of stiffness, mass, and added mass components, it can be estimated, that the natural period in heave would be reduced from the original value, and thus could become critical, if the scaling factor for the diameter of the upper columns exceeds 1.5. With the total scaling factors for the upper column diameter of 1.439 and 1.541 for the directly and successively upscaled designs, the decrease in the natural heave period of the IWT-based floater could already be predicted by means of this simple check.

The natural periods in surge and yaw were further increased, as it was already the case from the optimized DeepCwind platform to the floater design for the IWT-7.5-164. The same reason, as given in Subsection 8.2.1, applies for the DTU floaters, as again the mooring stiffness of the original OC4 system is maintained, and not further adjusted or optimized.

8.3.1.5 Controller Gains In order to adjust the blade-pitch controller gains, the damping should be set equal to $\zeta_c = 0.7$, following the recommendations given in Subsection 3.6.2. Based on Equation 48, the frequency is computed for both floater designs to $\omega_{c,\text{nat}} \approx 0.14 \text{ rad s}^{-1}$. With those values and the DTU turbine parameters, the proportional and integral blade-pitch controller gains are to be determined, following Equations 46 and 47 in Subsection 3.6.2.

8.3.2 Dynamic Analysis of the Upscaled Platform Designs for the DTU 10 MW

The dynamic analysis, based on HydroD, yields comparable sea state dependent standard deviations of the motions for both designs. Those are therefore only for the IWT-based floater presented in Figure 8.8. For a more detailed comparison, the maximum dynamic motions in surge, heave, and pitch are presented in Table 8.12, together with the values of the basic floaters.

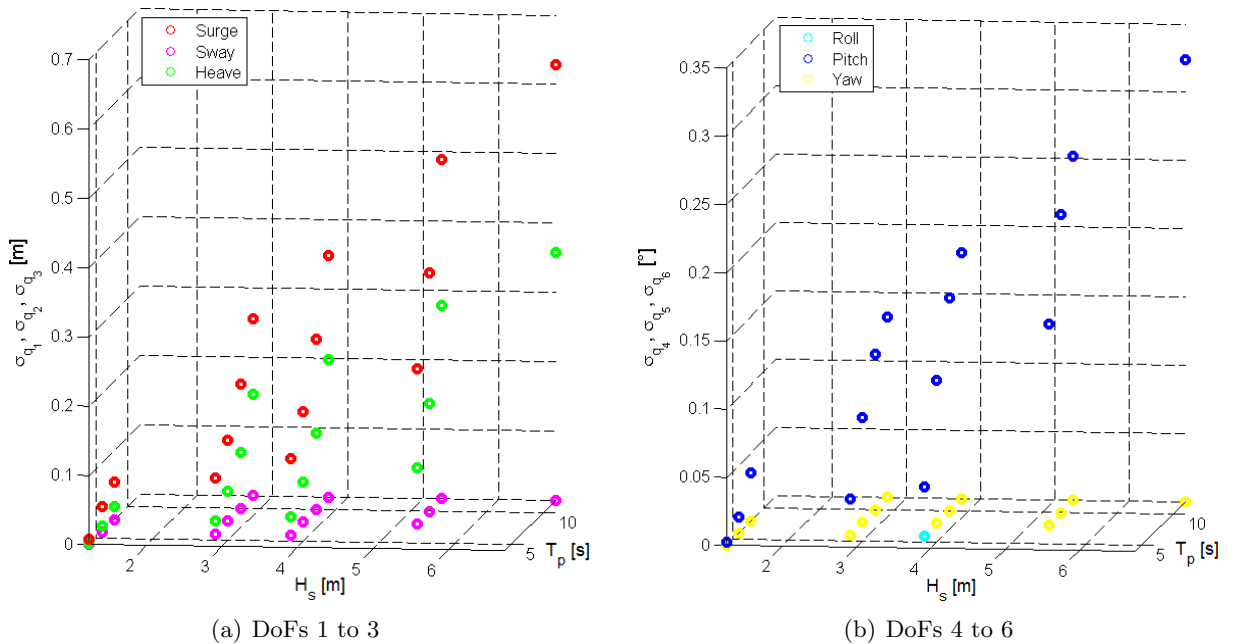


Figure 8.8: Dynamic response of the IWT-based upscaled platform for the DTU 10 MW, based on HydroD

Table 8.12: Dynamic response of the upscaled platforms for the DTU 10 MW, based on HydroD

| Parameter | Unit | DTU floater | Basic floater design | |
|-------------------|---------|-------------|----------------------|----------|
| $\sigma_{q1,max}$ | m | 0.62 | 0.73 | Opt. OC4 |
| | | 0.63 | 0.64 | IWT |
| $\sigma_{q3,max}$ | m | 0.31 | 0.48 | Opt. OC4 |
| | | 0.36 | 0.37 | IWT |
| $\sigma_{q5,max}$ | \circ | 0.34 | 0.51 | Opt. OC4 |
| | | 0.32 | 0.44 | IWT |

From Table 8.12 it can be seen that the dynamic motion response is further decreased, compared to the optimized DeepCwind semi-submersible platform and the upscaled floater for the IWT-7.5-164. This may be due to the increased weight of the total system, which makes the floating wind turbine system more inert, and the fact that the same sea states are considered in the analyses of all designed systems. However, again no statement on the more important relative motions can be made based on this analysis.

8.3.3 Structural Analysis of the Upscaled Platform Designs for the DTU 10 MW

The floating platform design for the DTU 10 MW based on the IWT floater has a by 1 m larger upper column diameter, than the design obtained by direct upscaling of the optimized OC4 floater. However, as the wall thickness of the upper columns is scaled with the main scaling factor, both platform designs have the same upper column wall thickness. Thus, it is expected that the IWT-based floater design has less structural strength, as a larger hollow cylinder is used with the same wall thickness. The results of the structural strength check, presented in Table 8.13, substantiate this presumption.

Table 8.13: Equivalent stress calculation for the upscaled platforms for the DTU 10 MW, values given in MPa

| Pressure combination | Basic floater design | Load point position | | |
|-------------------------------|----------------------|--------------------------------|-----------------------------------|--------------------------------|
| | | Outer wall ($\delta = 0$) | Wall center ($\delta = 0.5$) | Inner wall ($\delta = 1$) |
| $p_{tank,min}, p_{water,max}$ | Opt. OC4 | 53.5 | 53.7 | 54.0 |
| | IWT | 57.2 | 57.5 | 57.7 |
| $p_{tank,max}, p_{water,min}$ | Opt. OC4 | 14.7 | 14.8 | 14.8 |
| | IWT | 15.8 | 15.8 | 15.9 |

The yield stress for steel S355 amounts, for a wall thickness of 0.076 m , 325 MPa , based on Table 6.1 in Section 6.6. With the equivalent stresses from Table 8.13, a minimum safety factor of 6.0 is obtained, for the more critical pressure combination ($p_{tank,min}$ and $p_{water,max}$) and at the weaker location on the inner wall side, for the floater design based on the optimized OC4 platform. The safety factor for the IWT-based floater design, however, is at the same considered load point just 5.6. Still, both safety factors are sufficiently high for the performed strength check, however, a more detailed structural analysis is strongly recommended. Furthermore, the different safety factors demonstrate that the successively upscaled floater shows also a deficit regarding the structural strength, compared to the semi-submersible platform for the DTU 10 MW designed directly based on upscaling of the optimized DeepCwind floater.

9 Conclusion and Recommendation

9.1 Conclusion

In this thesis work, a guideline for the optimization and upscaling procedure of a semi-submersible platform is given, such that a predefined larger wind turbine could be supported. The designed floating systems are analyzed based on hand calculations, with the help of HydroD and Wadam, and by means of simulations in Dymola, based on models implemented in Modelica.

An initial floater for Fraunhofer's wind turbine IWT-7.5-164 is designed, based on an elementary upscaling of the DeepCwind semi-submersible floater, following mainly the power rating. Two variants, one with water as ballast, the other one with concrete, are analyzed and compared regarding their static properties and dynamic performances.

Based on those results, the following recommendations for upscaling and analyzation are given:

- The main scaling factor should be based on the mass ratio of the top structures, rather than on the power rating, as the latter one does not include any technical development in the turbine design, in which mass reduction is aimed.
- As the original DeepCwind semi-submersible floater is already over-conservatively designed, a change of the ballast from water to concrete for stability reasons is not needed, and also not recommended due to cost factors. A denser ballast is only required, if the needed water volume would exceed the available space within the columns.
- The natural frequencies should be moved further away from the wave excitation. This could be achieved for the heave DoF by applying a smaller scaling factor for the upper columns. The pitch natural frequency could be decreased by lifting up the ballast, to obtain a higher center of gravity. This, however, has to be proved with the stability criteria, as well as with the maximum allowable pitch.
- The mooring system should be included in the upscaling procedure, at least in a first approach. Thus, the radius to the anchor positions should also be scaled with the main scaling factor, and the mooring line length should be determined so that a certain mooring stiffness is obtained.
- In the hand calculations, the added mass components in heave and pitch should be determined by scaling the values of the basic design with the main scaling factor to the power of three and five, respectively. This would yield more accurate values than the equation-based computations, even if different scaling factors are used for upper and main columns.
- The equation-based determination of the stiffness components is very accurate.

Those conclusions and recommendations make up the basis for the criteria for the detailed optimization and upscaling procedure. Furthermore, the aims for the natural periods of at least 20 s in heave and at least 30 s in pitch are defined, and another criterion regarding structural integrity is introduced. This implies that a simplified strength check, based on equivalent stress computations due to the combination of maximum and minimum inner (tank) and outer (sea) pressure, should be performed at three locations at the base of the upper columns, in order to prove sufficiency of the wall thickness.

As the DeepCwind semi-submersible platform is found to be over-conservatively designed, quite heavy, and not yet good performing from an eigenfrequency point of view, an optimized floater is designed, which is later on used as basis for the upscaling processes. In the optimization procedure, the upper column diameter is adjusted, based on the aims of at least 20 s natural period in heave and a nominal pitch of around 5°. This way, the upper column diameter is

reduced by 17.5%, compared to the original DeepCwind floater. The analysis of the optimized platform design yields that a lighter, less over-conservative, but still stable system, with higher natural periods is obtained.

The final upscaling procedure includes three different scaling factors. The main scaling factor, for most of the platform components, is determined from the ratio of the top structure masses. A separate scaling factor for the main column has to be defined, based on the tower base diameter of the target wind turbine. The third scaling factor, used for upscaling of the upper column diameter, is determined in a detailed calculation and expressed in terms of parameters of the basic floating system design, the other two scaling factors, as well as known parameters of the target wind turbine. Based on those upscaled platform components, the drag coefficients are re-calculated, the effective mooring line length is determined, the tower base is cut at the elevation of the main column, and the required amount of ballast is computed and distributed between upper and base columns, such that the aimed nominal pitch (5°) is obtained. Finally, the blade-pitch controller gains are adjusted, based on the system natural frequency in pitch.

This upscaling procedure is applied to the optimized DeepCwind semi-submersible platform and the target reference wind turbine IWT-7.5-164. This yields a well-designed floating wind turbine system, which uses the cheapest possible ballast water, fulfills all stability criteria, has a nominal pitch of 4.8° , gained an improved eigenfrequency performance with natural periods of 20.6 s and 33.2 s in heave and pitch, respectively, experiences less dynamic motions, and is expected to remain structurally intact.

The guideline for upscaling is also used to obtain a floating platform for the DTU 10 MW reference wind turbine. Two floaters are designed: one based on the optimized DeepCwind semi-submersible, the other one based on the platform for the IWT-7.5-164. The obtained floater dimensions are the same except for the upper columns. The upscaling procedure based on the IWT floater yields a by 1 m larger upper column diameter. This has a by 4.5% heavier system, $2.24E + 5$ kg more processed steel, reduced but still sufficient stability, a heave natural period of just 19.3 s and thus fallen below the aim of 20 s, a slightly reduced natural period in pitch, slightly increased dynamic motions in surge and heave, but slightly decreased dynamic motion in pitch, and a smaller safety factor for the structural strength as consequences. Both designs, however, have a nominal pitch of 4.8° .

Some main parameters, as well as the eigenfrequency, static, and dynamic performances of the designed semi-submersible floating wind turbine systems and the original OC4 floating system, are summarized and compared in Tables A.1 and A.2 in Appendix A.7.

9.2 Recommendation

Regarding the upscaling procedure, it is recommended to use directly the critically optimized platform design as basis, and not an already upscaled floater. By means of a simple check, based on the calculated scaling factors, it could already be estimated ahead of any analysis, whether the natural period in heave would be reduced, and thus could become critical.

As the different analysis methods yield comparable results, except for the surge and yaw natural periods, it is strongly recommended to adjust the mooring line model in Modelica. The mooring line extensional stiffness should be included in the catenary equation formulation, and the initial bottom contact length calculation, provided in this work, should be directly included in the mooring line model. Furthermore, the nominal pitch computation could be adjusted, so that the determination of the overturning moment is more consistent with the stiffness calculation.

The mooring system, in general, has to be adjusted in future work, such that the natural frequencies in surge, sway, and yaw are improved, and the platform offsets are kept within the allowable limits. Those are mainly predefined by the location of the wind turbine, especially if it is placed within a wind farm, the allowable pitch angle during operation, and the maximum accepted nacelle acceleration of $0.2g$. The mooring lines can be adjusted in diameter, material, extensional stiffness, as well as by adding buoys or clump weights. Then, it has to be checked that the mooring system can bring up the required stiffness, the maximum tension in the mooring lines is not exceeding the breaking strength, and the anchors are not loaded by vertical forces.

For a more meaningful assessment of the designed semi-submersible platforms and floating systems, it is recommended to perform some more detailed analyses.

The effect on the tower frequency, when the tower base is cut, has to be elaborated. An alternative, that could be considered, is shortening the main column instead of the tower. For this option, however, it has to be ensured that the tower base could withstand wave impact.

The strength check should include buckling check, structural fatigue check, as well as sectional load calculations for all elements and at several locations, especially also the joints. Based on the results, the wall thickness could either be reduced or, if more structural stability is needed, inner struts have to be added. The latter one, however, would affect the available inner volume of the columns, which thus again has to be checked against the required ballast amount.

In addition, different limit states should be analyzed. The stability has to be checked for the case of a damaged column, the maximum pitch angle has to be determined for a fault situation, and extreme sea states, depending on the actual site where the wind turbine is to be installed, should be included in ultimate limit state calculations. The dynamic response should not only be analyzed by means of standard deviations, but also based on the more crucial relative motions. Furthermore, the effects of second order wave forces and turbulent wind on the platform motions have to be elaborated in further analyses.

In order to obtain a more realistic platform performance, the floating wind turbine system should be implemented as fully flexible structure in Modelica. This system then could be extensively simulated and tested in Dymola. The simulation time, however, has to be increased, so that also low-frequent motions are covered and represented with enough cycles in the evaluated time span.

Finally, a detailed cost analysis, including aspects like producibility, location of suitable docks, as well as associated possible increased transportation times and costs, would supplement the entire study.

References

- [1] I. Akkerman. Offshore Mooring Systems. Lecture, Delft University of Technology, 2015.
- [2] R. Antonutti, C. Peyrard, L. Johanning, A. Incecik, and D. Ingram. An investigation of the effects of wind-induced inclination on floating wind turbine dynamics: heave plate excursion. *Ocean Engineering*, 91:208–217, 2014.
- [3] E.E. Bachynski and Z. Gao. Integrated dynamic analysis of wind turbines. Lecture, Norwegian University of Science and Technology, 2015.
- [4] C. Bak, F. Zahle, R. Bitsche, T. Kim, A. Yde, L.C. Henriksen, M.H. Hansen, J. Blasques, M. Gaunaa, and A. Natarajan. The DTU 10-MW Reference Wind Turbine, Version 1.04, Revision 14. Data sheet, Technical University of Denmark, 2013.
- [5] C. Bak, F. Zahle, R. Bitsche, T. Kim, A. Yde, L.C. Henriksen, M.H. Hansen, J. Blasques, M. Gaunaa, and A. Natarajan. The DTU 10-MW Reference Wind Turbine. Presentation, Danish Wind Power Research 2013, Fredericia, Denmark, 27/05/2013.
- [6] A.B. Biran and R. López-Pulido. *Ship Hydrostatics and Stability*. Elsevier Ltd., 2nd edition, 2013.
- [7] O. Bleich. AP 1: Generierung von Input für den Monopile-Entwurf. Technical report, Fraunhofer Institute for Wind Energy and Energy System Technology, 2016.
- [8] O. Bleich, J. Dührkop, H. Hartmann, and M. Strach-Sonsalla. Gesamtvorhabenbeschreibung TANDEM - Towards an Advanced Design of Large Monopiles. Technical report, Fraunhofer Institute for Wind Energy and Energy System Technology, 2015.
- [9] H. Bredmose. Floating Wind Turbines. Presentation within the course "Offshore Wind Energy", Department of Wind Energy, Technical University of Denmark, 2014.
- [10] P. Catalano, M. Wang, G. Iaccarino, and P. Moin. Numerical simulation of the flow around a circular cylinder at high Reynolds numbers. *International Journal of Heat and Fluid Flow*, 24:463–469, 2003.
- [11] Naval Damage Control Training Center. *Handbook of Damage Control*. NavPers 16191, 1945.
- [12] S.K. Chakrabarti, editor. *Handbook of Offshore Engineering, Volume I*. Elsevier, 1st edition, 2005.
- [13] P.W. Cheng. Windenergienutzung I. Lecture, Endowed Chair of Wind Energy, University of Stuttgart, 2013.
- [14] N.E. Clausen. Offshore wind energy technology, outlook and economics. Presentation within the course "Offshore Wind Energy", Department of Wind Energy, Technical University of Denmark, 2014.
- [15] N.E. Clausen. Environmental impact of wind energy. Presentation within the course "Planning and Development of Wind Farms", Department of Wind Energy, Technical University of Denmark, 2015.
- [16] O.M. Faltinsen. *Sea Loads on Ships and Offshore Structures*. Cambridge Ocean Technology Series. Cambridge University Press, 1993.
- [17] P. Feja. Dynamische Modellierung von Verankerungsleinen für schwimmende Offshore-Windenergieanlagen mit Modelica. Bachelor thesis, RWTH Aachen University, Fraunhofer Institute for Wind Energy and Energy System Technology, 2013.

- [18] P. Fritzson. Principles of Object-Oriented Modeling and Simulation with Modelica 3.3: A Cyber-Physical Approach. Wiley-IEEE Press, 2nd edition, 2015.
- [19] R. Gasch and J. Twele, editors. Wind Power Plants - Fundamentals, Design, Construction and Operation. Springer, 2nd edition, 2012.
- [20] J. George. WindFloat design for different turbine sizes. Master's thesis, Mechanical Engineering Department of Instituto Superior Técnico, Universidade de Lisboa, Portugal, 2014.
- [21] P. Ghadimi, H.P. Bandari, and A.B. Rostami. Determination of the Heave and Pitch Motions of a Floating Cylinder by Analytical Solution of its Diffraction Problem and Examination of the Effects of Geometric Parameters on its Dynamics in Regular Waves. International Journal of Applied Mathematical Research, 1(4):611–633, 2012.
- [22] M. Greco. TMR 4215: Sea Loads. Lecture Notes, Department of Marine Hydrodynamics, Norwegian University of Science and Technology, 2012.
- [23] M.H. Hansen, A. Hansen, T.J. Larsen, S. Øye, P. Sørensen, and P. Fuglsang. Control design for a pitch-regulated, variable speed wind turbine. Risø-R-1500(en) Report, Risø National Laboratory, Roskilde, Denmark, 2005.
- [24] M.O.L. Hansen. Aerodynamics of Wind Turbines. Earthscan, 2nd edition, 2008.
- [25] M.O.L. Hansen. Wind Turbine Technology and Aerodynamics. Lecture, Department of Wind Energy, Technical University of Denmark, 2014.
- [26] J. Helsen, F. Vanhollebeke, D. Vandepitte, and W. Desmet. Some trends and challenges in wind turbine upscaling. Proceedings of ISMA International Conference On Noise And Vibration, 2012.
- [27] F. Huijs, J. Mikx, F. Savenije, and E.J. de Ridder. Integrated design of floater, mooring and control system for a semi-submersible floating wind turbine. EWEA Offshore Conference, Frankfurt, 2013.
- [28] R. Huijsmans. Offshore Hydromechanics Mod-3. Lecture, Delft University of Technology, 2015.
- [29] P. Jamieson. Innovation in Wind Turbine Design. John Wiley & Sons, Ltd, 1st edition, 2011.
- [30] X. Jiang and S. Sang. Hydrodynamic Analysis of Heave Plates of the Truss Spar Platform. In J.H. Lee and C. Ng, editors, Proceedings of the Sixth International Conference on Asian and Pacific Coasts (APAC 2011), pages 935–947. World Scientific, 2011.
- [31] J. Jonkman, S. Butterfield, W. Musial, and G. Scott. Definition of a 5-MW Reference Wind Turbine for Offshore System Development. Technical report, NREL, 2009.
- [32] A. Kolios, M. Borg, and D. Hanak. Reliability analysis of complex limit states of floating wind turbines. Journal of Energy Challenges and Mechanics, 2, 2015.
- [33] M.A. Lackner. Wind Turbine Control Systems: Current Status and Future Developments. Presentation, University of Massachusetts Amherst, 2009.
- [34] T.J. Larsen and T.D. Hanson. A method to avoid negative damped low frequent tower vibrations for a floating, pitch controlled wind turbine. Journal of Physics: Conference Series 75, 2007.

-
- [35] C. Lopez-Pavon and A. Souto-Iglesias. Hydrodynamic coefficients and pressure loads on heave plates for semi-submersible floating offshore wind turbines: A comparative analysis using large scale models. *Renewable Energy*, 81:864–881, 2015.
- [36] A. Monarcha and N. Fonseca. A static analytical method for the preliminary design of multiple line mooring systems. In T.A. Santos, C.G. Soares, Y. Garbatov, and S. Sutulo, editors, *Maritime Engineering and Technology*, pages 195–203. CRC Press, 2012.
- [37] U.S. Navy. *The Silent Service in World War II: The Fleet Type Submarine*. Periscope Film LLC, 1st edition, 2009.
- [38] F.G. Nielsen, Hanson T.D., and B. Skaare. *Integrated Dynamic Analysis of Floating Offshore Wind Turbines*. EWEA, 2006.
- [39] E.G. Paland, editor. *Technisches Taschenbuch*. Schaeffler KG, 2002.
- [40] A. Robertson. Introduction to the OC5 Project, an IEA Task Focused on Validating Offshore Wind Modeling Tools. Technical report, NREL, 2015.
- [41] A. Robertson, J. Jonkman, M. Masciola, H. Song, A. Goupee, A. Coulling, and C. Luan. Definition of the Semisubmersible Floating System for Phase II of OC4. Technical report, NREL, 2014.
- [42] A. Robertson, J. Jonkman, F. Vorpahl, and W. Popko et al. Offshore Code Comparison Collaboration Continuation Within IEA Wind Task 30: Phase II Results Regarding a Floating Semisubmersible Wind System. NREL, 2014.
- [43] D. Roddier, C. Cermelli, A. Aubault, and A. Weinstein. WindFloat: A floating foundation for offshore wind turbines. *Journal of Renewable and Sustainable Energy* 2, 2010.
- [44] S. Schløer. Wind and wave climate. Presentation within the course "Offshore Wind Energy", Department of Wind Energy, Technical University of Denmark, 2014.
- [45] A. Schweizer. Formelsammlung und Berechnungsprogramme für Anlagenbau. 'www.schweizer-fn.de/rohr/festigkeit/festigkeit.php', 2016, [Cited 2016-03-03].
- [46] A. Sevinc, M. Rosemeier, M. Bätge, R. Braun, F. Meng, L. Steer, M. Shan, D. Horte, C. Balzani, and A. Reuter. Reference Wind Turbine IWT-7.5-164 Specification, rev.03. Data sheet, Fraunhofer Institute for Wind Energy and Energy System Technology, Leibniz University Hannover - Institute of Wind Energy Systems, 2016.
- [47] G. Sieros, P. Chaviaropoulos, J.D. Sørensen, B.H. Bulder, and P. Jamieson. Upscaling wind turbines: theoretical and practical aspects and their impact on the cost of energy. *Wind Energy*, 15(1):3–17, 2012.
- [48] J.P. Sánchez de Lara García. Wind turbine database: Modelling and analysis with focus on upscaling. Master's thesis, Department of Applied Mechanics, Chalmers University of Technology, 2013.
- [49] H. Stöcker. DeskTop Taschenbuch mathematischer Formeln und moderner Verfahren. 'https://elearning.physik.uni-frankfurt.de/data/FB13-PhysikOnline/lm_data/lm_5563/daten/auto/part_2/node129.htm', Verlag Harri Deutsch, 2003, [Cited 2016-03-16].
- [50] SteelConstruction.info. Steel material properties. 'http://www.steelconstruction.info/Steel_material_properties', [Cited 2016-03-15].
-

- [51] K. Suzuki, H. Yamaguchi, M. Akase, A. Imakita, T. Ishihara, Y. Fukumoto, and T. Oyama. Initial Design of Tension Leg Platform for Offshore Wind Farm. Journal of Fluid Science and Technology, 6(3):372–381, 2011.
- [52] L. Tao and S. Cai. Heave motion suppression of a Spar with a heave plate. Ocean Engineering, 31:669–692, 2004.
- [53] Det Norske Veritas. Design of Floating Wind Turbine Structures. Offshore Standard DNV-OS-J103, DNV, 2013.
- [54] Det Norske Veritas. SESAM User Manual GeniE Vol. 1 - Concept design and analysis of offshore structures. DNV, 2013.
- [55] Det Norske Veritas. SESAM User Manual HydroD - Wave load & stability analysis of fixed and floating structures. DNV, 2013.
- [56] P. Walsh. Useful Moment of Inertia Formulas. Training document within the course "AER 316 Fluid Mechanics", Department of Aerospace Engineering, Ryerson University Toronto (Canada), 2007.
- [57] Q. Wang. Design of a Steel Pontoon-type Semi-submersible Floater Supporting the DTU 10MW Reference Turbine. Master's thesis, Delft University of Technology, Norwegian University of Science and Technology, 2014.
- [58] C. Watanabe. Fukushima Floating Offshore Wind Project Seeks to Halve Cost. '<http://www.bloomberg.com/news/articles/2013-11-28/fukushima-floating-offshore-wind-project-seeks-to-halve-cost>, Bloomberg L.P., 2013, [Cited 2015-09-26].
- [59] M. Wiedemann. Smart Blades News Nr. 2. DLR, 2013.
- [60] IEA Wind. Task 30 - OC4 Phase II: DeepCwind semisubmersible. 'https://www.ieawind.org/task_30/task30_Public.html, 2014, [Cited 2015-09-05].
- [61] Q. Yu and X. Chen. Design Guideline for Stationkeeping Systems of Floating Offshore Wind Turbines. Final Report, American Bureau of Shipping (ABS), 2013.
- [62] W. Yu. Dynamic Modeling of a Floating Wind Turbine. Technical report, Fraunhofer Institute for Wind Energy and Energy System Technology, 2015.

A Appendix

A.1 Detailed Stability Calculation

In order to obtain reliable results for the stability behavior of the floating wind turbine system by means of simulations in Dymola, the detailed stability calculations have to be implemented manually in Modelica, as this is an equation-based modelling language. This means that both gravity and buoyancy forces, as well as their application points have to be defined.

Gravity

The gravity force, as well as the center of gravity for each component are indirectly already specified by implementing the elements of the floating wind turbine system as bodies, with geometrical dimensions and material density as input parameters. By connecting the structures to the component world, which has the acceleration due to gravity of $g = 9.81 \text{ ms}^{-1}$ in negative z -direction as default parameter, a gravity force vector is acting at each component's body-fixed center of gravity. As the floating wind turbine is simulated as closed system, meaning that no mass could be added or removed during operation, weight and body-fixed center of gravity remain unchanged. The global position of the center of gravity may change, as it is the case for the rotating blades or moving entire floating system. This, however, is defined by a variable translation vector from the origin of the world's coordinate system to the body-fixed center of gravity, or by means of a free motion.

Buoyancy

Buoyancy force and center of buoyancy depend on the actual displaced water volume. This means, that those parameters have to be computed at each time step, considering the actual platform pitch and heave motion.

All forces, acting on the platform, thus also the hydrodynamic forces, are implemented in the model "SemiSubLoadElement". This load calculation is for one column set, consisting of upper and base part. The cross braces and pontoons are neglected in the Morison load calculation, but included in the buoyancy force computation. In the final model for the entire semi-submersible platform, "PlatformSemiSub", the "SemiSubLoadElement" is called with an array of four elements as input. Those are three offset column sets and one set for the main column, which is just subdivided into an upper part and a negligible short base part, both of the same diameter. To each of the three offset column sets belongs, besides upper and base column, also one cross brace, one upper D and Y pontoon, as well as one lower D and Y pontoon. For the fourth (main) column set, the input lengths of pontoons and cross brace are set equal to zero. From the free motion of the platform, the heave motion $q_{3,i}$ of each individual column, as well as the platform pitch θ are obtained as output. Those are needed for the computation at each time step, in order to determine the actual position of the considered column with respect to the water line.

As the columns are cylindrical bodies, the submerged water volume can be computed by means of Equation 85 for a cylindrical hoof, based on [49], and Equation 86 for a (sloped) circular cylinder.

$$V_{\text{cyl.hoof}}(D, h, \theta) = \frac{hD^3}{24|\tan\theta|} \left[2\sqrt{1 - \left(\frac{D - 2\frac{h}{|\tan\theta|}}{D}\right)^2} - \frac{D - 2\frac{h}{|\tan\theta|}}{D} \left(3\arccos\left(\frac{D - 2\frac{h}{|\tan\theta|}}{D}\right) - \frac{1}{2}\sqrt{1 - \left(2\frac{D - 2\frac{h}{|\tan\theta|}}{D}\right)^2} \right) \right] \quad (85)$$

$$V_{\text{cylinder}}(D, h) = \frac{D^2}{4}\pi h \quad (86)$$

The corresponding position of the center of the volume of the (sloped) circular cylinder is given in Equations 87 and 88, defined with respect to the bottom center of the cylinder. [39]

$$x_{\text{cylinder}}(D, h, \theta) = \frac{D^2 \tan \theta}{16h} \quad (87)$$

$$z_{\text{cylinder}}(D, h, \theta) = \frac{h}{2} + \frac{D^2 \tan^2 \theta}{32h} \quad (88)$$

The position of the center of the cylindrical hoof volume is determined based on Equations 89 and 90, and can be computed explicitly by means of Equations 91 and 92.

$$x_{\text{cyl.hoof}}(D, h, \theta) = \frac{1}{V_{\text{cyl.hoof}}(D, h, \theta)} \int_{\frac{D}{2} - \frac{h}{|\tan \theta|}}^{\frac{D}{2}} \int_{-\sqrt{\frac{D^2}{4} - x^2}}^{\sqrt{\frac{D^2}{4} - x^2}} \int_0^{h - |\tan \theta|(\frac{D}{2} - x)} x \, dz \, dy \, dx \quad (89)$$

$$z_{\text{cyl.hoof}}(D, h, \theta) = \frac{1}{V_{\text{cyl.hoof}}(D, h, \theta)} \int_{\frac{D}{2} - \frac{h}{|\tan \theta|}}^{\frac{D}{2}} \int_{-\sqrt{\frac{D^2}{4} - x^2}}^{\sqrt{\frac{D^2}{4} - x^2}} \int_0^{h - |\tan \theta|(\frac{D}{2} - x)} z \, dz \, dy \, dx \quad (90)$$

$$x_{\text{cyl.hoof}}(D, h, \theta) = \frac{|\tan \theta|}{12V_{\text{cyl.hoof}}(D, h, \theta)} \left[\frac{3}{16} D^4 \left(\frac{\pi}{2} - \arctan \left(\frac{D - \frac{2h}{|\tan \theta|}}{2\sqrt{\frac{h}{|\tan \theta|} \left(D - \frac{h}{|\tan \theta|} \right)}} \right) \right) \right. \\ \left. - \sqrt{\frac{h}{|\tan \theta|} \left(D - \frac{h}{|\tan \theta|} \right)} \left(\frac{3}{8} D^3 + \frac{D^2}{4} \frac{h}{|\tan \theta|} - \frac{3Dh^2}{|\tan \theta|^2} + \frac{2h^3}{|\tan \theta|^3} \right) \right] \quad (91)$$

$$z_{\text{cyl.hoof}}(D, h, \theta) = \frac{|\tan \theta|^2}{24V_{\text{cyl.hoof}}(D, h, \theta)} \left[\frac{3}{4} D^2 \left(\frac{4h^2}{|\tan \theta|^2} - \frac{4Dh}{|\tan \theta|} + \frac{5}{4} D^2 \right) \right. \\ \left(\frac{\pi}{2} - \arctan \left(\frac{D - \frac{2h}{|\tan \theta|}}{2\sqrt{\frac{h}{|\tan \theta|} \left(D - \frac{h}{|\tan \theta|} \right)}} \right) \right) \\ \left. - \sqrt{\frac{h}{|\tan \theta|} \left(D - \frac{h}{|\tan \theta|} \right)} \left(\frac{15}{8} D^3 - \frac{19D^2}{4} \frac{h}{|\tan \theta|} + \frac{3Dh^2}{|\tan \theta|^2} - \frac{2h^3}{|\tan \theta|^3} \right) \right] \quad (92)$$

For the exact position, also the y -coordinate is needed, and would follow a similar computation. This is, however, skipped in this work, as the roll motion is not analyzed.

Both volume and center position are expressed in terms of the cylinder diameter D , the slope angle θ , and the height h , measured at the cylinder axis for the (sloped) cylinder, and at the outer edge for the cylindrical hoof, as visualized in Figure A.1.

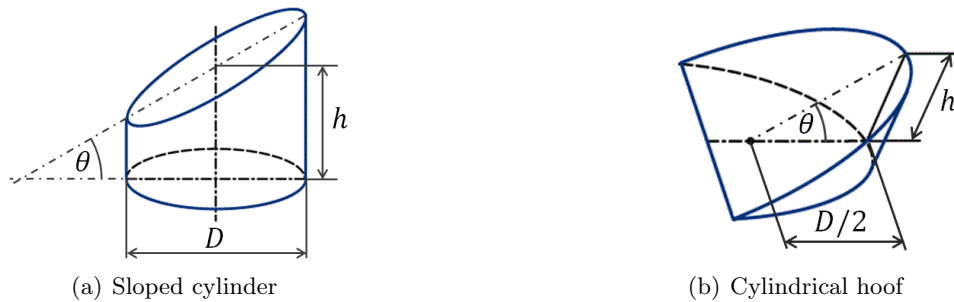


Figure A.1: Parameters of cylindrical geometries, based on [49]

Looking at one column, it can be distinguished between six cases how the displaced water volume can be determined. Those are listed in the following, and schematically shown in Figure A.2.

1. Nothing is submerged.
2. Only one bottom edge is submerged.
3. Bottom and upper edge of the same side are submerged.
4. Entire bottom circle is submerged, entire upper circle is emerged.
5. Only one upper edge is emerged.
6. Everything is submerged.

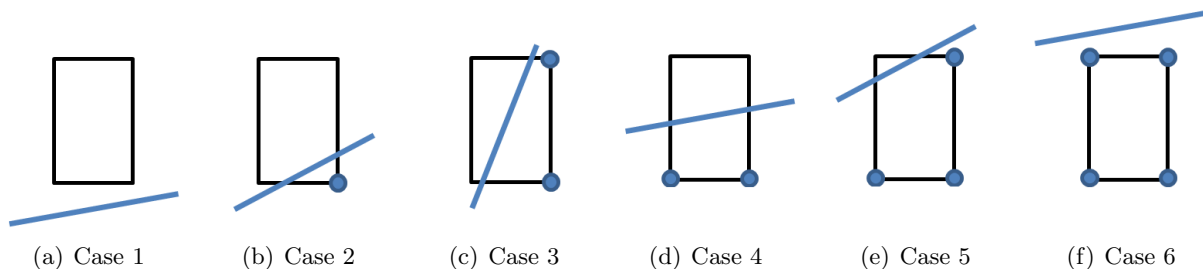


Figure A.2: Six cases of the column position with respect to the water line

Case 1 If nothing of the considered column i is submerged, the corresponding displaced water volume is equal to $V_{B,i} = 0 \text{ m}^3$ and no buoyancy force is acting on this component. However, still the center of buoyancy has to be defined, as Modelica requires a value. Thus, the center point at the bottom of the considered column is chosen, leading to $x_{B,i} = x_i$ and $z_{B,i} = z_{b,i}$.

Case 1 occurs for the considered column part, if Equation 93 is true.

$$q_{3,i} - |\tan \theta| \frac{D_i}{2} \geq -z_{b,i} \quad (93)$$

Case 2 If only one bottom edge of the column is submerged, the corresponding displaced water volume can be computed by means of Equation 94, based on Equation 85, and the position of the volume center by means of Equations 95 and 96, based on Equations 91 and 92.

$$V_{B,i} = V_{\text{cyl.hoof}} \left(D_i, |\tan \theta| \frac{D_i}{2} - q_{3,i} - z_{b,i}, \theta \right) \quad (94)$$

$$x_{B,i} = x_i + \text{sgn}(\theta) x_{\text{cyl.hoof}} \left(D_i, \left| \tan \theta \right| \frac{D_i}{2} - q_{3,i} - z_{b,i}, \theta \right) \quad (95)$$

$$z_{B,i} = z_{b,i} + z_{\text{cyl.hoof}} \left(D_i, \left| \tan \theta \right| \frac{D_i}{2} - q_{3,i} - z_{b,i}, \theta \right) \quad (96)$$

Case 2 occurs for the considered column part, if Equation 97 is true.

$$\begin{aligned} & q_{3,i} - \left| \tan \theta \right| \frac{D_i}{2} < -z_{b,i} \\ \&\& & q_{3,i} - \left| \tan \theta \right| \frac{D_i}{2} > -z_{t,i} \\ \&\& & q_{3,i} + \left| \tan \theta \right| \frac{D_i}{2} > -z_{b,i} \end{aligned} \quad (97)$$

Case 3 If bottom and upper edge of the same side of the considered column are submerged, the corresponding displaced water volume can be determined by subtracting the emerged column volume from the total column volume. As, however, the emerged part is in general a cylindrical hoof with a cut top edge, the emerged volume is first extended to a full cylindrical hoof. If this extended emerged volume is subtracted from the total column volume, the extension, thus the top edge, which is itself of the shape of a cylindrical hoof, has to be added again. Following this procedure, $V_{B,i}$ can be computed by means of Equation 98, based on Equations 85 and 86.

$$\begin{aligned} V_{B,i} = V_{\text{cylinder}}(D_i, h_i) - V_{\text{cyl.hoof}} \left(D_i, \left| \tan \theta \right| \frac{D_i}{2} + q_{3,i} + z_{b,i} + h_i, \theta \right) \\ + V_{\text{cyl.hoof}} \left(D_i, \left| \tan \theta \right| \frac{D_i}{2} + q_{3,i} + z_{b,i}, \theta \right) \end{aligned} \quad (98)$$

The corresponding volume center can be determined by means of Equations 99 and 100, based on Equations 87, 88, 91, 92, and Equation 8 for composed volumes, given in Paragraph 3.2.2.2.

$$\begin{aligned} x_{B,i} = x_i + \frac{\text{sgn}(\theta)}{V_{B,i}} \left[\{x_{\text{cyl.hoof}} V_{\text{cyl.hoof}}\} \left(D_i, \left| \tan \theta \right| \frac{D_i}{2} + q_{3,i} + z_{b,i} + h_i, \theta \right) \right. \\ \left. - \{x_{\text{cyl.hoof}} V_{\text{cyl.hoof}}\} \left(D_i, \left| \tan \theta \right| \frac{D_i}{2} + q_{3,i} + z_{b,i}, \theta \right) \right] \end{aligned} \quad (99)$$

$$\begin{aligned} z_{B,i} = z_{b,i} + \frac{1}{V_{B,i}} \left[z_{\text{cylinder}}(D_i, h_i, 0^\circ) V_{\text{cylinder}}(D_i, h_i) \right. \\ \left. - \left\langle h_i V_{\text{cyl.hoof}} \left(D_i, \left| \tan \theta \right| \frac{D_i}{2} + q_{3,i} + z_{b,i} + h_i, \theta \right) \right. \right. \\ \left. \left. - \{z_{\text{cyl.hoof}} V_{\text{cyl.hoof}}\} \left(D_i, \left| \tan \theta \right| \frac{D_i}{2} + q_{3,i} + z_{b,i} + h_i, \theta \right) \right\rangle \right. \\ \left. - \{z_{\text{cyl.hoof}} V_{\text{cyl.hoof}}\} \left(D_i, \left| \tan \theta \right| \frac{D_i}{2} + q_{3,i} + z_{b,i}, \theta \right) \right] \end{aligned} \quad (100)$$

Case 3 occurs for the considered column part, if Equation 101 is true.

$$\begin{aligned} & q_{3,i} - \left| \tan \theta \right| \frac{D_i}{2} \leq -z_{t,i} \\ \&\& & q_{3,i} + \left| \tan \theta \right| \frac{D_i}{2} > -z_{b,i} \end{aligned} \quad (101)$$

Case 4 If the entire bottom circle of the considered column is submerged and the entire upper circle emerged, the corresponding displaced water volume can be computed by means of Equation 102, based on Equation 86, and the position of the volume center by means of Equations 103 and 104, based on Equations 87 and 88.

$$V_{B,i} = V_{\text{cylinder}}(D_i, -q_{3,i} - z_{b,i}) \quad (102)$$

$$x_{B,i} = x_i + x_{\text{cylinder}}(D_i, -q_{3,i} - z_{b,i}, \theta) \quad (103)$$

$$z_{B,i} = z_{b,i} + z_{\text{cylinder}}(D_i, -q_{3,i} - z_{b,i}, \theta) \quad (104)$$

Case 4 occurs for the considered column part, if Equation 105 is true.

$$\begin{aligned} & q_{3,i} - |\tan \theta| \frac{D_i}{2} > -z_{t,i} \\ \&\& \quad & q_{3,i} + |\tan \theta| \frac{D_i}{2} \leq -z_{b,i} \end{aligned} \quad (105)$$

Case 5 If only one upper edge of the considered column is submerged, the corresponding displaced water volume can be determined by subtracting the emerged cylindrical hoof from the total column volume. Following this procedure, $V_{B,i}$ can be computed by means of Equation 106, based on Equations 85 and 86.

$$V_{B,i} = V_{\text{cylinder}}(D_i, h_i) - V_{\text{cyl.hoof}}\left(D_i, |\tan \theta| \frac{D_i}{2} + q_{3,i} + z_{t,i}, \theta\right) \quad (106)$$

The corresponding volume center can be determined by means of Equations 107 and 108, based on Equations 87, 88, 91, 92, and Equation 8 for composed volumes, given in Paragraph 3.2.2.2.

$$x_{B,i} = x_i + \frac{\text{sgn}(\theta)}{V_{B,i}} \{x_{\text{cyl.hoof}} V_{\text{cyl.hoof}}\} \left(D_i, |\tan \theta| \frac{D_i}{2} + q_{3,i} + z_{t,i}, \theta\right) \quad (107)$$

$$\begin{aligned} z_{B,i} = z_{t,i} - \frac{1}{V_{B,i}} \left[& z_{\text{cylinder}}(D_i, h_i, 0^\circ) V_{\text{cylinder}}(D_i, h_i) \right. \\ & \left. + \{x_{\text{cyl.hoof}} V_{\text{cyl.hoof}}\} \left(D_i, |\tan \theta| \frac{D_i}{2} + q_{3,i} + z_{t,i}, \theta\right) \right] \end{aligned} \quad (108)$$

Case 5 occurs for the considered column part, if Equation 109 is true.

$$\begin{aligned} & q_{3,i} - |\tan \theta| \frac{D_i}{2} \leq -z_{t,i} \\ \&\& \quad & q_{3,i} + |\tan \theta| \frac{D_i}{2} \leq -z_{b,i} \\ \&\& \quad & q_{3,i} + |\tan \theta| \frac{D_i}{2} > -z_{t,i} \end{aligned} \quad (109)$$

Case 6 If everything of the considered column is submerged, the corresponding displaced water volume can be computed by means of Equation 110, based on Equation 86, and the position of the volume center by means of Equations 111 and 112, based on Equations 87 and 88.

$$V_{B,i} = V_{\text{cylinder}}(D_i, h_i) \quad (110)$$

$$x_{B,i} = x_i \quad (111)$$

$$z_{B,i} = z_{b,i} + z_{\text{cylinder}}(D_i, h_i, 0^\circ) \quad (112)$$

Case 6 occurs for the considered column part, if Equation 113 is true.

$$q_{3,i} + |\tan \theta| \frac{D_i}{2} \leq -z_{t,i} \quad (113)$$

The cross braces and pontoons have a very small diameter, and displace quite less water compared to the voluminous columns. But still, they are included in the buoyancy calculation, however, not that detailed case distinction is implemented as for the columns. Thus, it is assumed that the upper D and Y pontoons are never submerged, but the lower D and Y pontoons are always with their full length l submerged. For the latter one, the corresponding displaced water volume could then be computed by means of Equation 114, based on Equation 86.

$$V_{B,i} = V_{\text{cylinder}}(D_i, l_i) \quad (114)$$

The corresponding center of the displaced water volume is independent of the platform motion, and could thus directly be determined based on the geometrical arrangement of the pontoons, presented in Figure 2.1(b) in Section 2.1. The x - and z -coordinates for the lower D and Y pontoons are expressed in Equations 115 and 116, using d_{OCs} as the spacing between the offset column centers.

$$\begin{aligned} i = \text{DL1} \parallel \text{DL2} : \quad x_{B,i} &= -\frac{d_{\text{OCs}}}{4\sqrt{3}} \\ i = \text{DL3} : \quad x_{B,i} &= \frac{d_{\text{OCs}}}{2\sqrt{3}} \\ i = \text{YL1} \parallel \text{YL3} : \quad x_{B,i} &= \frac{D_{\text{MC}} + l_i}{4} \\ i = \text{YL2} : \quad x_{B,i} &= -\frac{D_{\text{MC}} + l_i}{2} \end{aligned} \quad (115)$$

$$z_{B,i} = z_i \quad (116)$$

The water volume, displaced by the cross braces, is determined depending on the heave motion q_3 at the platform centerline and the platform pitch motion θ , as expressed in Equation 117, based on Equation 86.

$$V_{B,i} = V_{\text{cylinder}}\left(D_i, \frac{-z_{b,i}}{z_{t,i} - z_{b,i}}\right) - \frac{D_i^2}{4} \pi \frac{l_i}{z_{t,i} - z_{b,i}} (q_3 - x_{i,\text{SWL}} \tan \theta) \quad (117)$$

$x_{i,\text{SWL}}$ is the x -coordinate of the intersection point between cross brace and still water line, and computed for the three cross braces by means of Equation 118.

$$\begin{aligned} i = \text{CB1} \parallel \text{CB3} : \quad x_{i,\text{SWL}} &= \frac{D_{\text{MC}}}{4} - \frac{1}{2} \frac{z_{b,i}}{z_{t,i} - z_{b,i}} \left(\frac{d_{\text{OCs}}}{\sqrt{3}} - \frac{D_{\text{UC}} + D_{\text{MC}}}{2} \right) \\ i = \text{CB2} : \quad x_{i,\text{SWL}} &= \frac{z_{b,i}}{z_{t,i} - z_{b,i}} \left(\frac{d_{\text{OCs}}}{\sqrt{3}} - \frac{D_{\text{UC}} + D_{\text{MC}}}{2} \right) - \frac{D_{\text{MC}}}{2} \end{aligned} \quad (118)$$

The position of the volume center can be computed by means of Equations 119 and 120.

$$x_{B,i} = \frac{1}{2} \left[x_{i,SWL} + x_{i,MC} + \frac{x_{i,SWL} \tan \theta - q_3}{-z_{b,i} + \epsilon} (x_{i,SWL} - x_{i,MC}) \right] \quad (119)$$

$$z_{B,i} = \frac{1}{2} (x_{i,SWL} \tan \theta - q_3 + z_{b,i}) \quad (120)$$

$x_{i,MC}$ is the x -coordinate of the intersection point between cross brace and main column, and computed for the three cross braces by means of Equation 121.

$$\begin{aligned} i = \text{CB1} \parallel \text{CB3} : \quad x_{i,MC} &= \frac{D_{MC}}{4} \\ i = \text{CB2} : \quad x_{i,MC} &= -\frac{D_{MC}}{2} \end{aligned} \quad (121)$$

The variable ϵ , used in Equation 119, is needed to avoid a division by zero for the fourth column set, as there the cross brace parameters are set equal to zero. Thus, this ϵ amounts zero for the column sets one to three (the offset columns), but 1 m for the fourth column set.

As now, displaced water volume and corresponding volume center are determined for all platform components, the final buoyancy force can be implemented in the “SemiSubLoadElement” by means of adding a force vector with zeros in the x - and y -components, and the z -component, the actual buoyancy force F_B , following Equation 122.

$$F_B = \rho_{\text{water}} g \sum_i V_{B,i} \quad (122)$$

The point, in which this force acts, is defined by the x - and z -coordinates, given in Equations 123 and 124, respectively, based on Equation 8 for composed volumes, given in Paragraph 3.2.2.2.

$$x_B = \frac{\sum_i x_{B,i} V_{B,i}}{\sum_i V_{B,i}} \quad (123)$$

$$z_B = \frac{\sum_i z_{B,i} V_{B,i}}{\sum_i V_{B,i}} \quad (124)$$

If the buoyancy force is zero, the point of attack is set equal to the center of the considered column at SWL. This case, that nothing of the platform is submerged, is not realistic, however, has to be included for correct implementation in Modelica.

A.2 Parameters for Controller Gain Calculation

The blade-pitch sensitivity at rated $\left. \frac{\partial P}{\partial \theta} \right|_{\theta_{\text{rated}}}$, as well as the rotor-collective blade-pitch angle θ_K , at which the pitch sensitivity has doubled from its rated value, have to be determined for the controller gain calculation. Applying BEM theory [24], first, the required pitch angles for maintaining constant power are computed for wind speeds equal to or above rated. Based on those results, the variation in the power is determined by changing the pitch angle but keeping the induced velocities constant, following the procedure in [31]. Finally, the calculated blade-pitch sensitivities for different wind speeds are plotted with respect to the wind speed. From the best-fit line through those points, the two parameters, $\left. \frac{\partial P}{\partial \theta} \right|_{\theta_{\text{rated}}}$ and θ_K , can be identified.

In the following, the implementation of those steps in MATLAB is explained in more detail.

As the airfoil is an essential input for aerodynamic calculations, the blade twist angle ξ , chord length c , as well as the airfoil type at different radial positions r/R_{rotor} along the blade have to be read into MATLAB, as presented in Source Code A.1. For each airfoil type the lift and drag coefficients C_L and C_D for different angles of attack AOA have to be provided.

```

1 clear all
2 close all
3 clc

5 %% airfoil data
6 airfoildata=xlsread('AirfoilData','Data');
7 rR=airfoildata(:,2); % radial position [-]
8 twist=airfoildata(:,3); % twist [°]
9 c=airfoildata(:,4); % chord [m]
10 airfoil=airfoildata(1:end,5); % airfoil type
11 % airfoils
12 airfoil1=xlsread('AirfoilData','1');
13 airfoil2=xlsread('AirfoilData','2');
14 airfoil3=xlsread('AirfoilData','3');
15 ...

```

Source Code A.1: Reading in of airfoil data

Air density ρ_{air} , rotor diameter D_{rotor} , number of blades B , cut in, rated and cut out wind speeds, rated tip speed $v_{\text{tip,rated}}$, rated power P_{rated} , and generator efficiency η , are also needed as input. With those parameters, the solidity Σ , given in Equation 125, rotor radius $R_{\text{rotor}} = \frac{1}{2}D_{\text{rotor}}$, and maximum angular velocity $\omega_{\text{max}} = v_{\text{tip,rated}}R_{\text{rotor}}^{-1}$ can be computed. The implementation in MATLAB is presented in Source Code A.2, using the values for the NREL 5 MW.

$$\Sigma(r) = \frac{c(r)B}{2\pi r} \quad (125)$$

```

1 %% other parameters
2 rho=1.225; % air density [kg/m^3]
3 D=126; % diameter [m]
4 R=D/2; % radius [m]
5 B=3; % number of blades [-]
6 Vin=3; % cut in wind speed [m/s]
7 Vrated=11.4; % rated wind speed [m/s]
8 Vout=25; % cut out wind speed [m/s]
9 VtipRated=80; % rated tip speed [m/s]
10 omegamax=VtipRated/R; % maximal angular velocity [rad/s]
11 Prated=5*10^6; % rated power [W]
12 efficiency=0.944; % generator efficiency
13 sigma=c.*B./(2.*pi.*rR.*R); % solidity [-]
14 lambdaRated=VtipRated/Vrated; % tip speed ratio at rated [1/s]
15 V0=[11.4 12:25]; % velocity vector [m/s]

```

Source Code A.2: Input parameters for the BEM calculation, values for the NREL 5 MW

Based on BEM theory and [24], the blade-pitch angle at different wind speeds is determined iteratively by changing the pitch angle successively until the deviation from the rated mechanical power is less than a tolerated difference of maximum 1 kW. The power for wind velocities equal to or above rated wind speed, thus at maximum angular velocity, is determined by integration along the blade axis, as presented in Equation 126, based on [25].

$$P = \frac{1}{2} \rho_{\text{air}} B \omega_{\text{max}} R_{\text{rotor}}^2 v_0^2 \int_0^1 \frac{r}{R_{\text{rotor}}} \frac{(1-a)^2}{\sin^2 \chi} C_t c \, d \left(\frac{r}{R_{\text{rotor}}} \right) \quad (126)$$

The tangential load factor C_t can be determined from the lift and drag coefficients of the considered blade segment, and under the actual flow conditions, as given in Equation 127.

$$C_t = C_t \left(\frac{r}{R_{\text{rotor}}} \right) = C_L (AOA) \sin \chi - C_D (AOA) \cos \chi \quad (127)$$

Angle of attack AOA , flow angle χ , blade twist ξ , and rotor-collective blade-pitch angle θ are related to each other at each radial position of the blade, as presented in Equation 128.

$$AOA = \chi - (\theta + \xi) \quad (128)$$

The flow angle χ can be expressed in terms of the axial and tangential induction factors a and a' , respectively, as given in Equation 129.

$$\tan \chi = \frac{(1-a) v_0}{(1+a') \omega_{\text{max}} r} \quad (129)$$

The axial and tangential induction factors have to be computed iteratively for each blade segment, following the procedure given in [24]:

1. The initial values for the induction factors are set equal to zero.
2. The corresponding flow angle is computed, based on Equation 129.
3. The angle of attack at the radial position is determined, based on Equation 128.
4. The lift and drag coefficients are read from the airfoil data at the determined angle of attack.
5. The tangential and normal load factors C_t and C_n are to be calculated based on Equations 127 and 130, respectively.

$$C_n = C_n \left(\frac{r}{R_{\text{rotor}}} \right) = C_L (AOA) \cos \chi + C_D (AOA) \sin \chi \quad (130)$$

6. The new axial and tangential induction factors a_{i+1} and a'_{i+1} have to be computed by means of Equations 131 and 132, based on the thrust coefficient C_T , given in Equation 133, and including Glauert correction Γ and Prandtl's tip loss correction factor Π , given in Equations 134 and 135, respectively, based on the previous axial induction factor a_i . [25]

$$a_{i+1} = 0.1 \frac{C_T}{4\Pi (1 - \Gamma a_i)} + 0.9 a_i \quad (131)$$

$$a'_{i+1} = \frac{1}{\frac{4\Pi \sin \chi \cos \chi}{C_t \Sigma} - 1} \quad (132)$$

$$C_T = \frac{(1 - a_i)^2 C_n \Sigma}{\sin^2 \chi} \quad (133)$$

$$\Gamma = \begin{cases} 1 & \text{for } a_i \leq \frac{1}{3} \\ \frac{1}{4} (5 - 3a_i) & \text{for } a_i > \frac{1}{3} \end{cases} \quad (134)$$

$$\Pi = \frac{2}{\pi} \cos^{-1} \left[\exp \left(-\frac{B R_{\text{rotor}} - r}{2 r \sin \chi} \right) \right] \quad (135)$$

7. If the difference between the new and previous induction factors is larger than an acceptable discrepancy of 0.001, steps 2 to 7 have to be iterated.

This algorithm is executed for one wind speed at each radial position. Then the total power can be computed based on Equation 126. If this differs more than 1 kW from the rated mechanical power (rated power divided by generator efficiency), the blade pitch angle is adjusted, and the iteration procedure for the induction factors is performed anew. This is done for all concrete wind speeds, considered in the range from rated to cut out wind velocity, and thus the pitch angles for maintaining constant power at rated or above rated wind speed are determined. The implementation of this iterative computation in MATLAB is presented in Source Code A.3.

```

1 %% get optimum pitch angles for rated power
2 flowRadMatrix=zeros(length(V0),length(rR)); % flow angle [rad]
3 flowMatrix=zeros(length(V0),length(rR)); % flow angle [°]
4 CtMatrix=zeros(length(V0),length(rR)); % tangential load coefficient
5 aMatrix=zeros(length(V0),length(rR)); % axial induction factor
6 atMatrix=zeros(length(V0),length(rR)); % tangential induction factor
7 P=zeros(size(V0)); % power [W]
8 thetaMatrix=zeros(size(V0)); % pitch angle [°]
9 theta=0; % start with zero pitch
10 greater=0;
11 smaller=0;
12 greater2=0;
13 smaller2=0;
14 for V0i=1:length(V0)
15     while (abs(P(V0i)-Prated/efficiency)>1*10^3) && (~ (greater2==1 && smaller2
16         ==1))
17         for rRi=1:length(rR)
18             foil=eval(['airfoil' num2str(airfoil(rRi,:))]);
19             AOAdat=foil(:,1);
20             Cldat=foil(:,2);
21             Cddat=foil(:,3);
22             a=0;
23             aold=1;
24             at=0;
25             while abs(a-aold)>10^(-3)
26                 flowRad=real(atan((1-a)*V0(V0i)/((1+at)*R*omegamax*rR(rRi))));
27                 % flow angle [rad]
28                 flowRadMatrix(V0i,rRi)=flowRad;
29                 flow=real(flowRad*360/(2*pi)); % flow angle [°]
30                 flowMatrix(V0i,rRi)=flow;
31                 AOA=real(flow-(theta+twist(rRi))); % angle of attack [°]
32                 % determine coefficients
33                 Cl=interp(AOAdat,Cldat,AOA); % lift coefficient
34                 Cd=interp(AOAdat,Cddat,AOA); % drag coefficient
35                 Cn=real(Cl*cos(flowRad)+Cd*sin(flowRad)); % normal load
36                 coefficient

```

```

34         Ct=real(Cl*sin(flowRad)-Cd*cos(flowRad)); % tangential load
           coefficient
35         CtMatrix(V0i,rRi)=Ct;
36         CT=real((1-a)^2*Cn*sigma(rRi)/((sin(flowRad))^2)); % thrust
           coefficient
37         % computing next axial induction factor
38         F=real(2/pi*acos(exp(-B/2*(1-rR(rRi))/(rR(rRi)*sin(flowRad)))));
           ; % Prandtl's tip loss correction factor
39         if a<=1/3
40             f=1;
41         else
42             f=1/4*(5-3*a);
43         end
44         aold=a;
45         a=real(0.1*CT/(4*F*(1-f*a))+0.9*a);
46         at=real(1/(4*F*sin(flowRad)*cos(flowRad)/(sigma(rRi)*Ct)-1));
47     end
48     aMatrix(V0i,rRi)=a;
49     atMatrix(V0i,rRi)=at;
50 end
51 % Power P
52 int=rR.*(1-(aMatrix(V0i,:)).')^2./((sin((flowRadMatrix(V0i,:)).'))
           .^2.*(CtMatrix(V0i,:)).')*c;
53 P(V0i)=B.*omegamax.*trapz(rR,int).*1./2.*rho.*R.^2.*V0(V0i).^2;
54 if abs(P(V0i)-Prated/efficiency)<1*10^3
55     thetaMatrix(V0i)=theta;
56 elseif P(V0i)>Prated/efficiency
57     greater=1;
58     if smaller==0
59         theta=theta+0.1;
60     else
61         theta=theta+0.01;
62         greater2=1;
63     end
64 else
65     smaller=1;
66     if greater==0
67         theta=theta-0.1;
68     else
69         theta=theta-0.01;
70         smaller2=1;
71     end
72 end
73 end
74 thetaMatrix(V0i)=theta;
75 greater=0;
76 smaller=0;
77 greater2=0;
78 smaller2=0;
79 end
80 % save data for constant power
81 aOpt=aMatrix; % axial induction factor
82 atOpt=atMatrix; % tangential induction factor
83 POpt=P; % mechanical power [W]
84 flowOpt=flowMatrix; % flow angle [°]
85 flowRadOpt=flowRadMatrix; % flow angle [rad]
86 thetaOpt=thetaMatrix; % pitch angle [°]

```

Source Code A.3: Determination of the blade-pitch angles at wind speeds above rated

With the determined blade-pitch angles at different wind speeds for constant rated power, the sensitivity of the power to a variation in the blade-pitch angle is computed, following the same equations as already introduced above. However, neither an iteration for obtaining the rated power, nor an iteration for calculating the induction factors is performed, as the linearization analysis is executed assuming constant induced velocities, as done in [31]. This means that

both axial and tangential induction factors, as well as the flow angle are directly taken from the results obtained by running Source Code A.3. By varying the blade-pitch angle by $\pm 0.1^\circ$ from the determined value, the corresponding power is computed. Linearization at each considered wind speed and the corresponding optimum blade-pitch angle, yields the variation in power with respect to the variation in the blade-pitch angle. From the best-fit line through those obtained blade-pitch sensitivities at the different optimum blade-pitch angles, the blade-pitch sensitivity at rated, as well as the blade-pitch angle, at which the sensitivity has doubled from its value at rated, can directly be identified, as they follow Equation 43 in Subsection 3.6.2. In addition, also the blade-pitch sensitivity at zero pitch, as well as the corresponding pitch angle for doubled sensitivity, are computed from the best-fit line, as the determined rated pitch angle may differ from the original value of the wind turbine, which is zero in case of the NREL 5 MW.

Those final calculations are implemented in MATLAB by means of Source Code A.4.

```

1 %% compute sensitivity of aerodynamic power to blade pitch
2 thetaAdd=[-0.1 0 0.1].';
3 thetaLin=zeros(length(thetaAdd),length(thetaOpt));
4 PLin=zeros(length(thetaAdd),length(POpt));
5 linearization=zeros(2,length(V0));
6 for V0i=1:length(V0)
7     thetaLin(:,V0i)=thetaOpt(V0i)+thetaAdd;
8     for thetai=1:length(thetaAdd)
9         theta=thetaLin(thetai,V0i);
10        for rRi=1:length(rR)
11            foil=eval(['airfoil' num2str(airfoil(rRi,:))]);
12            AOAdat=foil(:,1);
13            Cldat=foil(:,2);
14            Cddat=foil(:,3);
15            a=aOpt(V0i,rRi); % same induced velocities
16            at=atOpt(V0i,rRi); % same induced velocities
17            flowRad=flowRadOpt(V0i,rRi); % flow angle [rad]
18            flow=flowOpt(V0i,rRi); % flow angle [°] % same induced velocities
19            AOA=real(flow-(theta+twist(rRi))); % angle of attack [°]
20            % determine coefficients
21            Cl=interp1(AOAdat,Cldat,AOA); % lift coefficient
22            Cd=interp1(AOAdat,Cddat,AOA); % drag coefficient
23            Cn=real(Cl*cos(flowRad)+Cd*sin(flowRad)); % normal load coefficient
24            Ct=real(Cl*sin(flowRad)-Cd*cos(flowRad)); % tangential load
                coefficient
25            CtMatrix(V0i,rRi)=Ct;
26            CT=real((1-a)^2*Cn*sigma(rRi)/((sin(flowRad))^2)); % thrust
                coefficient
27        end
28        % Power P
29        int=rR.*(1-(aMatrix(V0i,:)).')^2./((sin((flowRadMatrix(V0i,:)).'))
30            .^2.*(CtMatrix(V0i,:)).'*c);
31        PLin(thetai,V0i)=B.*omegamax.*trapz(rR,int).*1./2.*rho.*R.^2.*V0(V0i)
32            .^2;
33    end
34    linearization(:,V0i)=(polyfit(thetaLin(:,V0i)*pi/180,PLin(:,V0i),1)).';
35 end
36 dPdtheta=linearization(1,:);
37 dPdthetaFit=polyfit(thetaOpt,dPdtheta,1); % best-fit line
38 % parameters for controller gain calculation
39 dPdtheta0=dPdthetaFit(2); % pitch sensitivity at zero pitch [W/rad]
40 thetaK0=dPdthetaFit(2)/dPdthetaFit(1); % pitch angle for doubled pitch
    sensitivity [rad], using pitch sensitivity at zero pitch
41 dPdthetaRated=dPdthetaFit(1)*thetaOpt(1)+dPdthetaFit(2); % pitch sensitivity at
    rated pitch [W/rad]
42 thetaKrated=(2*dPdthetaRated-dPdthetaFit(2))/dPdthetaFit(1); % pitch angle for
    doubled pitch sensitivity [rad], using pitch sensitivity at rated pitch

```

Source Code A.4: Linearization analysis of the power for slightly varied blade-pitch angles

A.3 The OneWind® Modelica Library

The OneWind® Modelica Library for aero-hydro-servo-elastic Wind Turbine Simulation

Abstract

The OneWind® Modelica Library includes all major components needed for load calculations of current onshore and offshore wind turbines and is available for free for academic use. Models for environmental conditions and their respective influences on the structure are included (Table 1). The library constitutes a large effort in creation of a highly coupled multiphysics model with the modelling language Modelica. The source code of the library is available and can be adopted for application-specific components. This makes it possible to exchange / modify existing functionalities and further to expand the code by user-specific functionalities. The aim of this library is the ability to use it for certification load case calculation by IEC 61400-1 and 61400-3 and GL Guideline for the Certification of Wind Turbines. Results obtained with this library are continuously compared to results from the several projects in the IEA Offshore Code Comparison Collaboration [3] and continually verified with FAST [5] and Bladed [6].

Wind turbine system simulation

The OneWind® Modelica Library is able to perform aero-hydro-servo-elastic simulations of wind turbine systems, i.e. it comprises wind-inflow, aerodynamics (aero), waves and currents, hydrodynamics (hydro), control system (servo) and structural dynamic (elastic) models in a time domain coupled simulation environment. The models are grouped according to wind turbine components as seen in Figure 1 for an offshore wind turbine. This figure shows the model instances and corresponding interaction for the main wind turbine components: the rotor (with subcomponents of blade and hub), the tower, the substructure, the nacelle (with the subcomponents of drivetrain and generator), operating control, wind, waves, ice and soil. To simulate at different levels of detail, several models for almost every wind turbine component are available.

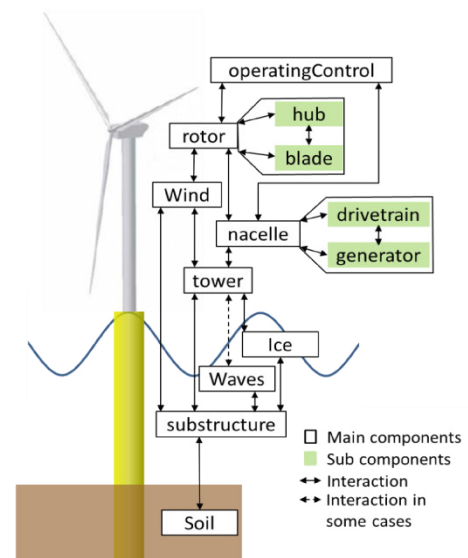


Figure 1: Major components of an offshore wind turbine in the OneWind® Modelica Library

Components of the Library

The particular components can be implemented independently due to the multibody system based structure of the OneWind® Modelica Library. In Table 1 a brief overview of the components of the OneWind® Modelica Library is given. Further information on the models can be found in [1] and [2].

Wind models

Deterministic and stochastic wind models are available. Deterministic wind uses several gust models. The stochastic wind data is read from binary or ASCII file in TurbSim [7] format.

Aerodynamic models

The aerodynamic load calculation uses either the blade element momentum (BEM) theory or the general dynamic wake method (GDW). The BEM theory is implemented as an iterative algorithm while the GDW is a set of differential equations. For the BEM, corrections for the dynamic wake and the dynamic stall can be used. Dynamic stall correction is also available for GDW.

Control system

The operating control system is implemented based on [4] and consists of a PI-pitch algorithm to control the power production above rated rotor rotation speed and a generator-torque controller which requests the counter torque from the electrical generator due to rotor torque. Several speed filters are available.

Table 1: Overview on the environmental and structural models of the OneWind® Modelica Library

| | | |
|-------------------|-----------------|---|
| Environment | Wind | <ul style="list-style-type: none"> • Exponential Wind Shear • Constant wind • Deterministic Wind • Turbulent Wind (Kaimal) • Gust models |
| | Waves | <ul style="list-style-type: none"> • Linear waves (Airy theory) • Linear irregular waves based on Pierson-Moskowitz and JONSWAP spectrum • Stretching Methods (Wheeler- and Delta stretching) |
| | Ice | <ul style="list-style-type: none"> • Floating ice loads |
| | Soil | <ul style="list-style-type: none"> • Linear spring-damper • <i>p-y-approach</i>* |
| Aerodynamics | | <ul style="list-style-type: none"> • Blade element momentum theory (BEM), dynamic stall Beddoes and Oye • General dynamic wake (GDW), dynamic stall Beddoes and Oye • Eddy viscosity wake |
| Hydrodynamics | | <ul style="list-style-type: none"> • Morison's equation |
| Structural Models | Rotor Blade | <ul style="list-style-type: none"> • rigid model • finite element model based on Euler-Bernoulli beam theory • modal reduced model as presented in [2] |
| | Hub and Nacelle | <ul style="list-style-type: none"> • Rigid Nacelle <ul style="list-style-type: none"> ○ rigid drivetrain ○ fixed speed generator model • Flexible nacelle <ul style="list-style-type: none"> ○ flexible drivetrain (torsional DOF) ○ variable speed generator model |
| | Tower | <ul style="list-style-type: none"> • rigid model • finite element model based on Euler-Bernoulli beam theory • modal reduced model as presented in [2] |
| | Substructure | <ul style="list-style-type: none"> • Monopile <ul style="list-style-type: none"> ○ rigid model ○ finite element model based on Euler-Bernoulli beam theory ○ modal reduced model as presented in [2] • <i>Jacket</i>* • <i>Tripod</i>* • <i>Spar Boye</i>* • <i>Semisubmersible</i>* |
| Operating control | | <ul style="list-style-type: none"> • Discrete and continuous (NREL 5-MW [4]) <ul style="list-style-type: none"> ○ including of dynamic link library (dll) possible ○ Pitch and torque control ○ Yaw control |

*under development

- [1] M. Strobel, F. Vorpahl, C. Hillmann, X. Gu, A. Zuga und U. Wihlfahrt, *The OnWind Modelica Library for Offshore Wind Turbines - Implementation and first results*, Bremerhaven.
- [2] P. Thomas, X. Gu, R. Samlaus, C. Hillmann und U. Wihlfahrt, *The OneWind Modelica Library for Wind Turbine Simulation with flexible Structure - Modal Reduction Method in Modelica*, Bremerhaven, 2014.
- [3] <https://www.ieawind.org/taskWebSites.html>
- [4] J. Jonkman, S. Butterfield, W. Musial und G. Scott, „*Definition of a 5-MW Reference Wind Turbine for Offshore System Development*“, February 2009.
- [5] J. M. Jonkman und M. L. Buhl, „FAST User's Guide,“ National Renewable Energy Laboratory, Colorado, 2005.
- [6] Garrad Hassan & Partners Ltd., „Bladed User Manual,“ Garrad Hassan & Partners Ltd., Bristol, 2010.
- [7] B. J. Jonkman und L. Kilcher, „TurbSim User's Guide: Version 1.06.00,“ National Renewable Energy Laboratory, Colorado, 2012.

A.4 Initial Bottom Contact Lengths of the Mooring Lines

The initial bottom contact lengths of the mooring lines is needed as input for calculations in Modelica. The horizontal projection of the total length $l_{\text{tot,hor}}$ and the height of the fairleads above the seabed h , defined in Section 3.5, have to be determined for each mooring line, based on the geometrical arrangement and the initial displacement, prescribed in the free decay tests.

For the undisplaced case, $l_{\text{tot,hor}}$ and h are the same for all mooring lines, and already known. Those parameters are given as input for the calculation in MATLAB, together with all free decay starting conditions, further geometrical dimensions (base column diameter D_{BC} , spacing between the offset column centers d_{OCs} , vertical position of fairleads below SWL Δz_{moor}), and mooring line parameters (total length l_{tot} , mooring line weight per length in water $\mu_{\text{moor,water}}$, g , extensional stiffness EA). This input is implemented in Source Code A.5, using the values of the original OC4 semi-submersible floater as example.

```

1  clear all
2  close all
3  clc

5  %% input parameters
6  surge = 22; % surge displacement [m] for free decay in surge
7  sway = 22; % sway displacement [m] for free decay in sway
8  heave = 6; % heave displacement [m] for free decay in heave
9  roll = 8*pi/180; % roll displacement [rad] for free decay in roll
10 pitch = 8*pi/180; % pitch displacement [rad] for free decay in pitch
11 yaw = 8*pi/180; % yaw displacement [rad] for free decay in yaw

13 dOCs = 50; % distance of centers of offset columns to each other [m]
14 DiameterBC = 24; % diameter of base columns [m]
15 fairleadZ = 14; % vertical position of fairleads below SWL [m]
16 L0=835.5; % total length of one mooring line [m]
17 w=108.63*9.81; % mooring line weight in water per length [N/m]
18 EA=753.6*10^6; % mooring line extensional stiffness [N]
19 l0=796.732; % mooring line: total horizontal projected length without any
    displacement [m]
20 h0=182.8536; % mooring line: height / vertical projected length without any
    displacement [m]

```

Source Code A.5: Input parameters for the initial bottom contact length calculation, values for the original OC4 floater

For the surge and sway free decay tests, $l_{\text{tot,hor}}$ can be determined by adding the surge or sway displacement and using a triangular calculation for determining the length in mooring line direction. However, $l_{\text{tot,hor}}$ remains unchanged for the free decay test in heave. h is constant in the surge, sway, and yaw free decay tests. For the free decay test in heave, however, the initial heave displacement has to be added to the original height.

The determination of $l_{\text{tot,hor}}$ and h for initial rotational displacement is more complex. Therefore, further parameters, like the absolute values of the x - and y -coordinates of the three fairleads, as well as the distance between undisplaced and displaced fairlead position, are determined based on the input parameters. The calculation is explained exemplarily for the roll motion. The corresponding geometrical arrangement is presented in Figure A.3 for the fairlead at column 3.

The absolute value of the y -coordinate of the fairleads at columns 1 and 3 can be determined based on Equation 136. The fairlead at column 2, however, is directly located on the x -axis, and thus has zero as y -coordinate.

$$\Delta y = \frac{1}{2} [d_{\text{OCs}} + D_{\text{BC}} \cos(30^\circ)] \quad (136)$$

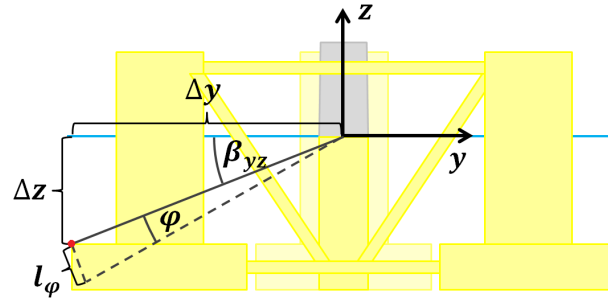


Figure A.3: Geometrical arrangement for the roll motion of the fairlead at column 3

The angle β_{yz} in the yz -plane, as indicated in Figure A.3, is defined in Equation 137. The distance l_φ between the fairlead position after roll displacement and the original fairlead position can be computed by means of Equation 138, based on the sine theorem for triangles.

$$\tan \beta_{yz} = \frac{\Delta z}{\Delta y} \quad (137)$$

$$l_\varphi = \frac{\sin \varphi}{\sin\left(\frac{\pi-\varphi}{2}\right)} \sqrt{(\Delta y)^2 + (\Delta z)^2} \quad (138)$$

This length, finally, has to be projected vertically, as well as in the xy -plane in the new mooring line direction, including the initial displacement. This follows just geometrical and angular calculations, and thus is not explicitly presented here.

The calculation for the other rotational initial displacements is similar as for roll. The entire computation of $l_{tot,hor}$ and h , is implemented in MATLAB by means of Source Code A.6.

```

1 %% calculated parameters for geometry and motion
2 fairleadY13 = dOCs/2+DiameterBC/2*cos(30*pi/180); % y-position (positive) of
   fairleads at columns 1 and 3
3 fairleadZY13Angle = atan(fairleadZ/fairleadY13); % projected angle between (
   origin to fairlead) and y-axis in y-z-plane for columns 1 and 3
4 Roll13 = sin(roll)/sin((pi-roll)/2)*sqrt(fairleadY13^2+fairleadZ^2); % roll
   motion: moved length of fairlead position at columns 1 and 3
5 fairleadX2 = dOCs/sqrt(3)+DiameterBC/2; % x-position (positive) of fairlead at
   column 2
6 fairleadZX2Angle = atan(fairleadZ/fairleadX2); % projected angle between (
   origin to fairlead) and x-axis in x-z-plane for column 2
7 Pitch2 = sin(pitch)/sin((pi-pitch)/2)*sqrt(fairleadX2^2+fairleadZ^2); % pitch
   motion: moved length of fairlead position at column 2
8 fairleadX13 = dOCs/sqrt(3)/2 + DiameterBC/2*cos(60*pi/180); % x-position (
   positive) of fairleads at columns 1 and 3
9 fairleadZX13Angle = atan(fairleadZ/fairleadX13); % projected angle between (
   origin to fairlead) and x-axis in x-z-plane for columns 1 and 3
10 Pitch13 = sin(pitch)/sin((pi-pitch)/2)*sqrt(fairleadX13^2+fairleadZ^2); % pitch
   motion: moved length of fairlead position at columns 1 and 3

12 %% matrices with:
13 % 3 columns for mooring lines 1, 2, 3
14 % 7 rows for cases:
15 % 1: no displacement
16 % 2: surge (22m)
17 % 3: sway (22m)
18 % 4: heave (6m)
19 % 5: roll (8°)
20 % 6: pitch (8°)
21 % 7: yaw (8°)

```



```

22 l=zeros(7,3); % total horizontal length (projected)
23 h=zeros(7,3); % height

25 % total horizontal length (projected)
26 l(1,:)=10;
27 l(2,2)=l(1,1)+surge;
28 l(2,1)=sqrt(l(1,1)^2+surge^2-2*l(1,1)*surge*cos(60*pi/180));
29 l(2,3)=sqrt(l(1,1)^2+surge^2-2*l(1,1)*surge*cos(60*pi/180));
30 l(3,2)=sqrt(l(1,1)^2+sway^2);
31 l(3,1)=sqrt(l(1,1)^2+sway^2-2*l(1,1)*sway*cos(30*pi/180));
32 l(3,3)=sqrt(l(1,1)^2+sway^2-2*l(1,1)*sway*cos(150*pi/180));
33 l(4,:)=l(1,1);
34 l(5,2)=sqrt(l(1,1)^2+(fairleadZ*sin(roll))^2);
35 l(5,1)=sqrt(l(1,1)^2+(Roll13*cos(pi-fairleadZY13Angle-(pi-roll)/2))^2-2*l(1,1)
    *(Roll13*cos(pi-fairleadZY13Angle-(pi-roll)/2))*cos(30*pi/180));
36 l(5,3)=sqrt(l(1,1)^2+(Roll13*cos((pi-roll)/2-fairleadZY13Angle))^2-2*l(1,1)*
    (Roll13*cos((pi-roll)/2-fairleadZY13Angle))*cos(150*pi/180));
37 l(6,2)=l(1,1)-Pitch2*cos(pi-fairleadZX2Angle-(pi-pitch)/2);
38 l(6,1)=sqrt(l(1,1)^2+(Pitch13*cos((pi-pitch)/2-fairleadZX13Angle))^2-2*l(1,1)*
    (Pitch13*cos((pi-pitch)/2-fairleadZX13Angle))*cos(120*pi/180));
39 l(6,3)=sqrt(l(1,1)^2+(Pitch13*cos((pi-pitch)/2-fairleadZX13Angle))^2-2*l(1,1)*
    (Pitch13*cos((pi-pitch)/2-fairleadZX13Angle))*cos(120*pi/180));
40 l(7,:)=sqrt(l(1,1)^2+(sin(yaw)/sin((pi-yaw)/2)*fairleadX2)^2-2*l(1,1)*
    (sin(yaw)/sin((pi-yaw)/2)*fairleadX2)*cos(pi-(pi-yaw)/2));

42 % height
43 h(1:3,:)=h0;
44 h(4,:)=h(1,1)+heave;
45 h(5,2)=h(1,1)+(fairleadZ-fairleadZ*cos(roll));
46 h(5,1)=h(1,1)+(Roll13*sin((pi-roll)/2-fairleadZY13Angle));
47 h(5,3)=h(1,1)-(Roll13*sin((pi-roll)/2-fairleadZY13Angle));
48 h(6,2)=h(1,1)+Pitch2*sin(pi-fairleadZX2Angle-(pi-pitch)/2);
49 h(6,1)=h(1,1)-(Pitch13*sin((pi-pitch)/2-fairleadZX13Angle));
50 h(6,3)=h(1,1)-(Pitch13*sin((pi-pitch)/2-fairleadZX13Angle));
51 h(7,:)=h(1,1);

```

Source Code A.6: Determination of $l_{\text{tot,hor}}$ and h for each mooring line at initial displacement

Finally, Equations 32 and 34, given in Subsection 3.5.2, are solved iteratively with respect to the effective mooring line length l_{eff} and the horizontal tension at the touch down point τ_{hor} . This calculation is performed for all mooring lines and each initial displacement, based on the determined values for $l_{\text{tot,hor}}$ and h . The MATLAB code is presented in Source Code A.7.

```

1 %% effective mooring line length Leff [m] and horizontal tension TH [N]
2 % x=[Leff; TH]
3 Leff=zeros(7,3);
4 TH=zeros(7,3);
5 for i=1:3
6     for j=1:7
7         F=@(x) [l(j,i)-L0+x(1)-x(2)/w*asinh(w*x(1)/x(2))-x(2)*x(1)/EA; w*(x
            (1))^2/(2*EA)-h(j,i)+x(2)/w*(sqrt(1+(w*x(1)/x(2))^2)-1)];
8         x0=[500; 8000];
9         x=fsolve(F,x0);
10        Leff(j,i)=x(1);
11        TH(j,i)=x(2);
12    end
13 end

```

Source Code A.7: Iterative computation of l_{eff} and τ_{hor}

The initial bottom contact lengths l_{rest} of the three mooring lines at an initial displacement can then be determined by subtracting the computed effective length l_{eff} from the total mooring line length l_{tot} , following Equation 29 in Subsection 3.5.2. If, however, the result for the effective mooring line length is larger than the total length, the initial bottom contact length is set equal to zero. In this case, the mooring line is under tension in the initial displaced position.

A.5 Mooring Line Length for the Upscaled System

In the upscaling procedure, the mooring system is designed in such a way, that fairlead and anchor positions are scaled with the main scaling factor, the water depth remains unchanged, and the total mooring line length is set, such that the mooring stiffness in surge of the original semi-submersible floater design is maintained.

As the original mooring stiffness is predefined, first, the horizontal tension at the touch down point τ_{hor} of the upscaled system can be computed based on Equation 40, presented in Subsection 3.5.3, using the new height of the fairleads above the seabed h of the upscaled platform. With the determined value for τ_{hor} , Equation 34, given in Subsection 3.5.2, can be solved iteratively with respect to the effective mooring line length l_{eff} , using the original effective length scaled up with the main scaling factor k as starting value for the iteration. Finally, the total mooring line length l_{tot} of the upscaled floater, which is needed to maintain constant mooring stiffness in surge, can be computed by means of Equation 32 in Subsection 3.5.2.

As this computation includes iterative calculations, and also has to be performed for each upscaled design anew, the entire computation procedure is implemented and carried out in MATLAB, based on Source Code A.8, using the values of the upscaled floater for Fraunhofer's IWT-7.5-164 as example.

```

1  clear all
2  close all
3  clc

5  %% input parameters
6  w=108.63*9.81; % mooring line weight in water per length [N/m]
7  EA=753.6*10^6; % extensional stiffness [N]

9  % original OC4 floater
10 hOrig=186; % vertical position of fairleads below SWL [m]
11 LtotOrig=835.5; % total mooring line length [m]
12 LtotHorOrig=796.732; % horizontal projection of total mooring line length [m]

14 % upscaled floater
15 k=1.172441063; % main scaling factor
16 lTotHor=934.122; % horizontal projection of total mooring line length [m]
17 h=183.5858; % vertical position of fairleads below SWL [m]

19 %% mooring stiffness of original OC4 floater used for upscaled floater
20 % xOrig=[LeffOrig; ThorOrig]
21 F1 = @(x) [LtotHorOrig-LtotOrig+x(1)-x(2)/w*asinh(w*x(1)/x(2))-x(2)*x(1)/EA; w
    *(x(1))^2/(2*EA)-hOrig+x(2)/w*(sqrt(1+(w*x(1)/x(2))^2)-1)];
22 x0=[500; 8000];
23 xOrig=fsolve(F1,x0);
24 Cmoor=3/2*w*(-2/sqrt(1+2*xOrig(2)/(w*hOrig))+acosh(1+w*hOrig/xOrig(2)))^(-1); %
    mooring system stiffness in surge of original OC4 floater [kg/s^2]

26 % horizontal tension Thor [N], determined from constant Cmoor
27 F2 = @(Thor) 3/2*w*(-2/sqrt(1+2*Thor/(w*h))+acosh(1+w*h/Thor))^(-1)-Cmoor;
28 Thor=fsolve(F2,xOrig(2));

30 % effective mooring line length Leff [m]
31 F3 = @(Leff) w*Leff^2/(2*EA)-h+Thor/w*(sqrt(1+(w*Leff/Thor)^2)-1);
32 Leff0=xOrig(1)*k; % upscaled effective length [m]
33 Leff=fsolve(F3,Leff0);

35 % total mooring line length lTot [m]
36 lTot=lTotHor+Leff-Thor/w*asinh(w*Leff/Thor)-Thor*Leff/EA;

```

Source Code A.8: Determination of l_{tot} of the upscaled system for constant stiffness in surge

A.6 Adjustment of the Ballast Position

The total ballast mass is indirectly predefined, based on the equilibrium condition between buoyancy and weight. This required ballast amount is equally distributed among the three offset columns. The concrete position within upper and base columns, however, has a relevant impact on the nominal pitch, because the center of gravity of the total system is a parameter of the stiffness component in pitch, as it can be seen from Equation 20 in Subsection 3.3.3. Including Equation 50 from Section 4.1, which defines the nominal pitch in terms of overturning moment and stiffness in pitch, the required system center of gravity $z_{G,\text{aimed}}$ can be determined based on Equation 139 for a certain aimed nominal pitch angle $q_{5,\text{rated,aimed}}$. This calculation can directly be carried out, as center of buoyancy z_B , displaced water volume V_B , second moment of waterplane area about the y -axis I_y , thrust force $F_{T,\text{rated}}$, and lever arm, defined in terms of hub height z_{hub} and center of buoyancy z_B , do not change when the ballast position is adjusted.

$$z_{G,\text{aimed}} = z_B - \frac{1}{V_B} \left(\frac{F_{T,\text{rated}} (z_{\text{hub}} - z_B)}{\rho_{\text{water}} g q_{5,\text{rated,aimed}} \left[\frac{\circ}{180} \right] \frac{\pi}{180}} - I_y \right) \quad (139)$$

Equation 139 is already written in such a way that the aimed nominal pitch could directly be substituted as angle in degrees.

With the required system center of gravity, Equation 140 can be defined for the equilibrium of mass and center of mass products for composed masses.

$$m z_G + \Delta m z_{G,\Delta\text{ballast,UC}} - \Delta m z_{G,\Delta\text{ballast,BC}} = m z_{G,\text{aimed}} \quad (140)$$

Δm is the amount of ballast that is moved between upper and base column, which has to be the same for both column parts, in order to maintain the total system mass m . The inverted correlation between adding (or removing) ballast in the upper column and removing (or adding) ballast in the base column, is included in Equation 140, by means of the opposite signs in front of the Δ -terms. The moving mass can be defined in two ways, as given in Equations 141 and 142 for the upper column and base column, respectively, using d_i for the wall thickness of the column.

$$\Delta m = 3\rho_{\text{ballast}} \frac{\pi}{4} (D_{\text{UC}} - 2d_{\text{UC}})^2 \Delta h_{\text{ballast,UC}} \quad (141)$$

$$\Delta m = 3\rho_{\text{ballast}} \frac{\pi}{4} (D_{\text{BC}} - 2d_{\text{BC}})^2 \Delta h_{\text{ballast,BC}} \quad (142)$$

Based on Equations 141 and 142, the changes in the ballast height in upper and base columns, $h_{\text{ballast,UC}}$ and $h_{\text{ballast,BC}}$, can be put in relation to each other, as presented in Equation 143.

$$\Delta h_{\text{ballast,BC}} = \left(\frac{D_{\text{UC}} - 2d_{\text{UC}}}{D_{\text{BC}} - 2d_{\text{BC}}} \right)^2 \Delta h_{\text{ballast,UC}} \quad (143)$$

The center of gravity of the moved ballast in upper and base columns can be determined by means of Equations 144 and 145, respectively, using the same sign convention as in Equation 140.

$$z_{G,\Delta\text{ballast,UC}} = z_{b,\text{UC}} + h_{\text{ballast,UC}} + \frac{1}{2} \Delta h_{\text{ballast,UC}} \quad (144)$$

$$z_{G,\Delta\text{ballast,BC}} = z_{b,\text{BC}} + h_{\text{ballast,BC}} - \frac{1}{2} \Delta h_{\text{ballast,BC}} \quad (145)$$

Substituting Equations 141 and 143 to 145 in Equation 140, yields Equation 146.

$$\begin{aligned} \frac{m(z_{G,\text{aimed}} - z_G)}{3\rho_{\text{water}}\frac{\pi}{4}(D_{\text{UC}} - 2d_{\text{UC}})^2} &= (z_{\text{b,UC}} + h_{\text{ballast,UC}} - z_{\text{b,BC}} - h_{\text{ballast,BC}}) \Delta h_{\text{ballast,UC}} \\ &+ \frac{1}{2} \left[1 + \left(\frac{D_{\text{UC}} - 2d_{\text{UC}}}{D_{\text{BC}} - 2d_{\text{BC}}} \right)^2 \right] \Delta h_{\text{ballast,UC}}^2 \end{aligned} \quad (146)$$

Equation 146 can finally be solved with respect to the variation in the ballast height in the upper columns, as presented in Equations 147, using the free variable parameters X , Y and Z , as defined in Equations 148 to 150. The physical reasonable solution for the change in the ballast height in the upper column, is obtained by addition of the square root in the nominator of Equation 147, for which reason the negative sign is already parenthesized.

$$\Delta h_{\text{ballast,UC}} = \frac{-Y \overset{+}{(-)} \sqrt{Y^2 - 4XZ}}{2X} \quad (147)$$

$$X = \frac{1}{2} \left[1 + \left(\frac{D_{\text{UC}} - 2d_{\text{UC}}}{D_{\text{BC}} - 2d_{\text{BC}}} \right)^2 \right] \quad (148)$$

$$Y = z_{\text{b,UC}} + h_{\text{ballast,UC}} - z_{\text{b,BC}} - h_{\text{ballast,BC}} \quad (149)$$

$$Z = \frac{4m(z_G - z_{G,\text{aimed}})}{3\rho_{\text{water}}\pi(D_{\text{UC}} - 2d_{\text{UC}})^2} \quad (150)$$

The corresponding variation in the ballast height in the base columns can then be computed by means of Equation 143.

For the final determination of the adjusted ballast heights, the initial sign convention in Equation 140 has to be used, meaning that the resulting $\Delta h_{\text{ballast,UC}}$ has to be added to the initial ballast height in the upper column, whereas $\Delta h_{\text{ballast,BC}}$ is to be subtracted from the initial ballast height in the base column.

A.7 Summary of the Designed Semi-Submersible Floating Wind Turbine Systems

Table A.1: Summary of the main dimensions of the semi-submersible floater designs

| Wind turbine | NREL | | IWT | | DTU | |
|---------------------------------|----------|--------------|-------------------|-----------|-----------|---------------------|
| | Original | Optimization | Initial upscaling | | | Optimized upscaling |
| Design | OC4 [41] | Orig. OC4 | Orig. OC4 | Opt. OC4 | Opt. OC4 | IWT floater |
| Ballast | water | water | water | concrete | water | water |
| Diameter MC | m | 6.50 | 7.00 | | 8.30 | |
| Diameter UC | m | 12.00 | 9.90 | 14.70 | 12.70 | 15.30 |
| Diameter BC | m | 24.00 | | 29.39 | 28.14 | 30.34 |
| Diameter pontoons/CB | m | 1.60 | | 1.96 | 1.88 | 2.02 |
| Spacing between OCs | m | 50.00 | | 61.24 | 58.62 | 63.21 |
| Elevation OC above SWL | m | 12.00 | | 14.70 | 14.07 | 15.17 |
| Elevation MC above SWL | m | 10.00 | | 12.25 | 11.72 | 12.64 |
| Draft below SWL | m | 20.00 | | 24.49 | 23.45 | 25.28 |
| Radius to anchors | m | 837.6 | | 982.0 | | 1058.9 |
| Unstretched mooring line length | m | 835.5 | | 972.4 | | 1045.3 |
| Effective mooring line length | m | 594.4 | | 475.2 | 586.7 | 582.6 |
| Mass top structure | kg | 0.600E+6 | | 0.937E+6 | | 1.203E+6 |
| Mass platform steel | kg | 3.852E+6 | 3.567E+6 | 7.016E+6 | 5.914E+6 | 7.822E+6 |
| Mass ballast | kg | 9.621E+6 | 8.354E+6 | 17.825E+6 | 14.329E+6 | 19.812E+6 |
| Mass total system | kg | 14.260E+6 | 12.715E+6 | 25.933E+6 | 21.376E+6 | 29.023E+6 |
| Center of Gravity | m | -11.59 | -12.43 | -14.29 | -16.31 | -13.30 |
| Center of Buoyancy | m | -13.17 | -13.93 | -16.18 | -15.97 | -16.96 |

Table A.2: Summary of the main performances of the semi-submersible floater designs

| Wind turbine | NREL | | IWT | | DTU |
|---------------------------------|----------|--------------|-------------------|---------------------|-------------|
| | Original | Optimization | Initial upscaling | Optimized upscaling | |
| Design | OC4 [41] | Orig. OC4 | Orig. OC4 | Opt. OC4 | IWT floater |
| Ballast | water | water | water | water | water |
| Natural period in surge | 112.2 | 104.9 | 152.1 | 136.9 | 156.7 |
| Natural period in heave | 17.4 | 20.4 | 19.3 | 20.6 | 20.4 |
| Natural period in pitch | 27.0 | 34.7 | 28.5 | 33.2 | 34.5 |
| Natural period in yaw | 79.3 | 73.7 | 132.3 | 113.2 | 139.6 |
| Maximum dynamic motion in surge | 0.78 | 0.73 | 0.64 | 0.64 | 0.62 |
| Maximum dynamic motion in heave | 2.11 | 0.48 | 0.36 | 0.37 | 0.31 |
| Maximum dynamic motion in pitch | 0.36 | 0.51 | 0.37 | 0.44 | 0.34 |
| Nominal pitch | 3.0 | 4.5 | 2.92 | 2.48 | 4.8 |

A.8 Successfully Submitted Paper

Attending the EERA DeepWind'2016 Deep Sea Offshore Wind R&D Conference in Trondheim with a poster presentation, I also submitted a full paper, which was accepted and will be published in Energy Procedia, expected in August 2016.

The paper is based on the preceding research project, mainly covered by Chapter 5. At the time of submission, however, I was working with Fraunhofer's onshore wind turbine design, as the data for the offshore equivalent was not yet accessible to me. Therefore, the concrete results, presented in the paper, differ from the findings in Chapter 5.

The successfully submitted paper is attached in the following.



13th Deep Sea Offshore Wind R&D Conference, EERA DeepWind'2016, 20-22 January 2016, Trondheim, Norway

Rational upscaling of a semi-submersible floating platform supporting a wind turbine

Mareike Leimeister^{a,d,*}, Erin E. Bachynski^b, Michael Muskulus^c, Philipp Thomas^d

^aDepartment of Marine Technology, NTNU, NO-7491 Trondheim, Norway

^bCentre for Ships and Ocean Structures, NTNU, NO-7491 Trondheim, Norway

^cDepartment of Civil and Transport Engineering, NTNU, NO-7491 Trondheim, Norway

^dFraunhofer Institute for Wind Energy and Energy System Technology (IWES), D-27572 Bremerhaven, Germany

Abstract

This work examines the procedure of upscaling of a semi-submersible platform in order to support a predefined wind turbine. As a result of technological progress and design changes, basic scaling based on the turbine rating cannot be used directly. Furthermore, additional factors that floating structures have to deal with - like coupled dynamic motions, wave interaction, low frequency response and mooring system - have to be considered and included in the upscaling procedure. It is shown and discussed here, how to develop a rational upscaling process for a semi-submersible structure, under all these constraints, when the goal is to find a reasonable design of a platform, which would fit a predefined wind turbine, is producible, and has realistic dynamic behavior.

© 2016 The Authors. Published by Elsevier Ltd.

Peer-review under responsibility of SINTEF Energi AS.

Keywords: Offshore wind energy; semi-submersible floating platform; upscaling; wind turbine

1. Introduction

Offshore wind energy has higher and more consistent wind resource potential, less size and noise limitations, and less visual impact than onshore wind energy. With floating wind turbines, promising sites at deeper water depths can be made accessible for the wind industry. Despite these advantages, the use of offshore wind power is still economically challenging because of higher installation and O&M costs, limited time windows for transport and installation, more difficult access, higher loads on the structure due to waves and current, and additional challenges like dynamic interaction between the floating structure and wind turbine or wave excitation frequencies.

One opportunity to reduce the costs is the installation of bigger but fewer wind turbines, which is more feasible offshore than onshore. Upscaling of smaller existing wind turbines to larger sizes is primarily based on geometric self-similarity. When aiming for the same optimal performance, similar aerodynamic behavior is needed and obtained by maintaining the tip speed ratio. The scaling factor is determined by the power rating and expressed in terms of

* Corresponding author. Tel.: +49-179-9843239.

E-mail address: mareike-leimeister@gmx.de

a length ratio. Due to the cubic increase in mass, however, buckling limit and yield strength are likely to limit the upscaling [1]. As the upscaling procedure does not consider Reynolds effects, wind shear, dynamic loads, and local or case-specific predefined constraints like noise limits or height requirements, existing wind turbines deviate from those theoretical scaling proportionalities [1]. By the same token, recent technology developments and new designs make simple geometrical upscaling insufficient. The support structure carrying the upscaled wind turbine also has to be adjusted, so that floatation and stability are maintained. Floating platforms are characterized by large coupled motions, low frequency modes, mooring system, and hydrodynamic interaction. As a consequence, simple upscaling based on the turbine rating cannot be applied in the case of floating offshore wind turbine systems.

This work examines the criteria that have to be fulfilled during upscaling of a semi-submersible floating system carrying a predefined wind turbine. Based on those factors, an adjusted upscaling procedure is developed, the resulting platform design is modelled, its hydrostatic and hydrodynamic parameters are determined, and its behavior is analyzed. As the main focus lies on the hydrodynamic behavior of the floating system and not on its structural integrity, structural scaling laws are not considered in this study. Section 2 covers the adjusted upscaling method and the derivation of system parameters. The results are presented in Section 3, divided into stability analysis, frequency-dependent behavior, natural periods and motion response. Finally, Section 4 provides recommendations for optimization and adaptation of the upscaling procedure.

Nomenclature

| | | |
|-----------------------|--|--|
| A | Added mass matrix (6×6) with components A_{ii} | [kg, kgm, kgm ²] |
| B | Damping matrix (6×6) with components B_{ii} | [kg/s, kgm/s, kgm ² /s] |
| bot | Bottom end | |
| C | Stiffness matrix (6×6) with components C_{ii} | [kg/s ² , kgm/s ² , kgm ² /s ²] |
| CoB, CoG | Center of buoyancy, gravity | |
| <i>D</i> | Diameter | [m] |
| F | Excitation force vector (6×1) with components F_i | [N, Nm] |
| f_n | Natural frequency | [Hz] |
| <i>g</i> | Acceleration due to gravity | [m/s ²] |
| <i>I</i> | Area moment of inertia | [m ⁴] |
| <i>l</i> | Length | [m] |
| M | Mass matrix (6×6) with components M_{ii} | [kg, kgm, kgm ²] |
| RAO | Response amplitude operator | |
| S_q, S_η | Response/Wave spectral density | [m ²] or [deg ²] |
| <i>s</i> | Scaling factor | |
| T_d, T_n | (Damped) Natural period | [s] |
| top | Top end | |
| <i>W</i> | Weight | [N] |
| <i>x, y, z</i> | Coordinate and direction of surge, sway, heave | |
| ρ_{water} | Water density | [kg/m ³] |
| σ | Standard deviation | [m] or [deg] |
| ω | Angular frequency | [rad/s] |

2. Methodology

The upscaling procedure was developed based on a case study: the OC4-DeepCwind semi-submersible floating platform [2], originally designed for the NREL 5 MW wind turbine, was modified to support Fraunhofer's 7.5 MW wind turbine IWT-7.5-164 [3].

The main upscaling of the semi-submersible floating platform was based on the simple upscaling procedure with the geometrical scaling factor determined by the power rating of the wind turbines, as follows $s = \sqrt{\frac{7.5 \text{ MW}}{5 \text{ MW}}} \approx 1.225$,

since the power is proportional to a length scale (the rotor diameter) squared. However, the upscaling of the main column (MC) had to be adjusted, such that the main column fits the tower base diameter of 8.4 m. With the original main column diameter of 6.5 m a slightly higher scaling factor of $s \approx 1.292$ resulted for the main column diameter and wall thickness. The draft, however, was scaled with the main scaling factor. The lengths of the cross braces (CB) and pontoons that interconnect the outer and main columns were determined from the geometrical arrangement. Another geometrical boundary condition was the hub height of 120 m, for which the IWT-7.5 wind turbine was designed. In order to avoid changing the complex hybrid tower design, the main column was cut at SWL and it was assumed that the tower bottom, made out of concrete, could withstand wave impact.

The mooring system parameters (line length and anchor position) were assumed to be unchanged as well as the water depth of 200 m. Due to the upscaled fairlead positions, however, the suspended mooring line length changed and thus also the weight and center of gravity of the suspended parts. The latter two were computed based on [4], considering elastic catenary mooring lines.

Finally, the upscaled platform was ballasted with the main focus on floatability and stability. The buoyancy was predefined by the upscaled draft of the platform and the resulting displaced water volume. The weight of the upscaled platform, lifted mooring lines and wind turbine had to be complemented by ballast so that balance with buoyancy was achieved. With the main focus on stability, a low system center of gravity was desired, meaning that the base columns (BC) were ballasted first and the upper columns (UC) were filled with ballast only if needed. Two different designs were considered, one with water, as used in the original DeepCwind floater, and the other one with concrete, as it has a higher density than water, and thus a deeper center of gravity could be obtained.

Fig. 1 (a) visualizes the floating system, including the main criteria of the upscaling procedure. A top view of the floater with indication of the wave direction is presented in Fig. 1 (b).

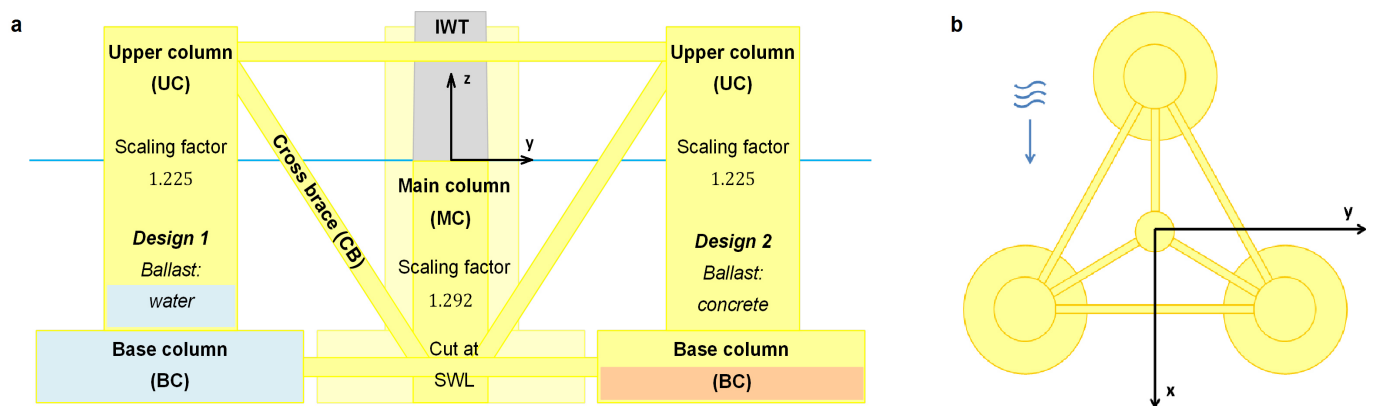


Fig. 1. (a) Components of the upscaled floating system; (b) Top view with coordinate system and wave direction

The theoretical scaling factor based on the power rating is not a strict rule. Comparisons of actual turbines suggest that the total tower top mass tends to scale with the power rating to 2 – 2.8 rather than 3, but there are uncertainties related to technological development [5]. In the case considered here, the nacelle mass increases at a higher rate due to the change from geared to direct drive. Similarly, there are uncertainties in the scaling of the loads due to the competing effects of tower height (reduced offshore) and extreme and fault loads (higher offshore).

The performance of the upscaled platform was analyzed based on hand calculations and computations by means of HydroD and Wadam by DNV GL. The focus lay on the stability limit in pitch, the natural periods, the nominal pitch at rated power, and the frequency-dependent behavior, considering only wave loads.

The simplified hand calculations used the wall-sided assumption in order to obtain the linear stiffness components of the system. The formulas for the hydrostatic components in heave and pitch are given in Equations 1 and 2, respectively. [6]

$$C_{33} = \rho_{\text{water}} g \frac{\pi}{4} \left[3 \left(D_{\text{UC}}^2 + D_{\text{CB}}^2 \frac{l_{\text{CB}}}{(z_{\text{top,CB}} - z_{\text{bot,CB}})} \right) + D_{\text{MC}}^2 \right] \quad (1)$$

$$C_{55} = W(z_{\text{CoB}} - z_{\text{CoG}}) + \rho_{\text{water}} g I_y \quad (2)$$

Besides the system stiffness, also the added mass had to be determined. For the hand calculations, two approaches were used. The first approximation was based on Equations 3 and 4 for heave and pitch, respectively [7,8]. Another approximation was obtained by scaling the given added mass values of the DeepCwind floating platform with the main scaling factor of $s \approx 1.225$ to the power of three for the heave DoF and to the power of five for pitch, neglecting the different scaling of the main column.

$$A_{33} = \frac{\rho_{\text{water}} D_{\text{MC}}^3}{6} + 3 \left\{ \frac{\rho_{\text{water}}}{3} D_{\text{BC}}^3 - \left[\frac{\pi \rho_{\text{water}}}{8} D_{\text{UC}}^2 \left(D_{\text{BC}} - \sqrt{D_{\text{BC}}^2 - D_{\text{UC}}^2} \right) + \frac{\pi \rho_{\text{water}}}{24} \left(D_{\text{BC}} - \sqrt{D_{\text{BC}}^2 - D_{\text{UC}}^2} \right)^2 \left(2D_{\text{BC}} + \sqrt{D_{\text{BC}}^2 - D_{\text{UC}}^2} \right) \right] \right\} \quad (3)$$

$$A_{55} = 3\rho_{\text{water}} \frac{\pi}{4} D_{\text{BC}}^2 \left(\frac{|z_{\text{bot,BC}}|^3}{3} + (z_{\text{CoG,BC}} - z_{\text{bot,BC}})^2 |z_{\text{bot,BC}}| + (z_{\text{CoG,BC}} - z_{\text{bot,BC}}) |z_{\text{bot,BC}}|^2 \right) + \rho_{\text{water}} \frac{\pi}{4} D_{\text{MC}}^2 \left(\frac{|z_{\text{bot,MC}}|^3}{3} + (z_{\text{CoG,MC}} - z_{\text{bot,MC}})^2 |z_{\text{bot,MC}}| + (z_{\text{CoG,MC}} - z_{\text{bot,MC}}) |z_{\text{bot,MC}}|^2 \right) \quad (4)$$

Based on the simplified hand calculations only the undamped natural periods could be computed, not accounting for the cross-diagonal coupling and using the determined low-frequency limit of the added mass. In the natural period calculation based on the HydroD results, the frequency-dependency of added mass, however, was taken into account. Furthermore, by including the damping terms obtained by Wadam calculations, the damped natural periods could be computed based on Equation 5. The Wadam calculations included linearized drag forces based on Morison's equation. The viscous drag forces are significantly smaller than the inertia forces due to the low Keulegan-Carpenter number of the considered flow conditions. Nonetheless, the contribution of the linearized viscous damping terms is important for the resonant response and is therefore included in the total damping matrix. In the present work, a simplification was made: the damping matrix was generated based on unit wave amplitude and was not updated for different sea states.

$$T_{d,i} = \left(f_{n,i} \sqrt{1 - \left(\frac{B_{ii}(f_{n,i})}{(M_{ii} + A_{ii}(f_{n,i})) 4\pi f_{n,i}} \right)^2} \right)^{-1} \quad \text{with} \quad f_{n,i} = \frac{1}{T_{n,i}} = \frac{1}{2\pi} \sqrt{\frac{C_{ii}}{M_{ii} + A_{ii}(f_{n,i})}} \quad (5)$$

3. Results

3.1. Stability analysis

As offshore wind turbines are facing the wind at high hub heights, but are supported by platforms with rather small footprints, attention has to be paid to the stability in pitch motion. Only considering static stability, the stability limit can be determined based on the location of the center of gravity with respect to the metacenter for different tilt angles. The stability limit can directly be taken from the righting lever GZ-curve as the first zero crossing point, which comes after the zero crossing point at the initial stable position. The main parameters of this static stability analysis are schematically visualized in Fig. 2.

This method is generally valid, but quite complex, so that computer programs have to be used or simplifying assumptions have to be made. For the hand calculations, all system components are assumed to be fixed, meaning that the center of gravity will not move within the local coordinate system of the structure. Furthermore, the change in the displaced water volume due to tilting is neglected. Thus, only accounting for the pitch motion and neglecting the required vertical translation for meeting the force equilibrium for floatation, the simplified hand calculations yield stability within the entire range of -19.0° to 18.9° used for the calculations, based on the geometrical arrangement shown in Fig. 2.

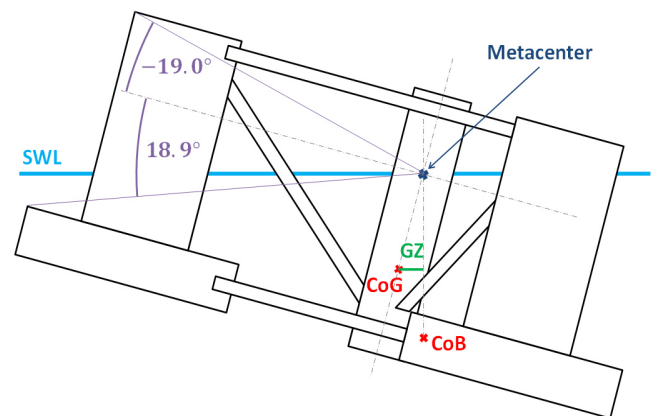


Fig. 2. Characteristic parameters and angles for the stability analysis

The more accurate stability analysis by means of HydroD shows that the stability limit is reached at a tilt angle of -73.2° for the water ballasted design and 92.8° for the concrete ballasted one. The maximum restoring force is achieved at -20° (and 30.0°) for both systems. Thus, the concrete ballasted design is more stable than the water ballasted one. This is as expected, since the center of gravity is lower.

3.2. Frequency-dependent hydrodynamic matrices

Based on the Wadam calculations, the frequency-dependent added mass and damping matrices were obtained, as shown in Fig. 3 (a) and (b). These matrices are independent of the ballasting. Due to symmetry, the surge and sway components, as well as the roll and pitch components, are the same.

In general, it is observed that the added mass in heave is much larger than in surge and sway, which is caused by the bigger base columns, acting as heave plates. At low frequencies, the added mass components in surge, sway and yaw reach around half of the double-body added mass, while the added mass components in heave, roll and pitch are not correlated with the double-body added mass values, as it is expected based on [9]. At higher frequencies, the added mass curves converge to a limit value. Comparing the heave and pitch low-frequency added mass limits with the hand calculated added mass components based on Equations 3 and 4, shown as dotted lines in Fig. 3 (a), confirms that the equation-based computations are only rough approximations, as they underestimate the results by 13 – 22%. The alternative of scaling up the original DeepCwind added mass components with the main scaling factor and just neglecting the different scaling of the main column, yields more accurate results, which still differ by 4.1 – 5.6% from the Wadam results.

The radiation damping curves, presented in Fig. 3 (b), show expected behavior, with the damping terms tending to approach zero at both small and high frequencies. The amount of damping in surge and sway is significantly higher than in heave. The same applies to the damping in yaw compared to roll and pitch. This is reasonable due to the geometry.

For semi-submersible platforms with large base columns, additional attention must be paid to the hydrodynamic excitation and damping on these columns. In the present work, viscous excitation has not been examined in detail. Simplified linearized viscous damping is included, but detailed analysis of the flow around the base plates is needed in order to correctly account for these effects. [10]

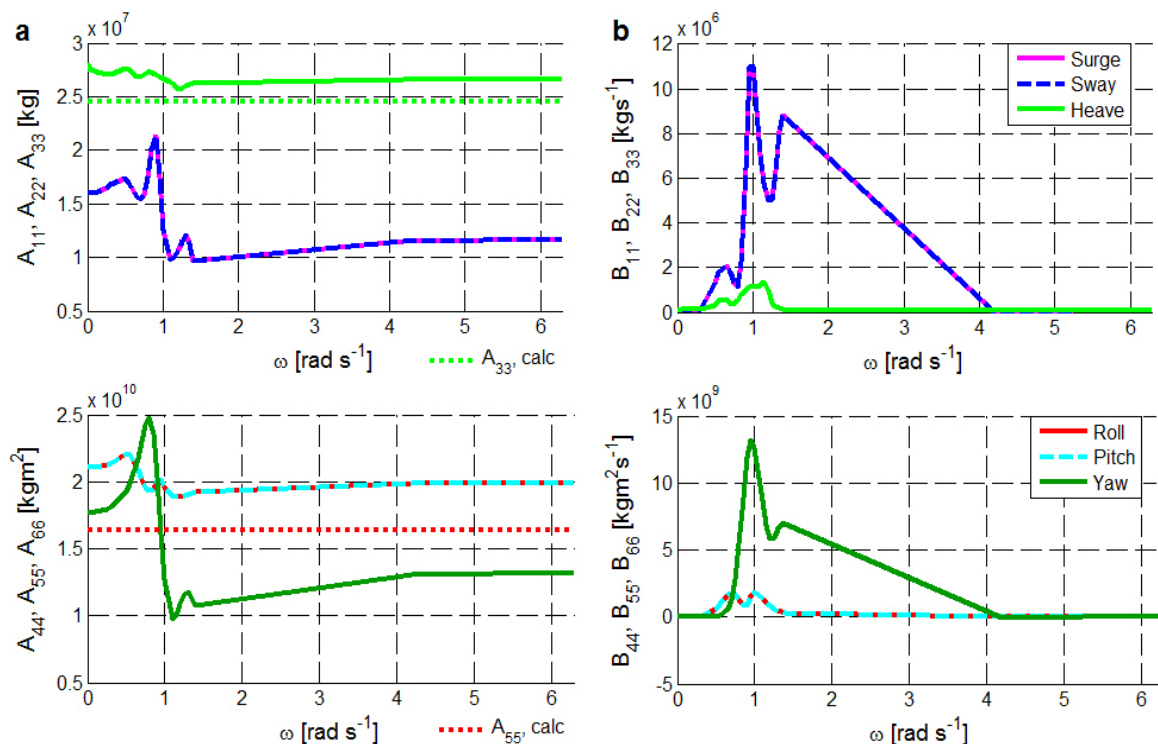


Fig. 3. (a) Diagonal added mass matrix terms; (b) Diagonal damping matrix terms.

3.3. Natural periods

As the hand calculations do not provide the system parameters, especially the added mass components, exactly, the damped natural periods were computed based on Equation 5 using the Wadam results and considering the frequency-dependency of the added mass and damping components. In order to include the station-keeping system in a first approach, the mooring stiffness of the catenary lines, directly taken from the original DeepCwind system [2], was added in the surge and yaw DoFs to the system stiffness. This way, the damped natural periods in surge, heave, pitch and yaw were computed explicitly. The results for both designs are presented in Table 1 together with the theoretical upscaled values of the original DeepCwind floating system (factor of \sqrt{s}), based on free decay load cases [11].

Table 1. Damped natural periods, given in s.

| DoF | Water ballasted | Concrete ballasted | Theoretical upscaled | Original DeepCwind |
|-------|-----------------|--------------------|----------------------|--------------------|
| Surge | 153.6 | 153.6 | 118.2 | 106.8 |
| Heave | 19.1 | 19.1 | 19.1 | 17.3 |
| Pitch | 34.1 | 31.4 | 29.9 | 27.0 |
| Yaw | 131.4 | 131.7 | 83.8 | 75.7 |

From Table 1 it can be seen that the damped natural period in heave lies at the lower bound of the typical range for semi-submersible platforms (17-40 s, [12]), but is considerably higher than the natural period in heave of the original DeepCwind floating system, and follows the theoretical scaling.

As the concrete ballasted design is the stiffer system, the damped natural period in pitch is smaller than in the water ballasted system. Both values lie in the lower region of the typical natural periods in pitch of a semi-submersible platform (25-50 s, [12]) and are higher than the theoretical upscaled value, because of the ballasting from bottom up.

The damped natural periods in surge and yaw are significantly higher than the theoretical upscaled values. As the stiffness components in surge and yaw are directly taken from the DeepCwind system without any scaling, the theoretical upscaled values should rather be based just on the mass and added mass proportionalities. Using a factor of $\sqrt{s^3}$ and $\sqrt{s^5}$ for the natural periods in surge and yaw, respectively, adjusted theoretical upscaled values (144.8 s and 125.7 s) closer to the computed values are obtained. The remaining difference is due to the fact that mass and added mass do not exactly scale with s^3 in surge and s^5 in yaw.

3.4. Motion response

The motion response can be represented by the response amplitude operator (RAO) as given in Equation 6, depending on the excitation \mathbf{F} , and presented in Fig. 4.

$$|\text{RAO}(\omega)| = \left| \left[\mathbf{C} + i\omega\mathbf{B}(\omega) - \omega^2(\mathbf{M} + \mathbf{A}(\omega)) \right]^{-1} \mathbf{F}(\omega) \right| \quad (6)$$

The RAOs for the translational DoFs are equal for both designs. From Fig. 4 (a) it can be observed that the heave RAO represents in a general way the typical behavior [9], with a damping-dependent peak at the heave natural frequency, a static behavior in the stiffness dominated low-frequency range and an inertia-dependent decrease to zero at infinitely high frequencies.

The RAOs for the rotational motions, presented in Fig. 4 (b) and (c), are slightly different for the two upscaled designs. Due to the fact that the concrete ballasted system is stiffer than the water ballasted one, the corresponding RAOs in the rotational DoFs are smaller in the static region below the system's natural frequency. At the natural frequencies, however, the RAOs of both systems are expected to be equal due to the same amount of damping. The results obtained by Wadam cannot represent this behavior exactly as the discrete frequencies are not at the system's natural frequencies. Above the natural frequencies, the RAOs of the two designs can barely be distinguished one from the other, as the mass matrix components in the rotational DoFs only differ by at most 4%.

The DoFs of highest response, in general, are surge, heave and pitch, as the wave excitation is in surge direction and these motions are coupled. The obtained responses in sway, roll and yaw are insignificant and purely numerical.

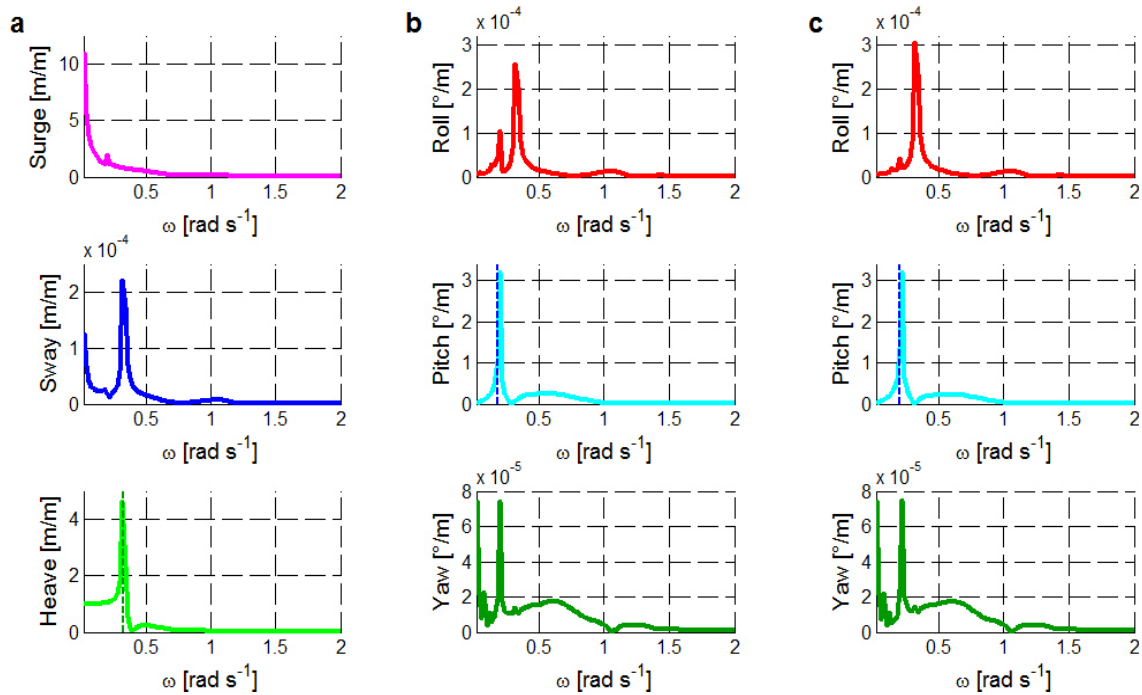


Fig. 4. RAOs in DoFs (a) 1 to 3 (both designs); (b) 4 to 6 (water ballasted); (c) 4 to 6 (concrete ballasted).

Based on 15 representative environmental conditions, response spectra ($S_q(\omega)$) and standard deviations (σ) of the motions were obtained, by means of Equation 7.

$$\sigma = \sqrt{\int_0^{\infty} S_q(\omega) d\omega} \quad \text{with} \quad S_q(\omega) = S_\eta(\omega) |\text{RAO}(\omega)|^2 \quad (7)$$

As the peak wave frequencies of the 15 conditions are beyond the system’s natural frequencies, there is almost no difference between the motion response of the two platform designs. The response spectra (not shown) are thus mainly affected by the wave excitation and not by the system’s eigenfrequencies, as the peak of the spectra occurs always at the peak wave frequency. The influence of the different significant wave heights is also only marginal compared to the peak wave frequencies. From the standard deviations of the motions, presented in Fig. 5, it can

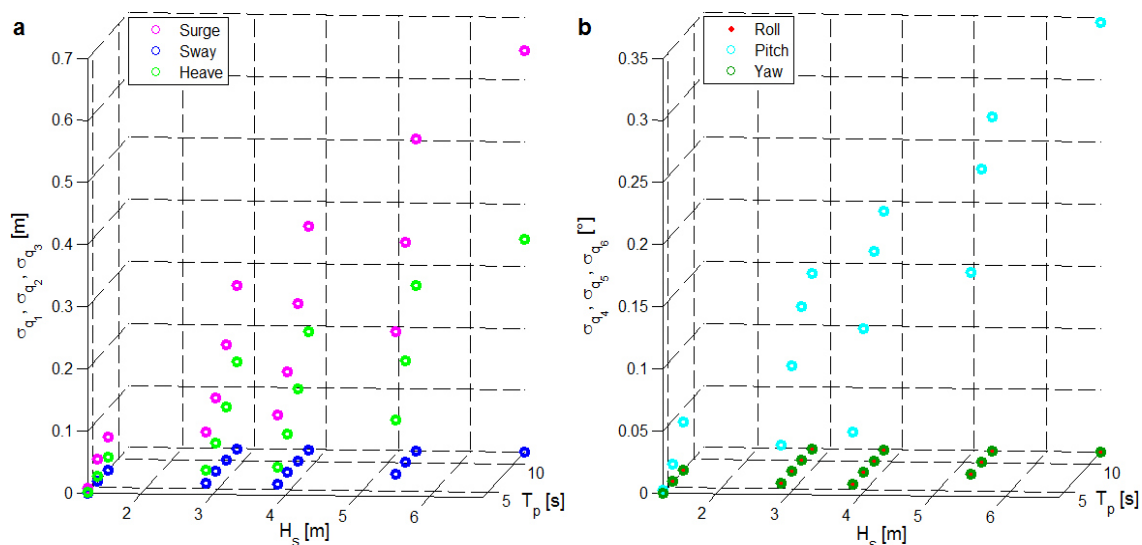


Fig. 5. Standard deviations in DoFs (a) 1 to 3; (b) 4 to 6.

be observed that the highest dynamic response occurs in surge, heave and pitch due to the directionality of the wave excitation, indicated in Fig. 1 (b). More severe environmental conditions also cause higher dynamic response. But still, the dynamic motions are quite small: at most 0.65 m in surge, 0.34 m in heave, and 0.34° in pitch. Comparing the dynamic response of both designs with different ballast systems shows that there is almost no difference for the considered environmental conditions, based on this linear frequency-domain analysis.

3.5. Nominal pitch displacement

As a proxy for the mean displacement of the floating wind turbine, the nominal pitch at maximum thrust was determined. The thrust force is the highest at rated wind speed and results with the hub height as lever arm in a moment in pitch of $1.386\text{E}+8$ Nm for the IWT-7.5-164 wind turbine [3]. Neglecting coupling terms, the nominal pitch displacement can be obtained by dividing the moment by the stiffness component in pitch. Due to the fact that this calculation is based on the static response and only includes the stiffness matrix, which is almost the same for the hand calculations and Wadam results, the obtained nominal pitch values are also comparable. As the concrete ballasted system is stiffer than the water ballasted one, the nominal pitch for the system with concrete as ballast (3.03°) is smaller than for the system with water as ballast (3.67°). Both values, however, are significantly higher than the theoretical upscaled nominal pitch displacement (2.31°) of the original DeepCwind floater, as the thrust force and corresponding moment cannot be compared directly for the two different turbine designs.

Comparing this maximum mean displacement with the standard deviations due to waves, it can be observed that the maximum dynamic pitch motion, occurring at the most severe sea state, is around 10% of the mean pitch displacement due to the maximum rotor thrust at rated wind speed.

4. Conclusion and outlook

In this work an initial upscaling of the OC4-DeepCwind semi-submersible floating platform was performed, such that Fraunhofer's wind turbine IWT-7.5-164 can be supported. Two upscaled floating platforms were designed with the focus on hydrodynamic performance, and compared regarding their static properties and dynamic behavior.

The high stability limits of -73.2° (water ballasted) and 92.8° (concrete ballasted), obtained by HydroD, indicate that both upscaled systems are too conservatively designed with respect to stability. A more detailed stability analysis including the mooring system and tower geometry is recommended.

The damped natural period in heave (19.1 s) is on the lower side of the typical range for semi-submersible platforms. Therefore, it is recommended to adjust the geometry such that the natural period in heave is increased. The water ballasted system yields a natural pitch period (34.1 s) more beyond the wave excitation than the concrete ballasted system (31.4 s), and is thus preferred from a frequency point of view. Due to the high stability limits, there is even room to increase the natural periods by elevating the center of gravity. Comparison with the original DeepCwind floating platform yields that both upscaled designs have higher natural periods, which is an advantageous aspect of upscaling. If the natural periods of the original DeepCwind floater are scaled up with the square root of the main scaling factor, however, it is found that the pitch natural frequency performance is better and the heave natural frequency performance is the same. The damped natural periods in surge and yaw are higher than the adjusted theoretical upscaled values. A more detailed analysis including the entire and exact mooring system stiffness is strongly recommended.

The maximum static pitch displacement at rated power is quite small (water: 3.67° , concrete: 3.03°), but - due to the different wind turbine designs - higher compared to the original DeepCwind floating system. Even in an extreme (fault) condition with a mean aerodynamic load of twice the rated load, the pitch displacement would still stay below the typical maximum allowable operational pitch of 10° . The dynamic motion is similar for both upscaled designs with a maximum of 0.65 m in surge, 0.34 m in heave and 0.34° in pitch.

For an optimized upscaling procedure, different scaling factors should be used for each component (smaller scaling factor for the upper columns, larger one for the base columns), in order to achieve higher natural frequencies in heave. This inhomogeneous scaling would most likely also influence the amount of displaced water volume. Thus, also adjustment of the amount of ballast and a change in the resulting total system mass, as well as the influence on the

stiffness in pitch and system's stability have to be considered in the optimization. The ballast system of the platform should be chosen such that an optimized balance between stability and natural frequencies further outside the wave excitation is found. Furthermore, the mooring system has to be analyzed more in detail and parameters like total length or location of the anchors have to be adjusted if needed.

Acknowledgements

This work has been partly supported by NOWITECH FME (Research Council of Norway, contract no. 193823). The authors also wish to acknowledge the financial support from Research Council of Norway through Center for Ships and Ocean Structures (CeSOS) and Centre for Autonomous Marine Operations and Systems (AMOS, RCN Project number 223254).

References

- [1] Sieros, G.; Chaviaropoulos, P.; Sørensen, J.D.; Bulder, B.H. and Jamieson, P. (2012). Upscaling Wind Turbines: theoretical and practical aspects and their impact on the cost of energy. *Wind Energy*, 15(1):3-17.
- [2] Robertson, A.; Jonkman, J.; Masciola, M.; Song, H.; Goupee, A.; Coulling, A. and Luan, C. (2014). Definition of the Semisubmersible Floating System for Phase II of OC4. Technical Report NREL/TP-5000-60601, NREL.
- [3] Sevinc, A.; Rosemeier, M.; Bätge, M.; Braun, R.; Meng, F.; Shan, M.; Horte, D.; Balzani, C. and Reuter, A. (2015). IWES Wind Turbine IWT-7.5-164 Specification, Revision 02. Data Sheet, Fraunhofer Institute for Wind Energy and Energy System Technology, Leibniz University Hanover - Institute of Wind Energy Systems.
- [4] Monarcha, A. and Fonseca, N. (2012). A static analytical method for the preliminary design of multiple line mooring systems. In Santos, T.A.; Soares, C.G.; Garbatov, Y. and Sutulo, S., *Maritime Engineering and Technology*, pages 195-203. CRC Press.
- [5] Jamieson, P. (2011). *Innovation in Wind Turbine Design*. John Wiley & Sons, Ltd, 1st edition.
- [6] Bredmose, H. (2014). Floating Wind Turbines. Presentation within the course "Offshore Wind Energy", Technical University of Denmark, Department of Wind Energy.
- [7] Tao, L. and Cai, S. (2004). Heave motion suppression of a Spar with a heave plate. *Ocean Engineering*, 31:669-692.
- [8] Ghadimi, P.; Bandari, H.P. and Rostami, A.B. (2012). Determination of the Heave and Pitch Motions of a Floating Cylinder by Analytical Solution of its Diffraction Problem and Examination of the Effects of Geometric Parameters on its Dynamics in Regular Waves. *International Journal of Applied Mathematical Research*, 1(4):611-633.
- [9] Newman, J.N. (1977). *Marine Hydrodynamics*. The MIT Press.
- [10] Benitz, M.A.; Schmidt, D.P.; Lackner, M.A.; Stewart, G.M.; Jonkman, J. and Robertson, A. (2015). Validation of Hydrodynamic Load Models using CFD for the OC4-DeepCwind Semisubmersible. Proceedings of the ASME 2015 34th International Conference on Ocean, Offshore and Arctic Engineering, St. John's, Newfoundland, Canada. Volume 9: Ocean Renewable Energy, V009T09A037.
- [11] Robertson, A.; Jonkman, J.; Vorpahl, F.; Popko, W.; et al. (2014). Offshore Code Comparison Collaboration Continuation Within IEA Wind Task 30: Phase II Results Regarding a Floating Semisubmersible Wind System. ASME 2014 33rd International Conference on Ocean, Offshore and Arctic Engineering, San Francisco, California, USA. Volume 9B: Ocean Renewable Energy, V09BT09A012.
- [12] Yu, Q. and Chen, X. (2013). Contract E12PC00027: Design Guideline for Stationkeeping Systems of Floating Offshore Wind Turbines, Final Report. American Bureau of Shipping (ABS).